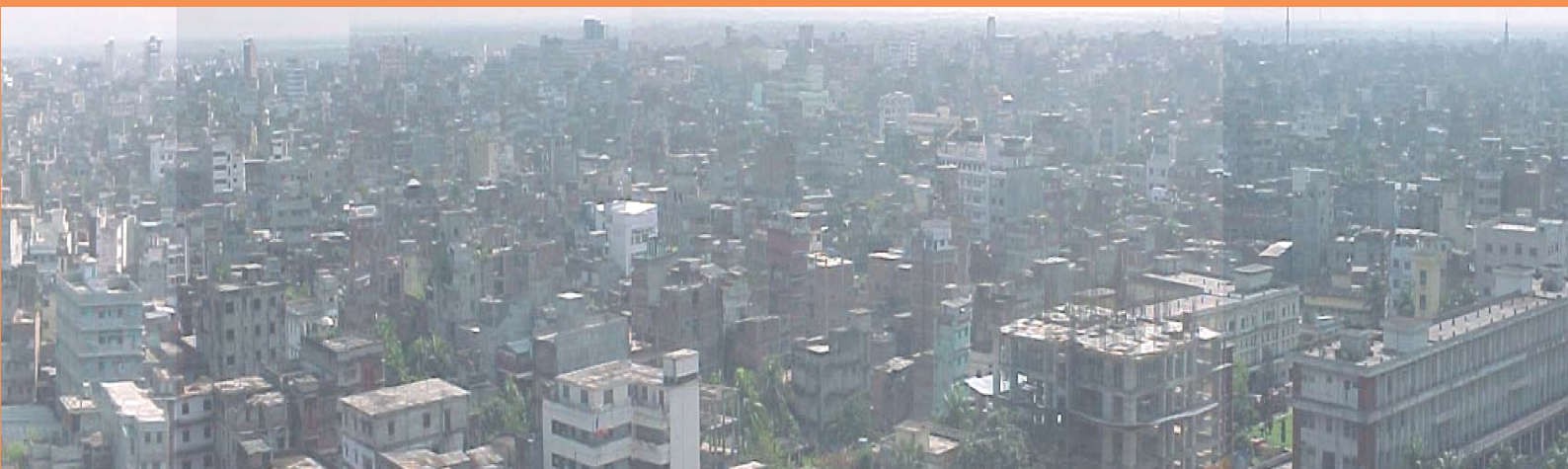




**BANGLADESH NETWORK
OFFICE FOR URBAN SAFETY**

BNUS ANNUAL REPORT-2011





**BANGLADESH NETWORK
OFFICE FOR URBAN SAFETY**



BNUS ANNUAL REPORT-2011

BANGLADESH
NETWORK OFFICE
FOR
URBAN
SAFETY



**BUET, DHAKA,
BANGLADESH**

Prepared By:

Mehedi Ahmed Ansary





**BANGLADESH NETWORK
OFFICE FOR URBAN SAFETY**



CONTENTS

PART-I: COMMUNITY UNDER FIRE THREAT: ASSESSMENT OF COMMUNITY FIRE HAZARD VULNERABILITY OF WARD 65 IN DHAKA CITY -----	1
PART-II: APPLICABILITY OF H/V MICROTREMOR TECHNIQUE FOR SITE RESPONSE ANALYSIS IN DHAKA CITY-----	27
PART-III: ESTIMATION OF SHEAR WAVE VELOCITY USING 3D MICROTREMOR MEASUREMENT IN SYLHET CITY -----	147
PART-IV: STRONG MOTION RECORDINGS DURING SEPTEMBER 18, 2011 SIKKIM EARTHQUAKE-----	159
PART-V: APPLICATION OF NON-DESTRUCTIVE TESTING TECHNIQUES FOR STRUCTURAL SAFETY EVALUATION IN BANGLADESH-----	175
PART-VI: VULNERABILITY EVALUATION FOR ZINDABAZAR GOVERNMENT PRIMARY SCHOOL, SYLHET, BANGLADESH-----	187
PART-VII: GEOPHYSICAL INVESTIGATION AT MEGHNA DHONAGODA IRRIGATION PROJECT (MDIP) USING GROUND PENETRATING RADAR METHOD-----	197
PART-VIII: TRAINING COURSES, SEMINARS AND WORKSHOPS -----	209



**BANGLADESH NETWORK
OFFICE FOR URBAN SAFETY**



PART-I

COMMUNITY UNDER FIRE THREAT: ASSESSMENT OF COMMUNITY FIRE HAZARD VULNERABILITY OF WARD 65 IN DHAKA CITY

**BANGLADESH NETWORK OFFICE FOR
URBAN SAFETY (BNUS), BUET, DHAKA**

Prepared By: Naima Rahman

Mehedi Ahmed Ansary

1. INTRODUCTION

Dhaka City has been experiencing many fire accidents at present and in most cases lack of proper precautionary measures along with the institutional inefficiency, insufficient equipment support and lack of public awareness are making the situation worse. To mitigate the impact of fire at community level, public participation is important. As a high risk area of fire hazard, no vulnerability assessment has been conducted in Dhaka City. In this study, a traditional community of ward 65 of Dhaka has been selected for vulnerability assessment. Community Vulnerability Assessment Tool (CVAT) (Lisa et al, 2002) method has been applied to assess vulnerability of the community to fire hazard. At first, a hazard map showing the different risk zones of fire has been developed by land use in the study area. Then four vulnerability analyses have been conducted namely social vulnerability, critical facilities vulnerability, economic vulnerability and structural vulnerability. To accomplish these vulnerability analyses different field surveys have been conducted for getting complete scenario of the community. By using some parameters and attributes, community vulnerability has been evaluated with respect to fire hazard. Finally some recommendations have been provided to improve the present condition of the community.

2. BACKGROUND

A fire hazard is any situation in which there is a greater than normal risk of harm to people or property due to fire. The physical vulnerability of the country's population and infrastructure is compounded by economic vulnerability. Extensive fire inevitably causes upheavals not only in the physical but also in the social and economic context where it occurs. Urban fires have devastating impact on the communities. An analysis of disaster impacts on urbanizing areas show that fires cause the greatest loss of life and property. Fires hazards occur frequently in Bangladesh especially in urban areas. Table 1 describes number of fire accidents originated by various causes in the last three years in Bangladesh. Electric fault, kitchen fire, cigarette, naked fire, burning ash, fireworks, friction of machine, sabotage, mob, unknown and misc (engine misfire, spontaneous ignition, and chemical reaction) are different causes of fire. Among these most of the fire occur due to electric fault and kitchen fire.

Table 1: Causes of Fire in Bangladesh

SL	Cause of Fire	Number of Fire Incident					
		2009		2010		2011	
1	Electric Fault	3754	43.27%	3188	39.44%	3760	43.86%
2	Kitchen Fire	2254	25.98%	2166	25.67%	2137	24.89%
3	Cigarette	865	9.97%	789	9.75%	828	9.64%
4	Naked fire	542	6.24%	528	6.52%	450	5.24%
5	Burning Ash	229	3.41%	267	3.16%	358	4.17%
6	Fire Works	162	2.41%	204	2.41%	161	1.87%
7	Friction of Machine	134	1.99%	170	2.01%	244	2.84%
8	Sabotage	85	1.26%	149	1.76%	104	1.21%
9	Mob	113	1.68%	241	2.85%	78	0.90%
10	Unknown	868	-	1105	-	726	-
11	Misc (Engine misfire, spontaneous ignition, Chemical reaction)	536	6.17%	389	4.61%	464	5.40%
	Total	12182		14682		13041	

Source: Bangladesh Fire Service and Civil Defense, 2012

Fire incidents are categorized into different causes. This categorization has been done according to the building use and electrical system in the building. Figure 1 describes the trends in fire accidents in Bangladesh with different categories from 2005 to April 2011. Residential fire events are increasing in every year tremendously and it causes loss of property and injures many people badly. Industrial fire is also in increasing trend.

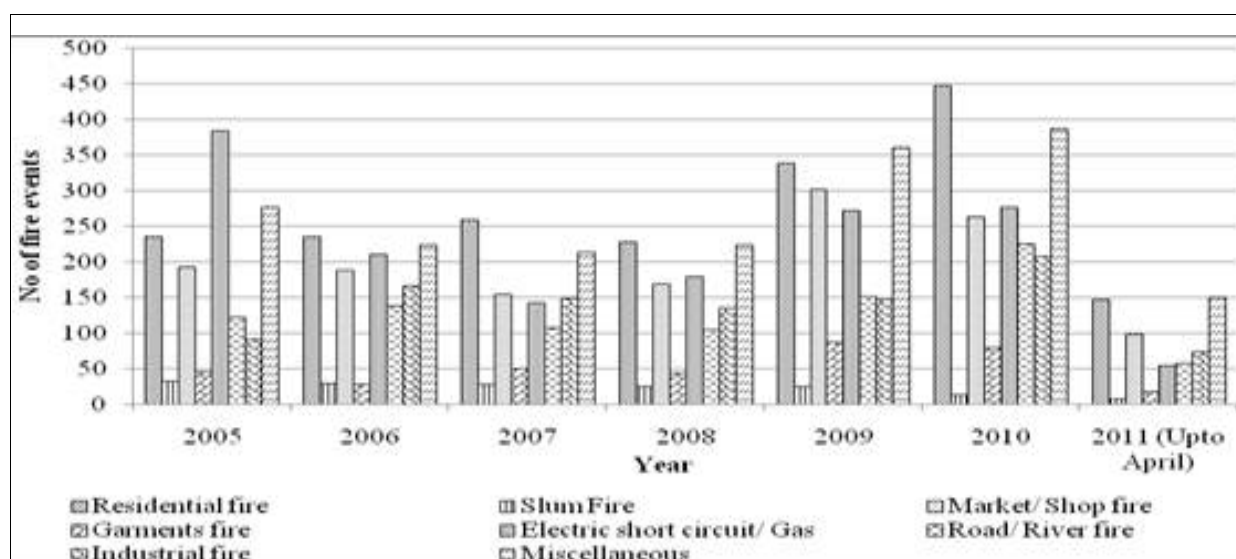


Figure 1: Trends in fire accidents in Bangladesh (2005 to April 2011)
(Source: Bangladesh Fire Service and Civil Defense)

Economic loss due to fire incidents is high. Figure 2 describes amount of loss due to residential fire in Taka crore from 2002 to 2010. Among these years the highest amount of loss (Tk. 272.64 crores) is seen in 2005. In most of the years the loss amount is above Tk. 100 crores. As Bangladesh is a developing country it cannot afford the huge amount of loss due to fire accidents every year.

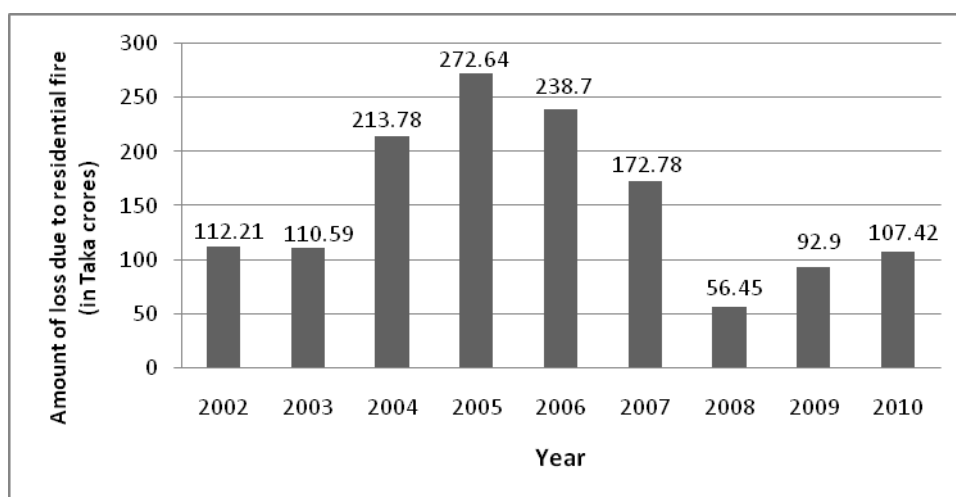


Figure 2: Extent of losses due to fire hazards in recent years (1 Million USD = Taka 8.6 crore)
 (Source: Bangladesh Fire Service and Civil Defense)

Dhaka the capital of Bangladesh often faces fire hazards due to its dense building concentrations, narrow roads, flammable building materials, aging water supply and electrical wire, chemical factory in residential areas as well as the lack of preparedness and response skills among local people and the fire authority. Figure 3 shows the trend of fire in Dhaka City in the last six years. Most of the fire events occurred in 2010 than the other statistical year.

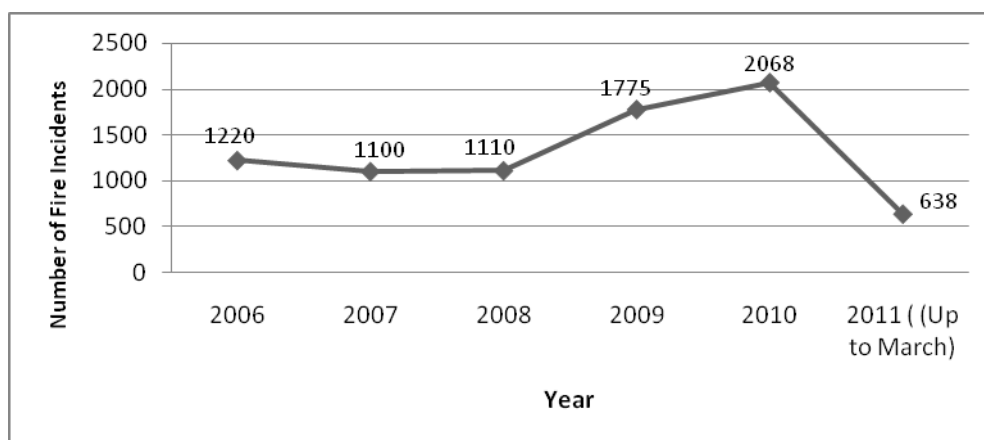


Figure 3: Number of fire event in Dhaka city
 (Source: Bangladesh Fire Service and Civil Defense, June 2011)

In 3rd June 2010, a devastating fire broke out in the densely-populated part of Old Dhaka city at Nimtoli. Fire killed at least 117 people and caused injury to a hundred people. Most of the affected peoples were women and children. Initially it was thought that explosion of two transformers at Nimtoli started the fire but later it has been known the fire originated from an oil stove and spread to the chemical warehouses nearby and resulted high casualties and damages.

Two back to back fires occurred in 15th and 16th January 2012 in Islambag and Lalbag areas in Ward 65 in Old Dhaka. The first incident occurred in a plastic warehouse near the Eidgah ground in West Islambag at around 10:45 PM started from a gas stove. The next day again at the same time another fire occurred in Shahid Nagar area at Lalbag around 10:30 PM. In this case fire originated from a tin shed house. Around 100 shanties, five shops and a printing press caught by fire. (BNUS field Survey, 2012).

This is a common situation in Old Dhaka where most of the buildings have small factories like chemical, plastic, rubber etc. and warehouse and food shops up to second floor of the residential building. In Old Dhaka no house is equipped with fire fighting equipments like extinguisher, hose pipe etc. They don't have sufficient width of staircase let alone the emergency exit. In this respect, assessment of fire hazard vulnerability in Dhaka City especially in the old part is very important. The old part 'Puran Dhaka' is the most vulnerable area in Dhaka City. In this study Ward 65 (Map 1) of Old Dhaka is selected for the vulnerability assessment. This ward is one of most vulnerable to fire hazard than other because of its traditional land use and population density. Fire incidents are very common phenomenon in this area. It is also one of the oldest areas of Dhaka City. This ward is mainly used as manufacturing industrial area. Besides several land uses like Warehouse, commercial use, chemical shop, clamber storage and processing shops are also prominent. Land use of this area makes it more unique than the other area of Dhaka City. In this study, assessment of fire hazard vulnerability of the community has been conducted to examine the existing risk of fire in the area and prepare the residents to face this sort of disaster.



Map 1: Study Area (ward 65 of Dhaka city)
Source: Dhaka City Corporation

3.METHODOLOGY

The research has been conducted with the following methodology:

3.1 Study Design

For achieving the objectives, depending on the literature review a checklist for the study has been designed which has been modified on the basis of findings from pilot survey. The checklist is given in Appendix-A.

3.2 Study Area Selection

The Ward 65 of Old Dhaka is selected as the study area to assess the fire hazard vulnerability. The study includes the vulnerability assessment of the building stocks. Buildings adjacent to the roads were surveyed.

3.3 Sampling

As the total number of buildings of Ward 65 is 3210, so the total sample size of this research is 3210. For these sample size, total 1078 buildings survey has been conducted keeping the confidence level at 95% and confidence interval is 2.43. That means the result of this

research varies from -2.43 to +2.43. (<http://www.surveysystem.com/sscalc.htm>, accessed on 25th March, 2011).

3.4 Data Collection

3.4.1 Base map collection and updating map from field survey

A base map of the study area was collected from Dhaka City Corporation (DCC) office to become familiar with the environment of the study area. Field survey of the buildings was conducted on the basis of the DCC base map.

3.4.2 Primary Data Collection

A checklist survey was conducted in the study area to find out the existing socio-economic condition of the residents.

3.5 Data Processing and Analysis

Through data collection, raw data have been collected. Information collected from the survey, have been inputted in MS Access and then converted to SPSS 12 for processing and analysis.

3.5.1 Fire hazard vulnerability analysis

To assess the community vulnerability of Ward 65 in Old Dhaka, Community Vulnerability Assessment Tool (CVAT) is used to find out the existing scenario of the area. This tool has 7 steps including:

- Hazard identification
- Hazard analysis
- Critical facilities analysis
- Social analysis
- Economic analysis
- Environmental analysis
- Mitigation opportunities analysis

In this report only critical facilities analysis, social vulnerability analysis, economic vulnerability analysis and in addition structural vulnerability analysis has been done to assess the vulnerability of the community. The tools and methodologies used in this analysis consist of GIS and spatial mapping analysis.

Critical facilities analysis

This analysis focuses on determining the vulnerabilities of key individual facilities, lifelines, or resources within the community. Critical facilities include emergency shelters, schools, hospitals, nursing homes, public buildings, and facilities for fire and rescue, police, utilities, communications, transportation, etc., or those identified as critical by the risk and vulnerability assessment working group. It is important to protect critical facilities (e.g., through relocation, elevation, or retrofit: backup of essential records; and backup of power supplies) to ensure that service interruption is reduced or eliminated, because these facilities play a central role in disaster response and recovery. Because it is not usually feasible to conduct a structural and operational analysis for every structure in a community, this step helps to prioritize which facilities are most vulnerable, so that individual assessments may be performed later. A structural analysis is used to examine the structural integrity of the building and its ability to withstand potential hazard damage; whereas, an operational analysis helps determine how daily activities will be affected if the building is damaged or if utility services are interrupted. The critical facilities vulnerability analysis has four components:

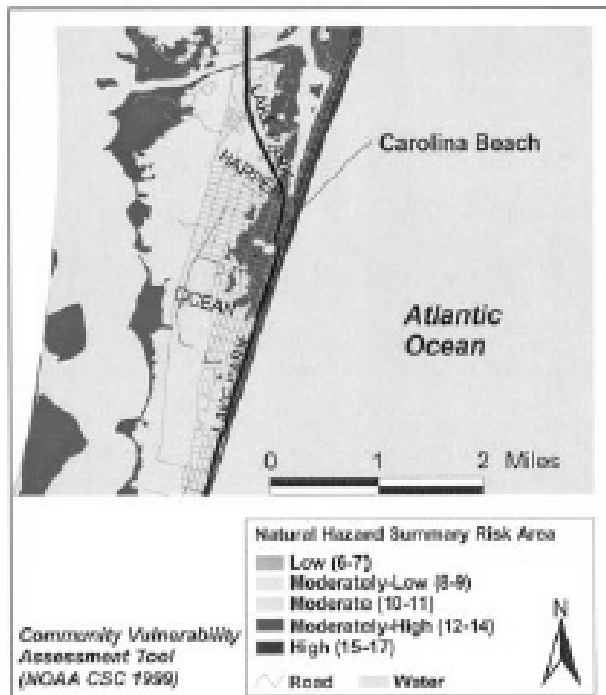
- First, critical facilities are identified by type and location to determine facilities that provide essential services to the community on a regular basis and are integral to disaster response and recovery operations.
- Second, a critical facilities inventory must be established by collecting general information on facility types and locations. The type and amount of information collected depends on the intended use of the database. Most local emergency management offices collect and maintain information on certain categories of critical facilities, which may provide a starting point for the critical facilities inventory. It is imperative to collect accurate information because these data will be essential for completing the individual facility assessments in the last step of this analysis.
- Third, critical facilities that are in and within close proximity to high-risk areas are identified by overlaying the critical facility locations over the map of hazard-risk areas.
- Next, critical facilities that will require further structural and operational assessments are identified by completing a critical facilities inventory, which should include but is not limited to construction type and quality, location, age, size, occupancy rates, monetary value, insurance coverage, auxiliary-power capability, backup capacity and process for electronic files, and protection and storage procedures for hard-copy documents. Assessment questions should be designed to meet the needs of the audience or investigators. Some questions may

require professionally trained inspectors or engineers, while others may rely on subjective evaluations from managers or property owners.

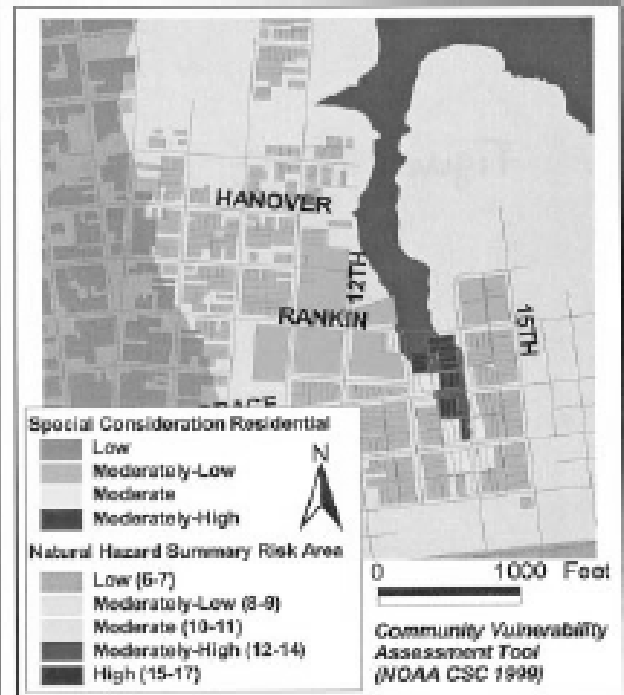
Social analysis

This analysis focuses on societal vulnerability by analyzing special consideration areas (preferably at the neighborhood level), where individual resources for loss prevention and disaster recovery tend to be minimal. Individuals that reside in special consideration areas are more likely to be uninsured or underinsured for hazard damages and have limited financial resources for pursuing individual hazard mitigation options. The population in these areas would be most dependent on public resources (e.g., disaster relief and recovery grants, unemployment assistance, subsidized health care and child care, social services, public transportation, etc.) after a disaster and therefore could indicate good investment areas for hazard mitigation activities. Special consideration areas can be identified by utilizing existing low-to-moderate income designations for community development grants or by analyzing key census data categories. Demographic characteristics can be selected to help identify special considerations such as mobility, literacy, or language, which can significantly hinder disaster recovery efforts. A societal vulnerability analysis is accomplished as follows:

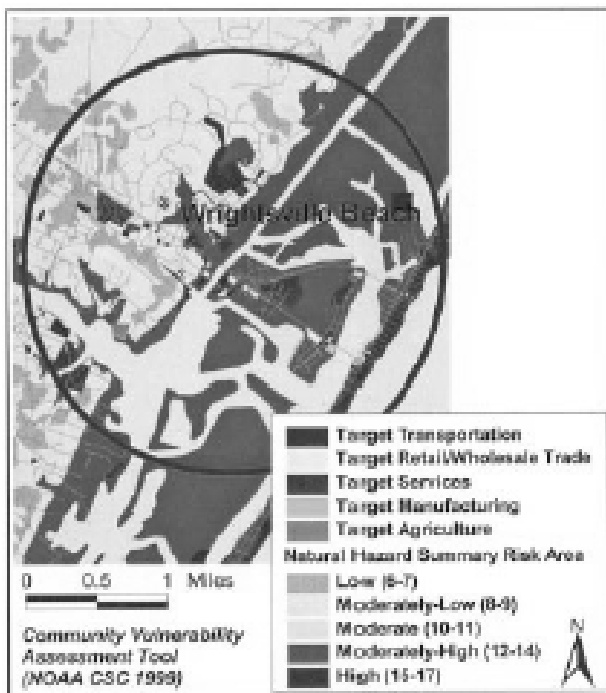
- First, special consideration areas (e.g., areas with high concentrations of poverty, elderly, minorities, single-parent households, rental dwellings, no high school diplomas, public assistance recipients, non-English speaking populations, no vehicle available, etc.) are identified by type and location to determine which populations may require special care or may have more difficulty with disaster response and recovery.
- Second, special consideration areas that are in high-risk areas are identified by overlaying the special consideration neighborhoods onto the risk areas.
- Next, a general inventory is completed of special consideration areas that are located in high-risk areas. There are several ways to complete this type of inventory. A community might elect to conduct a windshield survey to determine the number and type of vulnerable facilities in high-risk areas, unless these data are readily available from the local tax assessor's office. New Hanover County used a parcel-based land use inventory in a GIS format to distinguish the number and type of residential structures located in each census block group that was identified as a special consideration area. (Map 2)



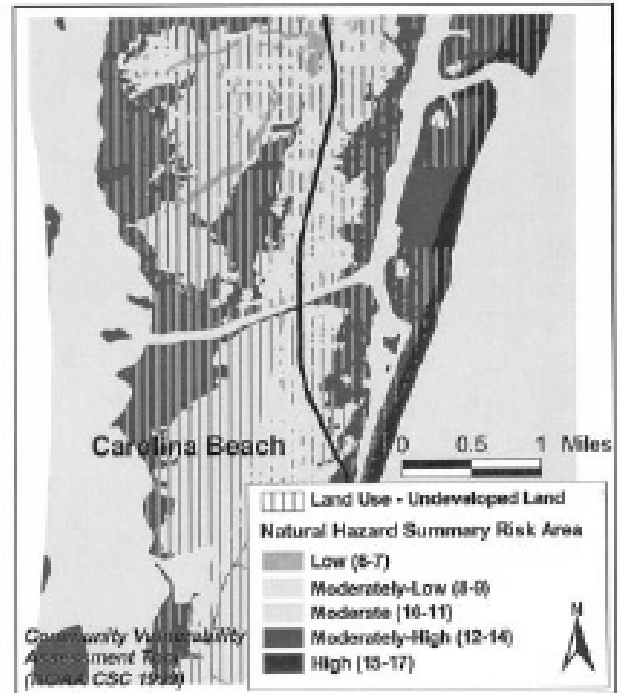
(a)



(b)



(c)



(d)

Map 2: Examples of GIS maps used for the Community Vulnerability Assessment Tool process in New Hanover County, North Carolina: (a) Natural hazard summary risk areas (Step 2-Hazard analysis); (b) Special consideration residential areas with high risk areas (Step 4-Societal vulnerability analysis); (c) Economic sectors in high-risk areas (Step 5-Economic vulnerability analysis); (d) Tracts of undeveloped land in high-risk areas (Step 7-Mitigation opportunities analysis)

Economic analysis

This analysis focuses on economic vulnerabilities to hazard impacts by identifying major economic sectors and mapping primary centers of activities in those sectors. Economic centers are areas where hazard impacts could have adverse effects on the local economy and would therefore be ideal locations for targeting certain hazard mitigation strategies. Some of the most devastating disaster costs to a community include the loss of income associated with business interruptions and the loss of jobs associated with business closures. A progressive community will actively pursue business continuity plans and hazard mitigation options to prevent or minimize such losses. It is important to begin this step by conducting a general overview of the local economy to provide a basis for targeting business sector partners in community-wide hazard mitigation efforts. The identification process will rely on local expertise such as the chamber of commerce or economic development council. Economic information can also be derived from widely available data sources such as the county business patterns located on the U.S. Census Bureau Web site (<http://www.census.gov/>). Land use or zoning data can often help in mapping business and industrial centers. Steps to accomplish an economic vulnerability analysis are as follows:

- First, the primary economic sectors and their geographic locations must be identified (i.e., economic centers) to determine which businesses are most important to the community (e.g., products and services, employment, tax revenue, disaster response and recovery capabilities, etc.).
- Second, primary economic centers that are located in high-risk areas are identified by overlaying the economic center locations over the risk areas.
- Third, a general inventory of high-risk economic centers is conducted. A community may choose to conduct a windshield survey to determine the number and type of vulnerable facilities in high-risk areas if this information is not readily available. A table (e.g., GIS attribute table or spreadsheet) can be used to summarize the type of industries, the number of facilities within each industry, the number of employees, the percentage of employees per industry and/or facility, and the annual payroll to help narrow the focus for facilities to be targeted for hazard mitigation.
- Fourth, large employers that are located in high-risk areas are identified to help prioritize the facilities on which to perform further analyses. Economic census data can help identify employment levels by economic sector and determine the size threshold.

- Next, a structural and operational vulnerability analysis is conducted. While this step is largely up to the private sector, it is recommended that vulnerability assessments for large employers be addressed in a manner similar to critical facilities. FEMA endorses engaging with key private sector establishments in hazard mitigation partnerships and asking them to assess their structural and operational vulnerability to hazards.

Environmental Vulnerability Analysis

This analysis focuses on identifying locations where secondary environmental impacts caused by natural hazards (primary impacts) may occur. Before embarking on this step, it is necessary to explain the terms “secondary impacts” and “secondary risk sites.” Secondary impacts occur when natural hazards (e.g., flood) trigger additional hazards such as toxic releases or hazardous spills. Therefore, a solid-waste facility or a building that stored hazardous materials would be characterized as “secondary risk sites” if they are in close proximity to areas of environmental concern (e.g., wetland). Although CVAT uses the term “secondary risk sites,” these are often called “hazardous facilities.” Environmental impacts are important to consider, as they not only jeopardize habitats and species, but can also threaten public health (e.g., water quality), various economic sectors (e.g., tourism and fishing), and quality of life (e.g., access to natural landscapes and recreational activities). For example, flooding (a primary hazard) can result in contamination (a secondary hazard) whereby raw sewage, animal carcasses, chemicals, pesticides, hazardous materials, etc. are transported through sensitive habitats, neighborhoods, and businesses. These circumstances can result in major cleanup and remediation activities, as well as natural resource degradation. Data can be obtained from state and local emergency management offices, local planning commissions, and environmental and natural resource management agencies to locate natural resources and secondary risk sites. Steps to accomplish an environmental vulnerability analysis are as follows.

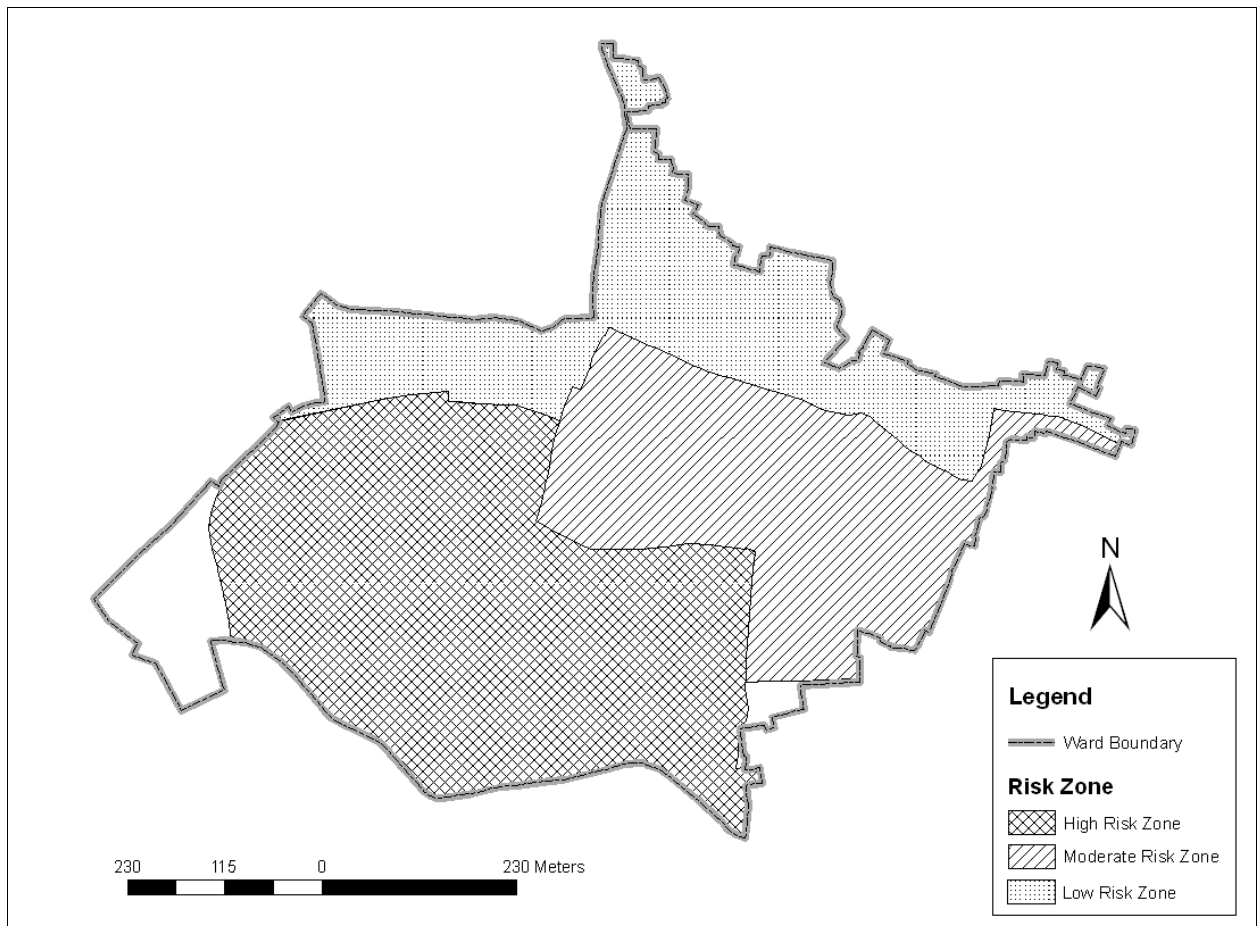
- First, secondary risk sites (e.g., hazardous materials, toxic release sites, solid-waste facilities, nuclear power plants, underground storage tanks, oil facilities, ports, marinas, discharge sites, etc.) and key natural resource sites (e.g., wetlands, sensitive/endangered species and habitats, fisheries, wildlife refuges, aquaculture sites, shellfish harvest areas, groundwater recharge areas, etc.) are identified.
- Next, secondary risk sites and environmentally sensitive areas are overlaid onto the risk areas to determine the types of hazardous materials and locations of potential releases into environmentally sensitive areas. (Lisa et al, 2002)

3.6 Preparation of Final Report

All information and finding are gathered and presented by tables, graphs and maps to prepare the final report. Some recommendations based on the findings are provided to improve the overall conditions of Ward 65 in the report.

4. FIRE HAZARD VULNERABILITY ANALYSIS

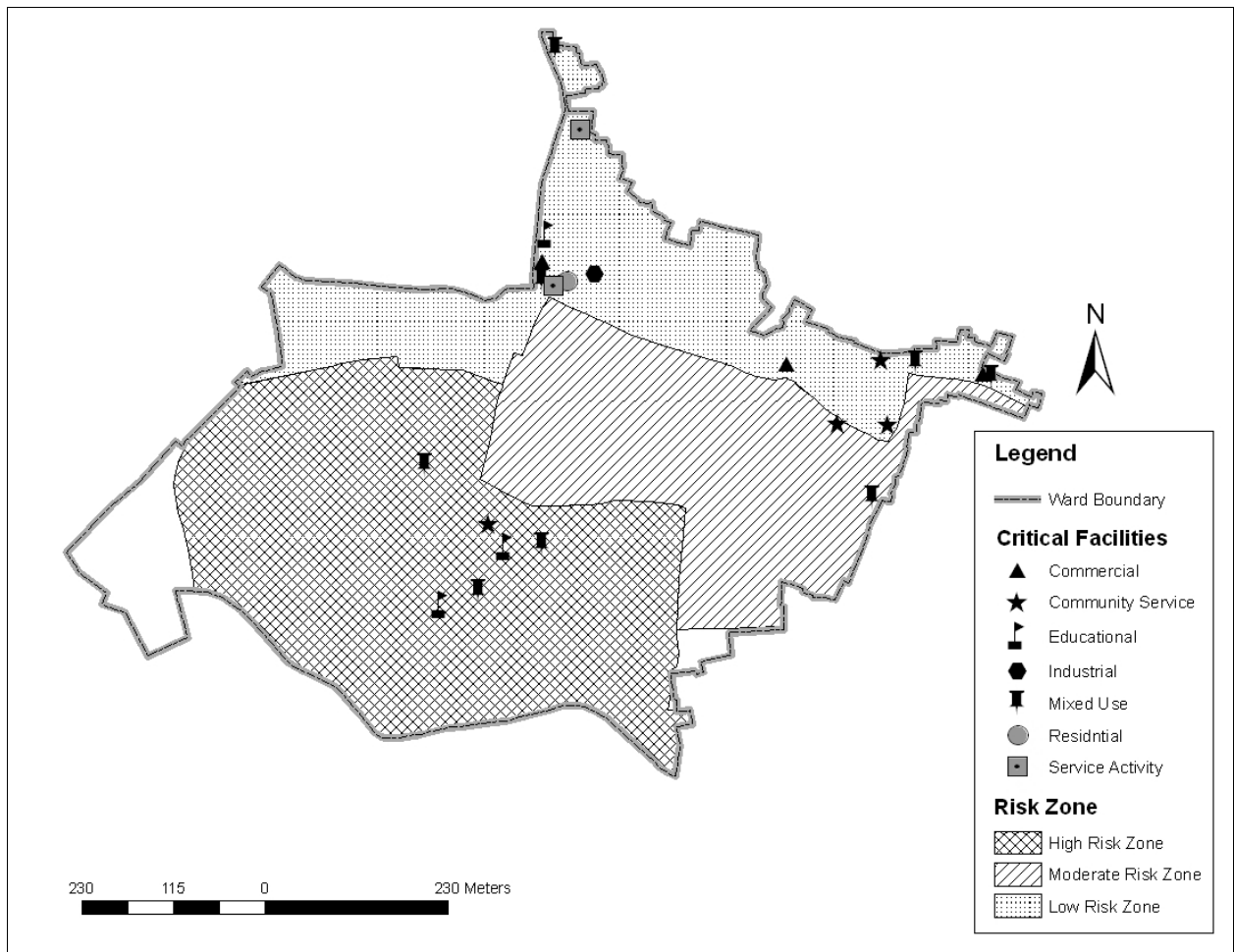
The study area is divided into three risk zones including high risk zone, moderate risk zone and low risk zone according to their land use from expert opinion. Land uses of various risk zones differ from other (map 3). The total area of Ward 65 is 118.1668 acres (0.478 Square Kilometer). Among this, high risk zone is 52.84 acres (44.72%), moderate risk zone is 30.89 acres (26.14%) and low risk zone is 27.95 acres (23.65%). (From GIS Map) The livelihoods of the inhabitants of a zone are primarily based on plastic processing industries like plastic manufacturing, recycling and processing factories. This zone is considered as high risk area. The name of this portion is Islambag. The zone also displays a high building density with multi-storey buildings and very few urban public spaces left. In the moderate risk area processing factory and different Warehouse (plastic Warehouse, cattle food storage) are dominant. Residential use with commercial (retail shop, office, bank and storage) use is considered as the low risk area.



Map 3: Fire risk zone in Ward 65

4.1 Critical Facilities Analysis

The critical facilities in ward 65 were identified and a complete inventory of these facilities was prepared. There are total 22 numbers of critical facilities in the study area. Then critical facilities that are in and within close proximity to high risk areas were identified by overlying the critical facilities location over the map of fire vulnerable areas. Map 4 shows critical facilities map in Ward 65. The most common critical facilities in the area are as follow:



Map 4: Critical facilities Map in Ward 65

Table 2: List of critical facilities of ward 65

Type	Name	Fire district
Educational institutions	School and Kindergarten	Lalbag Fire Station
Government organizations	Rapid Action Battalion (RAB) office	Lalbag Fire Station
Healthcare facilities	Dental Clinic	Lalbag Fire Station
Community facilities	Mosque and club	Lalbag Fire Station
Service facilities	Police stations, Bank/other office	Lalbag Fire Station
Utility facilities	Electrical sub station	Lalbag Fire Station

Figure 4 shows that 27.27% critical facilities are located at the high risk, 9.09% are located at moderate risk area and 63.64% are located at low risk zone. The critical facilities are mainly educational institution and religious center. Most of the critical facilities are located in the Lalbagh area which is comparatively low risk zone. In this area land use is mainly residential and in some case mixed (residential, retail shop, commercial) and the people in this area are less vulnerable to fire hazard. In high risk zone i.e. Islambag, plastic industries are located to very close proximity to critical facilities.

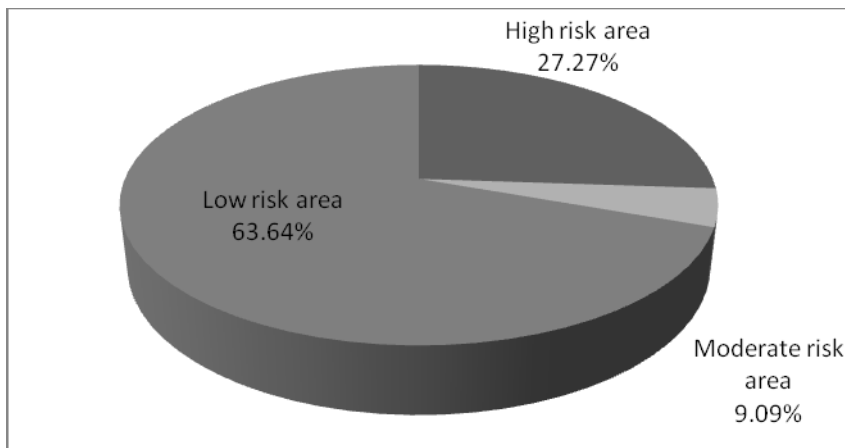


Figure 4: Percentage of critical facilities in different risk zones

Critical facilities of the study area are not vulnerable to fire. Besides these are located mainly adjacent to wider roads. In case of any fire, these can be used as shelter for the inhabitants.

4.2 Social Vulnerability Analysis

Number of population in any building of the study area varies from 0 to 400. Most of the buildings (28.53%) have 11 to 20 people. 22.03% have 21 to 30 persons and 18.93% have 6 to 10 persons. Building having population more than 100 is very low (1.6%). But most of the densely populated buildings are situated in the high risk zone (Map 5) which mainly consists of plastic recycling and processing factories. In these factories generally woman and child laborers work. With respect to these conditions of the area it can be said that the area is vulnerable to fire hazard.

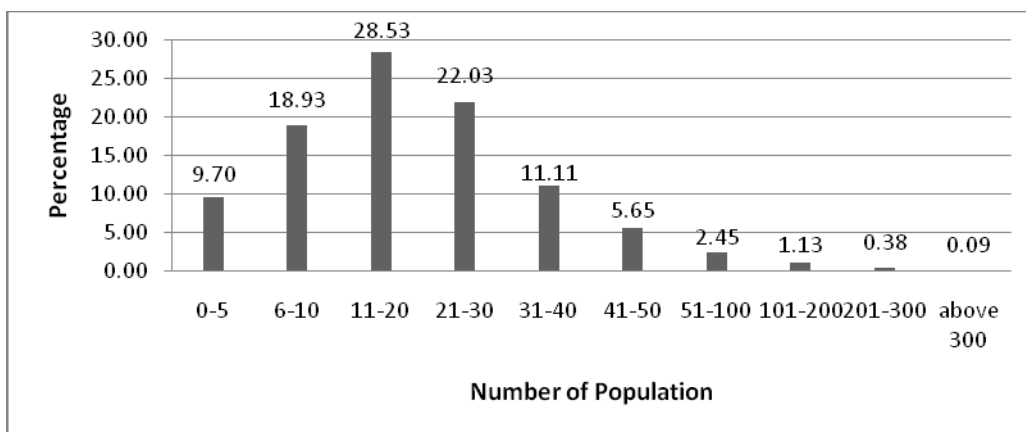
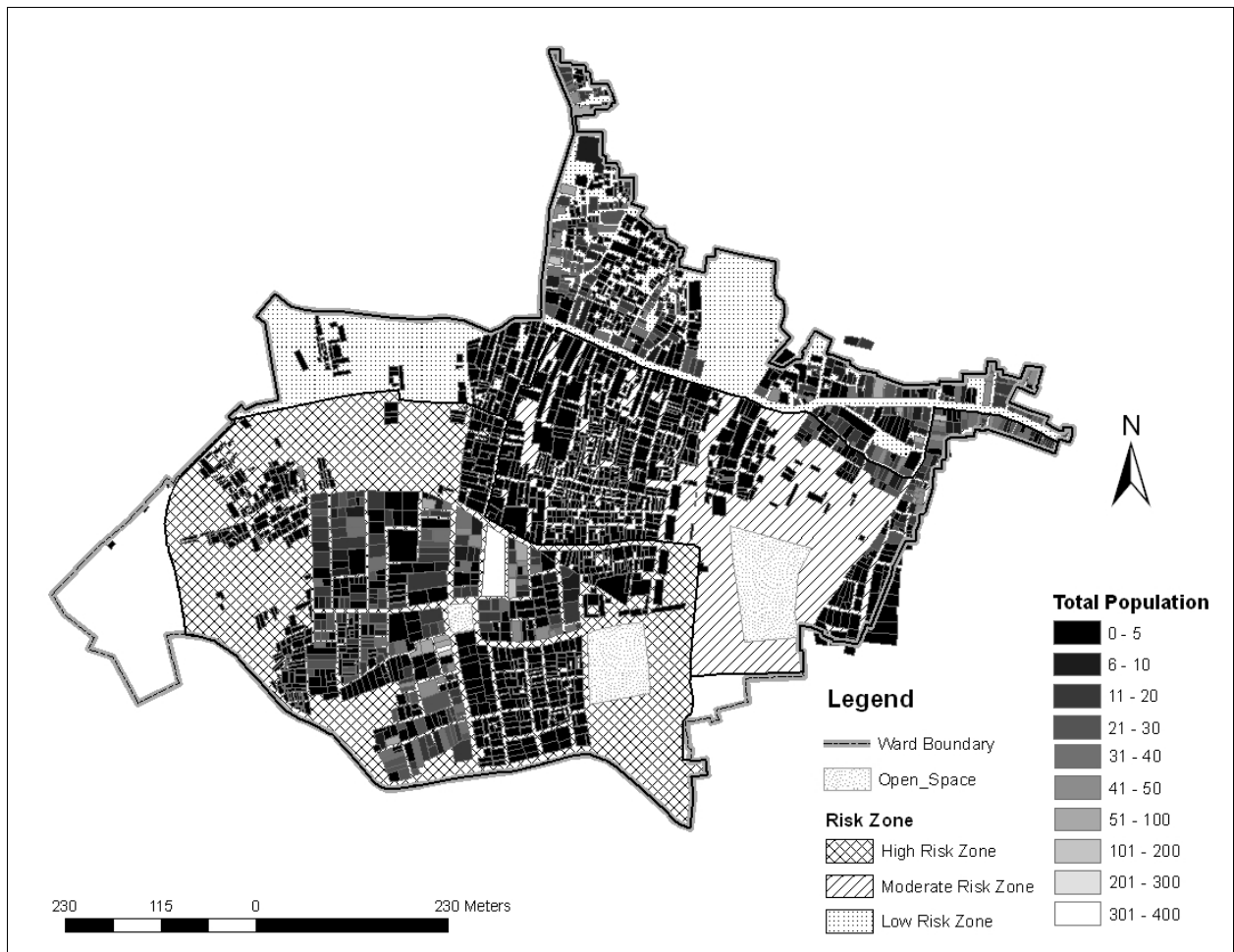


Figure 5: Population distribution in Ward 65.



Map 5: Population Map of Ward 65

4.3 Economic Vulnerability Analysis

Among the surveyed households, 57.22% have different types of economic activities. Plastic manufacturing and processing industry is dominating (20.22%); others are different type of factory (15.19%), warehouse (8.95%), iron/metal shop/factory (2.8%), gold and silver shop (1.49%), electric goods shop (1.3%), chemical shop/factory (1.21%) and other (6.06%) etc. Grocery shop, grocery shop and bank, medicine shop, tailoring shop/laundry, clamber storage, paper shop, bank/services, cloth store, hotel, market and phone shop are in other category. Figure 6 shows different types of economic activities of the study area.

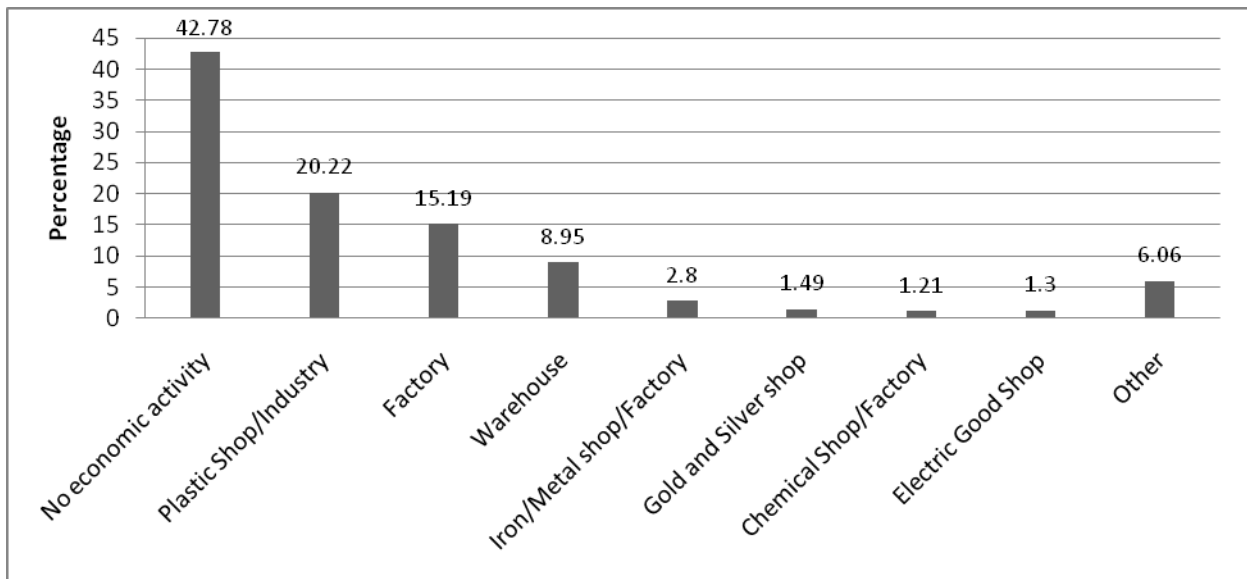


Figure 6: Economic Activities of the Study Area

Some economic activities make the study area vulnerable to fire hazard. Among them plastic manufacturing industry is totally based on chemicals which promote fire to spread within few seconds to the locality. From land use survey, it is found that the area is mainly a residential area (36.9%). Mixed activity is found in four categories: 1. residential and commercial (31.87%), 2. residential and industry (16.4%), 3. commercial and industry (0.93%), and 4. residential and education (0.1%). Figure 7 shows the present land use of the study area.

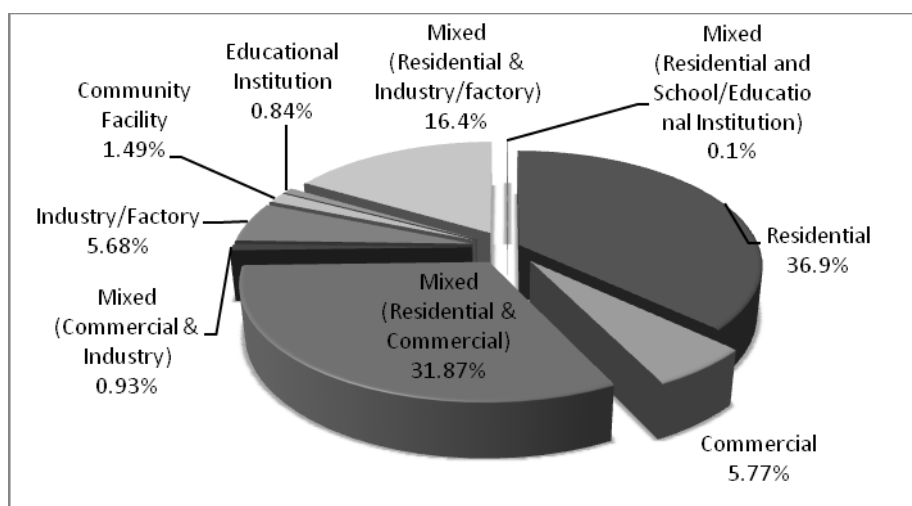
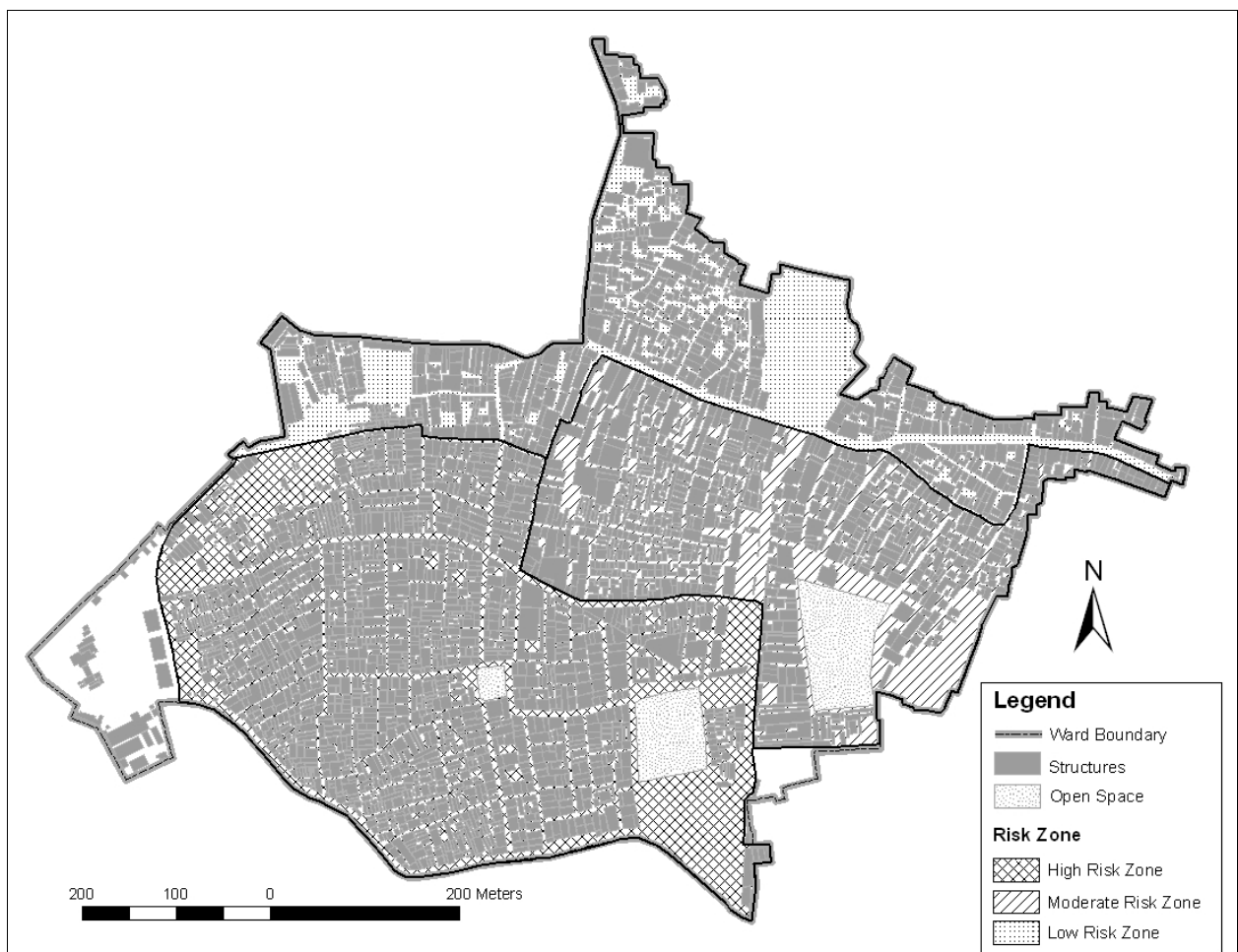


Figure 7: Present Land Use of the Study Area

4.4 Structural Vulnerability Analysis

There are other factors in the area which makes it vulnerable to fire hazard. These factors are width of staircase, road width of the area and accessibility to the building, position of transformer and electricity pole. If the roads are not accessible to fire service vehicle to douse/ put off the fire it may cause a loss to the community. For the emergency evacuation process staircase width is a vital issue to the resident of a building. That's why these factors get importance to the vulnerability assessment. The area consists of total 3210 structures. Among these, 55.66% of the structures are situated in high risk zone; 24.45% structures are situated in moderate risk zone and 19.89% structures are situated in low risk zone. (Map 6)



Map 6: Structure Map of Ward 65

4.4.1 Age of Structure

From the field survey, 2011, it is found that Ward 65 is composed of both old and newly developed buildings. 23.3% of surveyed buildings have been constructed 0-10 years ago. These are the newest structures of the area. Most of the buildings have been constructed around 11-20 years ago (25.7%). 23.2% and 11.6 % structures have been built 21-30 years

and 31-50 years before respectively. 15.9% building are 51-100 years old and 0.4% buildings are more than 100 years old.

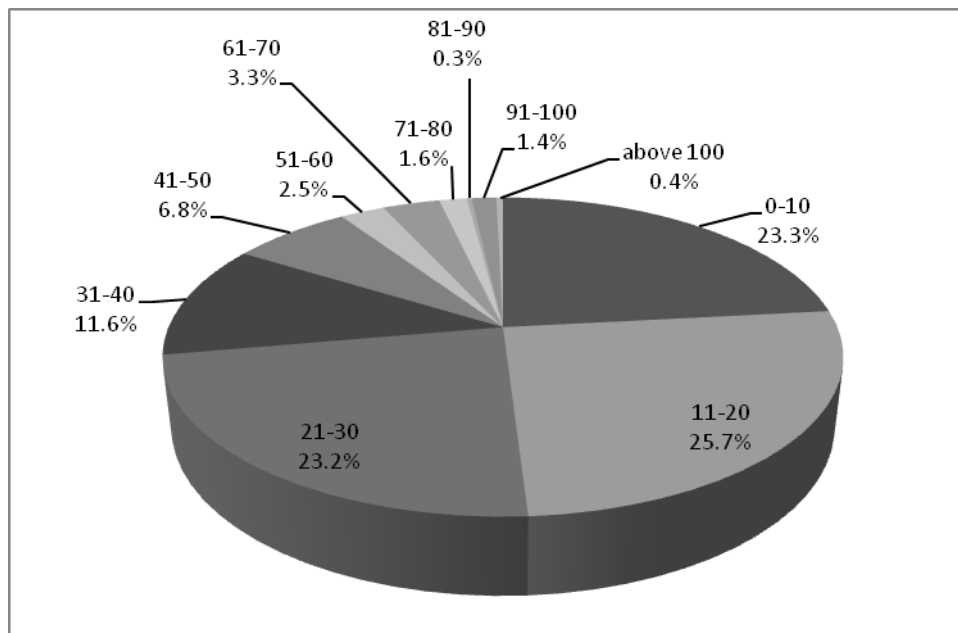


Figure 8: Age of building in the study area

4.4.2 Number of Floor

From field survey it has observed that in the study area most of the buildings (29.64% of surveyed buildings) are one storied. These buildings are mainly used as clamber storage and processing activity and plastic manufacturing and processing. In these structures fire can propagate very swiftly. 22.27% buildings are two storied and mainly used as residential and plastic processing activity. 3 storied are 14.35%, 4 storied are 13.05%, 5 storied are 12.3% and 6 to 14 storied are 7.36%. 1.03% buildings are under construction.

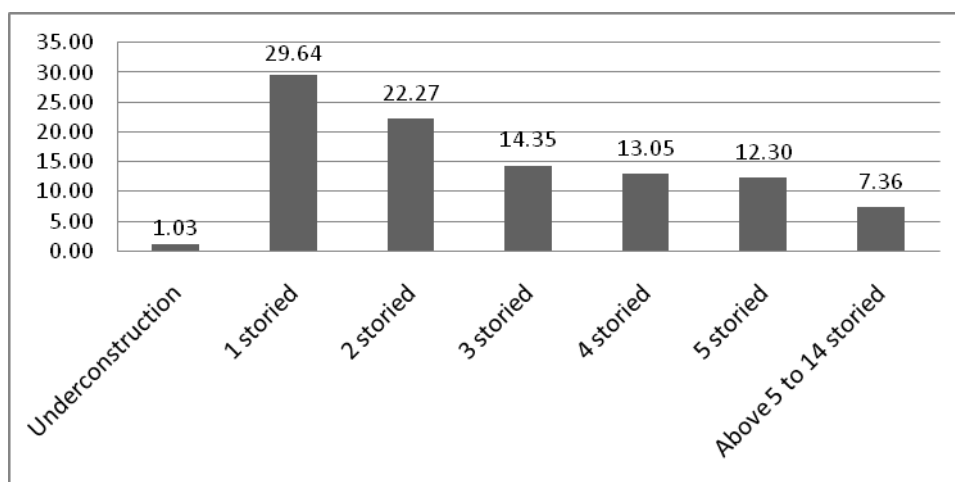


Figure 9: Number of floor of the building in the study area

4.4.3 Staircase Width

In the older portion of Dhaka city it is a tradition that the width of staircase is smaller than the new part of Dhaka. From the field survey it has been observed that staircase width of buildings varies from 1-5 feet. Most of the buildings (41.82%) have 3 feet wide staircase. 4 feet wide staircases are seen in 28.09% buildings. In case of some newly constructed buildings the width is 5 feet (11.73%). Wider staircase is essential for any building during the evacuation process for any disaster. For fire hazard it gets special priority because fire spreads very quickly in a building. So people need to protect themselves from the rage of fire in a very short time. In this respect the study area is vulnerable to fire hazard.

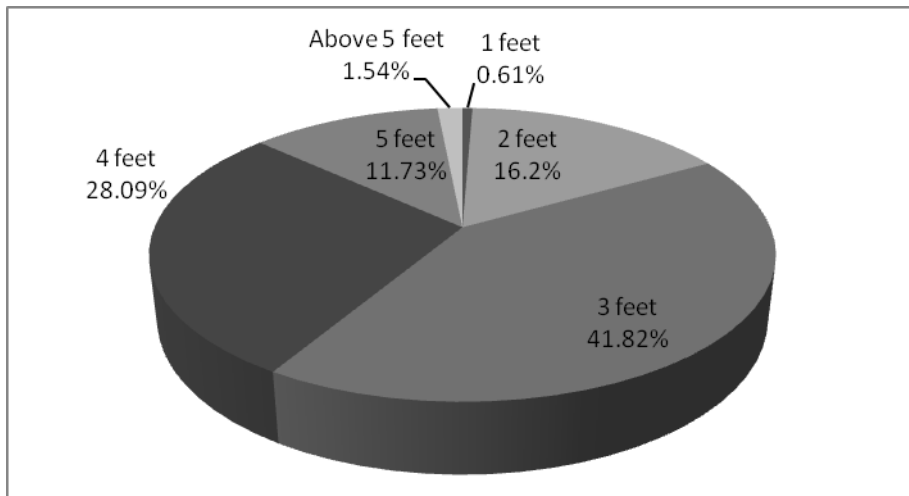
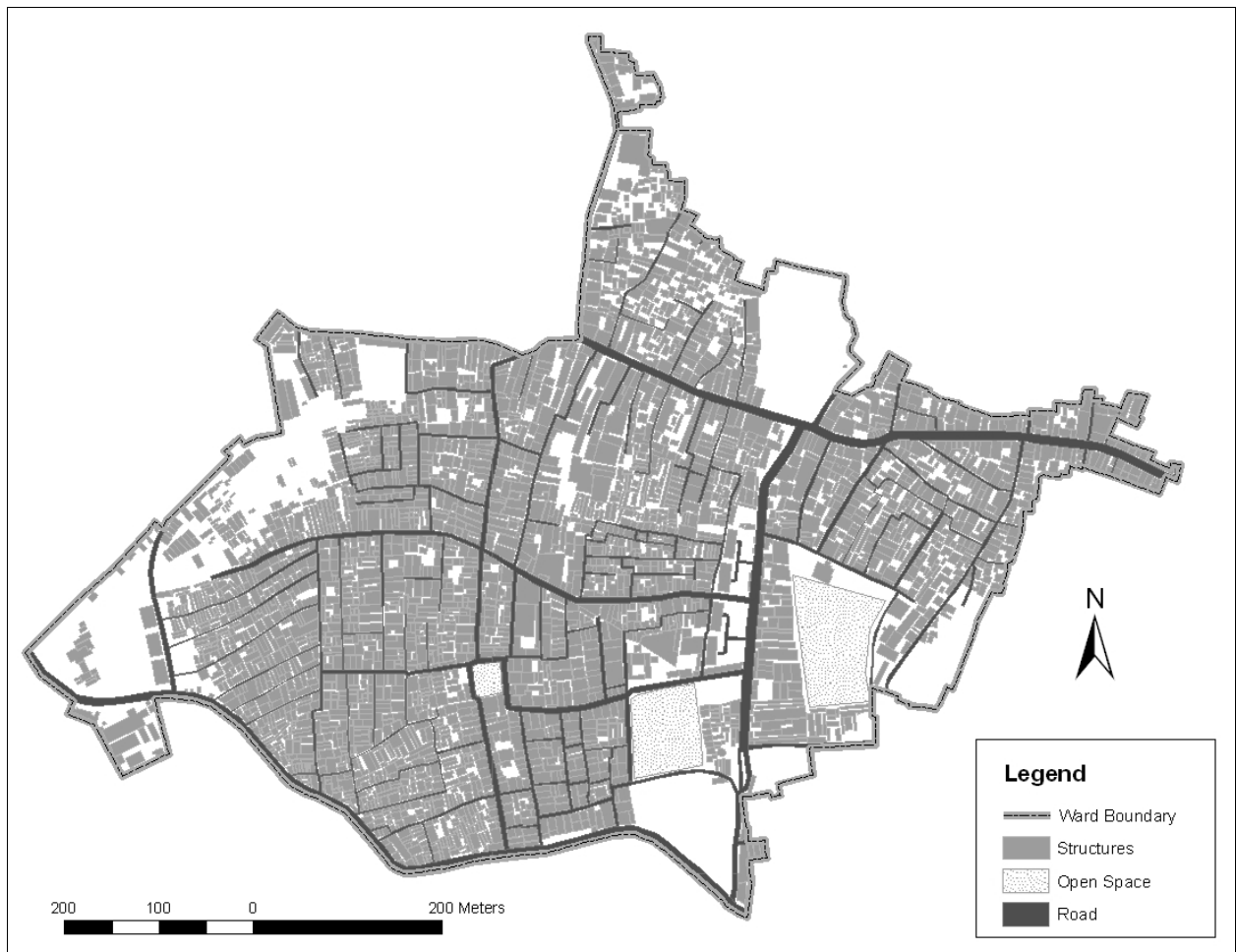


Figure 10: Staircase width (feet) of building in the study area

4.4.4 Road Width/ Accessibility to Building

For emergency response during any disaster road width is an important factor. If the road is not sufficiently wide to move fire service's vehicle it may cause another disaster to the people and it may extend the loss. Building fire can spread very quickly and can overwhelm properties and life. In the study area accessibility to each household is not good. The main roads are wide and accessible to the fire service vehicle but the local roads and connecting roads to the buildings are not accessible to the vehicle. (Map 7)



Map 7: Accessibility Map of Ward 65

Road width varies from 1-40 feet in the study area. Most of the residents have 6-10 feet roads in front of their houses (44.73%). 16.31% have 11-15 feet roads and 20.42% have above 15 feet roads. 18.55% households have only 0-5 feet roads which is inaccessible for fire truck. These narrow roads are totally impossible for evacuation and rescue process. In this respect this community is also vulnerable to fire hazard. They are not aware about widening the road.

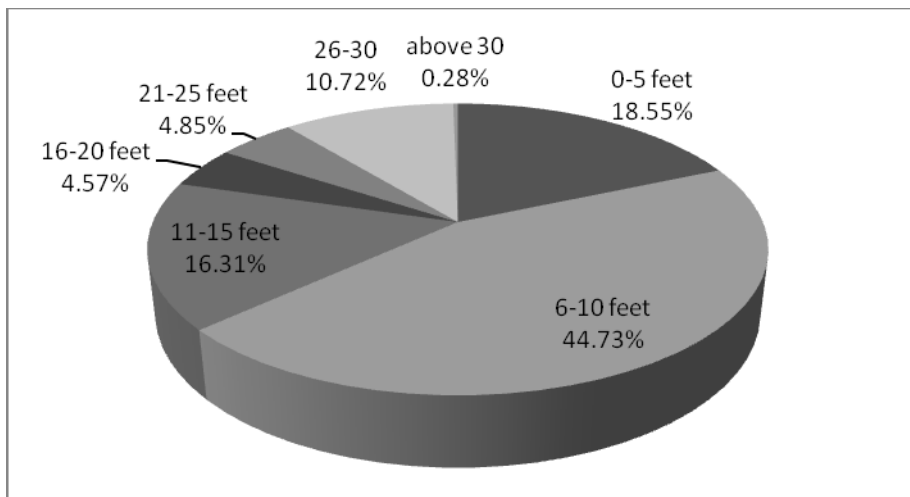


Figure 11: Road width (feet) / accessibility to building in the study area

4.4.5 Transformer and Electricity Pole

Position of transformer and electricity pole to a building is also assessed in this study because these may cause serious fire hazard to the locality. Recently in old Dhaka a fire incident occurred due to the blast of a transformer. The buildings in this area are constructed very closely to each other. So that fire can spread out to another building rapidly. Among the surveyed buildings electric pole is located in front of 13.51% buildings and transformer is located in front of 11.37 % building.

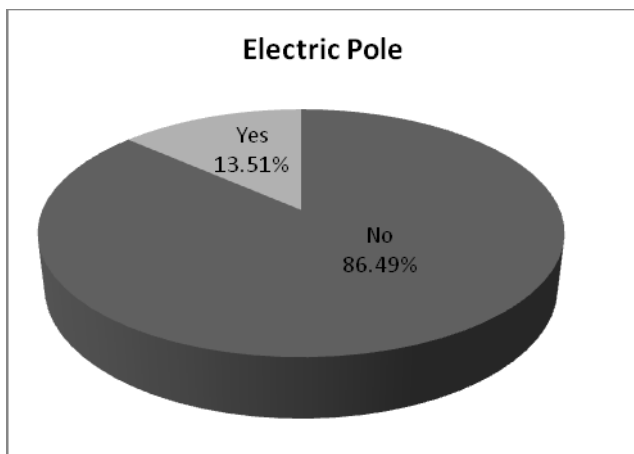


Figure 12: Electric pole in the study area

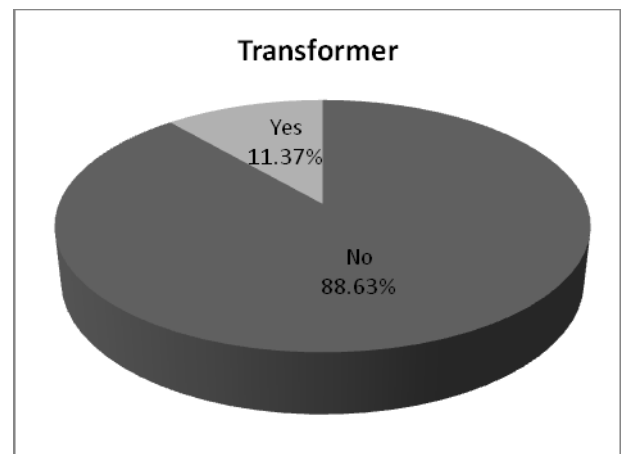


Figure 13: Transformer in the study area

4.4.6 Existence of Fire Source

Most of the buildings of the study area have different type of fire sources. Gas stove, electric wire, chemical factory and plastic factory are the main sources of fire. Besides, there are also some ornament factories, metal factories, recycled plastic shop, printing press and wholesale paper market in the area all of which can be source of great fire hazard. Residential houses

are vulnerable due to gas stove (38.4%) and electric wire (15.84%). Households with mixed use are mainly vulnerable due to plastic factory (17.8%), chemical shop (16.59%), metal factory (2.8%) and gold ornament factory (1.5%). 3.26% buildings have no fire source.

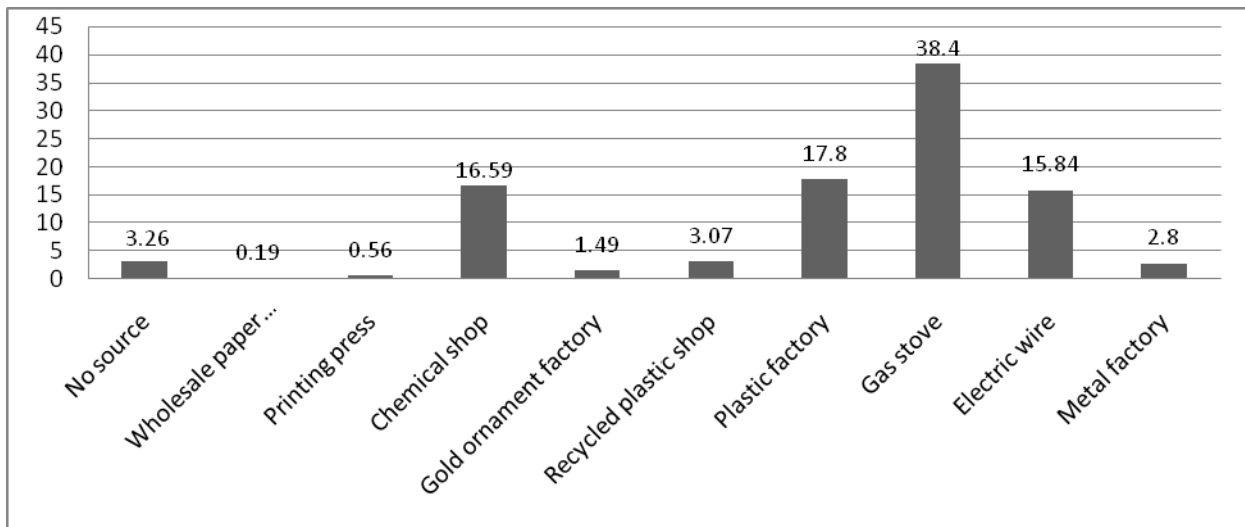


Figure 14: Existence of fire sources in the study area



Figure 15: Electric pole and transformer in front of building

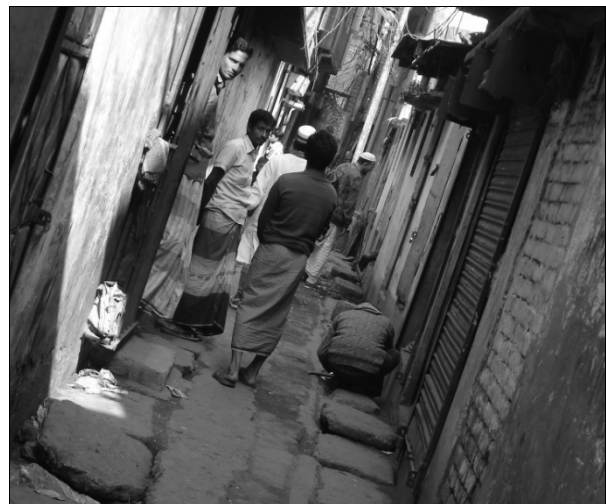


Figure 16: Narrow road within buildings

5. MAJOR FINDINGS

Severe fire incidents have occurred in ward 65. From the fire vulnerability analysis it has been found that maximum numbers of buildings of the study area are highly vulnerable (55.66%). Most of the highly fire vulnerable buildings are located in Islambag Road. Buildings of Water works Road and Lalbag area are less vulnerable because of being residential areas with mixed commercial use.

27.27% critical facility was found to be within the highly fire vulnerable areas. Most of these facilities (63.64%) are situated in the low risk zone. So critical facilities of the study area are moderately vulnerable to fire.

Population density in the high risk zone is high and the area consists of plastic recycling and processing industries. In these factories generally woman and child labors work. So it can be said that the area is socially vulnerable to fire hazard.

Most of the buildings of the study area have different kind of economic activities. Only 36.9% buildings are residential with no economic activity. 20.22% buildings have plastic manufacturing and processing industries which is highly vulnerable to fire hazard.

Most of the buildings (41.82%) have 3 feet wide staircase. 18.55% households have only 0-5 feet roads in front of their houses which is inaccessible for fire truck. Besides, electric pole is located in front of 13.51% buildings and transformer is located in front of 11.37 % building. 96.74% buildings of the study area have different type of fire sources. In this respect this community is vulnerable to fire hazard.

6.CONCLUSIONS

Urban fire incidents have been determined to have a high likelihood of occurrence in our country. But no mentionable fire risk assessment has been performed although fire hazard characterization information is available in the Fire Service and Civil Defense (FSCD). In this study after conducting vulnerability assessment using Community Vulnerability Assessment Tool (CVAT), it is found that ward 65 is vulnerable to fire hazard. The land use pattern of ward 65 indicates the possibility of this kind of hazard. The area comprises of residential use as well as commercial and industrial uses like plastic manufacturing and processing factory and chemical factory which may induce massive fire. As being a mixed use residential area, the loss due to fire may be catastrophic. To minimize the social and economic loss, Mitigation Planning is required. A change in present land use pattern is required. Chemical factory and plastic factory should be relocated. Road network as well as staircase of building should be wider to evacuate the community people. Community awareness should be raised. Although CVAT has been applied in this small area of Dhaka city, it can be applied to any type of hazard in any location of the country both at micro and macro levels.



PART-II

APPLICABILITY OF H/V MICROTREMOR TECHNIQUE FOR SITE RESPONSE ANALYSIS IN DHAKA CITY

**BANGLADESH NETWORK OFFICE FOR
URBAN SAFETY (BNUS), BUET, DHAKA**

Prepared By: Saidur Rahman

Mehedi Ahmed Ansary

1.1 GENERAL

In the recent past, Bangladesh has not suffered any damaging large earthquakes, but in the past few hundred years, several large catastrophic earthquakes struck this area. So far, all the major recent earthquakes have occurred away from major cities, and have affected relatively sparsely populated areas. In 1897, an earthquake of magnitude 8.7 caused serious damages to buildings in the northeastern part of India (including Bangladesh) and 1542 people were killed. Recently, Bilham et al. (2001) pointed out that there is high possibility that a huge earthquake will occur around the Himalayan region based on the difference between energy accumulation in this region and historical earthquake occurrence. The population increase around this region is at least 50 times than the population of 1897 and city like Dhaka has population exceeding several millions. It is a cause for great concern that the next great earthquake may occur in this region at any time.

The use of microtremor, an idea pioneered by Kanai et al. (1954) turns into one of the most appealing approaches in the site effects studies, due to its relatively low economic cost and the possibility of recordings without strict spatial or time restrictions (Rodriguez and Midorikawa, 2002). The H/V spectral ratio technique of microtremors gained popularity in the early nineties, after the publication of several papers (Nakamura, 1989; Field and Jacob, 1993; Lermo and Chávez-García, 1994) claiming the ability of this technique to estimate the site response of soft sedimentary deposits satisfactorily. This method is rather attractive in developing countries characterized by a moderate seismicity, where only very limited resources are available for seismic hazard studies. The H/V spectral ratio determined from microtremors has shown a clear peak that is well correlated with the fundamental resonance frequency at “soft” soil sites (Bard, 2004; Horike et al., 2001; Field et al., 1995; Lachet and Bard, 1994; Lermo and Chávez-García, 1993). Comparison of microtremor and earthquake spectral ratios at strong-motion instrument sites across SW British Columbia showed similar fundamental periods and in greater Victoria remarkably similar amplitudes, validating the use of the method for linear earthquake site response Molnar et al. (2007).

Ohmachi et al. (1991) and Lermo and Chávez-García (1994) applied the H/V ratio method to analyze microtremor measurements. Lermo and Chávez-García (1993) used it to assess the empirical function of the S-wave, part of an earthquake record, obtained from three cities in

Mexico. Their results clearly indicated that the H/V ratio could provide a robust estimate of frequency and amplitude of the first resonant mode, albeit not of the higher modes. In the meantime, Field and Jacob (1993) and Field et al. (1995) considered the response of sedimentary layers to ambient seismic noise and claimed that the H/V ratio method has been an effective and reliable tool to identify the fundamental resonance frequencies of all layered sedimentary basin. Further evidence has been given by Suzuki et al. (1995) who used both microtremor and strong-motion data in Hokkaido, Japan and ascertained that the peak frequency determined by the H/V ratio seemed to correspond with the predominant frequency estimated from the thickness of an alluvial layer. Based on numerical calculations, many other researchers (Lermo and Chávez-García, 1993, 1994; Lachet and Bard, 1994; Dravinski et al., 1996) have shown that the H/V ratio method is obviously able to predict fundamental resonant frequency well. Huang et al. (2002) found that the ground vulnerability index (Kg) values in the liquefied areas have been higher than those in the neighboring areas without liquefaction at 42 points in central Taiwan. This study shows supporting evidence for the first time that the H/V ratios of microtremor can be a good alternative indicator for an area's potential for liquefaction. Site amplification characteristics can be evaluated by one-point two-component surface recordings of earthquake ground motion, in a similar manner as proposed by Nakamura for microtremor (Ansary et al., 1996).

For seismic microzonation of Dhaka city, microtremor observation has been carried out at forty five reclaimed and Non-reclaimed area in and around the Dhaka city. Standard Penetration Test (SPT) has been executed at twenty seven locations of these points. Shear Wave velocity has been used to develop soil model. Six PS logging as well as SPT data, which are executed within the study area (CDMP, 2009) and eight Shear Wave Velocity as well as SPT data has been collected (Hossain, 2009). The SPT boring data of BUET campus has also been collected. Empirical SPT correlation developed by Ansary et al. (2010) has been used in this study to convert Field SPT N-value to Shear Wave Velocity. Finally, Soil model has been developed using 1D Response Analysis using the programme SHAKE. Comparison between microtremor and theoretical Transfer Function by the programme SHAKE has been carried out.

For Resonance analysis microtremor observation has been carried out at one hundred and thirty two selected locations within BUET campus and forty five buildings in BUET campus. Finally, seismic damage has been assessed using Nakamura (2000)'s Vulnerability Index.

Although it is not possible to prevent such calamities, it is however, possible to mitigate the impacts of earthquake. Specific roles and responsibilities relating to earthquake hazard should be emphasized in our disaster mitigation plan. Bangladesh is a country characterized by a moderate seismicity with almost no resources available for large scale seismic hazard studies. The objective of this thesis is to analyze seismic hazard in and around Dhaka city in terms of dynamic characteristics of soil (Predominant frequency and Amplification).

1.2 OBJECTIVE OF THE RESEARCH

The main purpose of this research is to estimate the dynamic response of soil using microtremor H/V technique. Dynamic response of soil is very important for the seismic hazard assessment of densely populated urban city like Dhaka. In order to carry out this research specific locations have been selected.

The followings are the specific objectives of the research:

- (i) To examine the effectiveness of using Horizontal to Vertical Spectral Ratio (H/V) of microtremor to estimate predominant frequency and amplification.
- (ii) To develop soil models to obtain transfer function using the computer programme SHAKE.
- (iii) To compare microtremor results with ID response analysis of SHAKE.
- (iv) To justify resonance criterion between soil and structure in the study area.
- (v) To estimate damage of soils using Nakamura's (2000) Vulnerability Index (Kg).

1.3 STUDY AREA AND SITE SELECTION

To check the stability of microtremor observation fourteen locations of West Palashi within BUET campus has been selected. For this purpose, observation has been made at different time instants within a day from morning to midnight. After checking the stability of microtremor data, microtremor observation has been carried out at one hundred and eighteen additional locations within the BUET campus, where latitude varies from 23°43'16.58" N to 23°43'59.44" N and longitude varies from 90°23'13.31"E to 90°23'43.56" E (see Figure 1.1).

To assess the characteristics of soils in the reclaimed and non-reclaimed area in and around the Dhaka city forty five locations have been selected to obtain microtremor observation (See Figure 1.2). These microtremor observation sites are situated at latitude from 23°38'15.10" N to 23°56'46.54" N and longitude from 90°20'24.92" E to 90°33'50" E. Among these forty five locations, at twenty seven locations sub-soil investigation has been carried out. The geology and geomorphology of the study area has been illustrated in section 1.5 of this chapter.

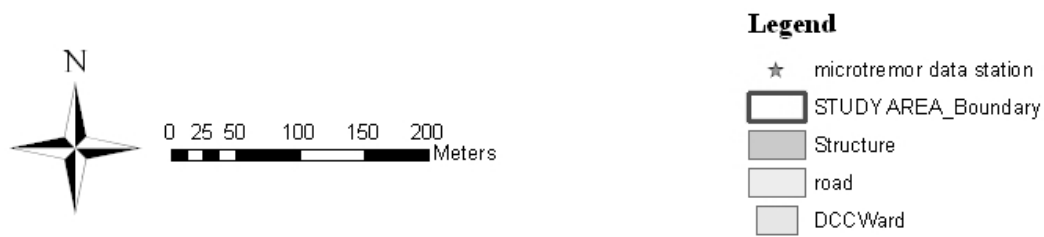
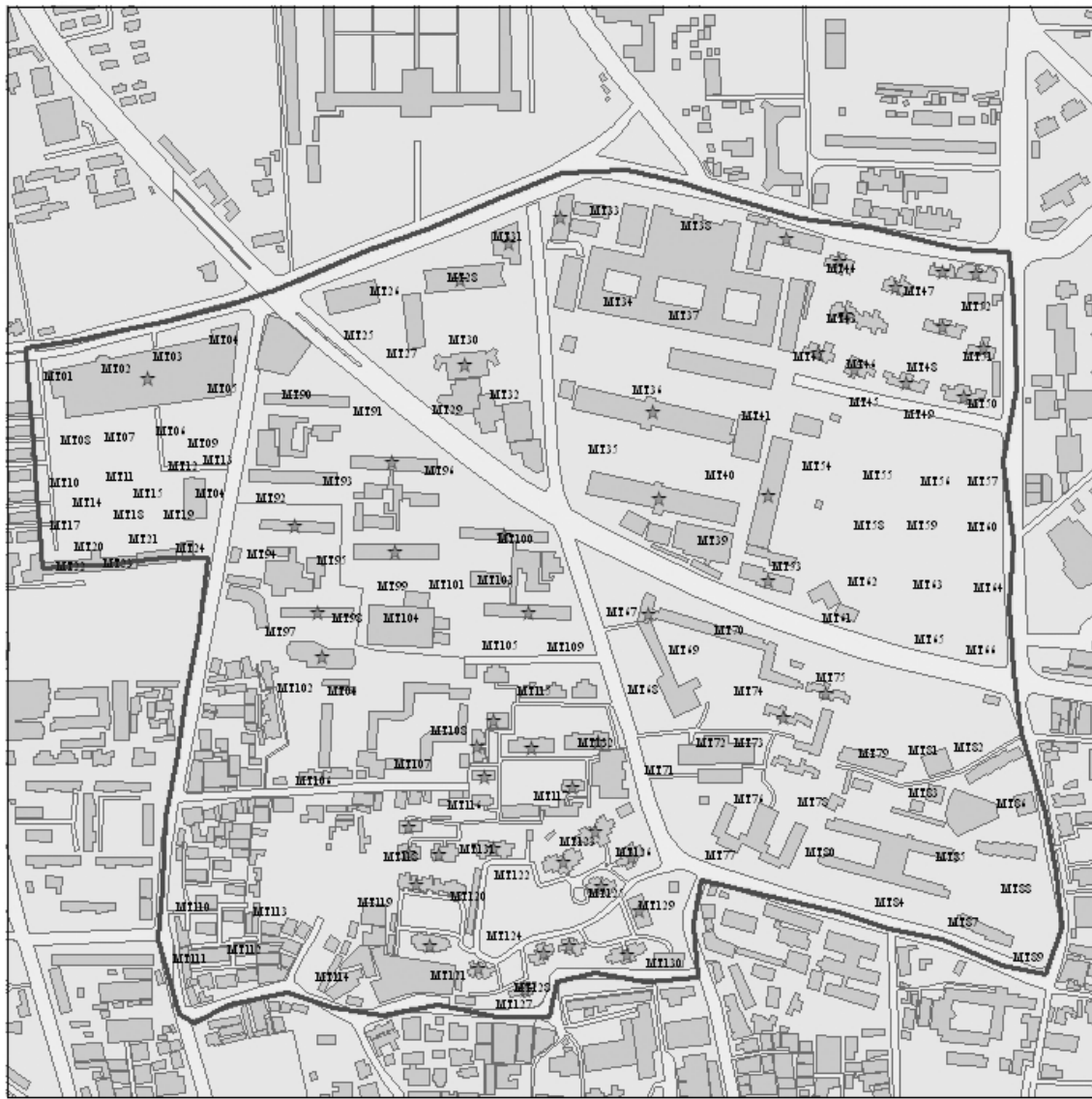


Figure 1.1: One hundred and thirty two microtremor observation in the free field locations of BUET campus.

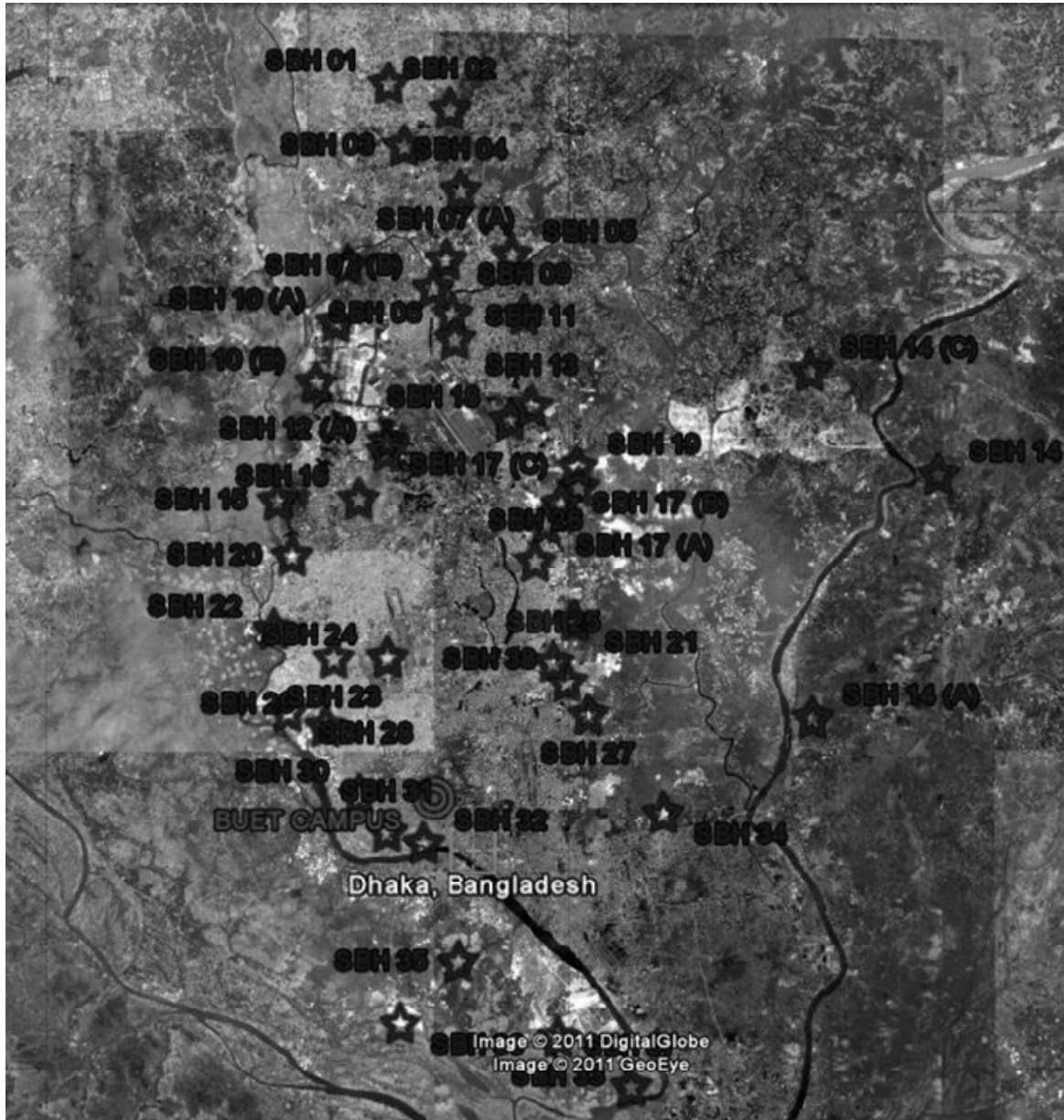


Figure 1.2: Forty five selected locations for microtremor observation in and around the Dhaka city. (Source: Google map)

1.4 OUTLINE OF METHODOLOGY

The amplitude ratio (H/V) of horizontal to vertical spectra of microtremor has become popular to determine predominant period and amplification of a site. It is well known that, degree of damage during earthquakes strongly depends on dynamic characteristics of buildings as well as amplification of seismic waves. Among the other time consuming and expensive approaches, microtremor is the easiest and cheapest way to understand the dynamic characteristics of soil as well as structural element. In a short period of time it provides several information including natural frequency, amplification and vibration characteristics of soil and structure at different frequencies.

Following steps have been followed in this research:

A. Microtremor Analysis

Microtremor observation has been carried out in selected locations of Dhaka city. Each record comprises of three components, viz., EW, NS and UD. For spectral analysis three noise-free segments of 20.48s of the recordings have been taken at 100 Hz instrumental sampling. At each point of sensor location microtremor data recording have been carried out at different time of the day.

Time domain data is not suitable for the clear identification of soil response due to ambient noise. This is why First Fourier Transformation (FFT) has been applied on the time domain records. After smoothing the corresponding spectra, spectral ratio (H/V) technique have been applied to derive transfer functions. The applied sequences are given below:

1. FFT Transformation:

At first, Fourier spectra of the two horizontal directions (East-West and North-South) and the vertical component (Up-Down) have been calculated.

2. Smoothing of the Spectra

After Fast Fourier transformation (FFT), the combined horizontal and vertical spectra have been digitally filtered applying a logarithmic window with a suitable bandwidth coefficient. These filtering techniques have been applied to reduce the distortion of peak amplitudes.

3. Calculation of the Soil Response functions:

The smoothed combined horizontal spectrum have been divided with the smoothed vertical component to plot Horizontal to vertical spectral ratio (H/V) which will provide the desired predominant frequency and corresponding amplification factor of the investigated portions (20.48 s) of records.

4. Estimation of Predominant Frequency and Amplification:

After calculating three sets of the H/V ratios at selected grid, they have been normalized to obtain a relatively non-biased site specific H/V ratio. Then, Normalized H/V ratios at different time of the day have been plotted in Logarithmic window. From this normalized H/V ratio the predominant frequency and corresponding amplification factor of this site have been taken.

B. Soil Investigation

Twenty seven Standard Penetration Test (SPT) have been carried out for subsoil investigations at study locations. Empirical soil correlation has been used to convert SPT N-value to Shear Wave Velocity.

C. Develop Soil Model for Site Response Analysis

Soil model of investigated locations have been developed using the program SHAKE.

D. Comparison between Theoretical Transfer Function with Microtremor H/V ratio

Theoretical transfer function obtained from one dimensional soil response analysis using the programme SHAKE has been compared with microtremor H/V ratio. This output data have been used for estimation of predominant frequency and site amplification.

The brief methodology of this research has been shown through a flowchart in Figure 1.3.

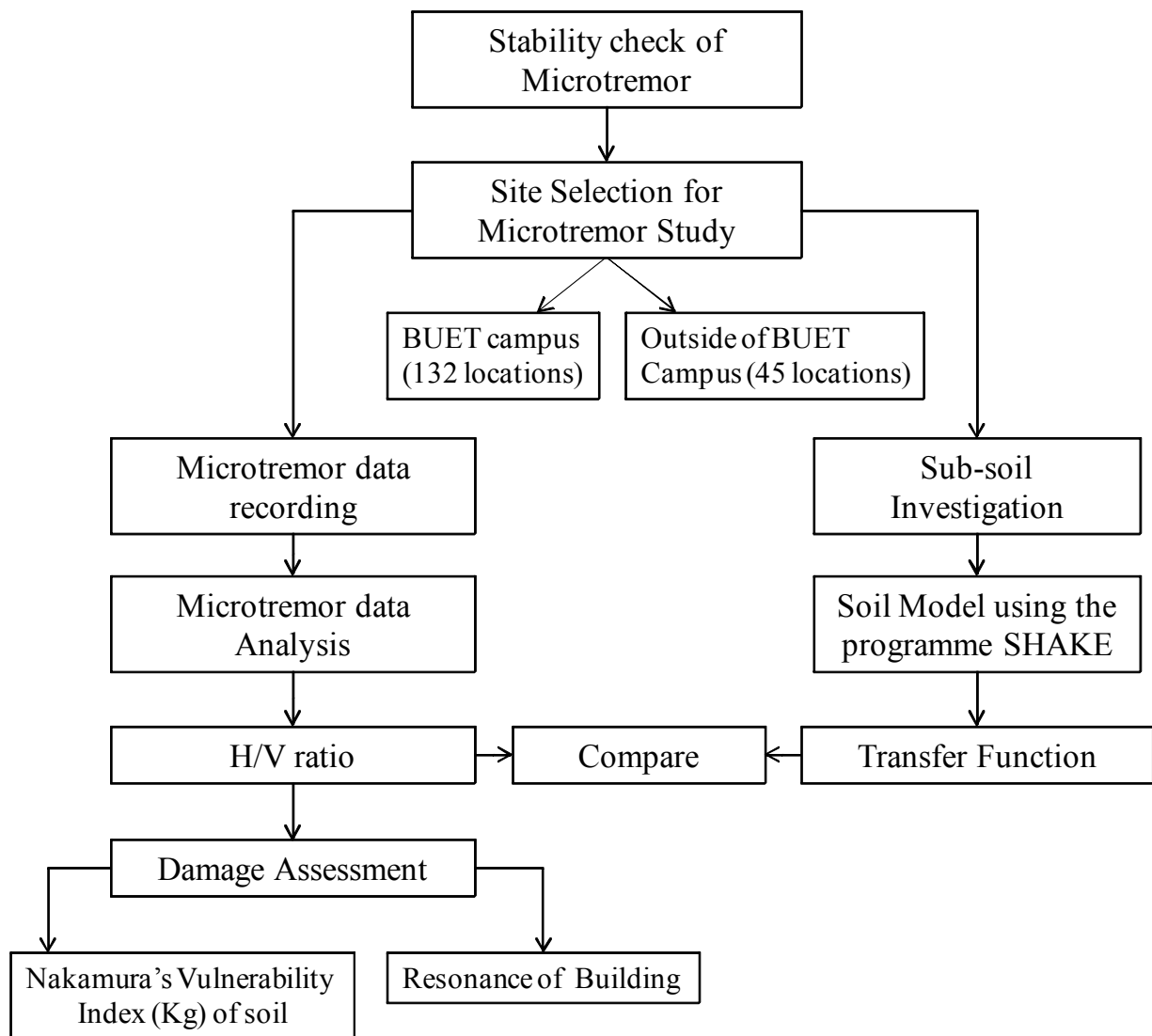


Figure 1.3: Flow chart for Microtremor Research in the Dhaka city.

The whole research has been carried out in the following phases according to Figure 1.3.:

- a. Stability of microtremor data has been carried out at fourteen different locations in different time instants from morning to midnight within a day. Time domain data has been converted to frequency domain data because time domain data do not show dynamic properties of soil. So, Fourier transformation of three segments of 20.48 s long time history data along EW, NS and UD of these locations has been carried out. Then, the stability of Fourier spectra data has been checked at different time instants. Fourier spectra data do not show the amplification and stable data for site response. Therefore, Horizontal to Vertical spectral ratio data

has been calculated from these Fourier spectra data. The mean H/V spectra data with half standard deviation with mean have been calculated and shown in logarithmic window. Stability of H/V ratio data at fourteen locations has been compared. H/V ratios are more stable than Fourier spectra data. From this conclusion, the analysis of Horizontal to Vertical spectra ratio (H/V) has been applied for microtremor data analysis.

- b. For details study of microtremor observations, one hundred and thirty two points have been selected within BUET campus from morning to midnight. These data are located in the same geological units. However, from the analysis of these data, most of the locations did not show significant amplification due to the presence of stiff soil within BUET campus. For this reason, forty five locations outside BUET have been selected. These locations include both reclaimed and non-reclaimed areas of Dhaka city.
- c. For the assessment of soil response of reclaimed and non-reclaimed sites outside the BUET campus microtremor observation has been conducted at forty five locations in and around the Dhaka city in consideration of different geological units. Microtremor observation has been carried out about ten geomorphic units (According to Figure 2.2) and nine geomorphic units (According to Figure 2.3).
- d. Field investigations include 27 (Twenty seven) boreholes up to a depth of 20 m out of 45 locations outside BUET. For another 15 locations SPT-N value data have been collected from other sources. PS-loggings at 6 locations and SSMM data at 8 locations for Shear Wave Velocity exist among these locations.
- e. Soil model has been developed at 42 locations out of 45. Among these locations, for 14 locations, shear-wave data have been directly obtained from the field. For rest 28 locations, empirical soil correlations developed by Ansary et al. (2010) and other empirical correlations (After TC4, ISSMFE, 1993) have been used to convert SPT-N value to shear-wave velocity.
- f. Microtremor H/V ratio has been compared with the transfer function obtained from 1D soil response analysis at 42 locations.
- g. Microtremor observation at forty five buildings in the BUET campus have already been carried out. The predominant frequency of these observed building

and adjacent soil obtained in this study has been compared to establish the resonance criteria.

- h. For the damage assessment of soils at the observed locations Nakamura's (2000) Vulnerability Index (Kg) has been used.

DATA COLLECTION AND ANALYSIS

2.1 GENERAL

Damage in recent earthquakes showed that local site conditions have a significant effect on ground motion. Site response studies play an important role in seismic microzonation studies. The application of microtremor is to determine dynamic characteristics (predominant frequency and amplification factor). Nowadays microtremor measurements are generalized in site characterization due to their simplicity, low cost and minimal disturbance to other activities.

In the traditional spectral ratio method, H_S/H_r , site and source effects are estimated from observation at a reference site. In practice, adequate reference site are not always available especially in flat areas where exposed rock is not available. Therefore, methods have been developed that do not need reference sites (Bard 1994). Several recent applications of this technique have proved to be effective in estimating predominant frequency (Field and Jacob 1973; Ohmachi et al. 1994) and amplification factors (Lermo and Chavez-Garcia 1994; Konno and Ohmachi 1995). The reality of microtremor H/V technique for site response analysis has been discussed in Chapter 2.

Several methods have been proposed for spectral calculation of ground motions including microtremor. Fourier spectrum is the most convenient one that is used widely. Some investigations showed that different methods give similar results (Dimitriu et al. 1998). However some researchers declare that a suitable spectral method gives more reliable results (Ghayamghamian and Kawakami 1997). That's why three segments of spectra have been selected to compute the mean segmental cross spectra. Standard deviation of mean has also been calculated to show the deviation of mean value from six spectra in East-West and North-South direction. Subsoil investigation has also been executed in the test location to compute the Shear Wave Velocity which has been used in 1D response analysis using the programme SHAKE.

2.2 LOCATION OF INVESTIGATED SITES WITHIN THE STUDY AREA

2.2.1 Geological and Geomorphological classification

Local site conditions substantially affect the characteristics of seismic waves during earthquakes. Soft alluvial deposits tend to amplify certain frequencies of ground motion and extend the duration of motion which may cause further earthquake damage. The expected variation in the ground motion, according to the geological site conditions, make it necessary to perform a more detailed seismic hazard assessment for a metropolitan area. To accurately identify the variation of seismic hazards at different locations within the metropolis, one may conduct seismic microzonation that requires subdividing an area into zones with respect to the geological characteristics of the sites.

Therefore, microtremor measurement at 45 selected locations in and around Dhaka city as well as 132 locations within BUET campus has been executed in consideration of diversified geological and geomorphological units. Most of the locations in and around Dhaka city are situated in various geomorphological units. But, all of the selected points in BUET campus are located in the same geological and geomorphological unit. 45 selected locations have been shown in Figure 2.1.

Two geomorphological maps of Dhaka city from different source are shown in Figure 2.2 and Figure 2.3. Microtremor measurements points have been superimposed in these two geomorphological maps. Some locations are situated out of the geomorphological map in Figure 2.2 and Figure 2.3. The geomorphological classifications of these locations have been presented in Table 2.1. Table 2.1 represents 45 test locations, their ID, latitude, longitude and geomorphological classification according to Figure 2.2 and Figure 2.3. The test locations have been classified in different geomorphological unit. Figure 2.2 has been divided by 15 geomorphological units. On the other hand, Figure 2.3 has been divided by 22 geomorphological units. 132 selected locations of BUET campus in Figure 2.55 has been classified as Upper Modhupur Terrace according to Figure 2.2 and Higher Pleistocene Terrace according to Figure 2.3.

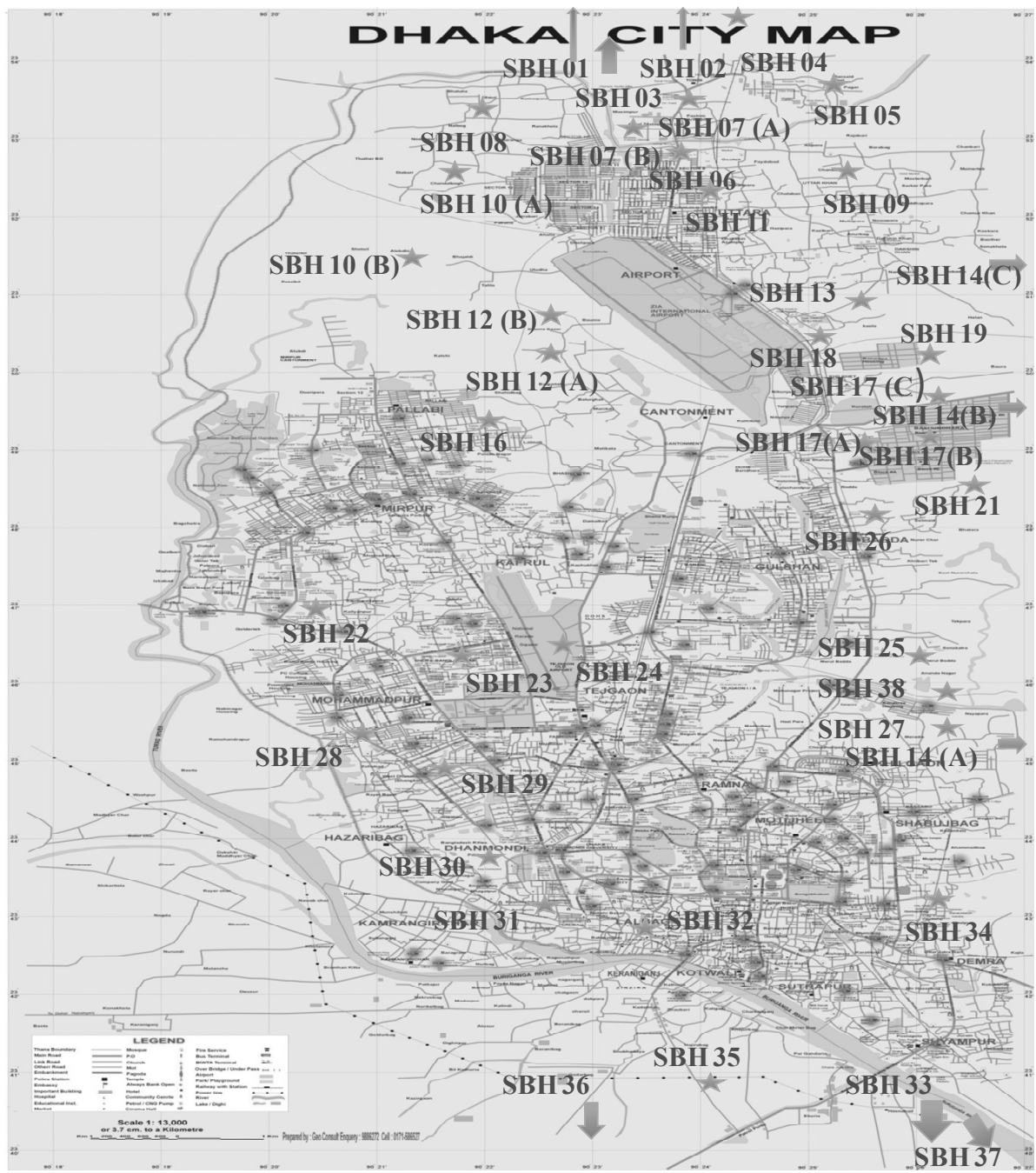


Figure 2.1: Microtremor observation at forty five selected locations in and around Dhaka City.

From Table 2.1, 45 selected locations are situated in 10 different geomorphic units according to Figure 2.2. On the other hand, same 45 locations are located in 9 different geomorphic units according to Figure 2.3. Most of the points in Table 2.1 have been selected on the basis of recent filling. But, there is no specific classification of geomorphological unit of filling area in Figure 2.2. However, Figure 2.3 shows specific geomorphic unit of recent filling. So, both Figure 2.2 and Figure 2.3 have been justified to classify 45 sites in different geomorphic units.

Table 2.1: Geological and Geomorphological classification of the study area

SL. No.	ID	Location	Latitude	Longitude	Geomorphological Classification	
					After Figure 2.2	After Figure 2.3
1	SBH-01	National University	23°56'46.54"	90°22'43.93"	Upper Modhupur Terrace	High Pleistocene terrace
2	SBH-02	Board Bazaar, Gazipur	23°56'18"	90°23'58"	Upper Modhupur Terrace	Moderately High Pleistocene terrace
3	SBH-03	Kaunia, Boro Bari, Moddopara	23°55'37"	90°23'03"	Shallow Alluvium Gully	Moderately High Pleistocene terrace
4	SBH-04	Tongi, Ershadnagar	23°54'48"	90°24'11"	Lower Modhupur Terrace	Moderately High Pleistocene terrace
5	SBH-05	Tongi BSCIC area	23°53'37.18"	90°25'13.35"	Lower Modhupur Terrace	Thick fill
6	SBH-06	Abdullahpur	23°52'31"	90°24'01"	Deep Alluvium Gully	Highly Erosional Lower Pleistocene terrace
7	SBH-07(A)	Ijtema field (North and East side)	23°53'31.13"	90°23'53.39"	Shallow Alluvium Gully	Deep alluvial valley
8	SBH-07 (B)	Ijtema Field (South and West side)	23°52'59.96"	90°23'37.91"	Shallow Alluvium Gully	Deep alluvial valley
9	SBH-08	Ashulia Toll Plaza	23°53'25.40"	90°21'54.61"	Deep Marshly Land	Deep marshly land

SL. No.	ID	Location	Latitude	Longitude	Geomorphological Classification	
					After Figure 2.2	After Figure 2.3
10	SBH-9	Uttar Khan	23°52'30"	90°25'28"	Lower Modhupur Terrace	Highly Erosional Lower Pleistocene terrace
11	SBH-10(A)	Uttara Phase 3 (North side)	23°52'22"	90°21'40"	Deep Marshly Land	Moderately thick fill
12	SBH-10(B)	Uttara Phase 3 (South side)	23°51'15"	90°21'16"	Deep Marshly Land	Moderately thick fill
13	SBH-11	Azampur School, Uttara	23°52'03"	90°24'04"	Upper Modhupur terrace	Moderately High Pleistocene terrace
14	SBH-12 (A)	Mirpur DOHS (South side)	23°49'59"	90°22'42"	Upper Modhupur terrace	High Pleistocene terrace
15	SBH-12 (B)	Mirpur DOHS (North side)	23°50'11"	90°22'42"	Upper Modhupur terrace	High Pleistocene terrace
16	SBH-13	Ashiyani city, Askona, Dakkhin Khan	23°50'49"	90°25'37"	Swamp/Depression	Moderately Thick fill
17	SBH-14(A)	Purbachal-1, Randokpur Hazi bari, Rupganj	23°45'03"	90°31'17"	Lower Modhupur Terrace	Thick fill
18	SBH-14(B)	Purbachal-2, American City	23°49'33"	90°33'50"	Lower Modhupur Terrace	Thick fill
19	SBH-14(C)	Purbachal Picnic Park, Gazipur	23°51'28"	90°31'14"	Lower Modhupur Terrace	Thick fill
20	SBH-15	Adjacent to Mirpur Zoo	23°49'04.14"	90°20'29.63"	Natural levee	Thick fill
21	SBH-16	Field Ground, Pallabi	23°49'06"	90°22'08"	Upper Modhupur terrace	Thick fill
22	SBH-17 (A)	Block-B, Basundhara	23°48'38"	90°25'54"	Lower Modhupur Terrace	Moderately High Pleistocene terrace
23	SBH-17 (B)	Block-D, Basundhara	23°49'00.49"	90°26'12.95"	Back swamp	Moderately High Pleistocene terrace

SL. No.	ID	Location	Latitude	Longitude	Geomorphological Classification	
					After Figure 2.2	After Figure 2.3
24	SBH-17 (C)	Block-H, Basundhara	23°49'19"	90°26'34"	Back swamp	Moderately High Pleistocene terrace
25	SBH-18	Civil Aviation Quarter	23°50'33.61"	90°25'11.22"	Upper Modhupur terrace	Higher Pleistocene terrace
26	SBH-19	Kuril Flyover	23°49'41.51"	90°26'32.06"	Swamp/Depression	Thick fill
27	SBH-20	Sarengbari, Mipur-2	23°48'03.24"	90°20'47.10"	Swamp/Depression	Deep marshly land
28	SBH -21	Purachal, Uttar Badda	23°46'51"	90°26'29"	Back swamp	Deep marshly land
29	SBH-22	City Corporation, Gabtoli	23°46'41.99"	90°20'24.92"	Flood plain	Moderately thick fill
30	SBH-23	Adabor	23°46'09.75"	90°21'37.62"	Shallow alluvium Gully	Moderately thick fill
31	SBH-24	Agargoan Trade Fair area	23°46'10.56"	90°22'42.73"	Upper Modhupur Terrace	Higher Pleistocene terrace
32	SBH-25	Aftab Nagar Housing Project	23°46'04.98"	90°26'03.22"	Flood plain	Thick fill
33	SBH-26	Umme Had Nagar, Nadda	23°47'57.17"	90°25'41.61"	Swamp/Depression	Moderately thick fill
34	SBH-27	South Banasree	23°45'07.17"	90°26'45.36"	Flood plain	Thick fill
35	SBH-28	Basila Garden City	23°45'10.29"	90°20'42.36"	Back Swamp	Thick fill
36	SBH-29	Royer Bazar Boddhobumi	23°44'54"	90°21'28"	River Bar	Gently sloping Erosional terrace edge
37	SBH-30	Kalunagar, Hazaribagh	23°43'38.50"	90°22'08.62"	River Bar	Thick fill
38	SBH-31	Rab-10, Plot, Kamrangirchar	23°42'57.58"	90°22'42.11"	River Bar	Moderately thick fill
39	SBH-32	Sosan Ghat, Kamrangirchar	23°42'44.81"	90°23'26.51"	Natural levee	Deep Marshly land
40	SBH-33	Basundhara River view	23°39'10"	90°26'09"	Flood plain	Moderately Thick fill
41	SBH-34	Matuail, Demra	23°43'18.24"	90°28'16.48"	Swamp/Depression	Younger active floodplain
42	SBH-35	Jilmil Project, Euria	23°40'33.40"	90°24'08.42"	Shallow alluvium Gully	Thick fill
43	SBH-36	Rajendapur	23°39'25"	90°22'58"	Deep alluvium Gully	Thick fill

SL. No.	ID	Location	Latitude	Longitude	Geomorphological Classification	
					After Figure 2.2	After Figure 2.3
44	SBH-37	Bramangaon	23°38'15.10"	90°27'37.35"	Flood plain	Deep alluvial valley
45	SBH-38	Meradia, Uttar Banasree	23°45'43.57"	90°26'19.67"	Flood plain	Thick fill

According to Figure 2.2, 45 selected locations have been classified into following groups: 8-Upper Modhupur Terrace [SBH 01; SBH 02; SBH 11; SBH 12(A); SBH 12(B); SBH 16; SBH 18 ; SBH 24], 5-Shallow Alluvium Gully [SBH 03; SBH 07(A); SBH 07(B); SBH 23; SBH 35], 7-Lower Modhupur Terrace [SBH 04; SBH 05; SBH 09; SBH 14(A); SBH 14(B); SBH 14(C); 17(A)], 2-Deep Alluvium Gully (SBH 06; SBH 3), 3-Deep Marshly Land [SBH 08; SBH 10(A); SBH 10(B)], 5-Swamp/Depression (SBH 13; SBH 19; SBH 20; SBH 26; SBH 34), 2-Natural Levee (SBH15; SBH 32), 4-Back Swamp [SBH (B); SBH 17(C); SBH 21; SBH 28], 6-Flood Plain (SBH 22; SBH 25; SBH 27; SBH 33; SBH 37; SBH 8) and 3- River Bar (SBH 29; SBH 30; SBH 31).

The common geomorphic unit is Deeply Marshly Land, which is found at SBH 8 (Ashulia Toll Plaza, Latitude-23°53'25.40" and Longitude- 90°21'54.61") in both Figure 2.2 and Figure 2.3. Out of 45 selected locations, 8 selected locations have been classified into Upper Modhupur Terrace geomorphological unit, which is the most predominant geomorphological unit in Figure 2.2. The second most common geomorphological unit is Lower Modhupur Terrace. However, it is not possible to classify filling area because of not having any geomorphological unit in Figure 2.2. Therefore, Figure 2.3 is required to justify these locations in actual geomorphic unit.

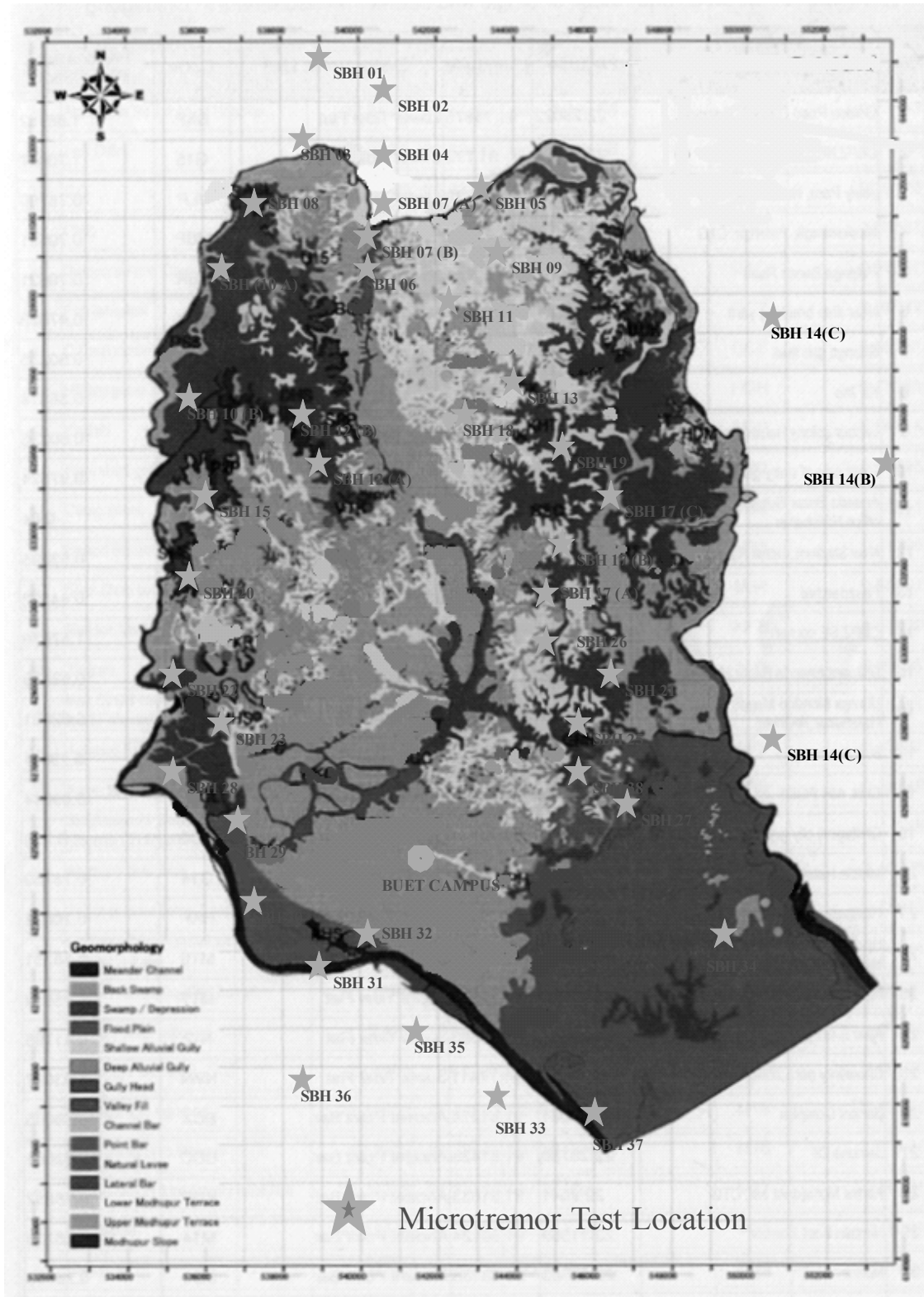


Figure 2.2: Superimposed study points on geomorphological map of Dhaka city. (Source: Geological Survey of Bangladesh, GSB)

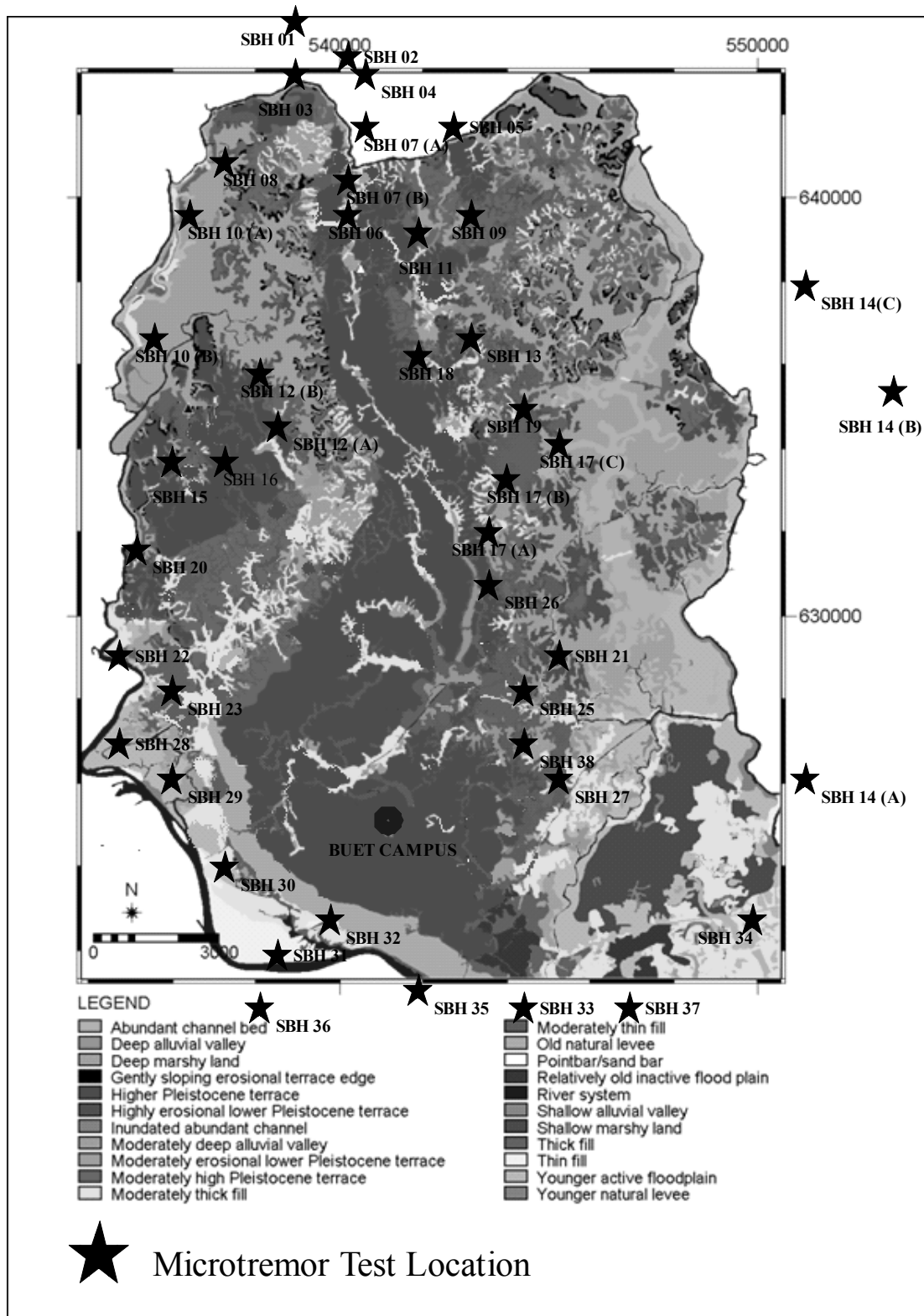


Figure 2.3: Superimposed study points on Geomorphological Map of Dhaka City.

(Source: A. S. M. Maksud Kamal)

According to Figure 2.3, 45 selected locations are classified into following groups:

14-Thick fill [SBH 05; SBH 14(A); SBH 14(B); SBH 14(C); SBH 15; SBH 16; SBH 19; SBH 25; SBH 27; SBH 28; SBH 30; SBH 35; SBH 36; SBH 38], 8-Moderately Thick fill [SBH 10(A); SBH 10 (B); SBH 13; SBH 22; SBH 23; SBH 26; SBH 31; SBH 33], 5-Higher Pleistocene Terrace [SBH 01; SBH 12(A); SBH 12(B); SBH 18; SBH 24], 7-Moderately Higher Pleistocene terrace [SBH 02; SBH 03; SBH 04; SBH 11; SBH 17(A); SBH 17(B); SBH 17(C)], 3-deep alluvium valley [07(A); 07(B); SBH 37], 4-Deep Marshly Land (SBH 08; SBH 20; SBH 21; SBH 32), 2-Highly Erosional Lower Pleistocene Terrace (SBH 06; SBH 09), 1-Younger active flood plain (SBH 34) and 1-Gently Sloping Erosional Terrace (SBH 29).

Out of 45 sites, the most predominant geomorphological unit is Thick fill, which is found in 14 locations in Figure 2.3. The second most common geomorphological unit is moderately thick fill. The geomorphological unit of Moderately Higher Pleistocene Terrace, which is 7, is higher than Higher Pleistocene Terrace.

Therefore, it can be said that the majority of the microtremor test locations are situated in recent fill area.

2.2.2 Sub-Soil Characteristics

Sub-soil investigation is necessary for the analysis of dynamic characteristics of soil. Shear wave velocity (SWV) is used to develop soil model. For this study Standard Penetration Test (SPT) has been carried out at 27 locations in and around the Dhaka city. SPT data has been collected from other sources as well. SPT is conducted in the area following procedure described in ASTM D1586. Shear wave velocity from 6 PS loggings as well as SPT data has been collected (CDMP, 2009). SWV from Small Scale Microtremor Measurement (SSMM) as well as SPT data has been collected at the microtremor Test location (Hossain, 2009). Finally, SWV has been estimated using SPT and SWV correlation (Ansary et al., 2010) where there is no SWV test result. The other three soil correlations (Ohta and Goto 1978; Imai and Yoshimura 1970; Ohba and

Toriumi 1970) have been used to compare SWV. Various sub-soil investigation results have been presented in this section and Appendix-A.

(1) Sub-Soil Characteristics of National University, Tongi (SBH 01)

SPT Results

The soil profiles of the borehole are shown in Table A3.1. From the disturbed soil sample, the borehole consists of two soil layers. The silty clay layer, which is light brown medium stiff and high plastic, varies from 0 to 5.0 m from EGL. On the other hand, the silty clay layer, which is light brown to brown stiff to very stiff, exists from 5 to 18.5 m from EGL. The uncorrected SPT N-value of this site varies from 4 to 19. The SPT-N value of medium stiff light brown silty clay varies from 4 to 7. The SPT N-value of stiff to very stiff light brown to brown silty clay layer varies between 7 and 19.

Shear Wave Velocity Results

There is no PS logging and SSMM test result in National University, Tongi. Therefore, shear wave velocity has been estimated using correlation. Table A3.1 shows estimated SWV using different soil correlation. According to soil correlation proposed by Ansary et al. (2010), the shear wave velocity varies from 135 to 229 m/sec. From soil correlation developed by Ohta and Goto (1978), SWV exists from 123 to 261 m/sec. On the other hand, SWV of Ohba and Toriumi (1970), which varies from 129 to 206 m/sec, shows slightly higher value than Imai and Yoshimura (1970), which shows ranging between 120 and 201 m/sec.

(2) Sub-Soil Characteristics of Board Bazaar, Gazipur (SBH 02)

SPT Results

The soil profiles of the borehole are shown in Table A2.2. The borehole consists of four soil layer. The silty clay layer, which is soft light brown and high plastic, varies from 0 to 2.50 m from EGL. The silty clay of stiff light brown with high plastic exists from 2.5 to 8.5 m from EGL. The medium dense brown silty fine sand varies from 8.5 to 10.0 m. The stiff to very stiff light brown silty clay varies between 10 and 20 m. The uncorrected SPT N-value of this site varies from 3 to 18. The SPT-N value of stiff light brown silty clay varies from 5 to 9. The SPT N-value of stiff to very stiff light brown to brown silty clay varies from 15 to 18.

Shear Wave Velocity Results

There is no PS logging and SSMM test result in Board Bazaar, Gazipur. Therefore, shear wave velocity has been estimated using soil correlation. Table A2.2 presents SWV using

different methods. From soil correlation proposed by Ansary et al (2010), SWV varies from 150 to 247 m/sec. From SPT correlation developed by Ohta and Goto (1978), SWV exists from 117 to 267 m/sec.

(3) Sub-Soil Characteristics of Kaunia, Boro Bari, Moddopara (SBH 03)

SPT Results

The soil profiles of the borehole are shown in Table A2.3. The borehole consists of five soil layers. The grey loose silty fine sand varies from 0 to 2.0 m from EGL. The stiff to very stiff light brown Silty Clay with trace fine sand high plastic exists from 5.5 to 15.5 m from EGL. The medium dense brown silty fine sand varies from 8.5 to 10.0 m. The very stiff brown clayey silt with fine sand med. compress varies between 15.5 to 18.5 m. The uncorrected SPT N-value of this site varies from 4 to 28. The SPT-N value of stiff to very stiff light brown silty clay with trace fine sand high plastic varies between 8 and 18. The SPT N-value of very stiff brown clayey silt with fine sand medium compress layer exists between 18 and 24.

Shear Wave Velocity Results

There is no PS logging and SSMM test result in Kaunia, Boro Bari. So, the value of shear wave velocity has been estimated using soil correlation. Table A2.3 presents SWV using different methods. From soil correlation proposed by Ansary et al. (2010), the shear wave velocity varies from 135 to 261 m/sec. From SPT correlation developed by Ohta and Goto (1978), SWV exists between 103 and 237 m/sec.

(4) Sub-soil Characteristics of Tongi, Ershadnagar (SBH 04)

SPT Results

The soil profile of the borehole has been demonstrated in Table A2.4. The borehole consists of six soil layers. The medium stiff to stiff light brown silty Clay with trace grits and fine sand high plastic varies from 0 to 3.5 m from EGL. The medium dense to loose brown sandy silt with trace mica exists from 6.5 to 9.5 m from EGL. The medium dense brown silty fine sand with trace mica varies from 8.5 to 10.0 m. The stiff grey to light brown silty clay with fine sand high plastic varies between 12.5 to 17.0 m. The uncorrected SPT N-value of this site varies from 6 to 17. The SPT N-value of stiff to medium stiff light brown silty clay varies between 2 and 11. The SPT N-value of medium

dense brown silty fine sand layer exists from 9 to 12. The SPT N-value of stiff grey to light brown silty clay varies between 10 and 12.

Shear Wave Velocity Results

Table A2.4 represents shear wave velocity using four different methods. From soil correlation proposed by Ansary et al. (2010), SWV varies from 182 to 221 m/sec. From SPT correlation developed by Ohta and Goto (1978), SWV exists from 132 to 244 m/sec. On the other hand, SWV of Ohba and Toriumi (1970), which varies from 146 to 202 m/sec, shows slightly higher value than Imai and Yoshimura (1970), which shows ranging between 137 to 194 m/sec.

(5) Sub-Soil Characteristics of Tongi BSCIC area (SBH 05)

SPT Results

The soil profile of the borehole has been shown in Table A2.5. The borehole consists of six soil layers. The grey loose silty Fine Sand with trace mica varies from 0 to 3.5 m from EGL. The soft dark grey silty clay with trace organic matter exists from 3.5 to 6.5 m from EGL. The medium stiff to stiff light brown to grey silty clay trace fine sand varies from 6.5 to 9.5 m. The medium dense brown silty fine sand with trace clay varies between 12.5 to 15.5 m. The uncorrected SPT N-value of this site varies from 4 to 37. The SPT N-value of soft dark grey silty clay varies from 4 to 5. The SPT N-value of medium dense brown silty fine sand varies from 13 to 20. The SPT N-value of medium dense to dense grey silty fine sand varies between 20 and 37.

Shear Wave Velocity Results

Table A2.5 represents shear wave velocity using four different methods. From soil correlation proposed by Ansary et al. (2010), SWV varies from 135 to 287 m/sec. From SPT correlation developed by Ohta and Goto (1978), SWV exists from 103 to 253 m/sec. On the other hand, SWV of Ohba and Toriumi (1970), which varies from 129 to 257 m/sec, shows slightly higher value than Imai and Yoshimura (1970), which shows ranging between 120 to 250 m/sec.

(6) Sub-Soil Characteristics of Abdullahpur (SBH 06)

SPT Results

The soil profile of the borehole is presented in Table A2.6. The borehole consists of four soil layers. The top layer of soil exist rubbish which varies from 0 to 2 m. The stiff reddish brown silty clay trace grits and fine sand high plastic exists from 2 to 5 m from

EGL. The stiff brown silty clay trace fine sand high plastic varies from 5 to 8 m. The medium dense to very dense brown silty clay trace mica varies between 8 and 20 m. The uncorrected SPT N-value of this site varies from 11 to 50. The SPT-N value of stiff reddish brown silty clay varies from 5 to 12. The SPT N-value of medium dense to very dense brown silty clay varies between 10 and 50.

Shear Wave Velocity Results

Table A2.6 represents shear wave velocity using four soil correlations. SWV varies from 122 to 318 m/sec (Ansary et al., 2010). SWV exists between 90 and 266 m/sec (Ohta and Goto, 1978). On the other hand, SWV of Ohba and Toriumi (1970), which varies from 118 to 282 m/sec, shows slightly higher value than Imai and Yoshimura (1970), which shows ranging between 109 to 276 m/sec.

(7) Sub-Soil Characteristics of Ijtema Field (SBH 07 (A))

SPT Results

The soil profile of the borehole is shown in Table A2.7. The borehole consists of four soil layers. The top layer of soil exist medium stiff to stiff light brown silty clay which varies from 0 to 5 m. The medium dense to dense brown silty fine sand trace clay varies between 8 and 20 m. The uncorrected SPT N-value of this site varies from 5 to 45. The SPT-N value of medium stiff to stiff light brown silty clay varies from 5 to 11. The SPT N-value of medium dense to dense brown silty fine sand varies from 17 to 45.

Shear Wave Velocity Results

Table A2.7 represents shear wave velocity using four different methods. SWV varies from 172 to 307 m/sec (Ansary et al., 2010). SWV exists between 128 and 262 m/sec (Ohta and Goto, 1978). On the other hand, SWV of Ohba and Toriumi (1970), which varies from 138 to 273 m/sec, shows slightly higher value than Imai and Yoshimura (1970), which shows ranging between 129 to 267 m/sec.

(8) Sub-Soil Characteristics of Ashulia Toll Plaza (SBH 08)

SPT Results

The soil profile of the borehole is shown in Table A2.8. The borehole consists of four soil layers. The top layer of soil exists filling grey very loose silty fine sand which varies from 0 to 2 m. The medium dense to dense reddish brown to brown silty fine sand varies between 5 and 20 m. The uncorrected SPT N-value of this site varies from 1 to 40. The SPT-N value of medium dense to dense reddish brown to brown silty fine sand varies between 5 and 39.

Shear Wave Velocity Results

Table A2.8 represents shear wave velocity using four different methods. SWV varies from 84 to 295 m/sec (Ansary et al., 2010). SWV exists between 82 and 256 m/sec (Ohta and Goto, 1978). On the other hand, SWV of Ohba and Toriumi (1970), which varies from 84 to 264 m/sec, shows slightly higher value than Imai and Yoshimura (1970), which shows ranging between 76 and 257 m/sec.

(9) Sub-Soil Characteristics of Uttar Khan (SBH 9)

SPT Results

The soil profiles of the borehole are shown in Table 2.2. The only thick clay layer exists in this borehole. The thick clay layer exists from 0 to 24 m. The SPT N-value of clay layer varies between 14 and 74.

Table 2.2: SPT-N and Shear Wave Velocity at Uttar Khan

Depth (m)	Soil Description	SPT-N Value	Shear wave velocity (m/s) from PS-logging				
			CDMP (2009)	Ansary et al. (2010)	Ohta and Goto (1978)	Imai and Yoshimura (1970)	Ohba and Toriumi (1970)
1.5	Clay	20	412	254	162	204	213
3.0	Clay	45	412	319	213	267	273
4.5	Clay	50	412	329	236	276	282
6.0	Clay	40	412	309	240	257	264
7.5	Clay	62	292	349	271	297	302
9.0	Clay	30	292	285	248	233	241
10.5	Clay	14	292	230	225	182	190
12.0	Clay	22	292	261	249	211	219
13.5	Clay	22	292	261	255	211	219
15.0	Clay	24	292	268	265	217	225
16.5	Clay	28	292	279	277	228	236
18.0	Clay	24	292	268	274	217	225
19.5	Clay	24	292	268	279	217	225
21.0	Clay	38	292	304	306	252	259
22.5	Clay	74	292	367	348	315	319
24.0	Clay	44	292	317	322	265	271

Shear Wave Velocity Results

Table 2.2 represents shear wave velocity by direct PS logging (CDMP, 2009) and four soil correlations. According to PS logging, SWV varies from 292 to 412. From soil correlation proposed by Ansary et al (2010), SWV varies between 254 and 349 m/sec. SWV exists from 162 to 348 m/sec (Ohta and Goto, 1978). On the other hand, SWV of

Ohba and Toriumi (1970), which varies from 190 to 319 m/sec, shows slightly higher value than Imai and Yoshimura (1970), which shows ranging between 182 to 315 m/sec.

(10) Sub-Soil Characteristics of Uttara Phase-3 (SBH 10 (A))

SPT Results

The soil profile of the borehole is represented in Table A2.9. The borehole consists of five soil layers. The top layer of soil exists filling grey very loose silty fine sand which varies from 0 to 3.5 m. The stiff grey silty clay trace fine sand varies between 3.5 to 8 m. The loose to medium dense grey sandy silt with clay varies between 9.5 and 17 m. The uncorrected SPT N-value of this site varies from 2 to 18. The SPT N-value of the stiff grey silty clay varies from 3 to 13. The SPT N-value of loose to medium dense grey sandy silt varies between 9 and 15.

Shear Wave Velocity Results

Table A2.9 represents shear wave velocity using four different methods. SWV varies from 107 to 225 m/sec (Ansary et al, 2010). From SPT correlation developed by Ohta and Goto (1978), SWV exists between 96 and 197 m/sec. On the other hand, SWV of Ohba and Toriumi (1970), which varies from 104 to 206 m/sec, shows slightly higher value than Imai and Yoshimura (1970), which shows ranging between 96 and 197 m/sec.

(11) Sub-Soil Characteristics of Azampur School, Uttara (SBH 11)

SPT Results

The soil profile of the borehole is shown in Table 2.3. This borehole exist three soil layers. The top layer exists clay from 0 to 6 m. The sandy silt layer varies between 6 and 13.5 m. The lower clay layer varies between 13.5 and 20. The uncorrected SPT N-value of this site varies from 12 to 20. The SPT N-value of the uppermost clay layer varies from 12 to 20. The SPT N-value of silty clay layer varies from 12 to 18. The SPT N-value of the bottom clay layer varies between 13 and 20.

Table 2.3: SPT-N and Shear Wave Velocity at Azampur School, Uttara

Depth (m)	Soil Description	SPT-N Value	Shear wave velocity (m/s) from SSMM				
			SSMM Hossain (2009)	Ansary et al. (2010)	Ohta and Goto (1978)	Imai and Yoshimura (1970)	Ohba and Toriumi (1970)
1.5	Clay	15	210	235	154	186	194
3.0	Clay	20	208	254	186	204	213
4.5	Clay	17	208	243	196	194	202
6.0	Clay	12	212	220	196	173	181
7.5	Sandy Silt	12	230	196	172	173	181
9.0	Sandy Silt	14	230	206	183	182	190
10.5	Sandy Silt	17	245	221	195	194	202
12.0	Sandy Silt	18	265	225	202	197	206
13.5	Sandy Silt	17	265	221	205	194	202
15.0	Clay	20	285	254	257	204	213
16.5	Clay	13	285	225	243	177	186
18.0	Clay	14	305	230	250	182	190
19.5	Clay	17	325	243	263	194	202
20.0	Clay	18	325	247	267	197	206

Shear Wave Velocity Results

Table 2.3 represents shear wave velocity using SSMM method (Hossain, 2009) and four soil correlations. According to SSMM, SWV varies from 208 to 325. SWV varies between 221 and 247 m/sec (Ansary et al., 2010). SWV exists between 154 and 267 m/sec (Ohta and Goto, 1978). On the other hand, SWV of Ohba and Toriumi (1970), which varies from 181 to 213 m/sec, shows slightly higher value than Imai and Yoshimura (1970), which shows ranging between 173 to 204 m/sec.

(12) Sub-Soil Characteristics of Mirpur DOHS (South side) (SBH-12(A))

SPT Results

The soil profile of the borehole is shown in Table 2.4 (Tanvir, 2009). The borehole exists three soil layers. The top layer exists filling sand layer from 0 to 3 m. The organic clay layer varies from 3 to 9 m. The bottom sand layer varies between 9 and 18 m. The uncorrected SPT N-value of this site varies from 2 to 19. The SPT N-value of the uppermost clayey silt layer varies from 6 to 8. The SPT N-value of sand layer varies from 4.5 to 18.

Table 2.4: SPT-N and Shear Wave Velocity at Mirpur DOHS (South side)

Depth (m)	Soil Description	SPT-N Value	Shear wave velocity (m/s) from SSMM				
			SSMM Hossain (2009)	Ansary et al. (2010)	Ohta and Goto (1978)	Imai and Yoshimura (1970)	Ohba and Toriumi (1970)
1.50	Filling Sand	3	78	122	98	109	118
3.00	Filling Sand	4	92	135	119	120	129
4.50	Organic Clay	1	102	110	121	76	84
6.00	Organic Clay	2	105	133	144	96	104
7.50	Organic Clay	3	115	150	162	109	118
9.00	Clay	5	115	145	153	129	138
10.50	Sand	7	125	163	168	144	154
12.00	Sand	9	135	178	180	157	166
13.50	Sand	10	135	184	187	162	172
15.00	Sand	17	142	221	209	194	202
16.50	Sand	18	142	225	215	197	206
18.00	Sand	20	150	233	223	204	213

Shear Wave Velocity Results

Table 2.4 represents shear wave velocity by direct SSMM method (Hossain, 2009) and four correlated methods. According to SSMM, SWV varies from 78 to 150. SWV varies from 110 to 233 m/sec (Ansary et al., 2010). From SPT correlation developed by Ohta and Goto (1978), SWV exists from 98 to 223 m/sec. On the other hand, SWV of Ohba and Toriumi (1970), which varies from 84 to 213 m/sec, shows slightly higher value than Imai and Yoshimura (1970), which shows ranging between 76 and 204 m/sec.

(13) Sub-Soil Characteristics of Mirpur DOHS (North Side) (SBH 12 (B))

SPT Results

The soil profile of the borehole is shown in Table A2.10. The borehole consists of five soil layers. The top layer of soil exists filling grey very loose silty fine sand which varies from 0 to 5.5 m. The stiff to very stiff light brown silty clay with trace fine sand high plastic varies between 16 and 22 m. The uncorrected SPT N-value of this site varies from 6 to 22. The SPT N-value of the grey very loose silty fine sand varies from 5 to 6. The

SPT N-value of stiff brown clayey silt with fine sand medium compress varies from 8 to 10. The SPT N-value of stiff to very stiff light brown silty clay varies between 16 and 22.

Shear Wave Velocity Results

Table A2.10 represents shear wave velocity using four different methods. SWV varies from 155 to 264 m/sec (Ansary et al., 2010). SWV exists from 111 to 278 m/sec (Ohta and Goto, 1978). On the other hand, SWV of Ohba and Toriumi (1970), which varies from 146 to 222 m/sec, shows slightly higher value than Imai and Yoshimura (1970), which shows ranging between 137 and 214 m/sec.

(14) Sub-Soil Characteristics of Ashiyan city, Askona, Dakkhin Khan (SBH 13)

SPT Results

The soil profile of the borehole is shown in Table A2.11. The borehole consists of six soil layers. The top layer of soil exists filling grey loose silty fine sand which varies from 0 to 3.5 m. The soft to medium stiff grey silty clay trace fine sand medium plastic varies between 7 and 12.5 m. The dense brown silty fine sand trace mica varies between 12.5 and 17 m. The uncorrected SPT N-value of this site varies from 4 to 42. The SPT N-value of soft to medium stiff grey silty clay varies from 3 to 7. The SPT N-value of stiff grey silty clay varies from 17 to 20.

Shear Wave Velocity Results

Table A2.11 represents shear wave velocity at four different methods. SWV varies from 135 to 300 m/sec (Ansary et al., 2010). SWV exists between 103 and 249 m/sec (Ohta and Goto, 1978). On the other hand, SWV of Ohba and Toriumi (1970), which varies from 129 to 268 m/sec, shows slightly higher value than Imai and Yoshimura (1970), which shows ranging between 120 to 261 m/sec.

(15) Sub-Soil Characteristics of Purbachal-1, Randokpur Hazi Bari, Rupganj (SBH 14(A))

SPT Results

The soil profile of the borehole is shown in Table A2.12. This borehole consists of six soil layers. The soft grey silty clay trace fine sand medium plastic varies from 2 to 8 m. The medium dense grey silty fine sand trace mica varies between 15.5 and 20 m. The uncorrected SPT N-value of this site varies from 2 to 17. The SPT N-value of soft grey silty clay varies from 2 to 4. The SPT N-value of medium dense grey silty fine sand varies from 13 to 16.

Shear Wave Velocity Results

Table A2.12 shows shear wave velocity using four different methods. SWV varies from 133 to 216 m/sec (Ansary et al., 2010). SWV exists between 117 and 219 m/sec (Ohta and Goto, 1978). On the other hand, SWV of Ohba and Toriumi (1970), which varies from 104 to 202 m/sec, shows slightly higher value than Imai and Yoshimura (1970), which shows ranging between 96 and 190 m/sec.

(16) Sub-Soil Characteristics of Purbachal-2, American City (SBH 14(B))

SPT Results

The soil profile of the borehole is represented in Table A2.13. This borehole consists of three soil layers. The top layer exists filling of very loose grey silty fine sand trace mica varies from 0 to 6.5 m. The very soft grey silty clay trace fine sand medium to high plastic varies between 6.5 and 18.5 m. The bottom layer of medium stiff grey silty clay varies from 18.5 to 20. The uncorrected SPT N-value of this site varies from 1 to 8. The SPT N-value of filling is 1. The SPT N-value of very soft grey silty clay varies between 1 and 2.

Shear Wave Velocity Results

Table A2.13 represents shear wave velocity using four different methods. SWV varies from 84 to 197 m/sec (Ansary et al., 2010). SWV exists between 98 and 233 m/sec (Ohta and Goto, 1978). On the other hand, SWV of Ohba and Toriumi (1970), which varies from 84 to 160 m/sec, shows slightly higher value than Imai and Yoshimura (1970), which shows ranging between 76 and 151 m/sec.

(17) Sub-Soil Characteristics of Purbachal Picnic Park, Gazipur (SBH 14(C))

SPT Results

The soil profile of the borehole is shown in Table A2.14. This borehole consists of four soil layers. The top layer exists filling of loose grey silty fine sand trace mica varies from 0 to 5.5 m. The bottom layer of stiff to very stiff light brown clayey silt varies between

11.5 and 20 m. The uncorrected SPT N-value of this site varies from 2 to 20. The SPT N-value of filling loose grey silty fine Sand varies from 4 to 6.

Shear Wave Velocity Results

Table A2.14 represents shear wave velocity using four different methods. SWV varies from 133 to 233 m/sec (Ansary et al., 2010). SWV exists between 107 and 228 m/sec (Ohta and Goto, 1978). On the other hand, SWV of Ohba and Toriumi (1970), which varies from 138 to 213 m/sec, shows slightly higher value than Imai and Yoshimura (1970), which shows ranging between 96 and 204 m/sec.

(18) Sub-Soil Characteristics of Adjacent to Mirpur Zoo (SBH 15)

SPT Results

The soil profile of the borehole is shown in Table A2.15. The borehole consists of six soil layers. The top layer exists filling of loose grey silty fine sand trace mica varies from 0 to 5.5 m. The medium stiff to stiff grey silty clay trace fine sand high plastic varies from 8 to 12.5 m. The bottom layer of medium dense brown silty fine sand trace mica varies between 16 and 26 m. The uncorrected SPT N-value of this site varies from 15.5 to 26. The SPT N-value of medium stiff to stiff grey silty clay varies from 6 to 11. The SPT N-value of the bottom layer varies between 16 and 26 m.

Shear Wave Velocity Results

Table A2.15 demonstrates shear wave velocity using four different methods. SWV varies from 145 to 255 m/sec (Ansary et al., 2010). From SPT correlation developed by Ohta and Goto (1978), SWV exists from 107 to 238 m/sec. On the other hand, SWV of Ohba and Toriumi (1970), which varies from 138 to 231 m/sec, shows slightly higher value than Imai and Yoshimura (1970), which shows ranging between 129 to 223 m/sec.

(19) Sub-Soil Characteristics of Field Ground, Pallabi (SBH 16)

SPT Results

The soil profile of the borehole is shown in Table 2.5. The borehole consists of four soil layers. The top layer exists filling of loose grey silty fine sand trace mica varies from 0 to 1.5 m. The clay layer varies from 3 to 18 m. The bottom layer of clay layer varies

between 21 and 24 m. The uncorrected SPT N-value of this site varies from 1 to 22. The SPT N-value of thick clay layer varies from 1 to 12. The SPT N-value of sand layer varies from 8 to 22 m.

Shear Wave Velocity Results

Table 2.5 demonstrates shear wave velocity using four different methods. SWV by PS logging varies from 78 to 230 (CDMP, 2009). From soil correlation proposed by Ansary et al. (2010), SWV varies from 84 to 247 m/sec. From SPT correlation developed by Ohta and Goto (1978), SWV exists from 82 to 277 m/sec. On the other hand, SWV of Ohba and Toriumi (1970), which varies from 84 to 206 m/sec, shows slightly higher value than Imai and Yoshimura (1970), which shows ranging between 76 and 197 m/sec.

Table 2.5: SPT-N and Shear Wave Velocity at Field Ground, Pallabi

Depth (m)	Soil Description	SPT-N Value	Shear wave velocity (m/s) from PS-logging				
			CDMP (2009)	Ansary et al. (2010)	Ohta and Goto (1978)	Imai and Yoshimura (1970)	Ohba and Toriumi (1970)
	Filling						
1.5	Sand	1	78	84	82	76	84
3.0	Clay	1	78	110	112	76	84
4.5	Clay	1	78	110	121	76	84
6.0	Clay	1	78	110	128	76	84
7.5	Clay	1	78	110	134	76	84
9.0	Clay	5	134	172	183	129	138
10.5	Clay	4	134	162	182	120	129
12.0	Clay	3	134	150	178	109	118
13.5	Clay	1	134	110	151	76	84
15.0	Clay	1	134	110	154	76	84
16.5	Clay	7	134	190	219	144	154
18.0	Clay	12	230	220	244	173	181
19.5	Sand	8	230	171	194	151	160
21.0	Sand	22	230	241	234	211	219
22.5	Clay	10	230	209	247	162	172
24.0	Clay	18	230	247	277	197	206

(20) Sub-Soil Characteristics of Block-B, Bashundhara (SBH 17 (A))

SPT Results

The soil profile of the borehole is shown in Table 2.6. This borehole exists three soil layers. The top layer exists filling of sand from 0 to 3 m. The thick clay layer exists between 3 and 13.5 m. The bottom layer of sand varies from 13.5 to 21 m. The

uncorrected SPT N-value of this site varies from 5 to 34. The SPT N-value of filling sand varies from 5 to 7. The SPT N-value of thick clay layer varies from 5 to 14. The SPT N-value of bottom sand layer varies from 10 to 34.

Shear Wave Velocity Results

Table 2.6 represents shear wave velocity using SSMM method and four correlated methods. According to SSMM, SWV varies from 120 to 270. SWV varies from 145 to 279 m/sec (Ansary et al., 2010). From SPT correlation developed by Ohta and Goto (1978), SWV exists between 107 and 252 m/sec. On the other hand, SWV of Ohba and Toriumi (1970), which varies from 138 to 251 m/sec, shows slightly higher value than Imai and Yoshimura (1970), which shows ranging between 129 and 243 m/sec.

Table 2.6: SPT-N and Shear Wave Velocity at Block-B, Bashundhara

Depth (m)	Soil Description	SPT-N Value	Shear wave velocity (m/s) from SSMM				
			SSMM Hossain (2009)	Ansary et al. (2010)	Ohta and Goto (1978)	Imai and Yoshimura (1970)	Ohba and Toriumi (1970)
1.5	Filling Sand	5	120	145	107	129	138
3.0	Filling Sand	7	120	163	130	144	154
4.5	Clay	5	140	172	159	129	138
6.0	Clay	11	170	215	193	168	177
7.5	Clay	14	190	230	210	182	190
9.0	Clay	7	190	190	194	144	154
10.5	Clay	8	212	197	204	151	160
12.0	Clay	10	225	209	218	162	172
13.5	Clay	12	225	220	230	173	181
15.0	Sand	10	230	184	191	162	172
16.5	Sand	11	230	190	198	168	177
18.0	Sand	27	245	258	235	226	233
19.5	Sand	30	270	268	243	233	241
21.0	Sand	34	270	279	252	243	251

(21) Sub-Soil Characteristics of Block-D, Bashundhara (SBH 17 (B))

SPT Results

The soil profile of the borehole is shown in Table 2.7. This borehole exists three soil layers. The top layer exists filling of very soft to soft light brown to brown silty clay trace fine sand from 0 to 11 m. The very soft silty dark grey silty clay trace fine sand varies

between 11 and 18.5 m. The bottom layer of medium dense grey silty fine sand varies from 18.5 to 21.5 m. The uncorrected SPT N-value of this site varies from 1 to 21. The SPT N-value of filling sand varies from 1 to 4. The SPT N-value of medium dense grey silty fine sand varies from 2 to 21.

Table 2.7: SPT-N and Shear Wave Velocity at Block-D, Bashundhara

Depth (m)	Soil Description	SPT-N Value	Shear wave velocity (m/s) from SSMM				
			SSMM Hossain (2009)	Ansary et al. (2010)	Ohta and Goto (1978)	Imai and Yoshimura (1970)	Ohba and Toriumi (1970)
1.5	Silty Clay	1	101	110	97	76	84
3.0	Silty Clay	2	101	133	126	96	104
4.5	Silty Clay	4	101	162	153	120	129
6.0	Silty Clay	3	101	150	155	109	118
7.5	Silty Clay	3	101	150	162	109	118
9.0	Silty Clay	4	137	162	176	120	129
10.5	Silty Clay	2	137	133	162	96	104
12.0	Silty Clay	1	137	110	147	76	84
13.5	Silty Clay	1	137	110	151	76	84
15.0	Silty Clay	1	137	110	154	76	84
16.5	Silty Clay	1	137	110	157	76	84
18.0	Silty Clay	2	137	133	180	96	104
19.5	Silty Fine Sand	17	137	221	221	194	202
21.0	Silty Fine Sand	21	231	237	232	208	216

Shear Wave Velocity Results

Table 2.7 represents shear wave velocity using SSMM method (Hossain, 2009) and four correlated methods. According to SSMM, SWV varies from 101 to 231. From soil correlation proposed by Ansary et al. (2010), SWV varies from 110 to 237 m/sec. From SPT correlation developed by Ohta and Goto (1978), SWV exists between 97 and 232 m/sec. On the other hand, SWV of Ohba and Toriumi (1970), which varies from 84 to 216 m/sec, shows slightly higher value than Imai and Yoshimura (1970), which shows ranging between 76 and 208 m/sec.

(22) Sub-Soil Characteristics of Block-H, Bashundhara (SBH 17 (C))**SPT Results**

The soil profile of the borehole is shown in Table 2.8 (CDMP, 2009). This borehole exists of two soil layers. The top layer exists filling of fine sand from 0 to 3 m. The thick clay layer varies between 3 and 21 m. The uncorrected SPT N-value of this site varies from 3 to 37. The SPT N-value of clay varies from 1 to 4. The SPT N-value of the bottom layer varies from 17 to 37.

Table 2.8: SPT-N and Shear Wave Velocity at Block-H, Bashundhara

Depth (m)	Soil Description	SPT-N Value	Shear wave velocity (m/s) from PS-logging				
			CDMP (2009)	Ansary et al. (2010)	Ohta and Goto (1978)	Imai and Yoshimura (1970)	Ohba and Toriumi (1970)
1.5	Fill	3	96	122	98	109	118
3.0	Fill	5	259	145	123	129	138
4.5	Clay	17	259	243	196	194	202
6.0	Clay	15	259	235	203	186	194
7.5	Clay	10	259	209	199	162	172
9.0	Clay	12	259	220	212	173	181
10.5	Clay	13	259	225	222	177	186
12.0	Clay	28	364	279	260	228	236
13.5	Clay	21	364	258	253	208	216
15.0	Clay	35	364	297	282	246	253
16.5	Clay	37	364	302	290	250	257
18.0	Clay	20	364	254	266	204	213
19.5	Clay	27	364	277	285	226	233
21.0	Clay	21	364	258	277	208	216

Shear Wave Velocity Results

Table 2.8 represents shear wave velocity using PS logging (CDMP, 2009) and four correlated methods. According to PS logging, SWV varies from 96 to 364. SWV varies from 122 to 302 m/sec (Ansary et al., 2010). SWV exists between 98 and 285 m/sec (Ohta and Goto, 1978). On the other hand, SWV of Ohba and Toriumi (1970), which

varies from 118 to 253 m/sec, shows slightly higher value than Imai and Yoshimura (1970), which shows ranging between 109 and 250 m/sec.

(23) Sub-Soil Characteristics of Kuril Flyover (SBH 19)

SPT Results

The soil profile of the borehole is shown in Table A2.16. This borehole consists of four soil layers. The top layer exists filling of loose grey silty fine sand trace mica varies from 0 to 3.5 m. The very soft grey silty clay trace fine sand medium plastic varies between 3.5 and 8 m. The stiff grey to light brown silty clay varies from 8 to 14.0. The bottom layer of very stiff light brown clayey silt with fine sand varies from 14 to 20. The uncorrected SPT N-value of this site varies from 1 to 27. The SPT N-value of filling is 4. The SPT N-value of very soft grey silty clay varies from 1 to 4.

Shear Wave Velocity Results

Table A2.16 represents shear wave velocity using four different methods. SWV varies from 135 to 258 m/sec (Ansary et al., 2010). SWV exists between 103 and 240 m/sec (Ohta and Goto, 1978). On the other hand, SWV of Ohba and Toriumi (1970), which varies from 84 to 233 m/sec, shows slightly higher value than Imai and Yoshimura (1970), which shows ranging between 76 and 226 m/sec.

(24) Sub-Soil Characteristics of Purachal, Uttar Badda (SBH 21)

SPT Results

The soil profile of the borehole is represented in Table A2.17. The borehole consists of five soil layers. The top layer exists filling of loose grey silty fine sand trace mica varies from 0 to 5 m. The medium stiff to stiff light brown silty clay varies between 8 and 14.5 m. The medium dense to dense brown sandy silt varies from 14.5 to 18.5. The bottom layer of dense brown silty fine sand varies from 33 to 38. The uncorrected SPT N-value of this site varies from 1 to 38. The SPT N-value of filling varies from 5 to 8. The SPT N-value of medium stiff to stiff light brown silty clay trace grits varies between 3 and 12.

Shear Wave Velocity Results

Table A2.17 represents shear wave velocity using four different methods. SWV varies from 163 to 290 m/sec (Ansary et al., 2010). SWV exists between 114 and 254 m/sec (Ohta and Goto, 1978). On the other hand, SWV of Ohba and Toriumi (1970), which

varies from 84 to 259 m/sec, shows slightly higher value than Imai and Yoshimura (1970), which shows ranging between 76 and 252 m/sec.

(25) Sub-Soil Characteristics of City Corporation, Gabtoli (SBH 22)

SPT Results

The soil profile of the borehole is shown in Table A2.18. This borehole consists of five soil layers. The top layer exists filling of loose grey silty fine sand trace mica varies from 0 to 5 m. The medium stiff dark grey silty clay trace organic matter medium plastic varies between 5 and 8 m. The loose to medium dense grey sandy silt with clay varies from 11 to 18.5 m. The bottom layer of medium dense grey silty fine sand trace mica varies from 13 to 15 m. The uncorrected SPT N-value of this site varies from 3 to 15. The SPT N-value of filling varies from 3 to 6. The SPT N-value of loose to medium dense grey sandy silt varies between 7 and 13.

Shear Wave Velocity Results

Table A2.18 represents shear wave velocity using four different methods. SWV varies from 155 to 211 m/sec (Ansary et al., 2010). From SPT correlation developed by Ohta and Goto (1978), SWV exists from 111 to 216 m/sec. On the other hand, SWV of Ohba and Toriumi (1970), which varies from 138 to 194 m/sec, shows slightly higher value than Imai and Yoshimura (1970), which shows ranging between 109 to 186 m/sec.

(26) Sub-Soil Characteristics of Adabor (SBH 23)

SPT Results

The soil profile of the borehole is shown in Table 2.9 (Tanvir, 2009). The borehole consists of four soil layers. The top layer exists filling of fine sand from 0 to 3 m. The clay layer varies between 3 and 10.5 m. The sand layer varies between 12 and 16.5. The uncorrected SPT N-value of this site varies from 2 to 37. The SPT N-value of clay varies between 2 and 13. The SPT N-value of sand layer varies from 22 to 37.

Shear Wave Velocity Results

Table 2.9 represents shear wave velocity by direct SSMM method (Hossain, 2009) and four correlated methods. According to SSMM, SWV varies from 85 to 230. From soil correlation proposed by Ansary et al. (2010), SWV varies from 107 to 287 m/sec. SWV exists between 92 and 258 m/sec (Ohta and Goto (1978). On the other hand, SWV of Ohba and Toriumi (1970), which varies from 104 to 216 m/sec, shows slightly higher value than Imai and Yoshimura (1970), which shows ranging between 96 and 250 m/sec.

Table 2.9: SPT-N and Shear Wave Velocity at Adabor

Depth (m)	Soil Description	SPT-N Value	Shear wave velocity (m/s) from SSMM				
			SSMM Hossain (2009)	Ansary et al. (2010)	Ohta and Goto (1978)	Imai and Yoshimura (1970)	Ohba and Toriumi (1970)
1.5	Filling Sand	2	85	107	92	96	104
3.0	Filling Sand	3	108	122	113	109	118
4.5	Clay	2	130	133	136	96	104
6.0	Clay	2	150	133	144	96	104
7.5	Clay	2	165	133	151	96	104
9.0	Clay	5	165	172	183	129	138
10.5	Clay	13	180	225	222	177	186
12.0	Sand	30	198	268	220	233	241
13.5	Sand	35	220	282	232	246	253
15.0	Sand	37	220	287	239	250	257
16.5	Sand	22	220	241	223	211	219
18.0	Clay	21	230	258	268	208	216

(27) Sub-Soil Characteristics of Agargoan Trade Fair area (SBH 24)

SPT Results

The soil profile of the borehole is shown in Table 2.10 (CDMP, 2009). This borehole consists of two soil layers. The top layer exists filling of fine sand from 0 to 4.5 m. The bottom thick clay layer varies between 4.5 and 24 m. The uncorrected SPT N-value of this site varies from 5 to 35. The SPT N-value of the uppermost filling sand varies from 5 to 23. The SPT N-value of the bottom clay layer varies between 21 and 35.

Shear Wave Velocity Results

Table 2.10 represents shear wave velocity by direct PS logging method (CDMP, 2009) and four correlated methods. According to PS logging, SWV varies from 150 to 300 m/sec. SWV varies from 145 to 297 m/sec (Ansary et al., 2010). From SPT correlation developed by Ohta and Goto (1978), SWV exists from 107 to 310 m/sec. On the other hand, SWV of Ohba and Toriumi (1970), which varies from 138 to 253 m/sec, shows slightly higher value than Imai and Yoshimura (1970), which shows ranging between 129 and 246 m/sec.

Table 2.10: SPT-N and Shear Wave Velocity at Agargoan Trade Fair area

Depth (m)	Soil Description	SPT-N Value	Shear wave velocity (m/s) from PS-logging				
			CDMP (2009)	Ansary et al. (2010)	Ohta and Goto (1978)	Imai and Yoshimura (1970)	Ohba and Toriumi (1970)
1.5	Filling Sand	5	150	145	107	129	138
3.0	Filling Sand	11	150	190	141	168	177
4.5	Filling Sand	23	200	244	173	214	222
6.0	Clay	21	200	258	215	208	216
7.5	Clay	21	200	258	225	208	216
9.0	Clay	21	239	258	234	208	216
10.5	Clay	22	239	261	243	211	219
12.0	Clay	22	239	261	249	211	219
13.5	Clay	22	239	261	255	211	219
15.0	Clay	27	300	277	270	226	233
16.5	Clay	26	300	274	273	223	231
18.0	Clay	23	300	264	272	214	222
19.5	Clay	28	300	279	286	228	236
21.0	Clay	30	300	285	294	233	241
22.5	Clay	30	300	285	298	233	241
24.0	Clay	35	300	297	310	246	253

(28) Sub-Soil Characteristics of Aftab Nagar Housing Project (SBH 25)

SPT Results

The soil profile of the borehole is shown in Table 2.11 (CDMP, 2009). The borehole consists of six soil layers. The top filling sand layer varies from 0 to 3 m. The thick sand layer exists between 12 and 24 m. The SPT N-value of filling sand varies from 2 to 3. The SPT N-value of the bottom thick sand layer varies between 18 and 29.

Table 2.11: SPT-N and Shear Wave Velocity at Aftab Nagar Housing Project

Depth (m)	Soil Description	SPT-N Value	Shear wave velocity (m/s) from PS-logging				
			CDMP (2009)	Ansary et al. (2010)	Ohta and Goto (1978)	Imai and Yoshimura (1970)	Ohba and Toriumi (1970)
1.5	Filling Sand	3	124	122	98	109	118
3.0	Filling Sand	2	124	107	105	96	104
4.5	Sand	2	124	107	114	96	104
6.0	Clay	8	211	197	183	151	160
7.5	Sand	10	211	184	166	162	172
9.0	Clay	13	211	225	215	177	186
10.5	Clay	18	211	247	235	197	206
12.0	Sand	18	211	225	202	197	206
13.5	Sand	24	211	248	217	217	225
15.0	Sand	20	211	233	215	204	213
16.5	Sand	17	211	221	213	194	202
18.0	Sand	24	211	248	230	217	225
19.5	Sand	27	211	258	239	226	233
21.0	Sand	27	211	258	242	226	233
22.5	Sand	25	211	251	242	220	228
24.0	Sand	29	211	264	252	231	239

Shear Wave Velocity Results

Table 2.11 represents shear wave velocity by direct PS logging method (CDMP, 2009) and four soil correlations. According to PS logging, SWV varies from 124 to 211 m/sec. From soil correlation proposed by Ansary et al. (2010), SWV varies between 107 to 264 m/sec. From SPT correlation developed by Ohta and Goto (1978), SWV exists from 98 to 252 m/sec. On the other hand, SWV of Ohba and Toriumi (1970), which varies from 118 to 239 m/sec, shows slightly higher value than Imai and Yoshimura (1970), which shows ranging between 96 to 231 m/sec.

(29) Sub-Soil Characteristics of Umme Had Nagar, Nadda (SBH 26)

SPT Results

The soil profile of the borehole is shown in Table A2.19. This borehole consists of nine soil layers. The top layer exists filling of very loose grey silty fine sand varies from 0 to 3.5 m. The medium stiff grey silty clay varies between 3.5 and 5 m. The stiff light brown silty clay varies from 8 to 11. The medium dense to dense light brown sandy silt varies from 12.5 to 15.5. The bottom layer of dense brown sandy silt trace clay varies from 18.5

to 20. The uncorrected SPT N-value of this site varies from 1 to 36. The SPT N-value of filling is 1. The SPT N-value of stiff light brown silty clay varies from 8 to 15. The SPT N-value of medium dense to dense light brown sandy silt varies between 13 and 33.

Shear Wave Velocity Results

Table A2.19 represents shear wave velocity using four different methods. SWV varies from 84 to 285 m/sec (Ansary et al., 2010). From SPT correlation developed by Ohta and Goto (1978), SWV exists from 82 to 251 m/sec. On the other hand, SWV of Ohba and Toriumi (1970), which varies from 84 to 253 m/sec, shows slightly higher value than Imai and Yoshimura (1970), which shows ranging between 76 and 246 m/sec.

(30) Sub-Soil Characteristics of South Banasree (SBH 27)

SPT Results

The soil profile of the borehole is shown in Table A2.20. This borehole consists of four soil layers. The top layer exists filling of very loose grey silty fine sand trace mica varies from 0 to 4 m. The medium stiff to very soft dark grey to grey silty clay varies between 4 and 14 m. The bottom layer of medium dense to dense brown silty fine sand varies from 16 to 20 m. The uncorrected SPT N-value of this site varies from 1 to 40. The SPT N-value of medium stiff to very soft dark grey to grey silty clay varies from 1 to 6. The SPT N-value of medium dense to dense brown silty fine sand varies from 9 to 40.

Shear Wave Velocity Results

Table A2.20 represents shear wave velocity using four different methods. From soil correlation proposed by Ansary et al. (2010), SWV varies from 133 to 295 m/sec. SWV exists between 107 and 273 m/sec (Ohta and Goto, 1978). On the other hand, SWV of Ohba and Toriumi (1970), which varies from 84 to 264 m/sec, shows slightly higher value than Imai and Yoshimura (1970), which shows ranging between 76 and 257 m/sec.

(31) Sub-Soil Characteristics of Kalunagar, Hazaribagh (SBH 30)

SPT Results

The soil profile of the borehole is shown in Table A2.21. This borehole consists of two soil layers. The top layer of soil exists filling of loose grey silty fine sand varies from 0 to 8 m. The bottom layer of medium dense grey silty fine sand varies from 8 to 20. The uncorrected SPT N-value of this site varies from 1 to 40. The SPT N-value of filling sand varies from 4 to 9. The SPT N-value of the bottom layer varies between 9 and 19.

Shear Wave Velocity Results

Table A2.21 represents shear wave velocity using four different methods. From soil correlation proposed by Ansary et al. (2010), SWV varies from 135 to 229 m/sec. SWV exists between 103 and 226 m/sec (Ohta and Goto, 1978). On the other hand, SWV of Ohba and Toriumi (1970), which varies from 129 to 209 m/sec, shows slightly higher value than Imai and Yoshimura (1970), which shows ranging between 120 and 201 m/sec.

(32) Sub-Soil Characteristics of Rab-10, Plot, Kamrangirchar (SBH 31)

SPT Results

The soil profile of the borehole is shown in Table A2.22. The borehole consists of five soil layers. The top layer exists filling of very loose to loose light brown silty fine sand varies from 0 to 3.5 m. The loose to medium dense grey fine sand and silt trace mica varies from 9.5 to 14 m. The bottom layer of medium dense grey silty fine sand trace mica varies from 14 to 20. The uncorrected SPT N-value of this site varies from 3 to 28. The SPT N-value of filling sand varies from 3 to 7. The SPT N-value of loose to medium dense grey fine sand and silt varies from 7 to 19. The SPT N-value of bottom layer varies from 19 to 28.

Shear Wave Velocity Results

Table A2.22 represents shear wave velocity using four different methods. SWV varies from 122 to 261 m/sec (Ansary et al., 2010). From SPT correlation developed by Ohta and Goto (1978), SWV exists from 98 to 261 m/sec. On the other hand, SWV of Ohba and Toriumi (1970), which varies from 118 to 236 m/sec, shows slightly higher value than Imai and Yoshimura (1970), which shows ranging between 109 and 228 m/sec.

(33) Sub-Soil Characteristics of Sosan Ghat, Kamrangirchar (SBH 32)

Table 2.12: SPT-N and Shear Wave Velocity at Sosan Ghat, Kamrangirchar

Depth (m)	Soil Description	SPT-N Value	Shear wave velocity (m/s) from SSMM				
			SSMM Hossain (2009)	Ansary et al. (2010)	Ohta and Goto (1978)	Imai and Yoshimura (1970)	Ohba and Toriumi (1970)
1.5	Filling Sand	7	100	163	114	144	154
3.0	Filling Sand	9	112	178	136	157	166
4.5	Filling Sand	10	134	209	179	162	172
6.0	Organic Clay	1	150	110	128	76	84
7.5	Organic Clay	2	160	133	151	96	104
9.0	Clay	12	160	220	212	173	181
10.5	Clay	13	165	225	222	177	186
12.0	Clay	15	170	235	234	186	194
13.5	Clay	14	170	230	236	182	190
15.0	Clay	15	180	235	244	186	194
16.5	Sand	22	180	241	223	211	219
18.0	Sand	25	200	251	232	220	228

SPT Results

The soil profile of the borehole is demonstrated in Table 2.12 (Tanvir, 2009). The borehole consists of four soil layers. The top layer exists filling of fine sand from 0 to 4.5 m. The organic clay layer varies between 4.5 and 7.5 m. The lower clay layer varies between 7.5 and 15. The uncorrected SPT N-value of this site varies from 1 to 25. The SPT N-value of filling sand varies from 7 to 10. The SPT N-value of clay layer varies between 12 and 15.

Shear Wave Velocity Results

Table 2.12 represents shear wave velocity by direct SSMM method (Hossain, 2009) and four correlated methods. According to SSMM, SWV varies from 100 to 200. SWV varies from 133 to 251 m/sec (Ansary et al., 2010). SWV exists between 114 and 244 m/sec (Ohta and Goto, 1978). On the other hand, SWV of Ohba and Toriumi (1970), which varies from 84 to 228 m/sec, shows slightly higher value than Imai and Yoshimura (1970), which shows ranging between 96 and 220 m/sec.

(34) Sub-Soil Characteristics of Basundhara River view (SBH 33)

SPT Results

The soil profile of the borehole is shown in Table A2.23. The borehole consists of six soil layers. The top layer exists filling of very loose to loose grey silty fine sand varies from 0 to 3.5 m. The medium stiff grey clayey silt with fine sand medium compress varies from

8 to 14 m. The uncorrected SPT N-value of this site varies from 2 to 10. The SPT N-value of filling sand varies from 3 to 5. The SPT N-value of medium stiff grey clayey silt varies from 4 to 10. The SPT N-value of soft silty grey silty clay trace fine sand varies from 2 to 5.

Shear Wave Velocity Results

Table A2.23 represents shear wave velocity using four different methods. SWV varies from 122 to 184 m/sec (Ansary et al., 2010). SWV exists from 98 to 202 m/sec (Ohta and Goto, 1978). On the other hand, SWV of Ohba and Toriumi (1970), which varies from 104 to 172 m/sec, shows slightly higher value than Imai and Yoshimura (1970), which shows ranging between 96 and 162 m/sec.

(35)

(36) Sub-Soil Characteristics of Matuail, Demra (SBH 34)

SPT Results

The soil profile of the borehole is shown in Table 2.13. This borehole exists five soil layers. The filling sand varies from 0 to 3.5 m. The stiff grey silty clay varies from 8.5 to 14 m. The bottom layer of grey clayey silt varies from 14 to 20 m. The uncorrected SPT N-value of this site varies from 2 to 23. The SPT N-value of the uppermost filling sand varies from 3 to 4. The SPT N-value of stiff grey silty clay varies from 7 to 17.

Shear Wave Velocity Results

Table 2.13 represents shear wave velocity using PS loggings method (CDMP, 2009) and four correlated methods. According to PS loggings, SWV varies from 101 to 231. SWV varies from 122 to 244 m/sec (Ansary et al., 2010). From SPT correlation developed by Ohta and Goto (1978), SWV exists from 98 to 244 m/sec. On the other hand, SWV of Ohba and Toriumi (1970), which varies from 118 to 222 m/sec, shows slightly higher value than Imai and Yoshimura (1970), which shows ranging between 96 and 214 m/sec.

Table 2.13: SPT-N and Shear Wave Velocity at Matuail, Demra

Depth (m)	Soil Description	SPT-N Value	Shear wave velocity (m/s) from PS-logging				
			CDMP (2009)	Ansary et al. (2010)	Ohta and Goto (1978)	Imai and Yoshimura (1970)	Ohba and Toriumi (1970)
1.5	Silty Fine Sand (Filling)	3	101	122	98	109	118
3.0	Silty Fine Sand (Filling)	4	101	135	119	120	129
4.5	Silty Clay	2	101	133	136	96	104
6.0	Silty Clay	2	101	133	144	96	104
7.5	Silty Clay	3	137	150	162	109	118
9.0	Silty Clay	8	137	197	198	151	160
10.5	Silty Clay	10	137	209	212	162	172
12.0	Silty Clay	14	137	230	231	182	190
13.5	Silty Clay	17	137	243	244	194	202
15.0	Clayey Silt	18	137	225	211	197	206
16.5	Clayey Silt	20	137	233	219	204	213
18.0	Clayey Silt	22	137	241	227	211	219
19.5	Clayey Silt	23	231	244	232	214	222
20.0	Clayey Silt	23	231	244	233	214	222

(37) Sub-Soil Characteristics of Jilmil Project, Equria (SBH 35)

SPT Results

The soil profile of the borehole is demonstrated in Table A2.24. This borehole consists of three soil layers. The top layer exists filling of very loose grey silty fine sand varies from 0 to 2 m. The soft to medium stiff grey silty clay varies from 2 to 8.5 m. The medium dense to dense grey silty fine sand varies from 8.5 to 20 m. The uncorrected SPT N-value of this site varies from 2 to 31. The SPT N-value of filling sand is 2. The SPT N-value of soft to medium stiff grey silty clay varies between 2 to 15. The SPT N-value of the bottom layer varies from 15 to 31.

Shear Wave Velocity Results

Table A2.24 represents shear wave velocity using four different methods. SWV varies from 107 to 271 m/sec (Ansary et al., 2010). SWV exists between 92 and 245 m/sec (Ohta and Goto, 1978). On the other hand, SWV of Ohba and Toriumi (1970), which varies from 104 to 244 m/sec, shows slightly higher value than Imai and Yoshimura (1970), which shows ranging between 96 and 236 m/sec.

(38) Sub-Soil Characteristics of Rajendapur (SBH 36)

SPT Results

The soil profile of the borehole is shown in Table A2.25. This borehole consists of five soil layers. The top layer exists filling of loose light grey silty fine sand varies from 0 to 5.5 m. The medium stiff to stiff grey clayey silt varies from 8 to 15.5 m. The uncorrected SPT N-value of this site varies from 4 to 26. The SPT N-value of filling sand varies from 4 to 5. The SPT N-value of medium stiff to stiff grey clayey silt varies from 5 to 9. The SPT N-value of the bottom layer varies between 21 and 26.

Shear Wave Velocity Results

Table A2.25 represents shear wave velocity using four different methods. SWV varies from 135 to 255 m/sec (Ansary et al., 2010). SWV exists between 103 and 238 m/sec (Ohta and Goto, 1978). On the other hand, SWV of Ohba and Toriumi (1970), which varies from 129 to 231 m/sec, shows slightly higher value than Imai and Yoshimura (1970), which shows ranging between 120 and 223 m/sec.

(39) Sub-Soil Characteristics of Bramangaon (SBH 37)

SPT Results

The soil profile of the borehole is shown in Table A2.26. This borehole exists four soil layers. The top layer exists filling of loose grey silty fine sand varies from 0 to 5 m. The medium stiff grey clayey silt with fine sand varies from 8 to 20 m. The uncorrected SPT N-value of this site varies from 4 to 8. The SPT N-value of filling sand varies from 4 to 5. The SPT N-value of the bottom layer varies from 5 to 8.

Shear Wave Velocity Results

Table A2.26 represents shear wave velocity using four different methods. SWV varies from 135 to 171 m/sec (Ansary et al., 2010). SWV exists from 103 to 195 m/sec (Ohta and Goto, 1978). On the other hand, SWV of Ohba and Toriumi (1970), which varies from 129 to 160 m/sec, shows slightly higher value than Imai and Yoshimura (1970), which shows ranging between 120 and 151 m/sec.

(40) Sub-Soil Characteristics of Meradia, Uttar Banasree (SBH 38)

SPT Results

The soil profile of the borehole is shown in Table 2.14. This borehole exists three soil layers. The top layer exists filling of fine sand from 0 to 4.5 m. The organic clay layer varies between 4.5 and 12 m. The lower clay layer varies between 12 and 18. The uncorrected SPT N-value of this site varies from 2 to 22. The SPT N-value of filling sand varies from 2 to 4. The SPT N-value of organic clay layer varies from 2 to 4. The SPT N-value of bottom clay layer varies from 17 to 22.

Shear Wave Velocity Results

Table 2.14 represents shear wave velocity using SSMM method (Hossain, 2009) and four correlated methods. According to SSMM, SWV varies from 90 to 195. From soil correlation proposed by Ansary et al (2010), SWV varies from 107 to 261 m/sec. SWV exists between 111 and 217 m/sec (Ohta and Goto, 1978). On the other hand, SWV of Ohba and Toriumi (1970), which varies from 104 to 209 m/sec, shows slightly higher value than Imai and Yoshimura (1970), which shows ranging between 96 and 201 m/sec.

Table 2.14: SPT-N and Shear Wave Velocity at Meradia, Uttar Banasree

Depth (m)	Soil Description	SPT-N Value	Shear wave velocity (m/s) from SSMM				
			SSMM Hossain (2009)	Ansary et al. (2010)	Ohta and Goto (1978)	Imai and Yoshimura (1970)	Ohba and Toriumi (1970)
1.5	Silty Fine Sand (Filling)	3	90	122	111	137	146
3.0	Silty Fine Sand (Filling)	4	102	135	130	144	154
4.5	Silty Fine Sand (Filling)	2	118	107	133	151	160
6.0	Organic Clay	2	130	133	111	96	104
7.5	Organic Clay	3	130	150	116	96	104
9.0	Organic Clay	8	138	197	120	96	104
10.5	Organic Clay	10	148	209	142	109	118
12.0	Organic Clay	14	157	230	154	120	129
13.5	Clay	17	157	243	184	162	172
15.0	Clay	18	170	247	194	173	181
16.5	Clay	20	170	254	207	190	198
18.0	Clay	22	195	261	217	201	209

(41) Sub-Soil Characteristics of BUET Play ground

SPT Results

The soil profile of the borehole is shown in Table 2.15. This borehole exists two soil layers. The top layer exist clayey silt layer from 0 to 4.5 m. The bottom sand layer exists from 4.5 to 18 m. The uncorrected SPT N-value of this site varies from 2 to 19. The SPT N-value of the uppermost clayey silt layer varies from 6 to 8. The SPT N-value of sand layer varies from 4.5 to 18.

Shear Wave Velocity Results

Table 2.15 represents shear wave velocity using SSMM method (Hossain, 2009) and four correlated methods. According to SSMM, SWV varies from 178 to 260 m/sec. SWV varies from 107 to 229 m/sec (Ansary et al., 2010). From Ohta and Goto (1978), SWV exists from 121 to 221 m/sec. On the other hand, SWV of Ohba and Toriumi (1970), which varies from 104 to 209 m/sec, shows slightly higher value than Imai and Yoshimura (1970), which shows ranging between 96 and 201 m/sec.

Table 2.15: SPT-N and Shear Wave Velocity at BUET Play ground

Depth (m)	Soil Description	SPT-N Value	Shear wave velocity (m/s) from SSMM				
			SSMM Hossain (2009)	Ansary et al. (2010)	Ohta and Goto (1978)	Imai and Yoshimura (1970)	Ohba and Toriumi (1970)
1.50	Clayey Silt	6	178	182	135	137	146
3.00	Clayey Silt	7	178	190	159	144	154
4.50	Clayey Silt	8	180	197	177	151	160
6.00	Sand	2	190	107	121	96	104
7.50	Sand	2	205	107	127	96	104
9.00	Sand	2	205	107	131	96	104
10.50	Sand	3	220	122	145	109	118
12.00	Sand	4	230	135	156	120	129
13.50	Sand	10	230	184	187	162	172
15.00	Sand	12	245	196	197	173	181
16.50	Sand	16	245	216	211	190	198
18.00	Sand	19	260	229	221	201	209

(42) Sub-Soil Characteristics of West Palashi, BUET campus

The BUET campus is situated in latitude 23°43'16.58" N to 23°43'59.44" N and longitude 90°23'13.31"E to 90°23'43.56" E. Microtremor observation has been executed at 132 selected points in soil. The geology of whole BUET campus is Upper Modhupur Terrace (Figure 2.2) and High Pleistocene terrace (Figure 2.3). There is no filling in this site.

SPT Results

Total 14 SPT boreholes data have been collected from West Palashi, BUET Campus. Table A2.27 to A2.31 shows soil profiles of five boreholes at BUET-JIDPUS building, West Palashi, BUET Campus (Dhaka Soil, 2008). Table 2.32 to 2.40 represent soil profiles of nine boreholes at New Academic building, West Palashi, BUET campus.

From Table A2.27 to A2.31, the uppermost silty clay varies from 0 to 6.0 m. Clayey silt exists below the silty clay layer between 4.5 to 7.5 m. The bottom layer of silty fine sand varies from 7.5 to 15 m.

From Table A2.32 to A3.40, clay silt exists between 0 to 1.5 m soils in most of the boreholes. The silty clay varies ranging between 1.5 and 7.5 m. In some borehole, fine sandy silt exists between 6 and 9 m. In all the boreholes, the bottom soil layer is silty fine sand.

Shear Wave Velocity Results

Table A2.27 to A2.40 represent shear wave velocity using four correlated methods.

From Table A2.27 to A2.31, SWV varies from 110 to 297 m/sec (Ansary et al., 2010). From SPT correlation developed by Ohta and Goto (1978), SWV exists between 92 and 242 m/sec. On the other hand, SWV of Ohba and Toriumi (1970), which varies from 84 to 266 m/sec, shows slightly higher value than Imai and Yoshimura (1970), which shows ranging between 76 and 259 m/sec.

From Table 2.32 to 2.40, SWV varies from 84 to 309 m/sec (Ansary et al., 2010). From SPT correlation developed by Ohta and Goto (1978), SWV exists from 82 to 259 m/sec. On the other hand, SWV of Ohba and Toriumi (1970), which varies from 84 to 275 m/sec, shows slightly higher value than Imai and Yoshimura (1970), which shows ranging between 76 and 269 m/sec.

2.3 MICROTREMOR DATA COLLECTION

The ground is always vibrating at minute amplitudes. Microtremors are ambient vibrations of the ground caused by natural or artificial disturbances such as wind, sea waves, traffic, human activities and industrial machinery. Microtremor data has been collected in consideration of noise in different geological and geomorphological unit (Figure 2.2 and Figure 2.3).

Microtremor measurement has been carried out in 132 selected locations (Figure 2.34) within BUET campus. In BUET campus, 240 second duration were recorded at different times in the specific locations. The measurements were carried out from morning to midnight in order to minimize artificial noises due to traffic and human activities. In BUET campus, most of the selected points were near the busy road. Special care has been taken during data recording. In West Polashi of BUET campus, there was an 8 MW with 1500 rpm Electric Power Plant. Although there is a machine foundation below the generator, this generator produces some noise in adjacent ground. So, microtremor observation has been executed at different times during ON and OFF condition to justify soil response due to this effect.

Microtremor observation at 45 sites has been carried out in and around Dhaka city. Traffic movement, human activities, any power plant and noise from other sources have been considered during data recording as well. Most of the microtremor observation has been executed in consideration of recent filling. However, some non recent filling areas have also been selected for observation. Figure 2.1 shows 45 selected locations in and around Dhaka city. Some location is not demonstrated specifically in Dhaka city map due to not having full area coverage map. These points are shown using arrow mark in Figure 2.1.

Figure 2.4 demonstrates microtremor measurement apparatus for data recording. This includes Geodas 15-HS equipment (Data logger and Laptop), Sensor, Cable, Battery and GPS. Mtobs.exe software is used to record microtremor data. Although there are five sensors in this observation system, two or three sensors have been used for data recording. Sensor has been used in consideration of surface condition, weather, time and geology of sites. CR4.5-1S velocity type sensor with sensitivity coefficient $0.0882\mu\text{m}/\text{sec}/\text{digit}$ has

been used in observation system. Sensors comprise three components, which can record the horizontal motion (in Latitude and Longitude directions) and the vertical motions (up and down). Microtremor sensor sensitivity was $295900\mu\text{m}/\text{sec}/\text{V}$. The converting speed was 50 kHz. The sampling frequency was 100 Hz. The amplification factor was used 20 db in observation system. Figure 2.5 shows some pictures of microtremor measurement at BUET campus, Demra and Ashulia Toll Plaza. These pictures are taken at different time during microtremor data recording.

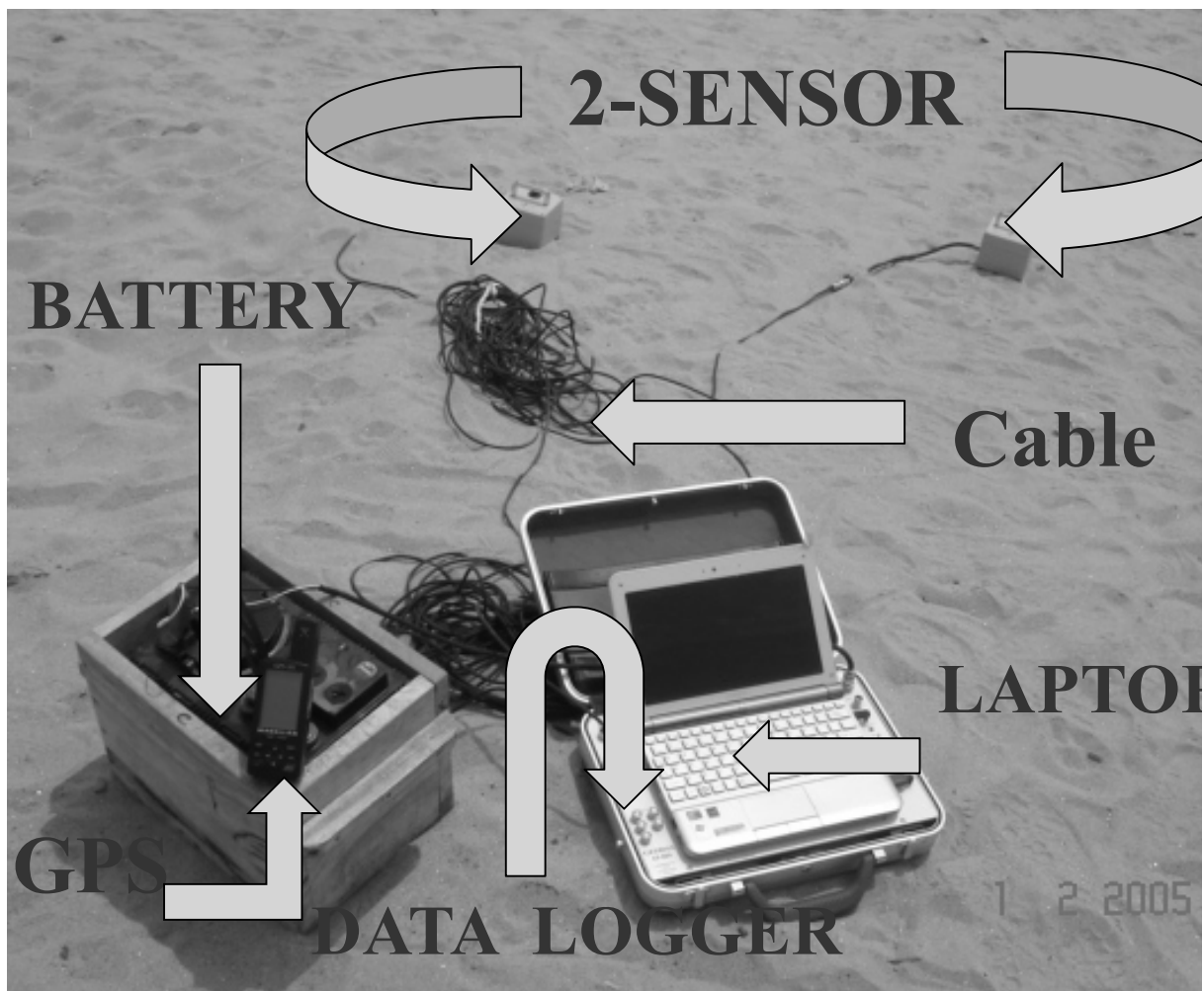


Figure 2.4: Microtremor measurement apparatus.



(a) West Polasi, BUET at 4:00 PM



(b) BUET campus at night



(c) Matuail, Demra (Left) and Ashulia Toll Plaza (Right) at afternoon

Figure 2.5: Microtremor data recording in and around Dhaka city.

2.4 MICROTREMOR DATA ANALYSIS

Velocity time history field microtremor data has been recorded in Mtobs.exe software with suitable number of observation channels, observation length, observation frequency, specific low or high pass filter code, amplification ratio, observation latitude and longitude, observation time and observation channel mode. Figure 2.6 shows a typical time history field data recording of Uttara Phase-3 (North side) at 4:30 PM on 9 April, 2011. The content of all input data are 2 CR4.5-1S velocity type sensors, 24000 observation data length, 100Hz sampling frequency, 0.05 Hz Low-pass filter, 20db amplification ratio, Latitude-23°52'22" and Longitude-90°21'40".

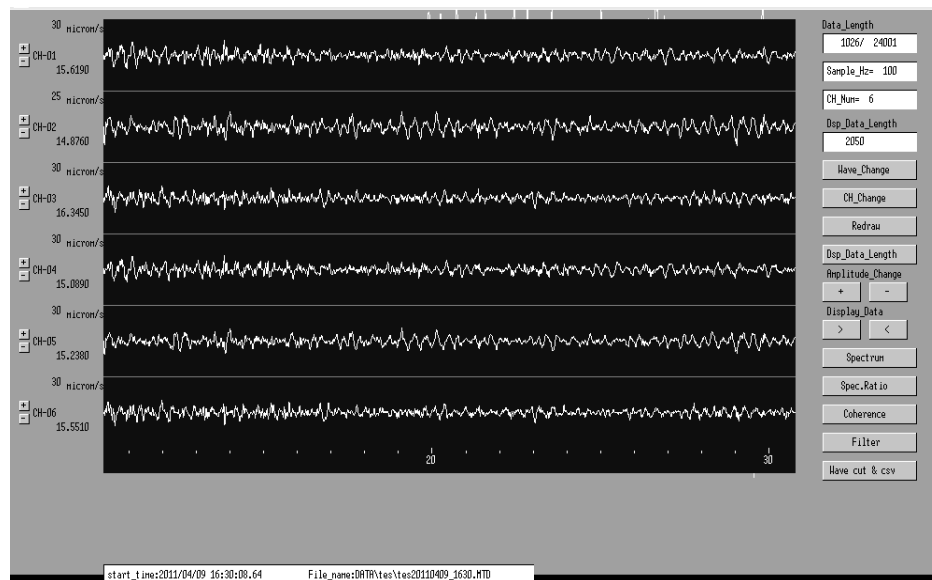


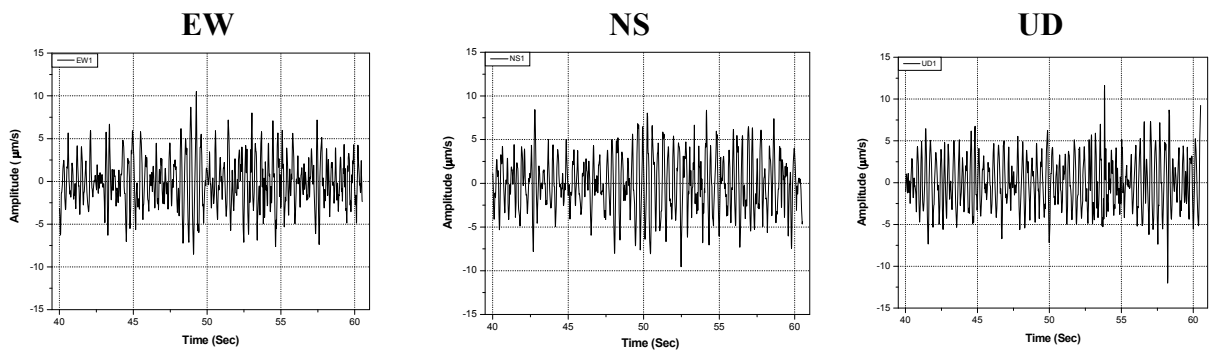
Figure 2.6: Time history field data recording at Uttara Phase-3 (North side).

Figure 2.7 [(a), (c) and (e)] shows time history microtremor data at segment 1, 2 and 3 with 2050 observed data length. Segment 1 illustrates time history data of 20.5 s from 40 s to 60.5 s. Segment 2 demonstrates time history data of 20.5 s from 100 s to 120.5 s. Segment 3 presents time history data of 20.5 s from 60 s to 80.5 s.

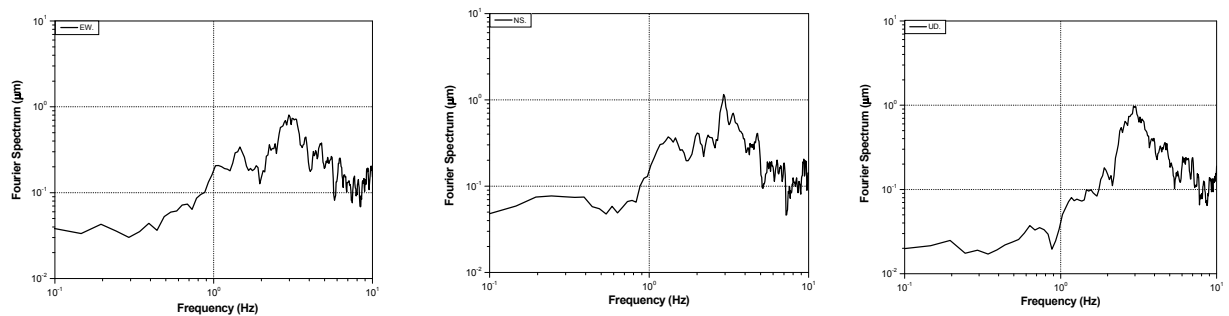
Time history data is not suitable to estimate the dynamic properties (predominant frequency and amplification ratio). So, transformation of time domain data to frequency domain data is required with Fourier Transformation. Therefore, Fast Fourier Transformation (FFT) has been used to transfer time domain data to frequency domain

data. Figure 2.7 [(b), (d) and (f)] presents Fast Fourier Transformation data at segment 1, 2 and 3 in EW, NS and UD directions, respectively. This transformation data is shown in logarithmic window in frequency from 0.1 Hz to 10 Hz and in Fourier Spectrum from 0.01 μm to 10 μm .

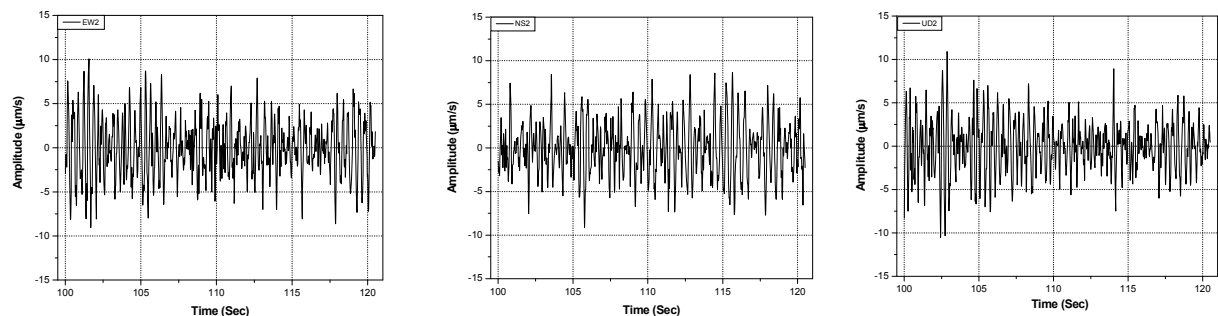
Only the Fourier Spectrum along three subsequent directions is not appropriate to estimate the predominant frequency and amplification. So, Horizontal to Vertical spectral ratio (H/V) is required to determine the dynamic properties of soil. Horizontal to Vertical Spectral Ratio (H/V) is determined dividing by Fourier Spectrum of UD direction to the Fourier Spectrum of EW or NS direction.



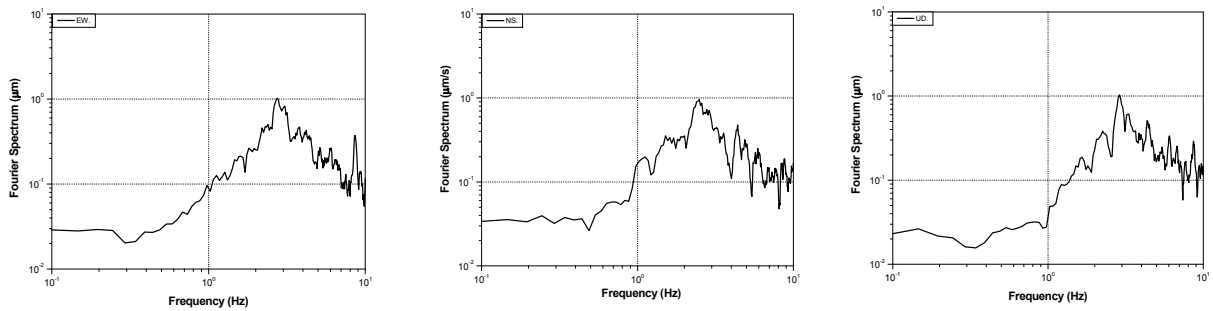
(a) Time History data of segment 1 from 40 sec to 60.5 sec



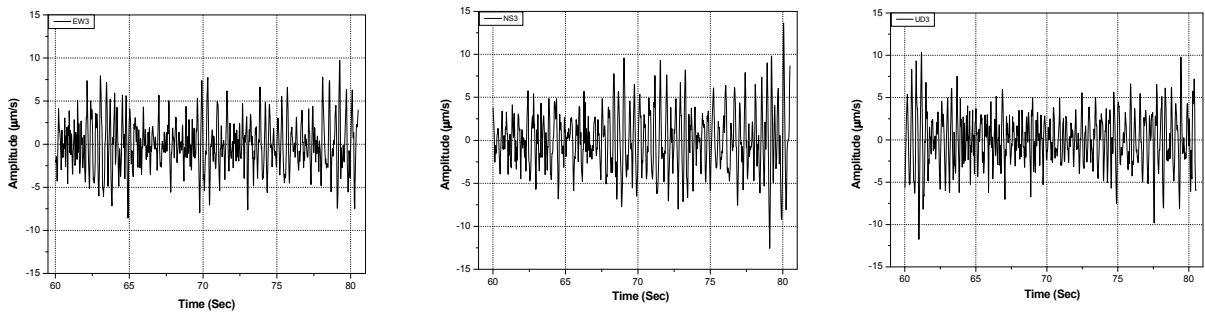
(b) Fourier Transformation of Segment 1 in EW, NS and UD direction



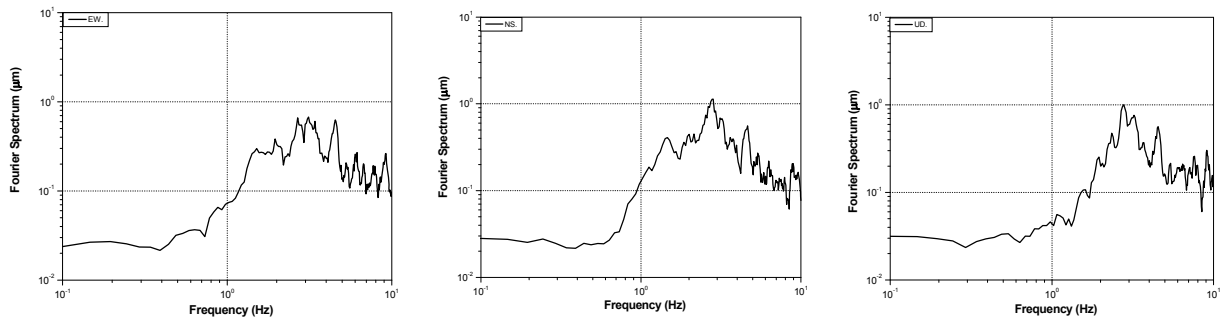
(c) Time History data of segment 2 from 100 sec to 120.5 sec



(d) Fourier Transformation of Segment 2 in EW, NS and UD direction

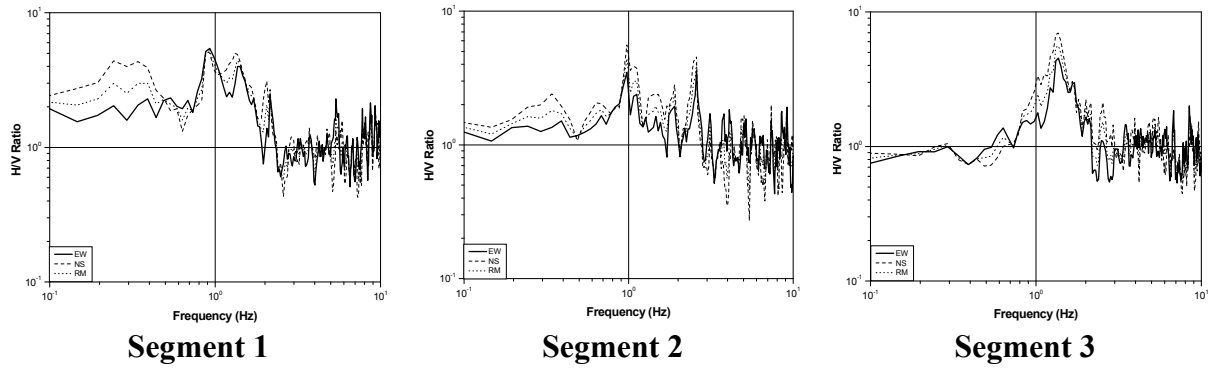


(e) Time History data of segment 1 from 60 sec to 80.5 sec

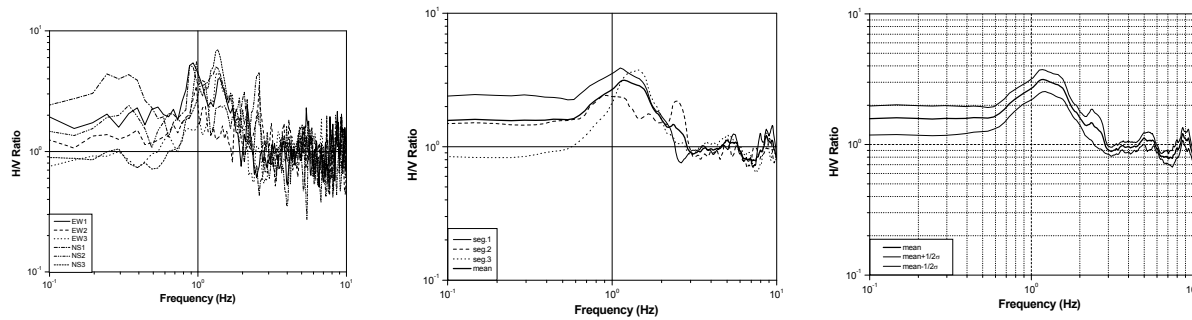


(f) Fourier Transformation of Segment 2 in EW, NS and UD direction

Figure 2.7: Fourier Transformation of three segments at Uttara Phase-3 (North side).



(a) H/V Ratio of EW, NS and their mean at Segment 1, 2 and 3



(b) Mean H/V ratio with Standard Deviation

Figure 2.8: Predominant Frequency and H/V ratio at Uttara Phase-3 (North side).

Figure 2.8 (a) shows the Horizontal to Vertical Spectral ratio (H/V) of segment 1, 2 and 3 in EW and NS directions, respectively. The square root of EW and NS direction H/V ratio in segment 1, 2 and 3 is calculated. Then, mean of the square root H/V ratio value is plotted with standard deviation 0.5σ . 0.5σ standard deviation represents the deviation of six H/V ratio data from mean in three segments. Figure 2.8 (b) presents the mean H/V ratio with six segmental H/V ratio in EW and NS direction. In addition to this, three segmental square root H/V ratio and their mean H/V Ratio is shown in Figure 2.8 (b). The plotted data is smoothed with suitable log- window to understand clearly the Predominant frequency (Hz) and Horizontal to vertical spectral ratio (H/V).

2.4.1 Stability of Microtremor Data

Microtremor is the combination of shear wave, Rayleigh wave and Love wave. The effect of different waves on microtremor data is significant. Therefore, stability check of microtremor data is important to estimate dynamic properties of any site soil. To carry out

this research velocity time history data have been recorded time ranging between morning to midnight at 14 locations in West Palashi, BUET. The observation microtremor data recording varies from 5 to 20 minutes. Ten minutes observation time has been taken in most of the observation points. Three segments of 20.48 s time domain data have been used to transform frequency domain spectrum. In order to get low noise data these Fourier spectra have been filtered using rectangular windows. The mean of these three segments of frequency domain data have been calculated using smoothing function with average smoothing point 5. Mean Fourier spectrum along EW, NS and UD directions have been plotted in logarithmic windows from 0.1 Hz to 10 Hz along predominant frequency and from $0.001\mu\text{m}$ to $1\mu\text{m}$ along Fourier amplitude spectrum, respectively. From these observations, stability of time variation microtremor data has been compared from Fourier spectrum. The horizontal to vertical spectral ratio has also been calculated in these locations to analyze the stability of H/V ratio with Fourier spectrum. Both Fourier spectrum and H/V ratio of fourteen observation points at different times have been included in this section.

2.4.1.1 Stability of Amplitude of Fourier Spectrum

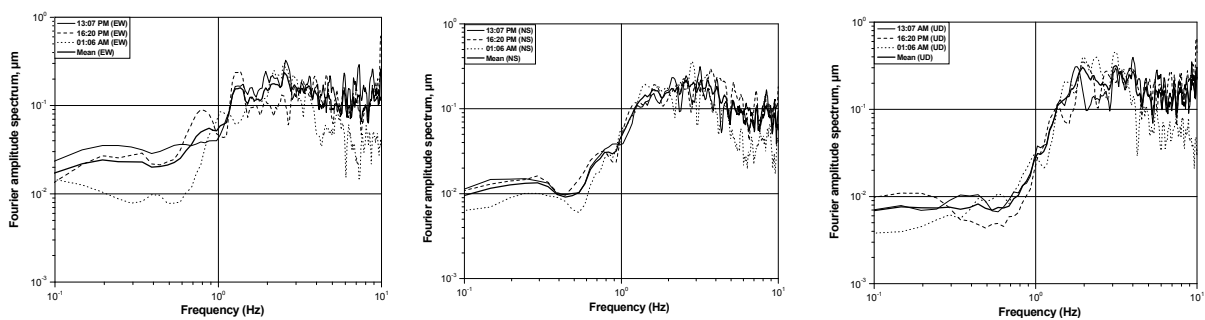
Frequency domain Fourier spectra of fourteen observation points have been demonstrated from Figure 2.9 to 2.13 along EW, NS and UD, respectively. Instead of using all the observed time records, three to four different times instants are selected from 24 hour observation for fourteen sites, for investigation. Figure 2.9 shows the vertical and horizontal Fourier spectra of microtremors observed at MT05, MT06 and MT07. The mean peak value of Fourier spectra varies from 2.1 Hz to 3.1 Hz for both the horizontal and vertical motions. Figure 2.9 (a) shows three time instants (13:07 PM, 16:20 PM and 01:06 AM) and their mean value. Figure 2.9 (b) shows three time instants (18:29 PM, 00:08 AM and 01:29 AM) where as Figure 2.9 (c) represents three time instants (11:34 AM, 16:55 PM and 19:41 PM). From figure 2.9, it can be concluded that Fourier spectra along EW, NS and UD directions are stable at these observation points. The stable Fourier spectra along vertical directions have been found around 3.0 Hz.

In Figure 2.10 Fourier spectra of microtremor observations at MT08, MT09 and MT10 have been illustrated along EW, NS and UD directions, respectively. The overall peak value of the Fourier spectra lies between 3.02 Hz and 3.84 Hz for both the horizontal and vertical motions. From Figure 2.10 (a), the horizontal motion of MT08 in the afternoon

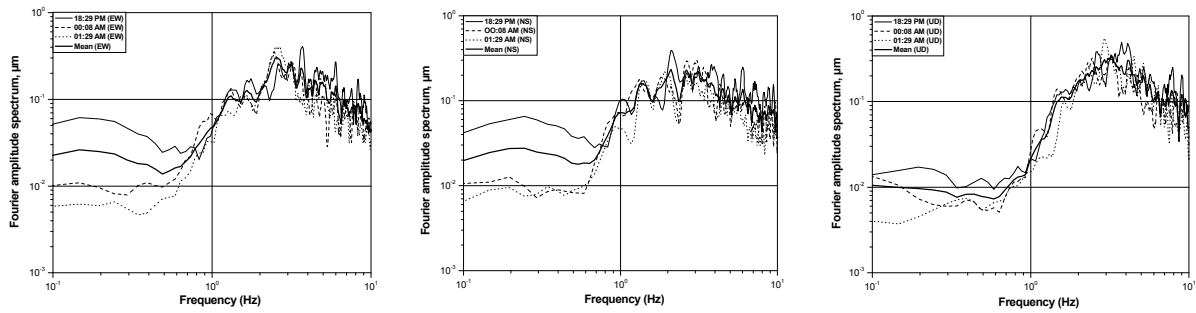
(11:34 AM and 16:55 PM) has a peak from 3.34 Hz to 4.4 Hz and in night (00:01 AM and 01:21 AM); it varies between 2.75 Hz and 2.95 Hz along EW direction. The peak along NS direction in the afternoon varies between 2.29 Hz and 2.57 Hz whereas it lies from 2.61 Hz to 2.94 Hz in night. The stable peak along vertical direction is 3.59 Hz in afternoon and it varies from 2.42 Hz to 3.02 Hz in night. The stable fourier spectra of MT 09 and MT 10 have been shown in Figure 2.10 (b) and Figure 2.10 (c). From Figure 2.10, it can be concluded that Fourier amplitude spectrum are stable along EW, NS and UD directions, respectively.

The frequency domain Fourier spectra at MT11, MT12 and MT13 are illustrated in Figure 2.11. The mean peak Fourier amplitude spectrum varies between 2.20 Hz and 3.74 Hz for both the horizontal and vertical motions for all three locations. The Fourier spectra at MT 11 and MT 12 are almost stable. The amplitude of these sites is around 3 Hz. But, the Fourier spectra at MT 13 are slightly different from MT 11 and MT 12. The mean peak of Fourier spectra at MT 13 varies from 2.72 Hz to 3.26 Hz. The peak Fourier spectra at MT 13 lies between 0.13 μm and 0.37 μm .

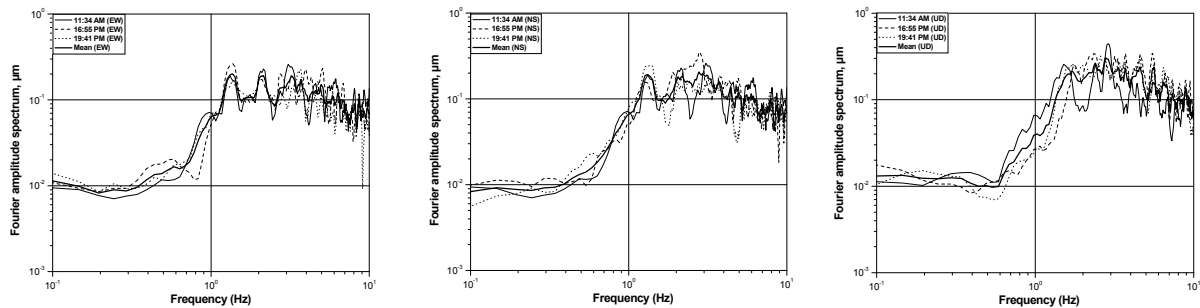
Figure 2.12 shows Fourier spectra of microtremor observations at MT15, MT16 and MT19 along EW, NS and UD directions, respectively. The mean peak amplitude of spectra varies from 1.94 Hz to 3.77 Hz for both the horizontal and vertical motions for all three locations. The mean peak Fourier amplitude has been found around 3.5 Hz along the vertical directions. The Fourier spectra at MT16 are more stable than other two locations along EW, NS and UD directions, respectively.



(a) MT05



(b) MT06

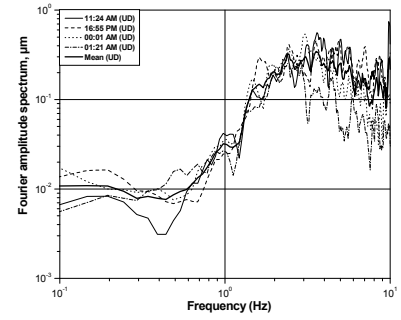
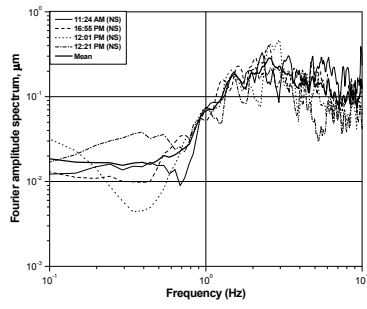
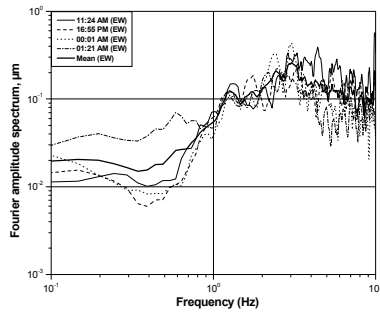


(c) MT07

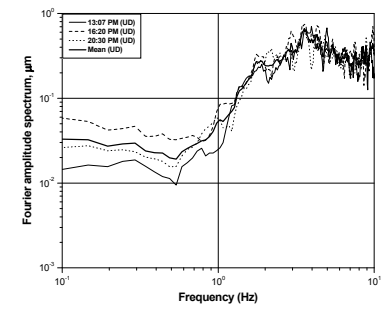
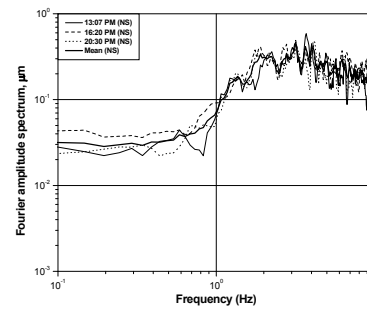
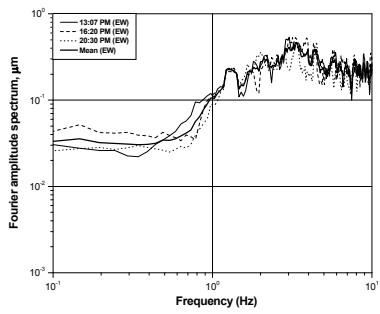
Figure 2.9 [(a), (b) and (c)]: Stability of Fourier Spectrum at different times along EW, NS and UD directions at MT05, MT06 and MT07.

The Fourier spectra of MT22 and MT23 are shown in Figure 2.13. The peak value of the spectra lies between 2.48 Hz and 4.08 Hz for both the horizontal and vertical motions for all three locations. Figure 2.13(a) shows the variation of Fourier spectra at MT22 at four time instants (12:48 PM, 15:53 PM, 11:31 and 00:38 PM) along EW, NS and UD directions, respectively. The variation of four time instants (12:48 PM, 15:53 PM, 11:46 PM and 00:46) of MT23 has been demonstrated in Figure 2.13 (b). From Figure 3.13, it can be said that the Fourier spectra in night are stable.

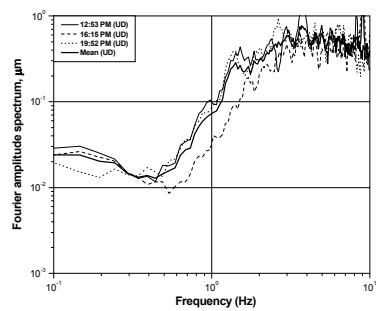
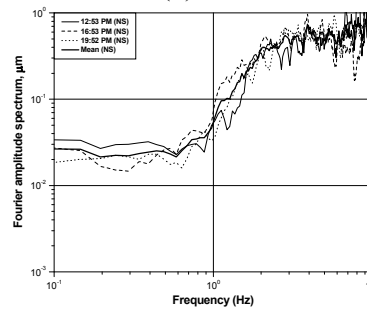
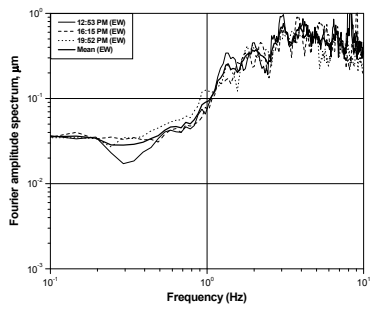
From the Fourier spectra analysis of 14 sites, it can be said that the amplitude level of Fourier spectra vary at different time instants of a day. The Fourier spectra at night are more stable than other time instants within a day. In the most of the sites Fourier spectra vary along EW and NS directions, respectively. It is not possible to estimate the dynamic characteristics (Predominant frequency and Amplification) of these sites on the basis of the amplitude level of Fourier spectra.



(a) MT08

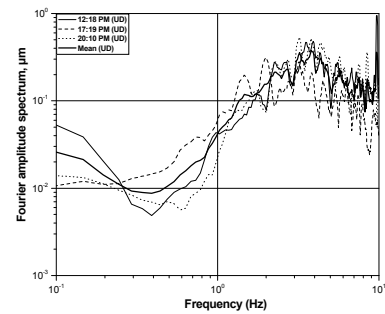
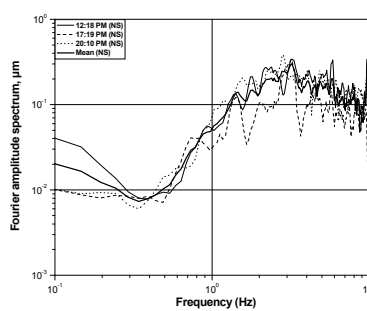
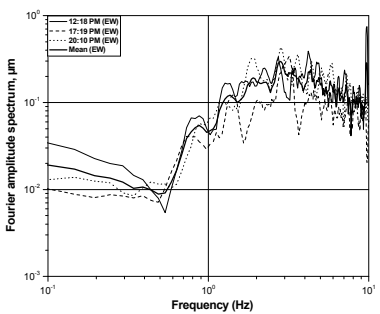


(b) MT09

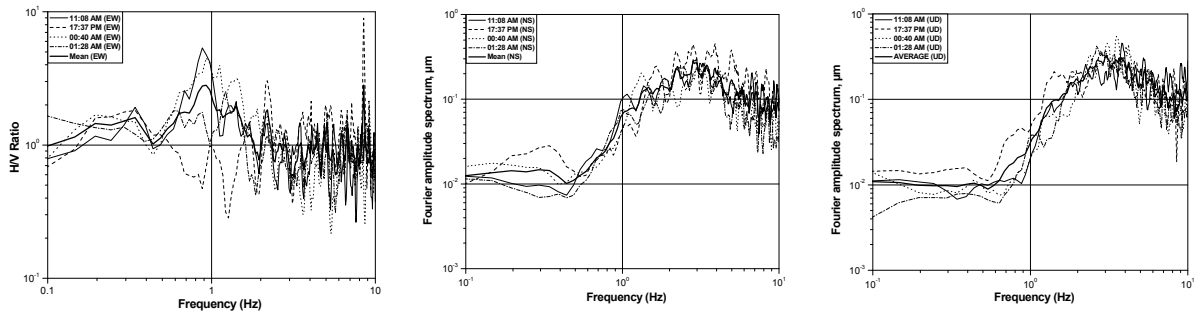


(c) MT10

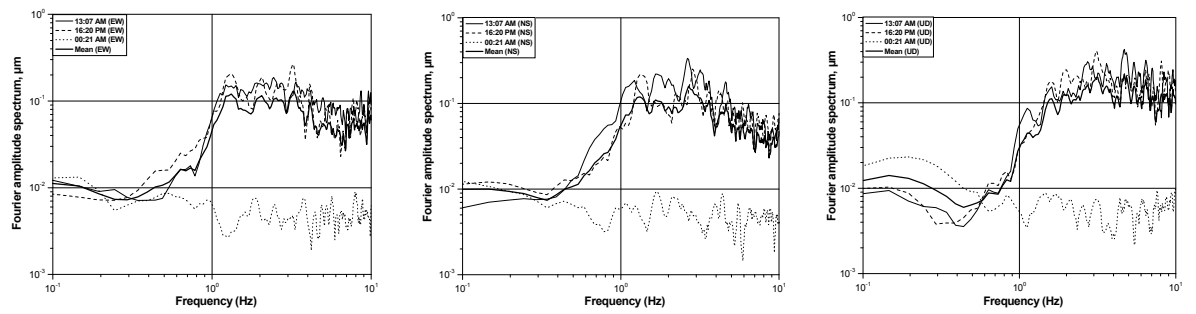
Figure 2.10 [(a), (b) and (c)]: Stability of Fourier Spectrum at different times along EW, NS and UD directions at MT08, MT09 and MT10.



(a) MT11

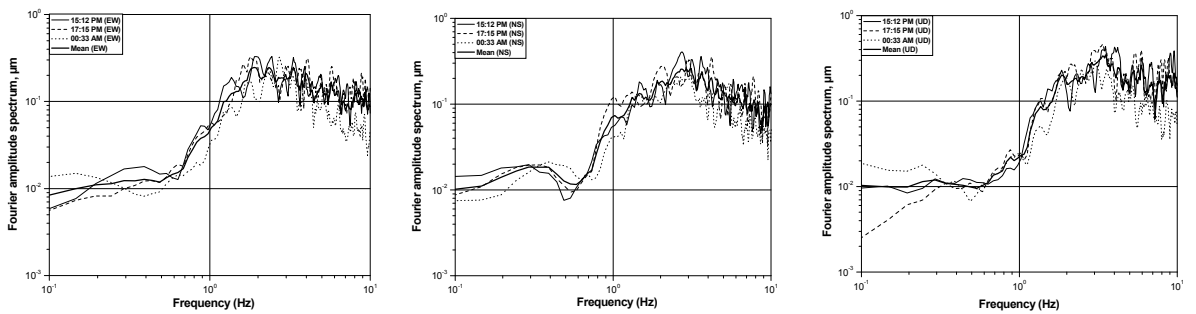


(b) MT12

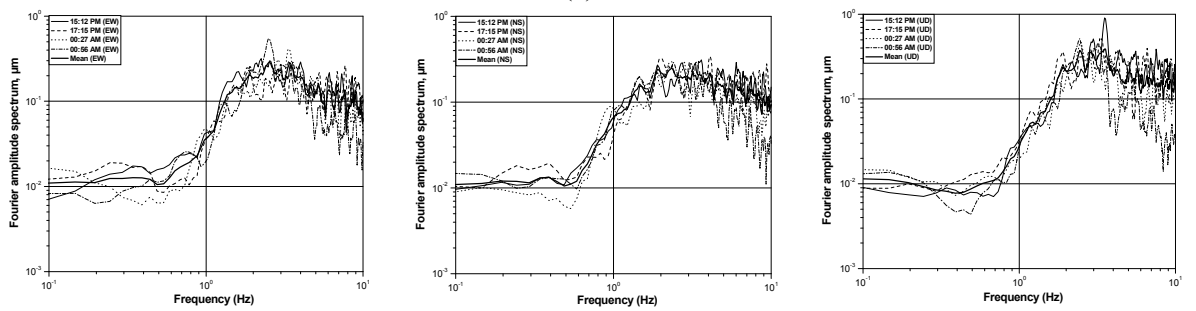


(c) MT13

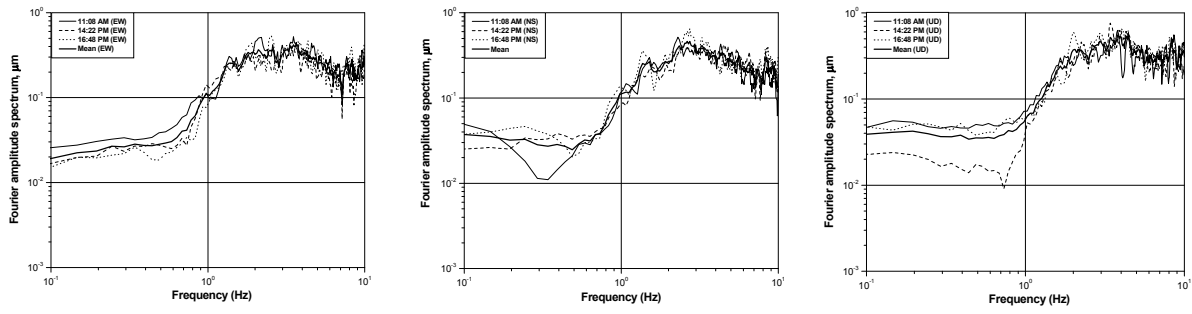
Figure 2.11 [(a), (b) and (c)]: Stability of Fourier Spectrum at different times along EW, NS and UD directions at MT11, MT12 and MT13.



(a) MT15

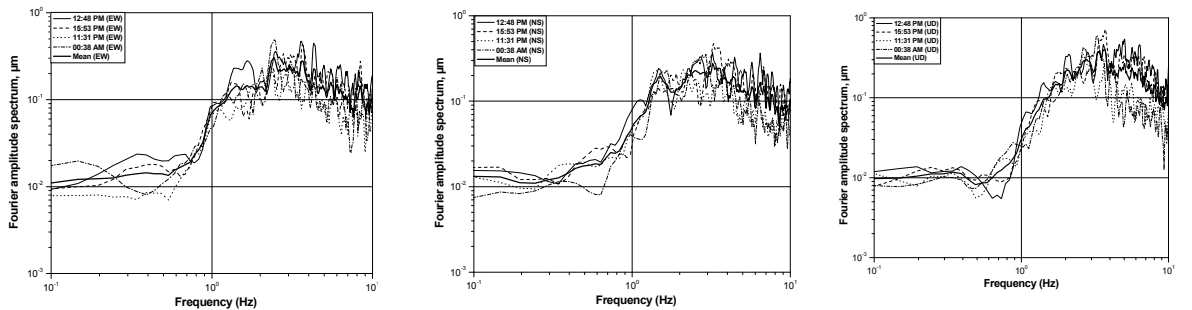


(b) MT16

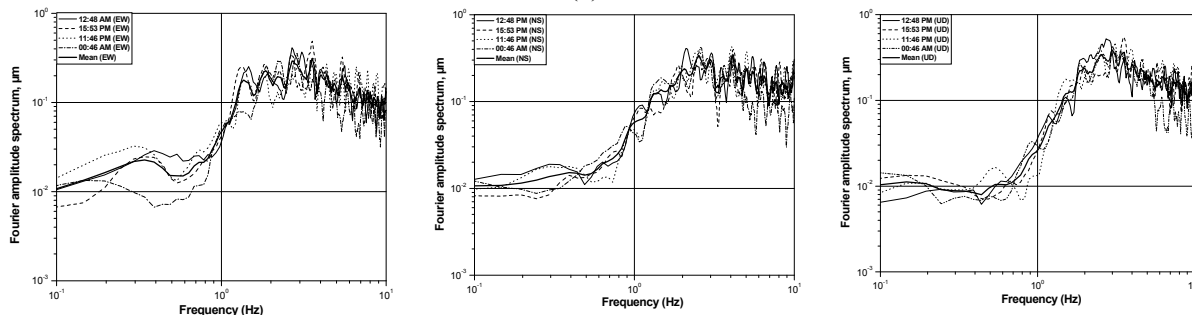


(c) MT19

Figure 2.12 [(a), (b) and (c)]: Stability of Fourier Spectrum at different times along EW, NS and UD directions at MT15, MT16 and MT19.



(a) MT22



(b) MT23

Figure 2.13 [(a) and (b)]: Stability of Fourier Spectrum at different times along EW, NS and UD directions at MT22 and MT23.

2.4.1.2 Stability of Horizontal to Vertical Spectral Ratio

The amplitude ratio calculated in this study is defined by Nakamura (1989). Amplitude ratios of Fourier amplitude spectra of EW and NS components, respectively, to that of the UD components, AR_{EW} and AR_{NS} , are obtained as follows:

$$AR_{EW} = \frac{F_{EW}}{F_{UD}} \quad AR_{NS} = \frac{F_{NS}}{F_{UD}} \quad (2.1)$$

Where, F_{EW} , F_{NS} and F_{UD} are the Fourier amplitude spectra in the EW, NS and vertical direction, respectively.

The Horizontal to Vertical spectral ratio along EW and NS directions are shown from Figure 2.14 to 2.18. In Figure 2.14, amplitude ratios, AR_{EW} and AR_{NS} of the Fourier spectra of two horizontal components, are shown for three different time instants (13:07 PM, 16:20 PM and 01:06 AM) of MT05, MT06 and MT07, respectively. The characteristics of the peak frequency of the amplitude ratios are different from those for Fourier spectra (Figure 2.9). The mean predominant frequency of two horizontal directions at MT05 and MT06 are stable. The mean predominant frequency of two horizontal directions at MT05 is around 0.77 whereas this value is around 0.94 at MT05 along EW and NS directions, respectively. The mean peak amplitude ratio is around 1.25 at MT07. Although the Fourier spectra are not stable with time, the amplitude ratios at different time instants along three directions within a day are stable at these sites.

Figure 2.15 shows stability of H/V ratio data at different time instants at MT08, MT09 and MT10 along EW and NS components, respectively. The peak Fourier amplitude ratios of MT08, which are around 1.20 Hz, are similar to the Fourier amplitude ratios at MT10. The peak amplitude ratio of MT09 is around 1.20 Hz along EW component and around 1.06 Hz along NS component, where the change of amplitude ratio of the spectra at different time instants of a day is comparatively small.

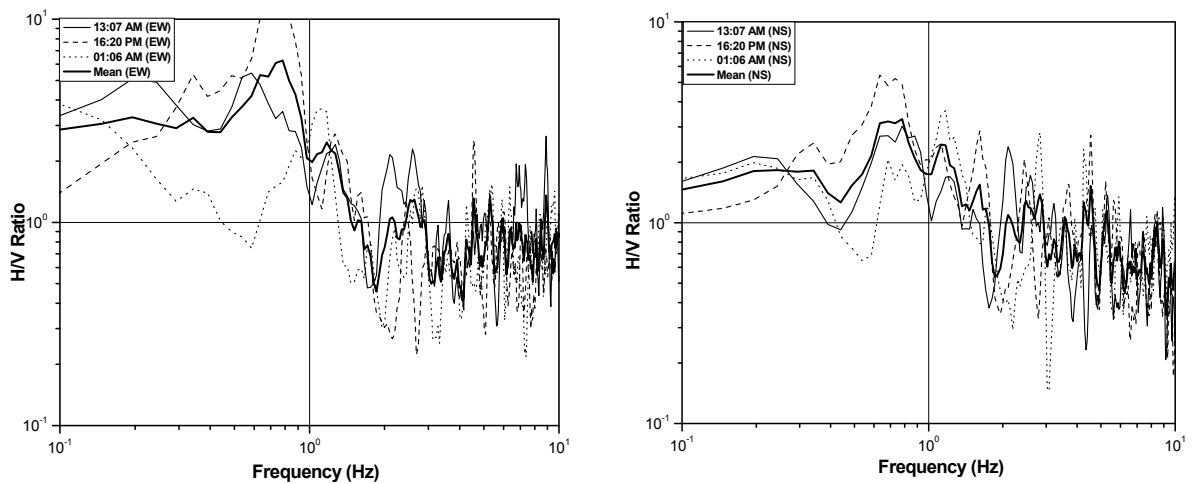
Figure 2.16 represents Stability of H/V ratio data at different time instants at MT11, MT12 and MT13 along EW and NS components, respectively. The peak Fourier amplitude ratios of MT10 varies between 0.78 Hz and 0.88 Hz where this value is around 0.93 Hz at MT12. The peak amplitude ratio of MT13 is around 1.22 Hz at MT13 in both Horizontal components.

The pattern of the amplitude spectra ratio at MT15, MT16 and MT19 are illustrated in Figure 2.17. Figure 2.17(a) and Figure 2.17(b) show the of amplitude change of Fourier spectra at three different time instants are comparatively small. The amplitude spectra ratio of four different time instants (15:12 PM, 17:15 PM, 00:27 AM and 00:56 AM) and their mean value are stable (Figure 2.17 (b)).

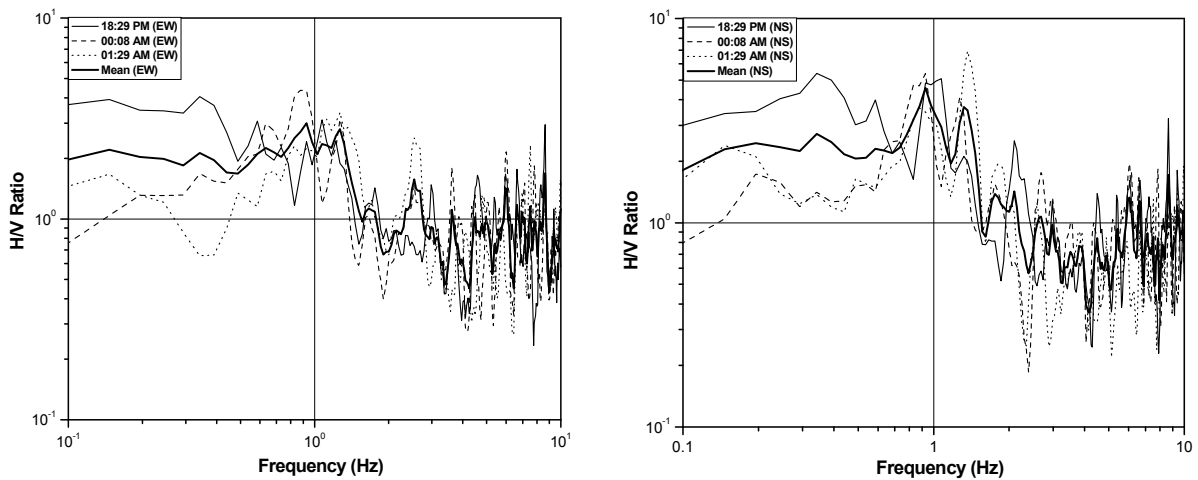
Figure 2.18 shows the stability of H/V ratio data at four different time instants at MT22 and MT23 along EW and NS components, respectively. Figure 2.18 (a) represent the amplitude spectra ratio of MT22 is around 0.96 Hz along EW component and around 0.73

Hz along NS component. The peak amplitude ratio of MT23 lies between 0.98 Hz and 1.32 Hz along the two horizontal directions. The change of amplitude spectra ratio at four different time instants (12:48 PM, 15:53 PM, 11:31 PM and 00:38 AM) at MT 22 and four different time instants (12:48 PM, 15:53 PM, 11:46 PM and 00:46 AM) at MT 23 are stable.

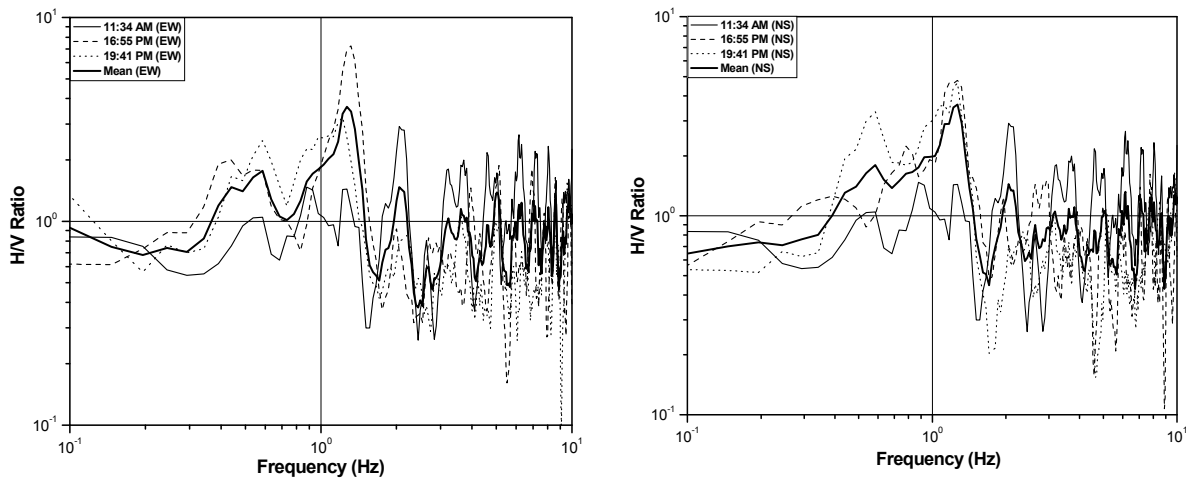
From analysis of Fourier spectra ratio from Figure 2.14 to 2.18, it can be concluded that the change of amplitude ratio at different time instants of a day is comparatively small. In addition to this, the amplitude ratio is less influenced by the source of vibration than the Fourier spectrum of any direction and may reflect the particular characteristics of the site. Therefore, the Horizontal to Vertical spectra ratio has been found more reliable to estimate dynamic properties (Predominant frequency and Amplification) of any particular soil.



(a) MT05

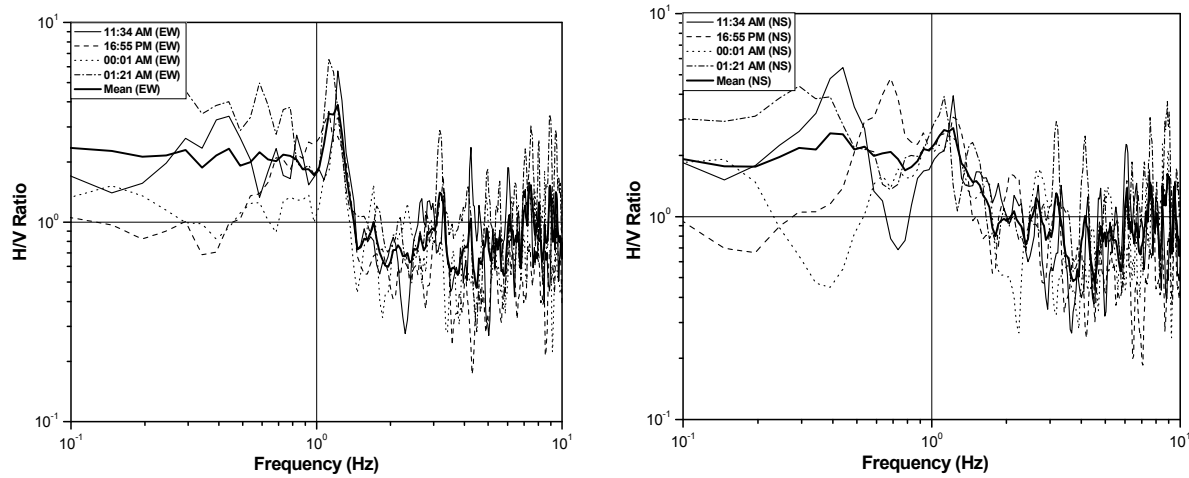


(b) MT06



(c) MT07

Figure 2.14 [(a), (b) and (c)]: Stability of H/V ratio data at different times along EW and NS direction at MT05, MT06 and MT07.



(a) MT08

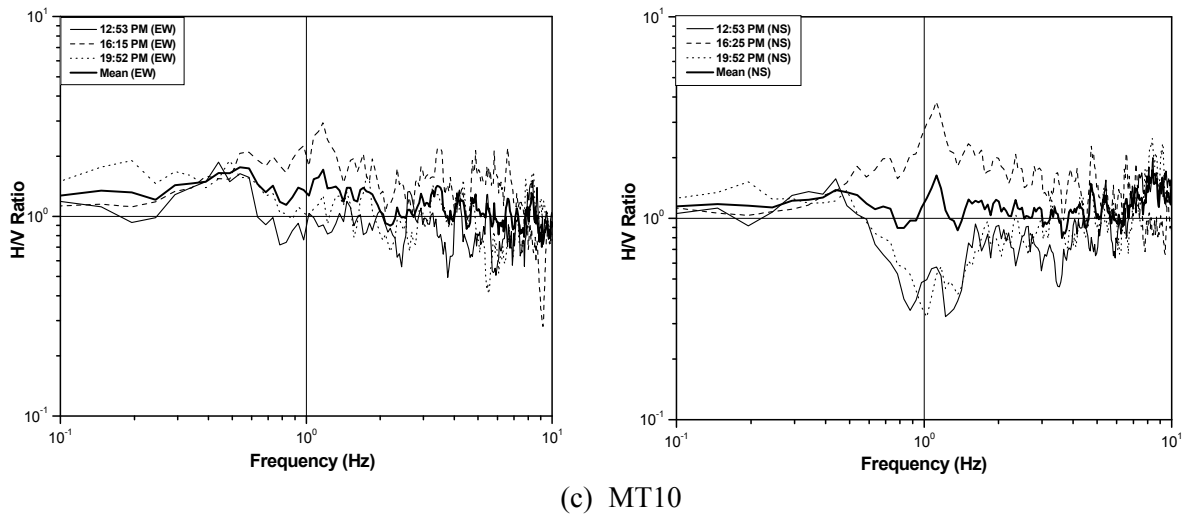
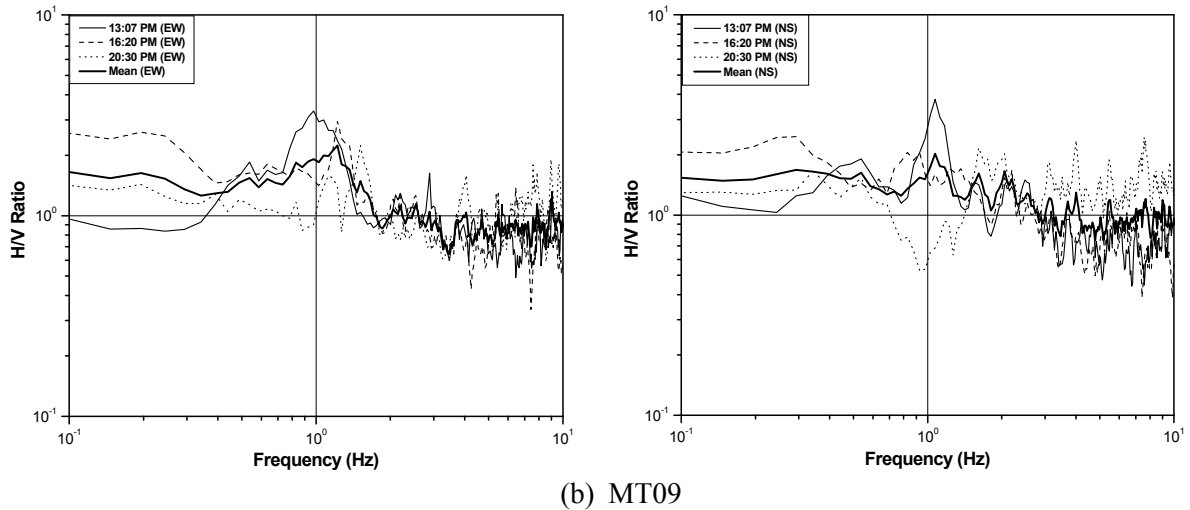
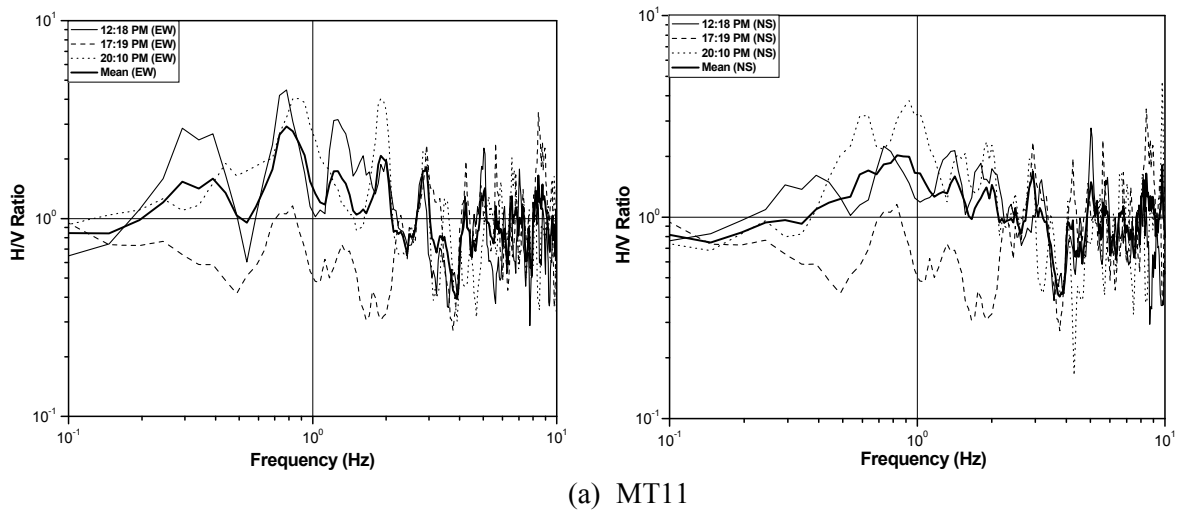
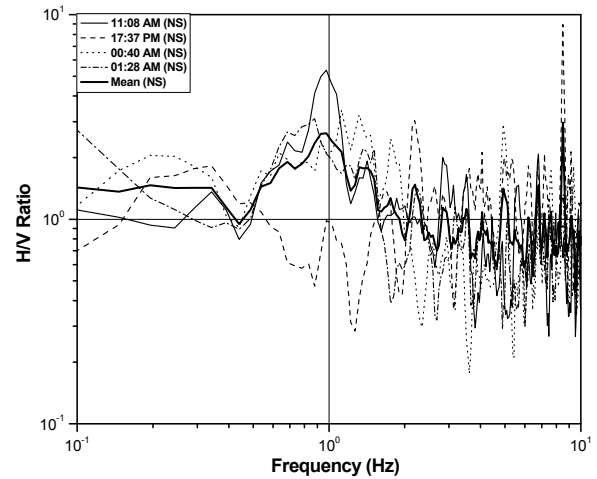
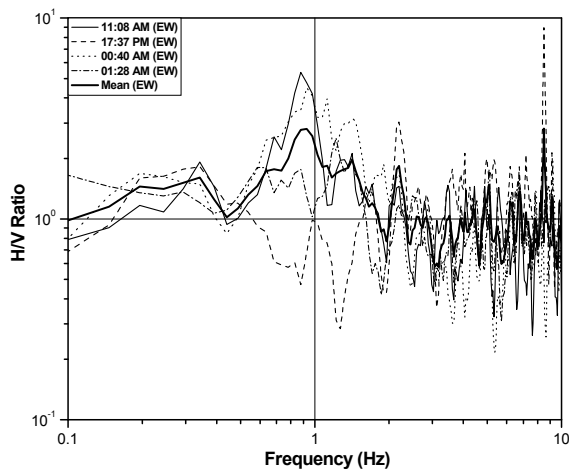
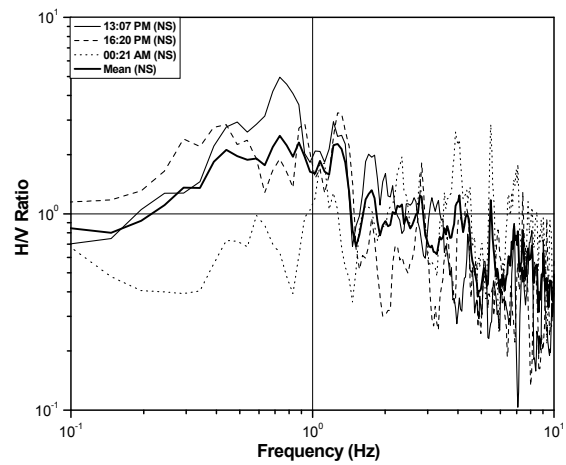
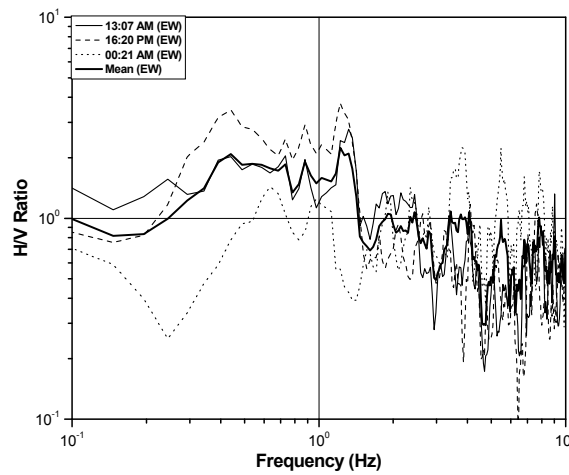


Figure 2.15 [(a), (b) and (c)]: Stability of H/V ratio data at different times along EW and NS direction at MT08, MT09 and MT10.



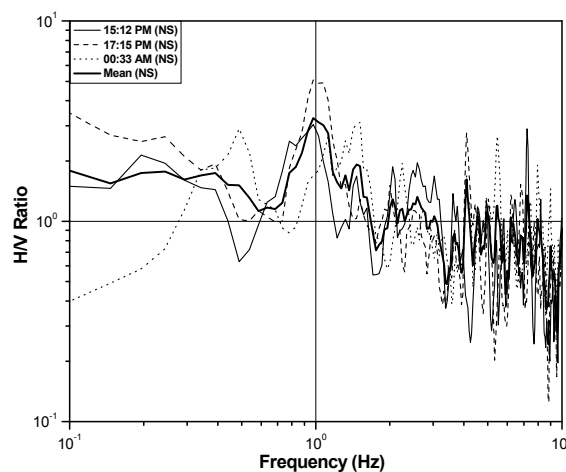
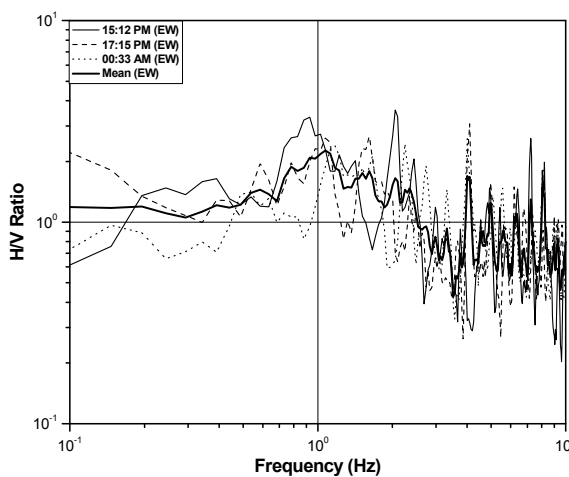


(b) MT12

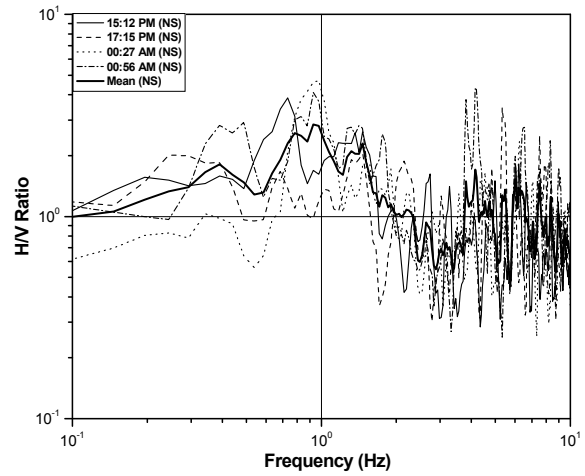
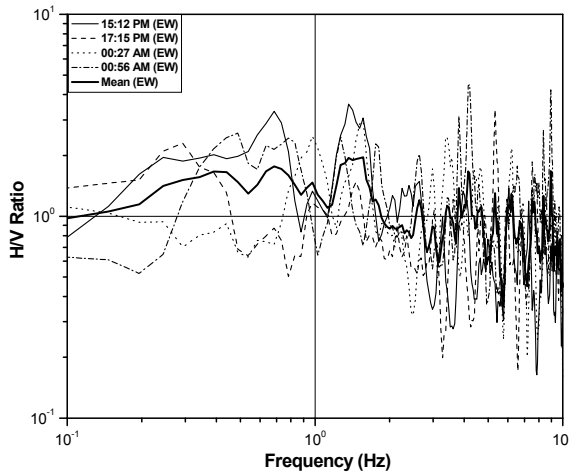


(c) MT13

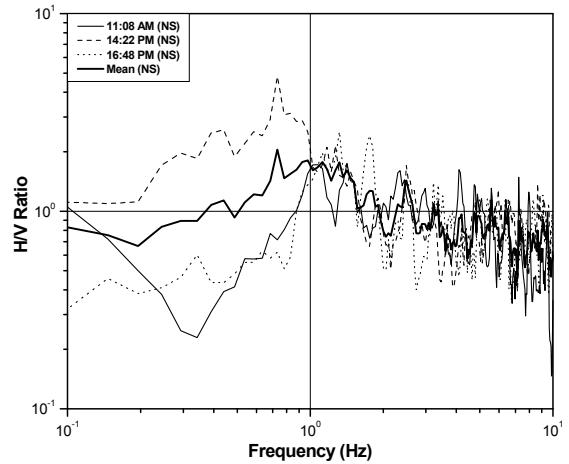
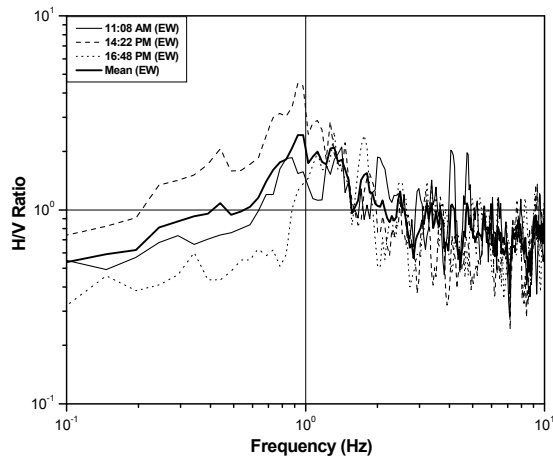
Figure 2.16 [(a), (b) and (c)]: Stability of H/V ratio data at different times along EW and NS direction at MT11, MT12 and MT13.



(a) MT15

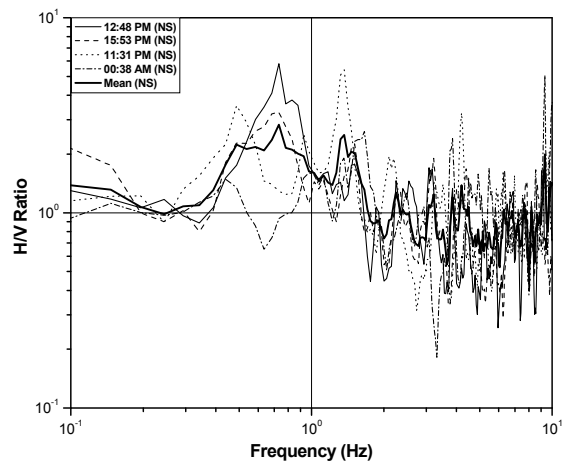
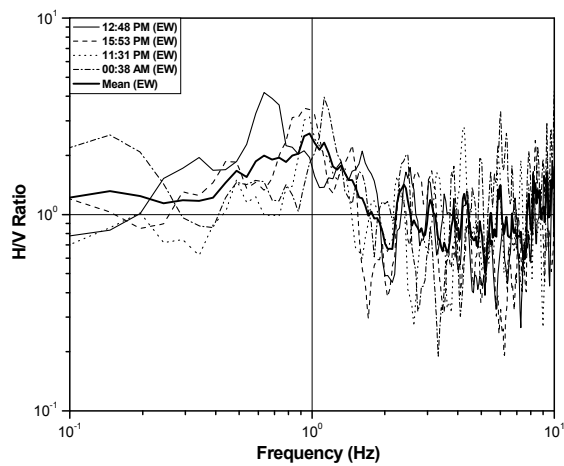


(b) MT16



(c) MT19

Figure 2.17 [(a), (b) and (c)]: Stability of H/V ratio data at different times along EW and NS direction at MT15, MT16 and MT19.



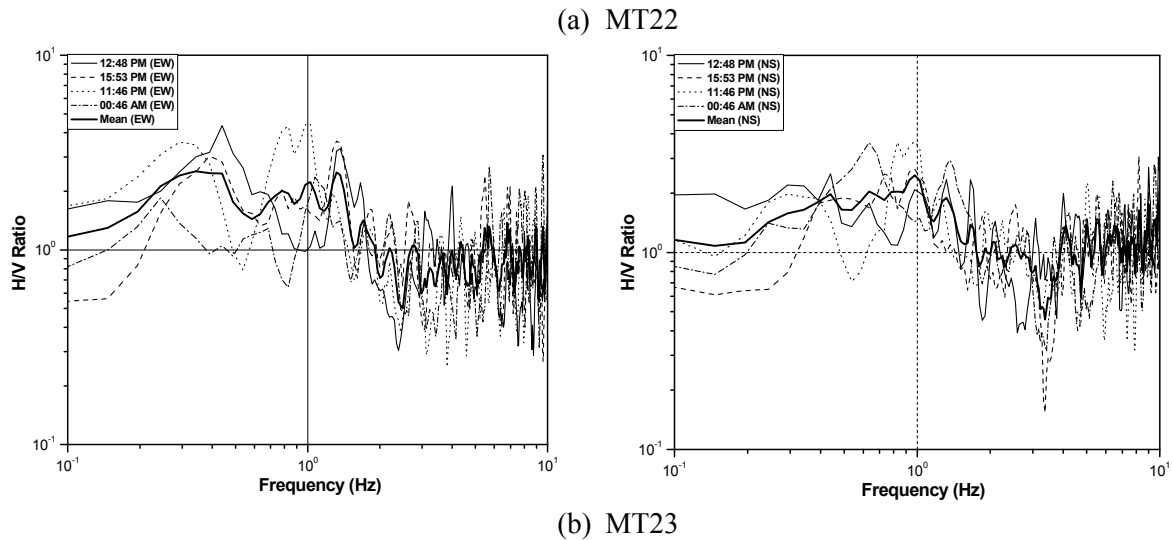


Figure 2.18 [(a) and (b)]: Stability of H/V ratio data at different times along EW and NS direction at MT22 and MT23.

2.4.2 Resultant of H/V Ratio Curve

Microtremor H/V ratio has been found along East-West and North-South direction, respectively. To estimate Predominant frequency and H/V ratio resultant of two direction spectrum is necessary. Four resultant of two direction H/V ratio curve are RM, RMS, RS and mean. The resultant H/V ratio can be represented in four ways. These are follows:

(a) Root multiplication, RM:

$$RM = \sqrt{HV_{EW} * HV_{NS}}$$

(b) Root mean square, RMS:

$$RMS = \sqrt{\frac{HV_{EW}^2 + HV_{NS}^2}{2}}$$

(c) Root square, RS:

$$RS = \sqrt{HV_{EW}^2 + HV_{NS}^2}$$

(d) Mean = $\frac{HV_{EW} + HV_{NS}}{2}$

Where,

HV_{EW} = Horizontal to Vertical Spectral Ratio along East-West direction

HV_{NS} = Horizontal to Vertical Spectral Ratio along North-South direction

The resultant H/V ratio has been shown from Figure 2.19 to Figure 2.21. These three graphs represent the comparison of H/V ratio resultant in four ways.

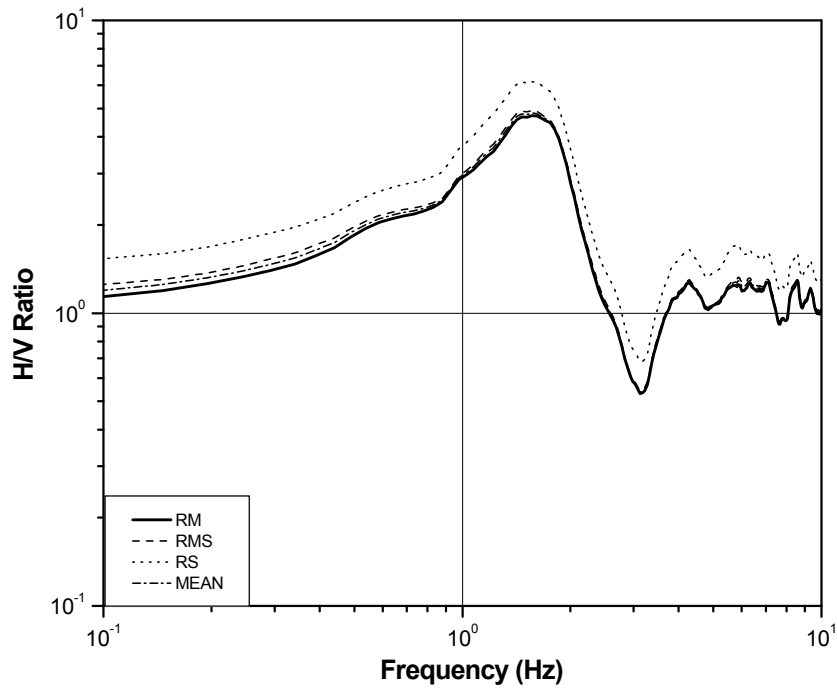


Figure 2.19: Comparison of RM, RMS, RS and MEAN resultant H/V ratio of EW and NS direction at Bashundhara, Block-D.

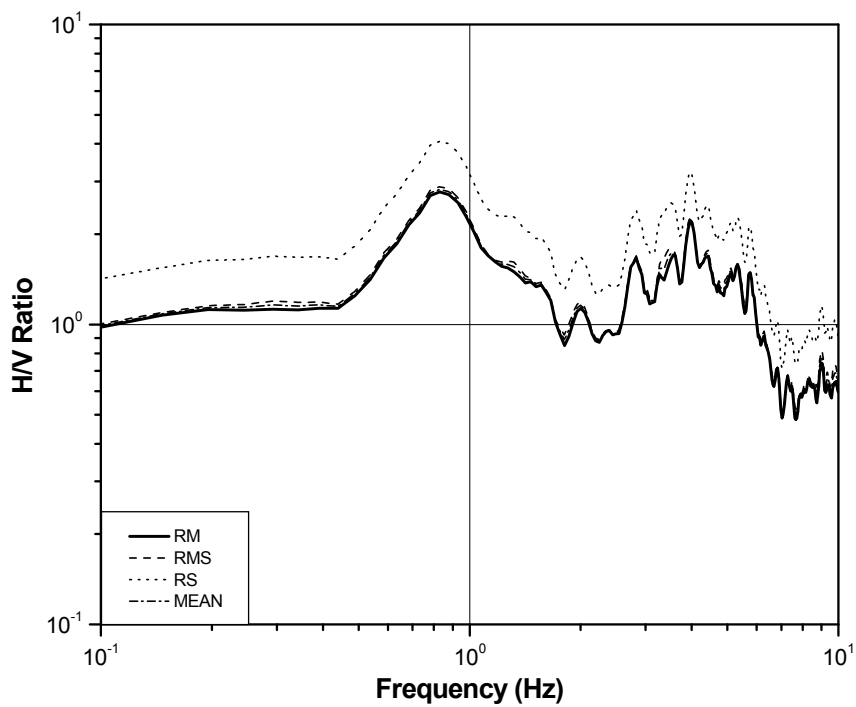


Figure 2.20: Comparison of RM, RMS, RS and MEAN resultant H/V ratio of EW and NS direction at Board Bazar, Gazipur.

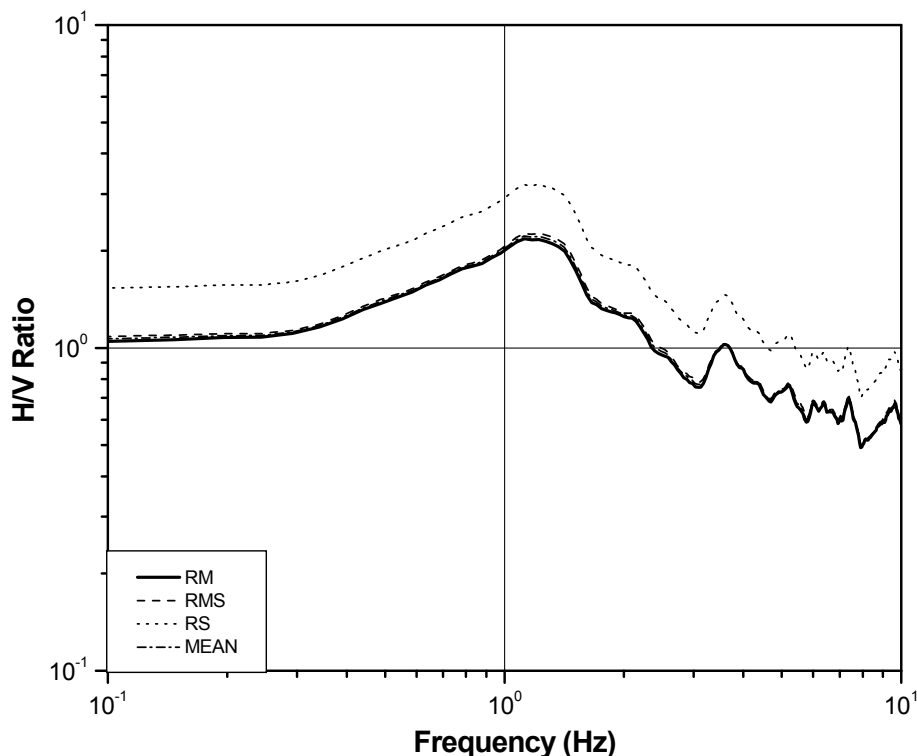


Figure 2.21: Comparison of RM, RMS, RS and MEAN resultant H/V ratio of EW and NS direction at Uttar Khan.

Figure 2.19 shows comparison of RM, RMS, RS and MEAN resultant H/V ratio of EW and NS direction at Bashundhara, Block-D. Figure 2.20 and 2.21 demonstrate comparison of H/V ratio in Board Bazar, Gazipur and Uttar Khan, respectively. From Figure 2.19 to Figure 2.21, it can be said that square root H/V ratio shows higher value than others. The RM, RS and mean H/V ratio show almost similar value. For this study, Root multiplication H/V ratio has been analyzed to estimate predominant frequency and H/V ratio.

2.4.3 Window Effect on Microtremor data

Fourier transformation using various analysis windows has significant effect on Horizontal to Vertical spectral ratio (H/V). The most common five types of analysis windows are Rectangular, Hanning, Hamming, Welch and Blackman windows. Fast Fourier transformation can be done in five time windows. The equations of five windows are shown from Equation 2.2 to Equation 2.6. These equations are follows:

- 1) Rectangular Window

$$W[n] = 1 \text{ for } 0 \leq n \leq N \text{ and zero otherwise} \tag{2.2}$$
- 2) Welch Window:

$$W[n] = 1 - \left[\frac{n - \frac{1}{2}(N-1)}{\frac{1}{2}(N+1)} \right]^2 \quad (2.3)$$

3) Hanning Window:

$$W[n] = \frac{1}{2} \left[1 - \cos \left(\frac{2\pi n}{N-1} \right) \right] \quad (2.4)$$

4) Hamming Window

$$W[n] = 0.54 - 0.46 \cos \left(\frac{2\pi n}{N-1} \right) \quad (2.5)$$

5) Blackman Window:

$$W[n] = 0.42 - 0.5 \cos \left(\frac{2\pi n}{N-1} \right) + 0.08 \cos \left(\frac{4\pi n}{N-1} \right) \quad (2.6)$$

Where,

$W[n]$ = Windows function, n = Index number and N = Total number of data points

Figure 2.22 to 2.25 show the analysis result of microtremor data of three segments at Bramangaon. Microtremor Time history data of three segments has been Fourier transformed using five windows. Figure 2.22 shows the analysis result of segment 1 in five windows at Bramangaon. From Figure 2.22, rectangular window shows different H/V ratio result than other four windows. The other four H/V curve gives almost similar pattern. However, predominant frequency is same in all the five cases. Rectangular window gives lower peak value of H/V ratio than other methods at segment 2 (Figure 2.23). From Figure 2.24, the rectangular window shows similar predominant frequency and H/V ratios to other windows. The mean H/V ratio and predominant frequent of five methods are represented in Figure 2.25. According to Figure 2.25, the pattern of H/V ratio curve in rectangular window is similar to other four windows. From the analysis of mean H/V ratio curve in five windows, it can be said that rectangular window is more suitable than other windows to estimate predominant frequency and H/V ratio. Therefore, rectangular window is selected to analyze the microtremor data in this study. This rectangular windows is suitable than others to assess dynamic properties.

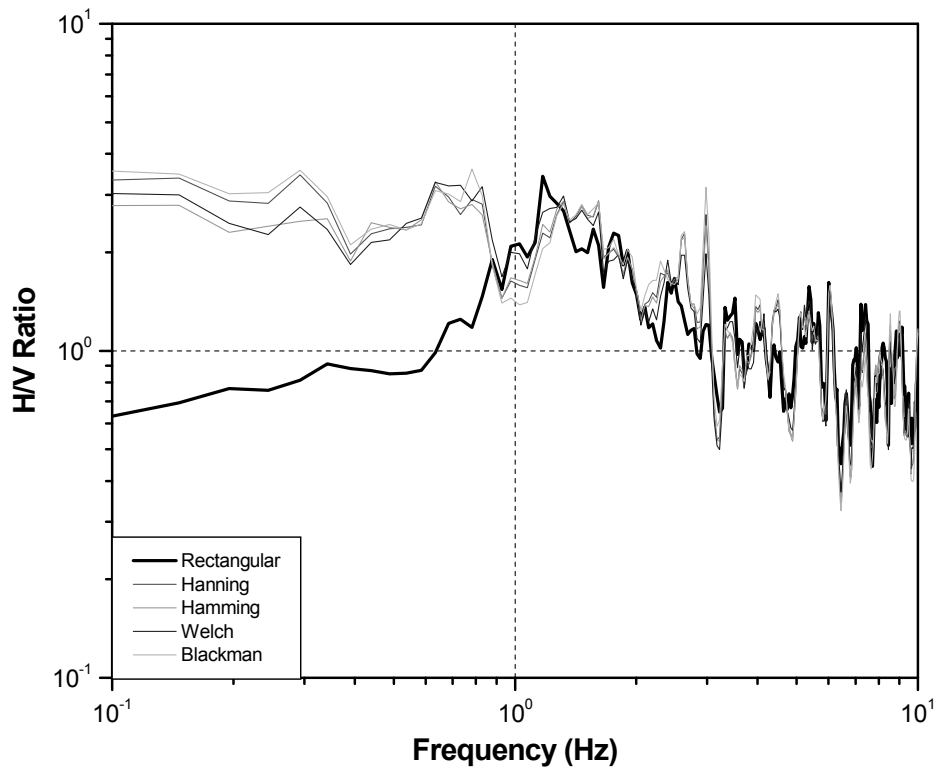


Figure 2.22: Five different windows effect on Microtremor data at segment 1 of Bramangaon.

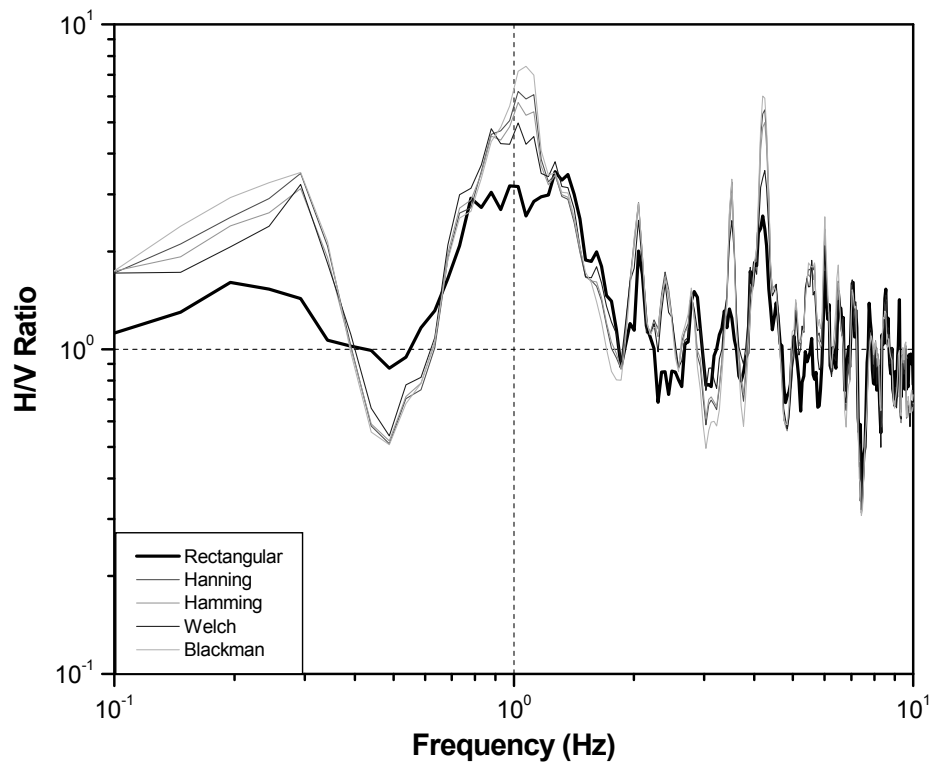


Figure 2.23: Five different windows effect on Microtremor data at segment 2 of Bramangaon.

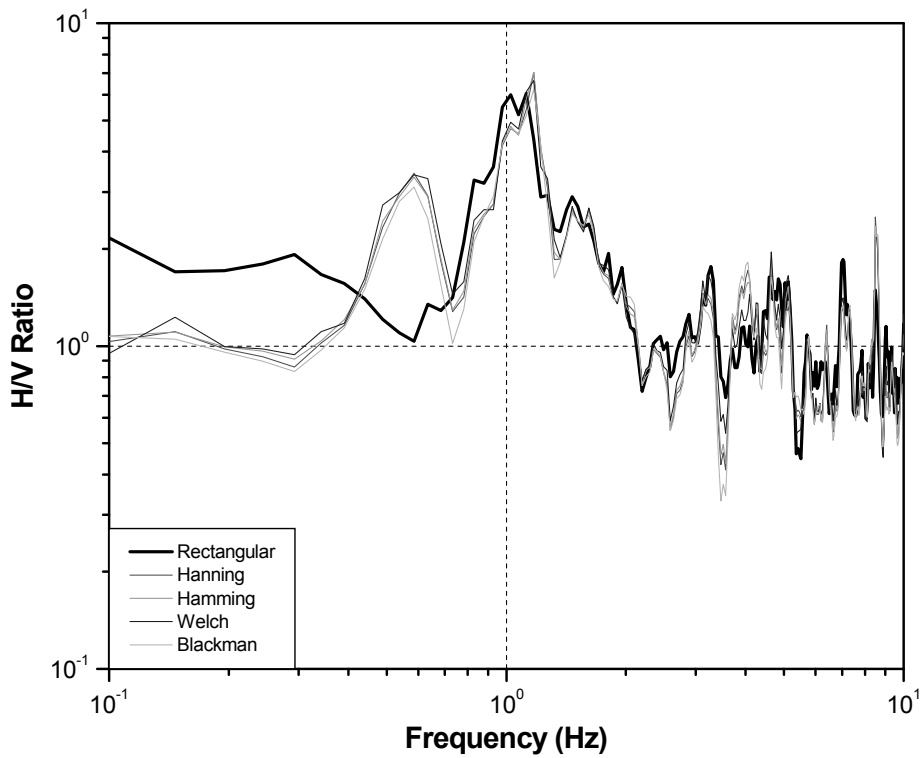


Figure 2.24: Five different windows effect on Microtremor data at segment 3 of Bramangaon.

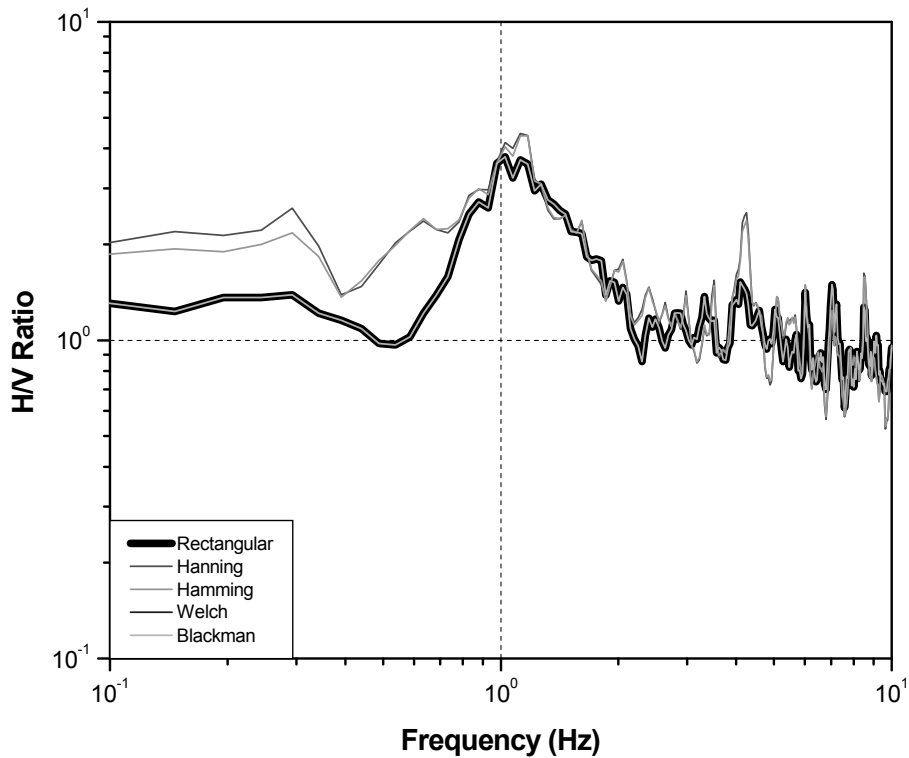


Figure 2.25: Five different windows effect on mean microtremor data at Bramangaon.

2.4.4 Smoothing Effect on Microtremor Data

Smoothing of microtremor data has significant effect to estimate predominant frequency and H/V ratio of any particular site. In some microtremor measurement locations, it is difficult to estimate dynamic properties. In that case, smoothing of data with suitable smoothing point gives accurate data. Therefore, almost all the microtremor locations data has been smoothed with suitable smoothing point. Generally, H/V ratio decreases and predominant frequency changes with the increase of smoothing point. So, proper justification is required before applying smoothing point on microtremor logarithmic window. Figure 2.26 to 2.29 show four mean microtremor data with smoothing effect. Different smoothing points have been applied to determine predominant frequency and H/V ratio. Figure 2.26 shows that the peak H/V becomes decreases due to applying different smoothing point. Figure 2.27, 2.28 and 2.29 illustrate the application of suitable smoothing point to determine Predominant frequency and H/V ratio of soil. It is difficult to determine predominant frequency and H/V ratio.

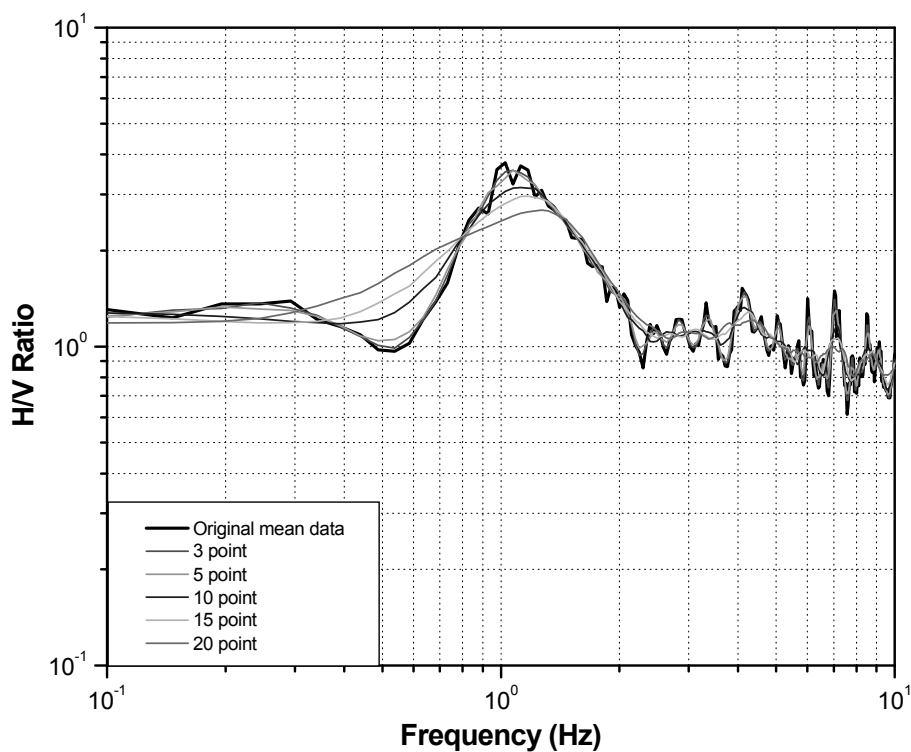


Figure 2.26: Variation of predominant frequency and H/V ratio due to smoothing effect at Bramangaon.

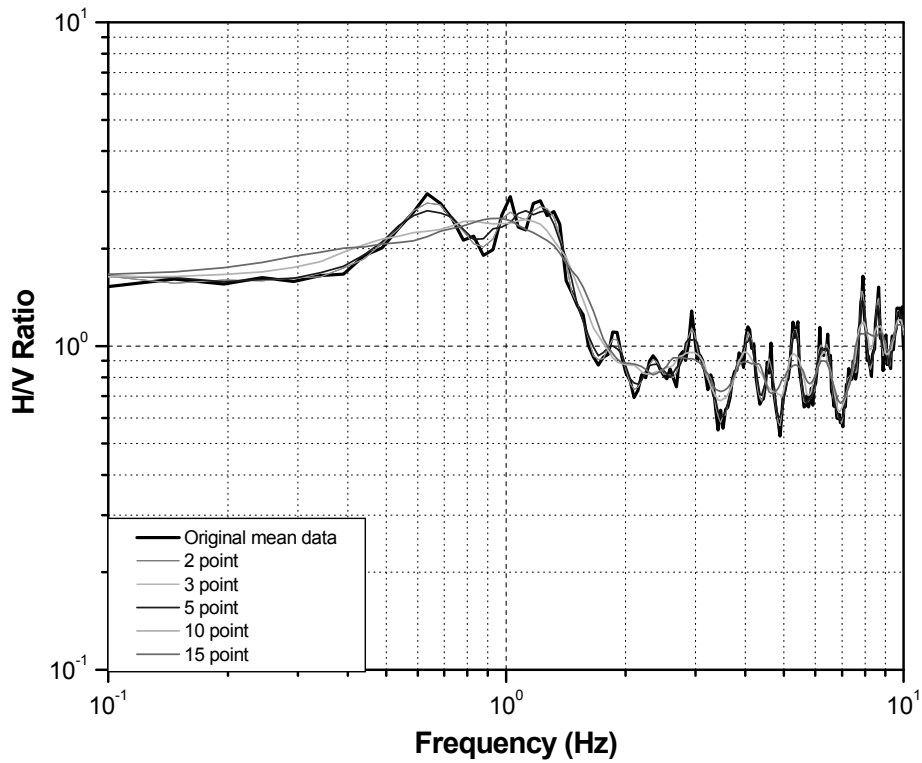


Figure 2.27: Variation of predominant frequency and H/V ratio due to smoothing effect at Tongi, Ershadnagar.

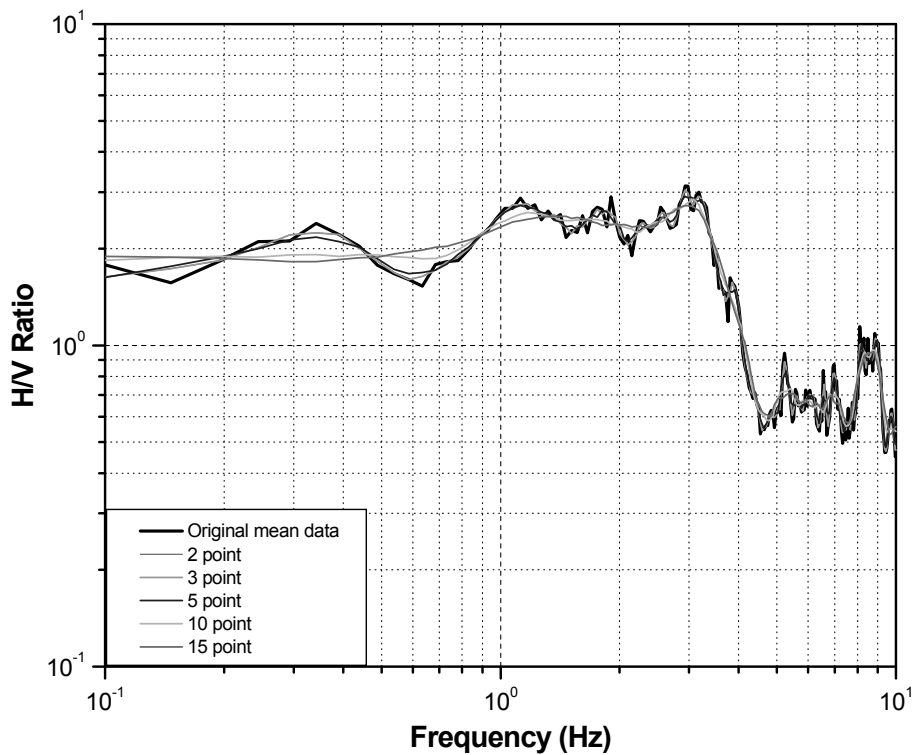


Figure 2.28: Variation of predominant frequency and H/V ratio due to smoothing effect at Ashiyan city.

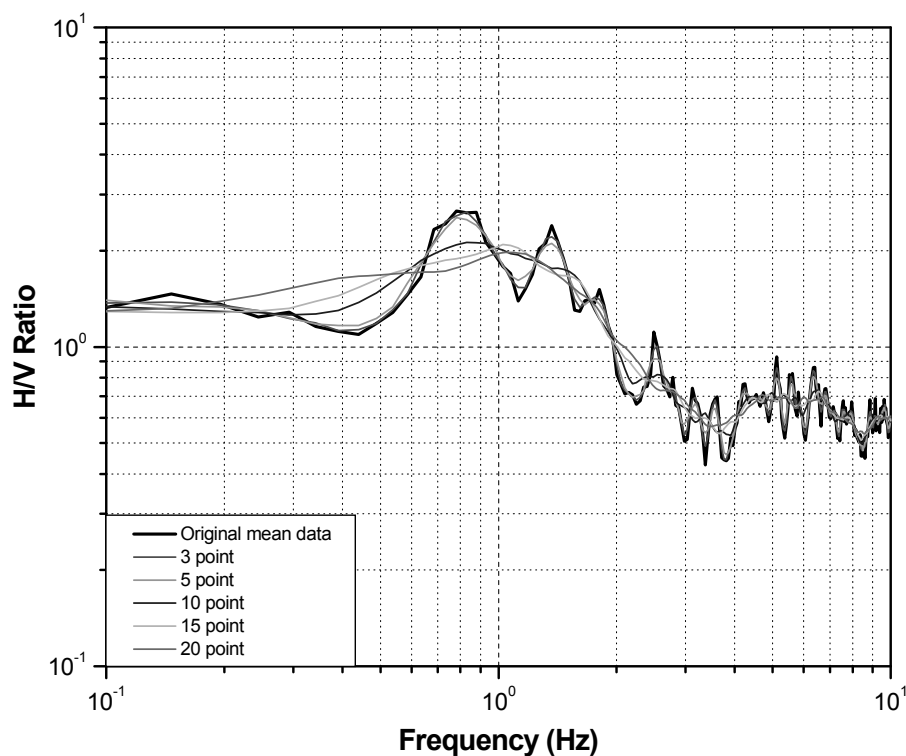


Figure 2.29: Variation of predominant frequency and H/V ratio due to smoothing effect at Agargaon Trade Fair.

2.5 ANALYSIS RESULT

Field time history microtremor data of 132 locations within BUET campus and 45 sites in and around Dhaka city has been analyzed according to section 2.4. The mean H/V ratio and standard deviation at 45 locations has been included in this chapter. The remains of analysis results of these locations are shown in APPENDIX-B. Microtremor analysis results at 132 locations in soil and 45 buildings within BUET campus are presented in this chapter. But, details Figures are illustrated in APPENDIX-C and APPENDIX-D.

2.5.1 Microtremor Analysis Result in and around Dhaka City

Microtremor measurement has been carried out in 45 locations at latitude lies from $23^{\circ}38'15.10''$ to $23^{\circ}56'46.54''$ and longitude lies from $90^{\circ}20'24.92''$ to $90^{\circ}33'50''$. Obtained velocity records are converted from time domain to frequency domain to get the Fourier Spectrum and it has been smoothed by using rectangular window with average smoothing point 5.

Table 2.16: Microtremor Test Location, Predominant Frequency and H/V ratio in and around the Dhaka city

Serial Number	ID	Location	Latitude	Longitude	Predominant Frequency	H/V Ratio (RM)
1	SBH-01	National University	23°56'46.54"	90°22'43.93"	1.24	2.59
2	SBH-02	Board Bazaar, Gazipur	23°56'18"	90°23'58"	0.82	2.73
3	SBH-03	Kaunia, Boro Bari, Moddopara	23°55'37"	90°23'03"	0.72	2.79
4	SBH-04	Tongi, Ershadnagar	23°54'48"	90°24'11"	0.97	2.51
5	SBH-05	Tongi BSCIC area	23°53'37.18"	90°25'13.35"	0.95	2.73
6	SBH-06	Abdullahpur	23°52'31"	90°24'01"	1.32	2.33
7	SBH-07(A)	Ijtema field (North and East side)	23°53'31.13"	90°23'53.39"	1.17	3.37
8	SBH-07(B)	Ijtema Field (South and West side)	23°52'59.96"	90°23'37.91"	0.86	3.26
9	SBH-08	Ashulia Toll Plaza	23°53'25.40"	90°21'54.61"	1.14	1.75
10	SBH-9	Uttar Khan	23°52'30"	90°25'28"	1.09	2.09
11	SBH-10(A)	Uttara Phase 3 (North side)	23°52'22"	90°21'40"	1.18	3.16
12	SBH-10(B)	Uttara Phase 3 (South side)	23°51'15"	90°21'16"	0.97	4.47
13	SBH-11	Azampur School, Uttara	23°52'03"	90°24'04"	3.65	2.73
14	SBH-12(A)	Mirpur DOHS (South side)	23°49'59"	90°22'42"	1.54	2.46
15	SBH-12(B)	Mirpur DOHS (North side)	23°50'11"	90°22'42"	1.21	3.44
16	SBH-13	Ashiyon city, Askona, Dakkhin Khan	23°50'49"	90°25'37"	1.12	3.19
17	SBH-14(A)	Purbachal-1, Randokpur Hazi bari, Rupganj	23°45'03"	90°31'17"	0.94	3.04
18	SBH-14(B)	Purbachal-2, American City	23°49'33"	90°33'50"	2.00	2.69
19	SBH-14(C)	Purbachal Picnic Park, Gazipur	23°51'28"	90°31'14"	1.34	2.23
20	SBH-15	Adjacent to Mirpur Zoo	23°49'04.14"	90°20'29.63"	1.52	2.43
21	SBH-16	Field Ground, Pallabi	23°49'06"	90°22'08"	1.24	2.64
22	SBH-17(A)	Block-B, Basundhara	23°48'38"	90°25'54"	2.09	3.12
23	SBH-17(B)	Block-D, Basundhara	23°49'00.49"	90°26'12.95"	1.57	4.71
24	SBH-17(C)	Block-H, Basundhara	23°49'19"	90°26'34"	2.52	2.94

Serial Number	ID	Location	Latitude	Longitude	Predominant Frequency	H/V Ratio (RM)
25	SBH-18	Civil Aviation Quarter	23°50'33.61"	90°25'11.22"	0.64	3.70
26	SBH-19	Kuril Flyover	23°49'41.51"	90°26'32.06"	1.97	2.73
27	SBH-20	Sarengbari, Mipur-2	23°48'03.24"	90°20'47.10"	0.59	2.84
28	SBH-21	Purachal, Uttar Badda	23°46'51"	90°26'29"	2.11	2.59
29	SBH-22	City Corporation, Gabtoli	23°46'41.99"	90°20'24.92"	0.82	3.67
30	SBH-23	Adabor	23°46'09.75"	90°21'37.62"	3.35	2.26
31	SBH-24	Agargoan Trade Fair area	23°46'10.56"	90°22'42.73"	0.86	2.12
32	SBH-25	Aftab Nagar Housing Project	23°46'04.98"	90°26'03.22"	0.95	2.76
33	SBH-26	Umme Had Nagar, Nadda	23°47'57.17"	90°25'41.61"	1.32	3.83
34	SBH-27	South Banasree	23°45'07.17"	90°26'45.36"	1.39	3.86
35	SBH-28	Basila Garden City	23°45'10.29"	90°20'42.36"	1.12	4.47
36	SBH-29	Royer Bazar Boddhobumi	23°44'54"	90°21'28"	2.57	1.08
37	SBH-30	Kalunagar, Hazaribagh	23°43'38.50"	90°22'08.62"	0.83	3.86
38	SBH-31	Rab-10, Plot, Kamrangirchar	23°42'57.58"	90°22'42.11"	0.48	3.91
39	SBH-32	Sosan Ghat, Kamrangirchar	23°42'44.81"	90°23'26.51"	1.21	4.78
40	SBH-33	Basundhara River view	23°39'10"	90°26'09"	1.05	3.51
41	SBH-34	Matuail, Demra	23°43'18.24"	90°28'16.48"	2.77	2.48
42	SBH-35	Jilmil Project, Equria	23°40'33.40"	90°24'08.42"	1.00	3.26
43	SBH-36	Rajendapur	23°39'25"	90°22'58"	1.17	2.59
44	SBH-37	Bramangaon	23°38'15.10"	90°27'37.35"	1.08	3.55
45	SBH-38	Meradia, Uttar Banasree	23°45'43.57"	90°26'19.67"	1.26	2.84

Table 2.16 shows predominant frequency and square root of Horizontal to Vertical spectral ratio (H/V) at 45 locations in and around the Dhaka city. The locations, latitude and longitude of 45 locations are also demonstrated in Table 2.16. Figure B2.30 represents the comparison of predominant frequency and H/V ratio among these locations. Details of predominant frequency, mean H/V ratio and standard deviation are illustrated

from Figure B2.31 to Figure A2.75. The basic six H/V ratio, square root of H/V ratio in three segments and their mean H/V ratio are also illustrated in APPENDIX-B.

Table 2.16 shows the predominant frequency and H/V ratio at 45 locations. Out of 45 microtremor observation locations, the maximum predominant frequency is 3.65 Hz, where H/V ratio is 2.73, at Azampur School, Uttara (Lat. 23°52'03" and Long. 90°24'04"). The geology of this location is Upper Modhupur terrace (Figure 3.2) and Moderately High Pleistocene terrace (Figure 2.3). Figure 2.30 shows the Horizontal to Vertical spectral ratio (H/V) ranging between 1.81 and 3.74. The basic six H/V ratio in three segments along EW and NS direction, H/V ratio of three segments and their mean value are shown in Figure B2.43. On the other hand, the minimum predominant frequency is 0.48 Hz, where H/V ratio is 3.91, Rab-10, Plot, Kamrangirchar (Lat. 23°42'57.58" and Long. 90°22'42.11"). This location is classified as River Bar (Figure 3.2) and Moderately Thick fill (Figure 3.3). Figure 2.31 demonstrates square root of Horizontal to Vertical spectral ratio (H/V) ranging between 2.23 and 5.65.

From Table 2.16, the maximum Horizontal to Vertical spectral ratio (H/V) is 4.78 where as predominant frequency is 1.22 Hz, at Sosan Ghat, Kamrangirchar (Lat. 23°42'44.81" and Long. 90°23'26.51"). The geology of this site is flood plain (Figure 2.2) and thick fill (Figure 2.3). Figure 2.32 shows Horizontal to Vertical spectral ratio (H/V) ranging between 4.07 and 5.71. The basic six H/V ratio in three segments along EW and NS direction, H/V ratio of three segments and their mean value are shown in Figure B2.69. The minimum Horizontal to Vertical spectral ratio (H/V) is 1.08 where as predominant frequency is 2.57 Hz at Royer Bazar (Lat. 23°44'54" and Long. 90°21'28"). The geology of this location is River Bar (Figure 2.2) and gently sloping Erosional terrace edge (Figure 2.3). Figure 2.33 shows Horizontal to Vertical spectral ratio (H/V) ranging between 0.87 and 1.28. The basic six H/V ratio in three segments along EW and NS direction, H/V ratio of three segments and their mean value are illustrated in Figure B2.66.

Out of 45 locations, the overall predominant frequency is 1.25 Hz with standard deviation 0.014. On the other hand, the overall H/V ratio is 2.72 with standard deviation 0.177. The predominant frequency of 45 locations has been classified into five types which are **Type I** (0 – 0.49), **Type II** (0.50 – 0.99), **Type III** (1.0 – 1.99), **Type IV** (2.0 – 2.99) and **Type V** (> 3.00).

The classifications of predominant frequency at 45 locations are as follows:

Type I: SBH-31

Type II: SBH-02, SBH-03, SBH-04, SBH-05, SBH-07(B), SBH-10(B), SBH-14(A), SBH-18, SBH-20, SBH-22, SBH-24, SBH-25 and SBH-30.

Type III: SBH-01, SBH-06, SBH-07(A), SBH-08, SBH-09, SBH-10(A), SBH-12(A), SBH-12(B), SBH-13, SBH-14(C), SBH-15, SBH-16, SBH-17(B), SBH-19, SBH-26, SBH-27, SBH-28, SBH-32, SBH-33, SBH-35, SBH-36, SBH-37 and SBH-38.

Type IV: SBH-14(B), SBH-17(A), SBH-17(C), SBH-21, SBH-29 and SBH-34.

Type V: SBH-11 and SBH-23.

From this classification of predominant frequency, it can be said that most of the locations predominant frequency varies from 1.0 Hz to 1.99 Hz. These are classified as **Type III**. This classifications show the second most common predominant frequency ranging between 0.50 and 0.99. The number of locations predominant frequency ranging between 2.0 and 2.99 is six. Only SBH-31 is classified as **Type I** predominant frequency.

On the other hand, Horizontal to Vertical spectral ratio (H/V) has been classified into four types. **Type I** (0-0.99), **Type II** (1.0 – 1.99), **Type III** (2.0 – 2.99) and **Type IV** (>3.0).

The classifications of H/V ratio at 45 locations are as follows:

Type I: None

Type II: SBH-08, SBH-12(B), SBH-14(C), SBH-15, SBH-16, SBH-17(B), SBH-29 and SBH-39.

Type III: SBH-01, SBH-02, SBH-03, SBH-04, SBH-05, SBH-06, SBH-09, SBH-11, SBH-12(A), SBH-14(B), SBH-17(A), SBH-17(C), SBH-19, SBH-20, SBH-21, SBH-23, SBH-24, SBH-25, SBH-34, SBH-36 and SBH-38.

Type IV: SBH-07(A), SBH-07(B), SBH-10(A), SBH-10(B), SBH-13, SBH-14(A), SBH-18, SBH-22, SBH-26, SBH-27, SBH-28, SBH-30, SBH-31, SBH-32, SBH-33, SBH-37 and SBH-39.

From the above classification of H/V ratio, the common H/V ratio is **Type III** in 45 locations. The second most common H/V ratio is **Type IV**. The number of locations H/V ratio ranging between 1.0 and 1.99 is eight.

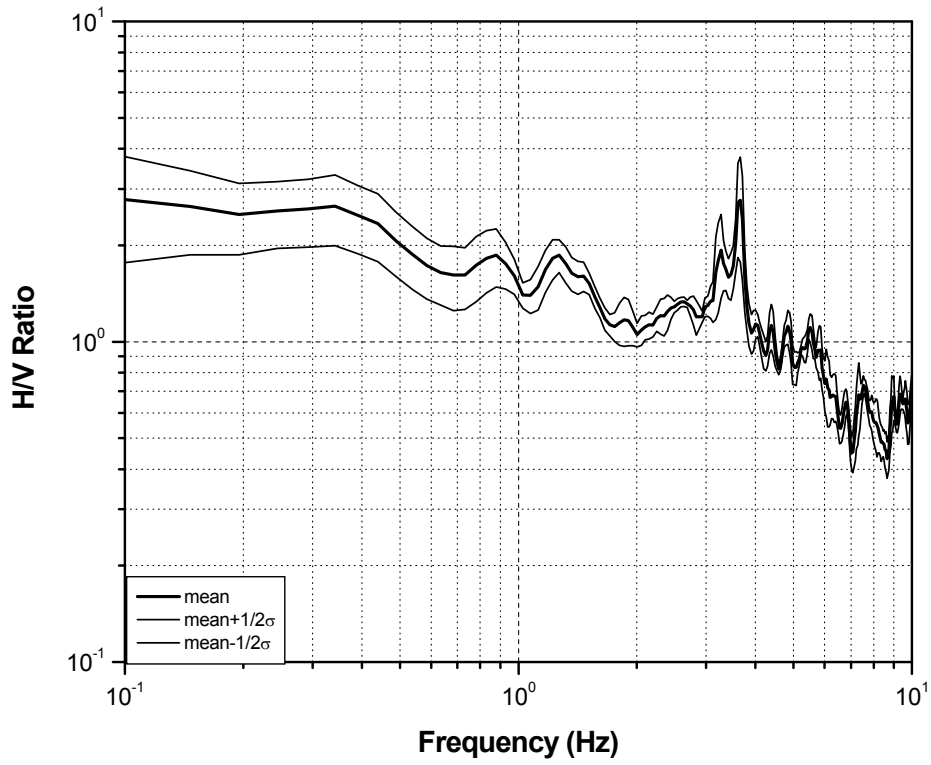


Figure 2.30: Predominant frequency and H/V ratio at Uttara Azampur.

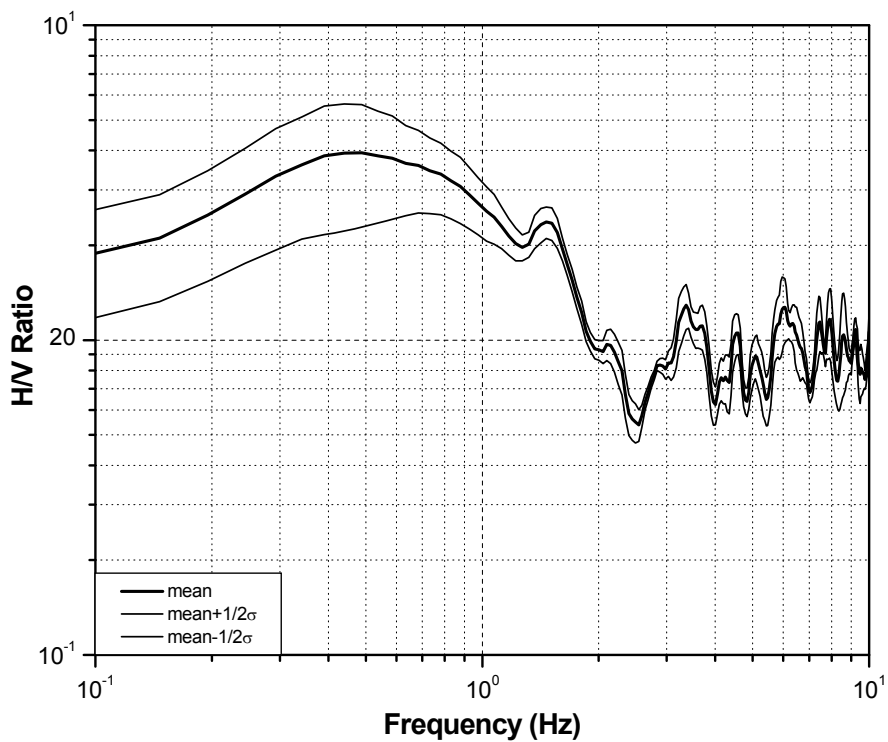


Figure 2.31: Predominant frequency and H/V ratio at Rab-10 Plot, Kamrangirchar.

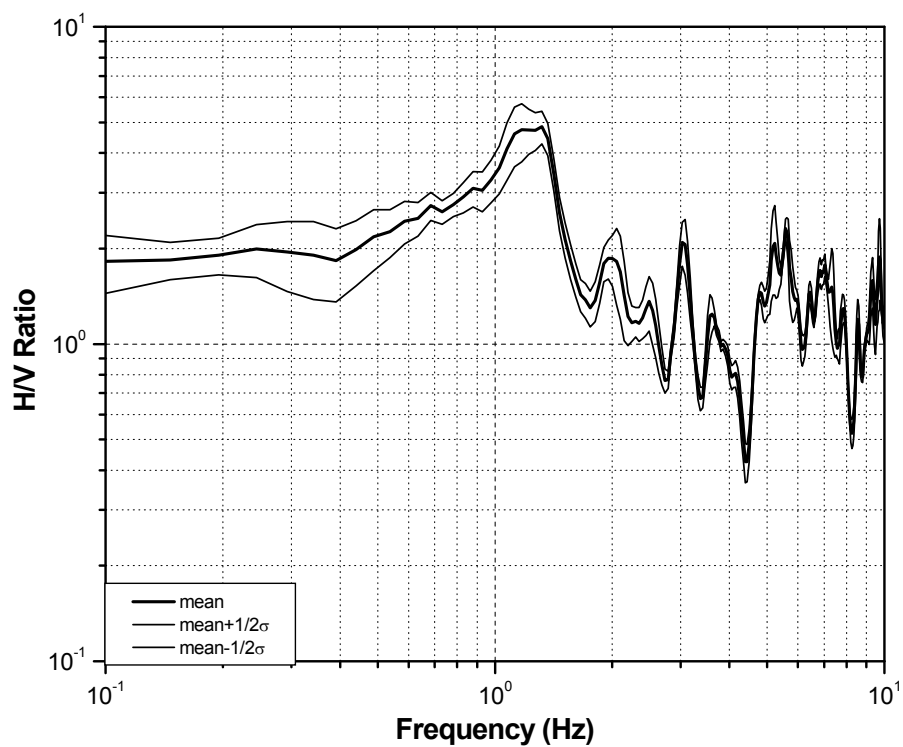


Figure 2.32: Predominant frequency and H/V ratio at Sosan Ghat, Kamrangirchar.

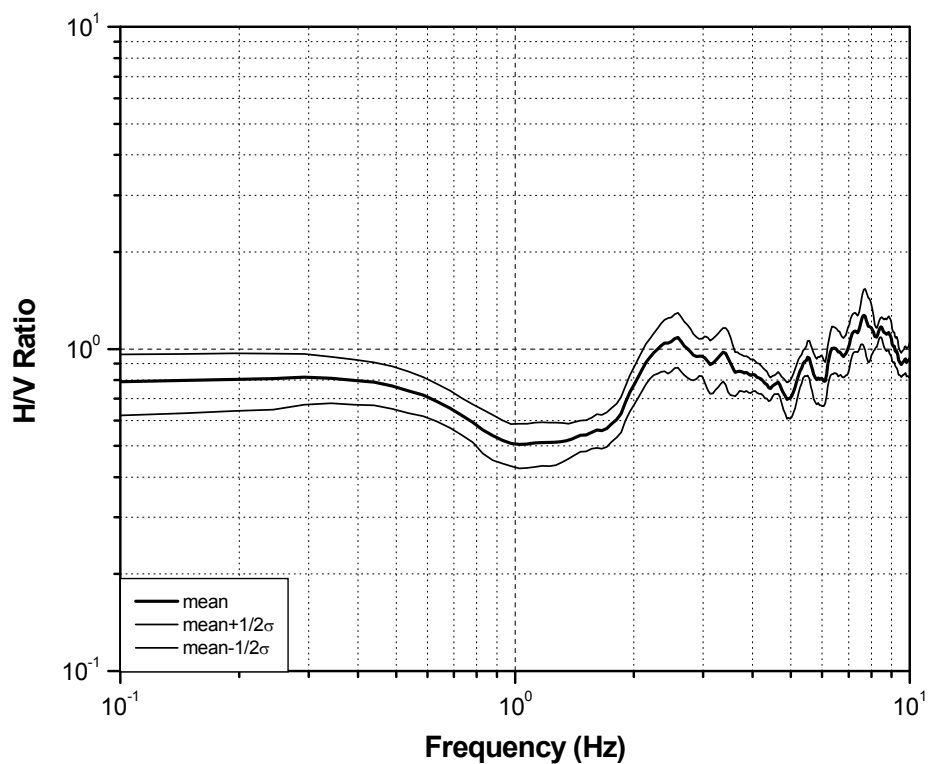


Figure 2.33: Predominant frequency and H/V ratio at RoyerBazar.

2.5.2 Microtremor Analysis Result within BUET Campus

The BUET campus is situated in latitude ranging from 23°43'16.58" N to 23°43'59.44" N and longitude from 90°23'13.31"E to 90°23'43.56" E. Microtremor observation at 132 selected points in soil and 45 locations in building have been carried out in BUET campus. The analysis results of these points are shown in this chapter and APPENDIX-C and APPENDIX-D.

2.5.2.1 Soil Sites

Table 2.17 shows predominant frequency and RM value of H/V ratio of 132 locations. Figure 2.34 demonstrates the observed microtremor locations at 132 selected locations. The details analysis results at 132 points are illustrated in APPENDIX-C from Figure C2.76 to Figure C2.207.

Out of 132 sites, the overall mean predominant frequency is 1.39 Hz where as standard deviation is 0.289. On the other hand, the overall peak mean H/V ratio is 2.09 where as standard deviation is 0.523.

Table 2.17 shows the predominant frequency and mean H/V ratio in 132 locations. Out of 132 microtremor observation locations, the maximum predominant frequency is around 9.62 Hz where as H/V ratio is 2.43 at MT82. The geology of this site is Upper Modhupur terrace (Figure 2.2) and Higher Pleistocene Terrace (Figure 2.3). Figure 2.35 (f) and C2.157 shows Horizontal to Vertical spectral ratio (H/V) ranging from 1.65 to 2.51. The basic six H/V ratio in three segments along EW and NS direction, square root of H/V ratio of three segments and their mean value are also shown in Figure C2.157. On the other hand, the minimum predominant frequency is around 0.25 Hz where as H/V ratio is 9.51 at MT72. This is the highest peak of H/V ratio in 132 selected locations in BUET campus. Figure 2.35(e) and Figure C2.147 demonstrates Horizontal to Vertical spectral ratio (H/V) ranging between 6.85 and 11.85. This lower predominant frequency and higher amplification ratio show that this site is highly susceptible due to any seismic hazard.

The predominant frequency of 132 locations has also been classified into five types. **Type I** (0 – 0.49), **Type II** (0.50 – 0.99), **Type III** (1.0 – 1.99), **Type IV** (2.0 – 2.99) and **Type V** (> 3.00).

The classifications of predominant frequency at 45 locations are as follows:

Type I: MT 02, MT 14, MT 17, MT 36, MT 62, MT 67, MT 72, MT 76, MT 77, MT 78, MT 80, MT 83, MT 84, MT 86, MT 108 and MT 120.

Type II: MT 03, MT 04, MT 05, MT 06, MT 11, MT 12, MT 15, MT 16, MT 18, MT 19, MT 22, MT 23, MT 24, MT 29, MT 30, MT 35, MT 41, MT 47, MT 48, MT 51, MT 52, MT 54, MT 56, MT 71, MT 79, MT 81, MT 85, MT 93, MT 99, MT 101, MT 103, MT 109 and MT 111.

Type III: MT 01, MT 07, MT 08, MT 09, MT 10, MT 13, MT 20, MT 21, MT 25, MT 26, MT 33, MT 34, MT 37, MT 38, MT 39, MT 40, MT 43, MT 44, MT 45, MT 46, MT 49, MT 50, MT 53, MT 58, MT 59, MT 60, MT 61, MT 63, MT 64, MT 65, MT 74, MT 87, MT 88, MT 90, MT 98, MT 102, MT 104, MT 106, MT 107, MT 110, MT 112, MT 113, MT 114, MT 115, MT 116, MT 121, MT 122, MT 128, MT 129, MT 130 and MT 132.

Type IV: MT 27, MT 28, MT 66, MT 89, MT 95, MT 105, MT 118, MT 119 and MT 123.

Type V: MT 31, MT 32, MT 42, MT 55, MT 57, MT 68, MT 69, MT 70, MT 73, MT 75, MT 82, MT 91, MT 94, MT 96, MT 97, MT 100, MT 117, MT 124, MT 125, MT 126 and MT 131.

From this classification of predominant frequency, it can be said that most of the locations predominant frequency ranging between 1.0 Hz and 1.99 Hz. These predominant frequencies are classified as **Type III**. The second most common type of predominant frequency is **Type II**. The number of locations predominant frequency classified as Type V is 21. In addition to this, there are sixteen Type I locations.

On the other hand, Horizontal to Vertical spectral ratio (H/V) has been classified into four types. **Type I** (0 - 0.99), **Type II** (1.0 - 1.99), **Type III** (2.0 - 2.99) and **Type IV** (>3.0).

The classifications of H/V ratio at 132 locations are as follows:

Type I: None

Type II: MT 01, MT 09, MT 10, MT 19, MT 20, MT 27, MT 28, MT 38, MT 47, MT 52, MT 58, MT 61, MT 66, MT 67, MT 68, MT 69, MT 70, MT 71, MT 73, MT 74, MT 75, MT 76, MT 77, MT 78, MT 80, MT 85, MT 86, MT 90, MT 91, MT 94, MT 97, MT 100, MT 104, MT 105, 108, MT 116, MT 117, MT 123, MT 124, MT 126, MT 127, MT 128 and MT 129.

Type III: MT 03, MT 04, MT 08, MT 11, MT 12, MT 13, MT 14, MT 15, MT 16, MT 17, MT 18, MT 21, MT 22, MT 23, MT 24, MT 25, MT 29, MT 30, MT 31, MT 32, MT 33, MT 34, MT 35, MT 37, MT 40, MT 41, MT 42, MT 43, MT 44, MT 45, MT 46, MT 48, MT 49, MT 50, MT 51, MT 53, MT 54, MT 55, MT 56, MT 57, MT 59, MT 63, MT 64, MT 65, MT 71, MT 79, MT 81, MT 82, MT 83, MT 87, MT 89, MT 92, MT 93, MT 95, MT 96, MT 98, MT 99, MT 102, MT 106, MT 107, MT 110, MT 111, MT 112, MT 113, MT 114, MT 115, MT 118, MT 119, MT 120, MT 121, MT 122, MT 125, MT 130, MT 131 and MT 132.

Type IV: MT 02, MT 05, MT 06, MT 07, MT 26, MT 36, MT 39, MT 60, MT 62, MT 72, MT 84, MT 88, MT 101, MT 103 and MT 109.

According to the above classification of H/V ratio, most of the selected locations are classified as **Type III**. There are seventy five Type III locations. **Type II** is the second most predominant H/V ratio. There is no H/V ratio ranging between 0 and 0.99. The number of locations H/V ratio greater than 3 is 15.

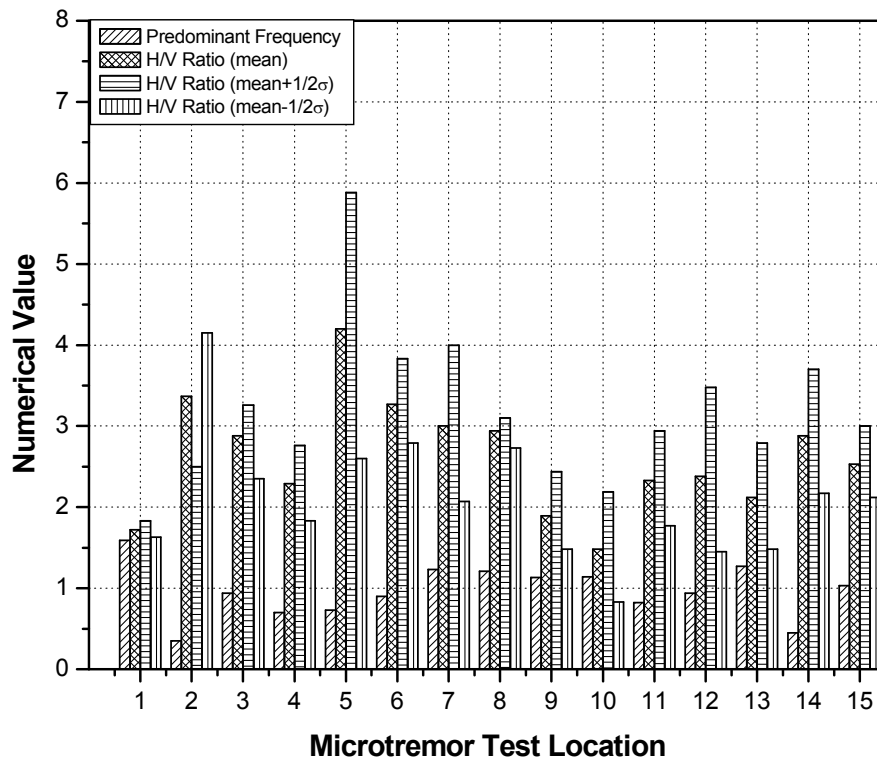
From Table 2.17, the minimum mean Horizontal to Vertical spectral ratio (H/V) is 1.24 where as predominant frequency is around 0.29 at MT 108. Figure 2.35(h) shows the Horizontal to Vertical spectral ratio (H/V) ranging between 0.93 and 1.56. The basic six H/V ratio in three segments along EW and NS direction, H/V ratio of three segments and their mean value are illustrated in Figure C2.183.

Table 2.17: Microtremor Test Location, Predominant Frequency and H/V Ratio within at 132 selected locations in soil within BUET campus

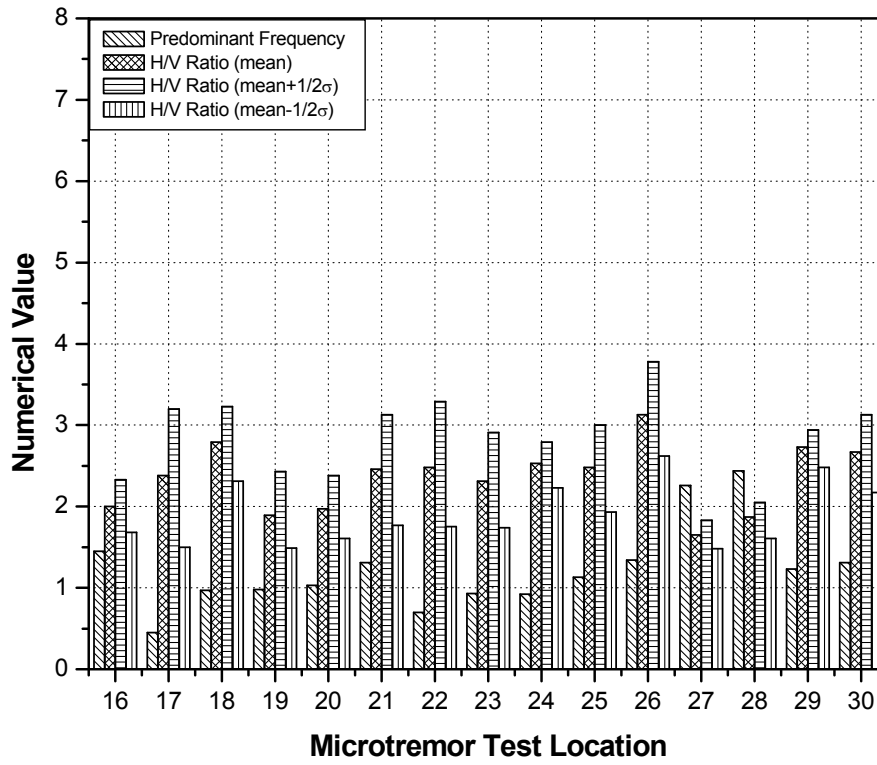
Serial Number	ID	Predominant Frequency	H/V Ratio (RM)	Serial Number	ID	Predominant Frequency	H/V Ratio (RM)
1	MT-01	1.59	1.72	2	MT-02	0.35	3.37
3	MT-03	0.94	2.88	4	MT-04	0.70	2.29
5	MT-05	0.73	4.20	6	MT-06	0.90	3.27
7	MT-07	1.23	3.0	8	MT-08	1.21	2.94
9	MT-09	1.13	1.89	10	MT-10	1.14	1.48
11	MT-11	0.82	2.33	12	MT-12	0.94	2.38
13	MT-13	1.27	2.12	14	MT-14	0.45	2.88
15	MT-15	1.03	2.53	16	MT-16	1.45	2.00
17	MT-17	0.45	2.38	18	MT-18	0.97	2.79
19	MT-19	0.98	1.89	20	MT-20	1.03	1.97
21	MT-21	1.31	2.46	22	MT-22	0.70	2.48
23	MT-23	0.93	2.31	24	MT-24	0.92	2.53
25	MT-25	1.13	2.48	26	MT-26	1.34	3.13
27	MT-27	2.26	1.65	28	MT-28	2.44	1.87
29	MT-29	1.23	2.73	30	MT-30	1.31	2.67
31	MT-31	3.65	2.12	32	MT-32	3.98	2.03
33	MT-33	1.37	2.14	34	MT-34	1.21	2.06
35	MT-35	0.57	2.88	36	MT-36	0.48	3.67
37	MT-37	1.24	2.31	38	MT-38	1.23	1.89
39	MT-39	1.24	3.74	40	MT-40	1.27	2.38
41	MT-41	0.65	2.03	42	MT-42	3.81	2.31
43	MT-43	1.35	2.79	44	MT-44	1.31	2.33
45	MT-45	1.07	2.29	46	MT-46	1.27	2.31
47	MT-47	0.66	1.41	48	MT-48	0.77	2.73
49	MT-49	1.24	2.59	50	MT-50	1.27	2.03
51	MT-51	0.82	2.00	52	MT-52	0.84	1.85
53	MT-53	1.15	2.70	54	MT-54	0.85	2.19

Serial Number	ID	Predominant Frequency	H/V Ratio (RM)	Serial Number	ID	Predominant Frequency	H/V Ratio (RM)
55	MT-55	3.02	2.00	56	MT-56	0.50	2.48
57	MT-57	7.31	2.17	58	MT-58	1.65	1.60
59	MT-59	1.30	2.45	60	MT-60	1.29	3.23
61	MT-61	1.27	1.74	62	MT-62	0.40	6.20
63	MT-63	1.29	2.97	64	MT-64	1.34	2.21
65	MT-65	1.24	2.14	66	MT-66	2.75	1.68
67	MT-67	0.39	1.98	68	MT-68	5.80	1.58
69	MT-69	7.06	1.41	70	MT-70	4.89	1.65
71	MT-71	0.80	2.14	72	MT-72	0.25	9.51
73	MT-73	3.13	1.75	74	MT-74	1.37	1.85
75	MT-75	4.89	1.59	76	MT-76	0.38	1.27
77	MT-77	0.34	1.94	78	MT-78	0.34	1.48
79	MT-79	0.83	2.51	80	MT-80	0.34	1.58
81	MT-81	0.96	2.03	82	MT-82	9.62	2.43
83	MT-83	0.44	2.43	84	MT-84	0.42	4.38
85	MT-85	0.94	1.98	86	MT-86	0.39	1.29
87	MT-87	0.82	2.38	88	MT-88	0.90	3.37
89	MT-89	1.28	2.35	90	MT-90	0.91	1.77
91	MT-91	3.72	1.65	92	MT-92	0.87	2.67
93	MT-93	0.74	2.70	94	MT-94	3.10	1.31
95	MT-95	2.75	2.19	96	MT-96	3.38	2.12
97	MT-97	4.45	1.95	98	MT-98	1.27	2.48
99	MT-99	0.64	2.33	100	MT-100	7.5	1.51
101	MT-101	0.92	3.19	102	MT-102	1.27	2.35
103	MT-103	0.52	4.97	104	MT-104	2.64	1.61
105	MT-105	2.54	1.35	106	MT-106	1.33	2.85
107	MT-107	1.32	2.82	108	MT-108	0.29	1.24
109	MT-109	0.54	3.70	110	MT-110	1.36	2.82
111	MT-111	0.98	2.48	112	MT-112	1.21	2.51

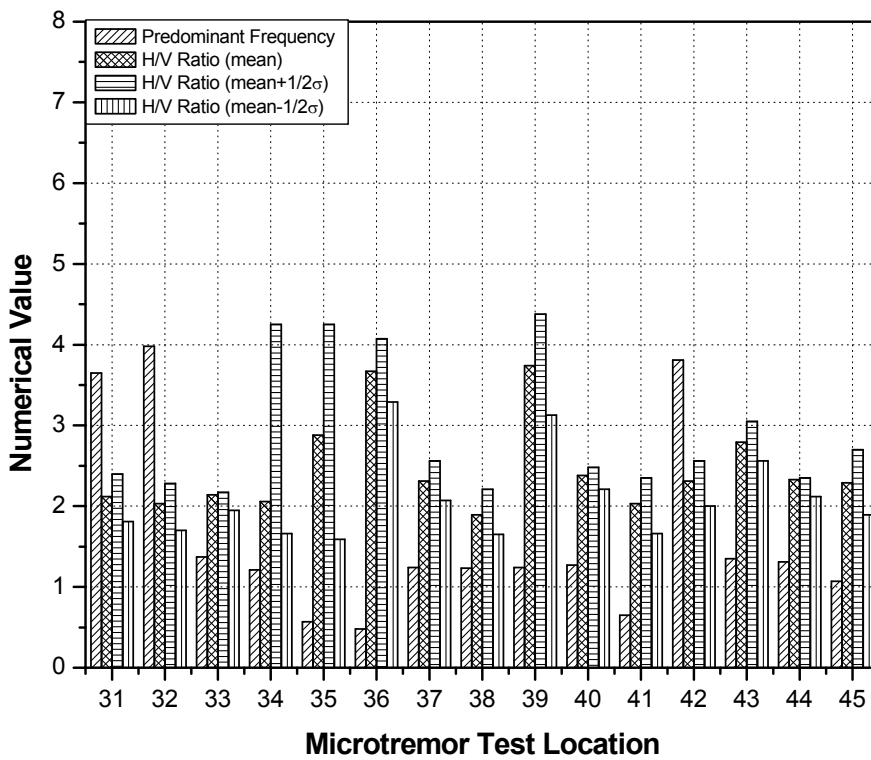
Serial Number	ID	Predominant Frequency	H/V Ratio (RM)	Serial Number	ID	Predominant Frequency	H/V Ratio (RM)
113	MT-113	1.03	2.35	114	MT-114	1.27	2.14
115	MT-115	1.16	2.10	116	MT-116	1.39	1.95
117	MT-117	6.11	1.61	118	MT-118	1.33	2.59
119	MT-119	1.27	2.33	120	MT-120	0.39	2.08
121	MT-121	1.27	2.82	122	MT-122	1.27	2.35
123	MT-123	2.68	1.89	124	MT-124	4.00	1.42
125	MT-125	4.85	2.33	126	MT-126	5.95	1.77
127	MT-127	6.11	1.95	128	MT-128	2.52	1.47
129	MT-129	1.80	1.31	130	MT-130	1.26	2.35
131	MT-131	4.65	2.21	132	MT-132	1.18	2.46



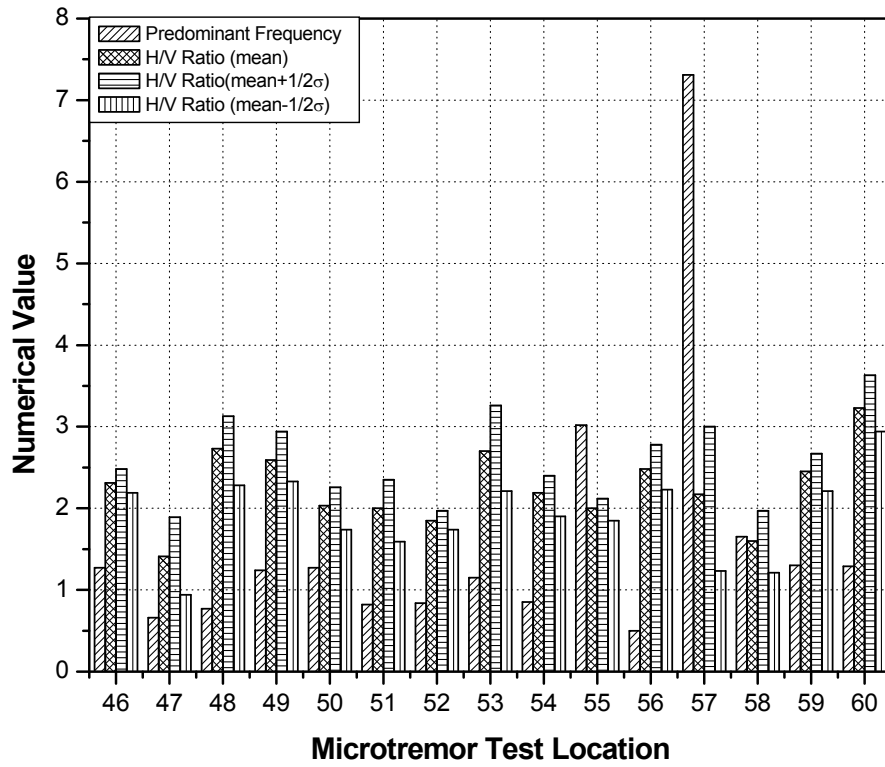
(a) Microtremor Test Location 1 to 15



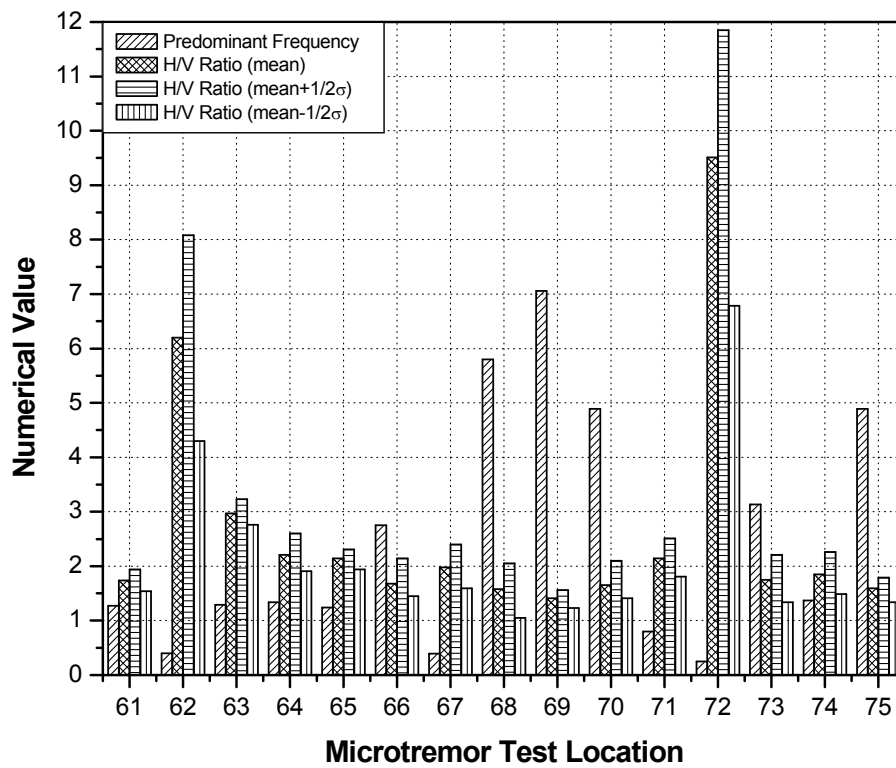
(b) Microtremor Test Location 16 to 30



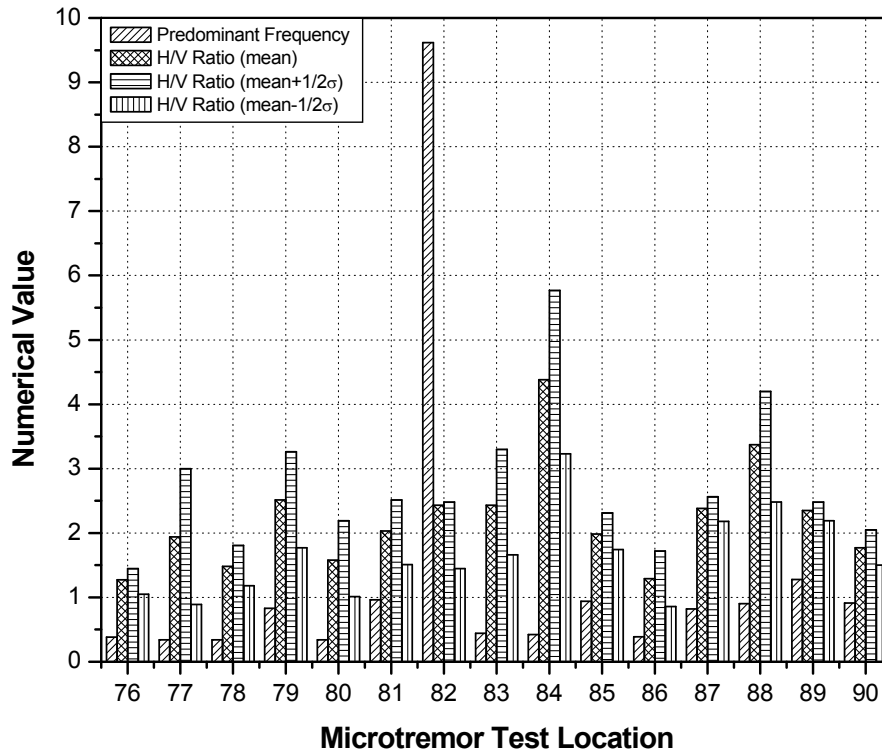
(c) Microtremor Test Location 31 to 45



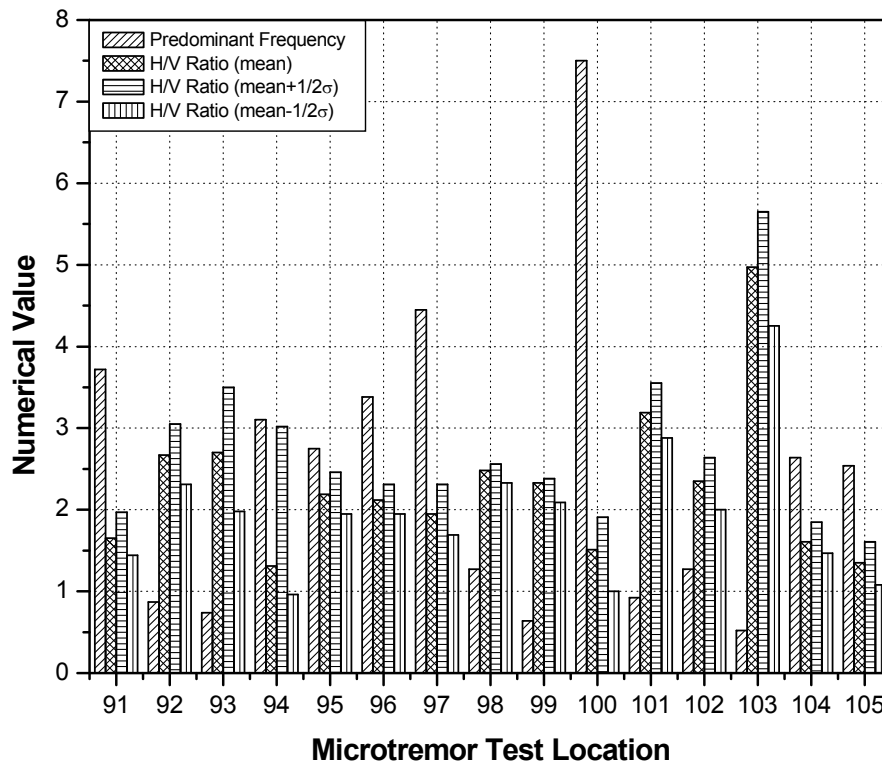
(d) Microtremor Test Location 46 to 60



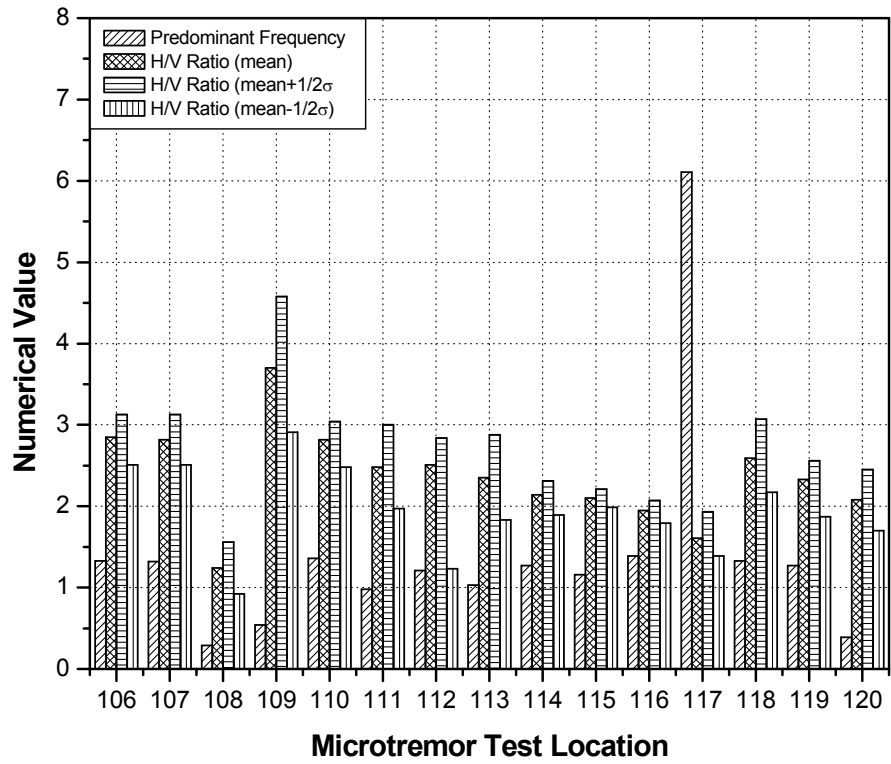
(e) Microtremor Test Location 61 to 75



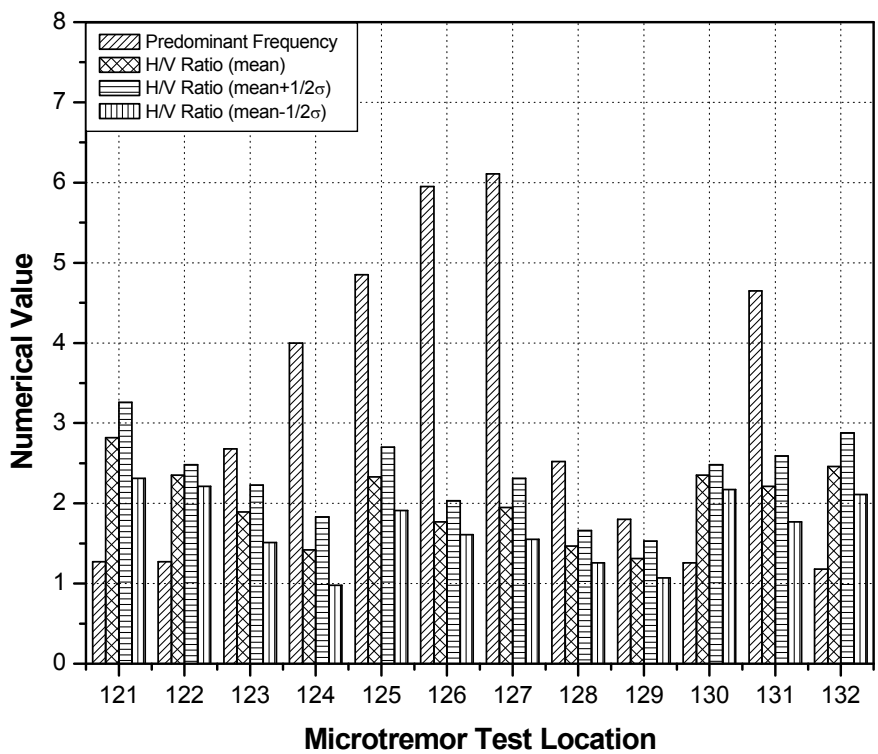
(f) Microtremor Test Location 76 to 90



(g) Microtremor Test Location 91 to 105



(h) Microtremor Test Location 106 to 120



(i) Microtremor Test Location 121 to 132

Figure 2.35 [(a), (b), (c), (d), (e), (f),(g),(h) and (i)]: Predominant frequency and H/V ratio at 132 selected locations in soil within BUET campus.

2.5.2.2 Building Sites

Microtremor observations at 45 residential and academic buildings of BUET campus are shown in Figure 2.36 and google map in Figure 2.37. The Horizontal to Vertical spectra ratio at building does not provide reliable dynamic characteristics. In that case Fourier Spectrum provides better result of predominant frequency at building. Table 2.18 shows the mean predominant frequency of Fourier spectrum in EW and NS directions at 45 buildings. Fourier spectra of 45 buildings along EW, NS and UD directions are shown in APPENDIX-D from Figure D208 to D252. In some buildings, microtremor data is recorded at different floors or different locations in the same floor. Out of 45 microtremor observation in buildings, the maximum predominant frequency is 5.56 Hz along both EW and NS directions in MTB10 at Controller of Examination Building. This is a four-storied frame structure building with 324sqm floor area. There are no lift and shear wall in this building. The foundation of the building is individual footing. There are no structural irregularities in building. But torsional irregularity, re-entrant corner and diaphragm discontinuity exist.

The minimum predominant frequency is 2.00 Hz along EW and NS directions at MTB02 at the Eleven Story Tower Building. This is an eleven-storied frame structure with 673sqm floor area. There are three lift cores and a shear wall in the building. The foundation of the building is pile-raft system. No structural irregularity exist in this building. But torsional irregularity, re-entrant corner and diaphragm discontinuity exist.

The predominant frequency of 45 building has also been classified into five types. **Type I** (0 – 0.49), **Type II** (0.50 – 0.99), **Type III** (1.0 – 1.99), **Type IV** (2.0 – 2.99) and **Type V** (> 3.00).

The classifications of predominant frequency along EW at 45 buildings are as follows:

Type I: None

Type II: None

Type III: None

Type IV: MT 01, MT 02, MT 03, MT 04 and MT 06.

Type V: MT 05, MT 07, MT 08, MT 09, MT 10, MT 11, MT 12, MT 13, MT 14, MT 15, MT 16, MT 17, MT 18, MT 19, MT 20, MT 21, MT 22, MT 23, MT 24, MT 25, MT 26, MT 27, MT 28, MT 29, MT 30, MT 31, MT 32, MT 33, MT 34, MT 35, MT 36, MT 37, MT 38, MT 39, MT 40, MT 41, MT 42, MT 43, MT 44 and MT 45.

In addition to this, classifications of predominant frequency along NS direction at 45 buildings are as follows:

Type I: None

Type II: None

Type III: None

Type IV: MT 02, MT 03, MT 04, MT 05, MT 06, MT 07, MT 13 and MT 45.

Type V: MT 01, MT 08, MT 09, MT 10, MT 11, MT 12, MT 14, MT 15, MT 16, MT 17, MT 18, MT 19, MT 20, MT 21, MT 22, MT 23, MT 24, MT 25, MT 26, MT 27, MT 28, MT 29, MT 30, MT 31, MT 32, MT 33, MT 34, MT 35, MT 36, MT 37, MT 38, MT 39, MT 40, MT 41, MT 42, MT 43 and MT 44.

Table 2.18: Predominant period and frequency of forty five BUET buildings (after Russel et al., 2006)

Serial Number	Building Name/Number	No. of story	Predominant period (sec)		Predominant Frequency (Hz)	
			EW direction	NS direction	EW direction	NS direction
1	IFCDR Building	4	0.38	0.30	2.63	3.33
2	Eleven Story Tower Building	11	0.50	0.50	2.00	2.00
3	Civil Engineering Building	7	0.50	0.40	2.00	2.50
4	EME Building	6	0.40	0.39	2.50	2.56
5	Library Building	4	0.26	0.37	3.85	2.70
6	Architectural Building	5	0.37	0.36	2.70	2.78
7	URP Building	5	0.33	0.38	3.03	2.63
8	ARI Building	6	0.26	0.30	3.85	3.33
9	New Academic Building	13	0.27	0.30	3.70	3.33

Serial Number	Building Name/Number	No. of story	Predominant period (sec)		Predominant Frequency (Hz)	
			EW direction	NS direction	EW direction	NS direction
10	Controller of Examination Building	4	0.18	0.18	5.56	5.56
11	Engg. University School Building	4	0.27	0.23	3.70	4.35
12	Titumir Hall	4	0.32	0.31	3.13	3.23
13	Sher-e-Bangla Hall	4	0.27	0.40	3.70	2.50
14	Dr. M.A. Rashid Hall	5	0.24	0.27	4.17	3.70
15	Ahsan-Ullah Hall	4	0.27	0.25	3.70	4.00
16	Shahid Smrity Hall (Middle Building)	4	0.27	0.21	3.70	4.76
17	Shahid Smrity Hall (North Building)	4	0.30	0.28	3.33	3.57
18	Register Building	2	0.20	0.20	5.00	5.00
19	# 1	4	0.25	0.25	4.00	4.00
20	# 2	4	0.25	0.26	4.00	3.85
21	# 3	4	0.28	0.22	3.57	4.55
22	# 4	5	0.33	0.29	3.03	3.45
23	# 5	4	0.22	0.26	4.55	3.85
24	# 6	4	0.23	0.27	4.35	3.70
25	# 7	4	0.25	0.27	4.00	3.70
26	# 8	4	0.32	0.28	3.13	3.57
27	# 9	4	0.24	0.22	4.17	4.55
28	# 12	5	0.30	0.28	3.33	3.57
29	# 13	5	0.28	0.28	3.57	3.57
30	# 14	5	0.31	0.31	3.23	3.23
31	# 18	5	0.33	0.29	3.03	3.45
32	# 21	4	0.23	0.30	4.35	3.33
33	# 22	4	0.33	0.29	3.03	3.45
34	# 23	4	0.25	0.30	4.00	3.33
35	# 24	4	0.24	0.29	4.17	3.45

Serial Number	Building Name/Number	No. of story	Predominant period (sec)		Predominant Frequency (Hz)	
			EW direction	NS direction	EW direction	NS direction
36	# 25	4	0.25	0.30	4.00	3.33
37	# 26	4	0.25	0.30	4.00	3.33
38	# 27	4	0.23	0.29	4.35	3.45
39	# 28	5	0.33	0.28	3.03	3.57
40	# 30	4	0.26	0.24	3.85	4.17
41	# 43	5	0.29	0.25	3.45	4.00
42	# 45	5	0.27	0.29	3.70	3.45
43	# 46	5	0.30	0.26	3.33	3.85
44	# 47	6	0.32	0.32	3.13	3.13
45	# 62	6	0.39	0.34	2.56	2.94

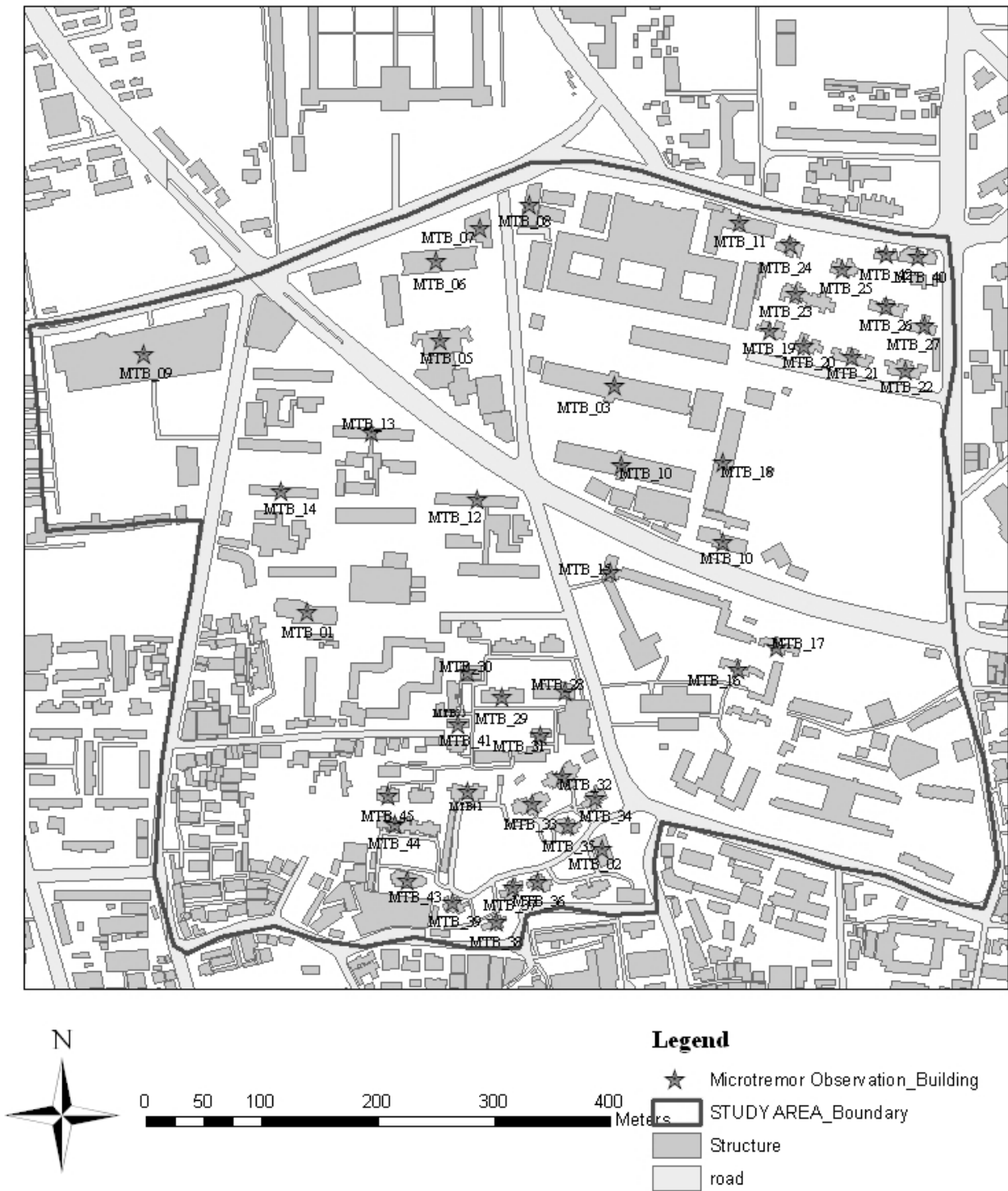


Figure 2.36: 45 microtremor observation points in various building of BUET campus.



Figure 2.37: Google Map of BUET Campus.

COMPARISON OF MICROTREMOR DATA WITH THEORETICAL ANALYSIS

3.1 GENERAL

The reliability of microtremor observation to estimate predominant frequency and amplification of any particular site has been illustrated in Chapter 2. These parameters may be used to assess the response of site soil due to any seismic activities. Comparison of H/V ratio of microtremor observation with theoretical transfer function of site soil using the 1D site response program SHAKE is important. This chapter provides comparison of these two ratios for 42 locations of Dhaka city. In 14 locations shear-wave velocity are obtained directly using PS-logging and SSMM method and in other 28 locations correlations are used to obtain shear-wave velocity from SPT-N value. Resonance between site soil and building within BUET campus as well as Nakamura's seismic vulnerability index (K_g) for soils for 45 locations has also been estimated.

3.2 COMPARISON OF MICROTREMOR DATA WITH 1D RESPONSE ANALYSIS USING THE PROGRAMME SHAKE

From the existing borelogs, SSMM and PS-loggings, soil model at each site has been established for theoretical analysis. The transfer function of the shear wave (the surface motion versus the incidental motion at depth) has been calculated using the soil models. For the calculation of transfer function of shear-wave and a damping ratio of 2% has been used, assuming input motion at the outcrop.

Figure 3.1 and Figure 3.2 show the typical graphs for comparison of amplitude ratio between the transfer function of shear wave and microtremor H/V ratio. The comparison of amplitude ratio between transfer function and microtremor H/V ratio for forty two sites in and around the Dhaka city have been illustrated in Appendix-E. Characteristics transfer function curve have been found from the 1D response analysis using the programme SHAKE. On the other hand, microtremor H/V ratio curve has been found from the Horizontal to Vertical spectral ratio (H/V) of Fourier spectra.

From the comparison of microtremor and transfer function, four types of characteristics curves have been observed. These curves are classified as similar, dissimilar, right side shifted and left side shifted compared to the microtremor H/V ratio curve. Among 42 models

thirty five transfer function have been shifted in the right side of microtremor and only one has been shifted in the left side. There are six sites where two curves have similar pattern. The rest two sites have been found where no similarity between microtremor H/V ratio and transfer function.

Figure E3.38 shows the comparison of amplitude ratio between microtremor and Transfer Function at Rajendapur. The amplitude ratio of Transfer function is similar to microtremor H/V ratio. However, peak of transfer function has been moved into right side slightly. The amplitude ratio of both curves is around 2.65. The predominant frequency of microtremor H/V ratio is 1.17 Hz whereas transfer function shows 2.5 Hz. Similar curves between transfer function and microtremor have been found in nine locations which are shown in Figure E3.1, E3.4, E3.5, E3.6, E3.11, E3.13, E3.17, E3.19 and Figure E3.24.

Figure E3.35 demonstrates that the peak amplitude ratio of transfer function has been moved toward right side of microtremor at Bashundhara River view Project. But, the peak value of transfer function is lower amplified than microtremor H/V ratio. The predominant frequency of microtremor H/V ratio is 1.05 Hz where as transfer function shows this value is 1.85 Hz. On the other hand, peak H/V ratio of microtremor is 3.51 whereas transfer function shows this value 3.03. The similar types of right shifted and lower amplified locations of transfer function have been found in Figure E3.2, E3.3, E3.7, E3.8, E3.10, E3.14, E3.15, E3.16, E3.17, E3.21, E3.23, E3.26, E3.29, E3.30, E3.31, E3.33, E3.34, E3.42 and Figure E3.35.

Figure E3.20 shows that amplitude ratio of transfer function is higher than microtremor H/V ratio at Pallabi. The predominant frequency of microtremor is 1.24 Hz whereas the predominant frequency of transfer function is 1.60 Hz. The amplitude ratio of microtremor is 2.64 whereas this value is 4 Hz in Transfer Function. The similar pattern of curves between microtremor and Transfer function have been observed in Figure E3.9, E3.13, E3.18, E3.20, E3.26 and Figure E3.41.

Figure E3.36 shows the left side shifted transfer function curve at Matuail, Demra. The peak value of H/V ratio of microtremor is similar to Transfer Function. The Predominant frequency of transfer function is around 1.7 Hz whereas this value is 2.73 Hz in microtremor. The peak value of amplitude ratio of transfer function is 2.48 where as microtremor shows 2.3.

The similar predominant frequency of microtremor and transfer function has been found in nine locations. Figure E3.12 represents the similar predominant frequency between microtremor and transfer function. The predominant frequency of microtremor and transfer function is around 3.65 Hz. The peak amplitude ratio of microtremor is 2.73 whereas this

value is 1.90 in transfer function. The similar patterns of curve have been illustrated in Figure E3.22.

The similar predominant frequency but higher amplification has been found in Figure E3.27 at Adabor. The predominant frequency in both curves is 3.35 Hz. The peak amplitude ratio of microtremor is 2.26 Hz whereas this value is 2.9 in Transfer Function.

The dissimilarity between transfer function and microtremor H/v ratio has been found in Figure E3.29 at Aftab Nagar Housing project. The transfer function curve is right shifted. The predominant frequency and amplitude ratio of transfer function are 6 Hz and 2 where as these value are 0.95 Hz and 2.76 in microtremor. Figure E3.37 demonstrates that amplitude ratio of transfer function is right shifted at Jilmil Project. The predominant frequency and H/V ratio of microtremor are 1.0 Hz and 3.26. The predominant frequency and H/V ratio of transfer function have been found 8.0 Hz and 3.0.

From these result, it can be said that although amplitude values of the ratios are close, the predominant frequency for the two cases differs slightly. The reason of this difference is that microtremor consists of different types of waves, but the theoretical transfer function is based on shear-wave only. Rayleigh wave has significant effect on microtremor result. If these waves are dispersed from the microtremor, microtremor results may be more close to the transfer function.

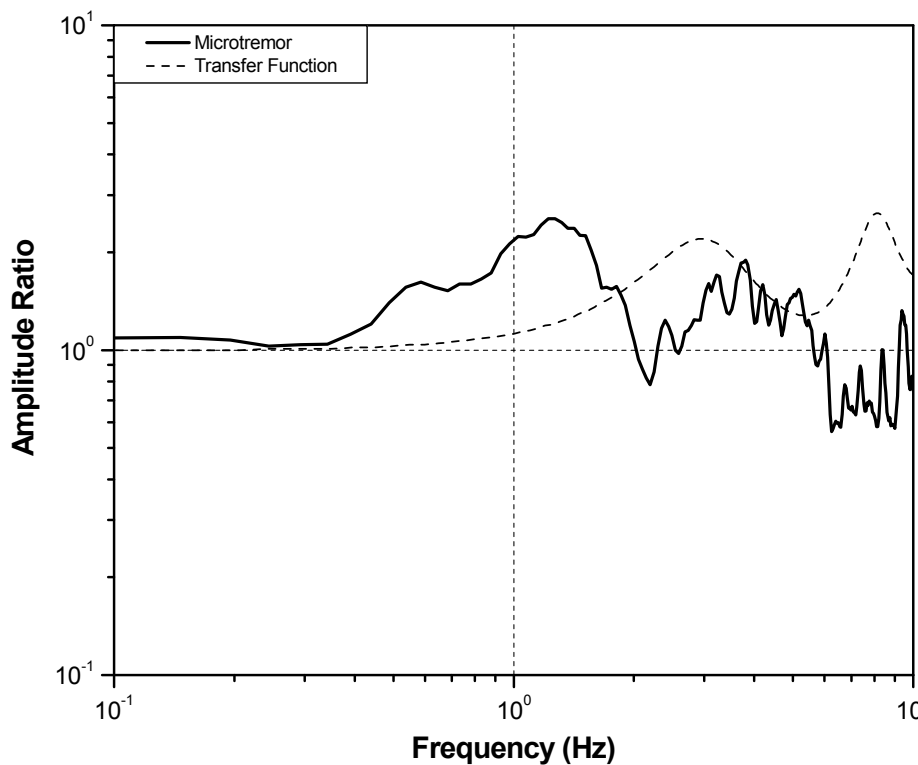


Figure 3.1: Amplitude ratios of microtremor and theoretical transfer function of shear

wave at National University.

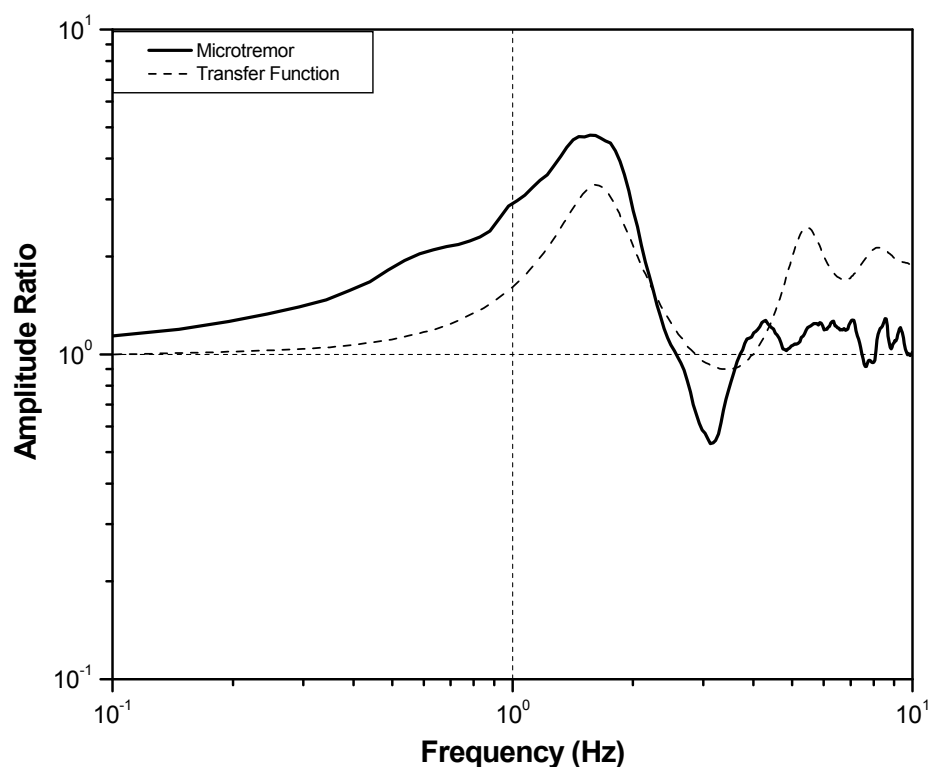


Figure 3.2: Amplitude ratios of microtremor and theoretical transfer function of shear wave at Block-D, Bashundhara.

3.3 VULNERABILITY ASSESSMENT

Earthquake vulnerability of the 45 buildings within BUET campus is carried out from predominant frequency obtained by the analysis of microtremor data. Microtremor observation has been carried out at 132 selected free-field locations within BUET campus which has been discussed in Chapter 2. The Horizontal to Vertical spectra ratio (H/V) of these locations have been compared with the predominant frequency of building along EW and NS direction, respectively. Fourier spectra of 45 buildings of BUET campus have been shown in APPENDIX-D from Figure D208 to D252. The mean square root of H/V ratio (RM) obtained from microtremor observations of nearby soils have been compared with Fourier spectra of microtremor observations at the top floor of the buildings. The occurrence of resonance between building and soil has been discussed in article 3.3.1. The damage assessment of consolidated soil using Nakamura's Seismic Vulnerability Index (Kg) has been included in article 3.3.2.

3.3.1 Resonance between Site Soil and Building

The resonance criteria of building and soil can be explained using the following simple relation:

$$\text{Resonance criteria, } \beta_R = \frac{f_B}{f_S} \quad (3.1)$$

Where, β_R = Coefficient for resonance occurrence, f_B = Predominant frequency of building and f_S = Predominant frequency of soil.

In equation (3.1), if β_R becomes close to 1 (1 ± 0.20), resonance may occur. The resonance between buildings and soil has been analyzed using this resonance criterion, β_R , in both EW and NS directions. Table 3.1 presents the predominant frequency of the buildings and their adjacent soils and shows possibility of resonance to occur. Four buildings have been found as vulnerable due to resonance occurrence. These buildings are Eleven Story Tower Building, URP Building, Titumir Hall and Building # 1.

Table 3.1: Analysis of resonance criteria of 45 buildings at BUET campus

Serial No.	Building Name/ Number	Predominant Frequency of Building (Hz)		Predominant Frequency of site soil (Hz)	Remarks on resonance occurrence
		EW direction	NS direction	Resultant, RM	
1	IFCDR Building	2.63	3.33	0.96	No
2	Eleven Story Tower Building	2.00	2.00	1.80	Yes
3	Civil Engineering Building	2.00	2.50	0.75	No
4	EME Building	2.50	2.56	1.24	No
5	Library Building	3.85	2.70	2.17	No
6	Architectural Building	2.70	2.78	1.88	No
7	URP Building	3.03	2.63	3.05	Yes
8	ARI Building	3.85	3.33	2.26	No
9	New Academic Building	3.70	3.33	0.96	No
10	Controller of Examination Building	5.56	5.56	1.24	No
11	Engg. University School Building	3.70	4.35	1.37	No
12	Titumir Hall	3.13	3.23	3.52	Yes
13	Sher-e-Bangla Hall	3.70	2.50	1.65	No

Serial No.	Building Name/ Number	Predominant Frequency of Building (Hz)		Predominant Frequency of site soil (Hz)	Remarks on resonance occurrence
		EW direction	NS direction	Resultant, RM	
14	Dr. M.A. Rashid Hall	4.17	3.70	1.87	No
15	Ahsan-Ullah Hall	3.70	4.00	5.92	No
16	Shahid Smrity Hall(Middle Building)	3.70	4.76	0.34	No
17	Shahid Smrity Hall(North Building)	3.33	3.57	3.13	No
18	Register Building	5.00	5.00	0.65	No
19	# 1	4.00	4.00	3.81	Yes
20	# 2	4.00	3.85	1.07	No
21	# 3	3.57	4.55	1.24	No
22	# 4	3.03	3.45	1.27	No
23	# 5	4.55	3.85	1.31	No
24	# 6	4.35	3.70	1.31	No
25	# 7	4.00	3.70	0.66	No
26	# 8	3.13	3.57	0.77	No
27	# 9	4.17	4.55	0.82	No
28	# 12	3.33	3.57	1.18	No
29	# 13	3.57	3.57	1.18	No
30	# 14	3.23	3.23	1.16	No
31	# 18	3.03	3.45	6.11	No
32	# 21	4.35	3.33	2.68	No
33	# 22	3.03	3.45	1.27	No
34	# 23	4.00	3.33	5.95	No
35	# 24	4.17	3.45	4.85	No
36	# 25	4.00	3.33	1.80	No
37	# 26	4.00	3.33	2.52	No
38	# 27	4.35	3.45	1.27	No
39	# 28	3.03	3.57	6.11	No
40	# 30	3.85	4.17	0.84	No
41	# 43	3.45	4.00	1.39	No
42	# 45	3.70	3.45	0.66	No
43	# 46	3.33	3.85	1.36	No
44	# 47	3.13	3.13	0.88	No
45	# 62	2.56	2.94	1.39	No

3.3.2 Seismic Damage assessment of soil using Nakamura's Technique

Seismic vulnerability index (K_g) is an index indicating the level of vulnerability of a layer of soil to deform. Therefore, this index is useful for the detection of areas that are weak zone (unconsolidated sediment) at the time of occurrence of earthquakes. Some studies like Daryono (2009) and Nakamura (2000) showed a good correlation between seismic vulnerability index (K_g) and the distribution of earthquake disaster damage. This index is obtained from the peak value of HVSR squared, divided by the value of the predominant frequency. For this research area (K_g) values for 45 locations are shown in Table 3.2.

The seismic vulnerability index has been classified into four major types. These are Low (0-5), Moderate (6-10), High (11-20) and Very High (>20). Table 3.2 demonstrates the highest (K_g) value at Rab-10, Plot, Kamrangirchar. Most of the zones having higher Vulnerability Index (K_g) are situated in reclaimed areas.

Table 3.2: Damage assessment of site soil using Nakamura's empirical formula

SL. No	ID	Location	Predominant Frequency, F_g (Hz)	H/V Ratio, A_g	Vulnerability Index, $K_g = \frac{A_g^2}{F_g}$	Remarks
1	SBH-01	National University	1.24	2.59	5.41	Low to moderate
2	SBH-02	Board Bazaar, Gazipur	0.82	2.73	9.09	Moderate
3	SBH-03	Kaunia, Boro Bari, Moddopara	0.72	2.79	10.81	Moderate to high
4	SBH-04	Tongi, Ershadnagar	0.97	2.51	6.49	Moderate
5	SBH-05	Tongi BSCIC area	0.95	2.73	7.85	Moderate
6	SBH-06	Abdullahpur	1.32	2.33	4.11	Low
7	SBH-07(A)	Ijtema field (North and East side)	1.17	3.37	9.71	Moderate
8	SBH-07(B)	Ijtema Field (South and West side)	0.86	3.26	12.35	High

SL. No	ID	Location	Predominant Frequency, F_g (Hz)	H/V Ratio, A_g	Vulnerability Index, $K_g = \frac{A_g^2}{F_g}$	Remarks
9	SBH-08	Ashulia Toll Plaza	1.14	1.75	2.69	Low
10	SBH-9	Uttar Khan	1.09	2.09	4.01	Low
11	SBH-10(A)	Uttara Phase 3 (North side)	1.18	3.16	8.46	Moderate
12	SBH-10(B)	Uttara Phase 3 (South side)	0.97	4.43	20.48	Very high
13	SBH-11	Azampur School, Uttara	3.65	2.73	2.04	Low
14	SBH-12 (A)	Mirpur DOHS (South side)	1.54	2.46	3.93	Low
15	SBH-12 (B)	Mirpur DOHS (North side)	1.21	3.44	9.78	Moderate
16	SBH-13	Ashiyani city, Askona, Dakkhin Khan	1.12	3.19	9.08	Moderate
17	SBH-14(A)	Purbachal-1, Randokpur Hazi bari, Rupganj	0.94	3.04	9.83	Moderate
18	SBH-14(B)	Purbachal-2, American City	2.00	2.69	3.62	Low
19	SBH-14(C)	Purbachal Picnic Park, Gazipur	1.34	2.23	3.71	Low
20	SBH-15	Adjacent to Mirpur Zoo	1.52	2.43	3.88	Low
21	SBH-16	Field Ground, Pallabi	1.24	2.64	5.62	Low to moderate
22	SBH-17 (A)	Block-B, Basundhara	2.09	3.12	4.66	Low
23	SBH-17 (B)	Block-D, Basundhara	1.57	4.71	14.13	High

SL. No	ID	Location	Predominant Frequency, F_g (Hz)	H/V Ratio, A_g	Vulnerability Index, $K_g = \frac{A_g^2}{F_g}$	Remarks
24	SBH-17 (C)	Block-H, Basundhara	2.52	2.94	3.43	Low
25	SBH-18	Civil Aviation Quarter	0.64	3.70	21.39	Very high
26	SBH-19	Kuril Flyover	1.97	2.73	3.78	Low
27	SBH-20	Sarengbari, Mipur-2	0.59	2.84	13.67	High
28	SBH -21	Purachal, Uttara Badda	2.11	2.59	3.18	Low
29	SBH-22	City Corporation, Gabtoli	0.82	3.67	16.42	High
30	SBH-23	Adabor	3.35	2.26	1.52	Low
31	SBH-24	Agargoan Trade Fair area	0.86	2.12	5.23	Low to moderate
32	SBH-25	Aftab Nagar Housing Project	0.95	2.76	8.02	Moderate
33	SBH-26	Umme Had Nagar, Nadda	1.32	3.83	11.11	Moderate
34	SBH-27	South Banasree	1.39	3.86	10.72	Moderate to high
35	SBH-28	Basila Garden City	1.12	4.47	17.84	High
36	SBH-29	Royer Bazar Boddhobumi	2.57	1.08	0.45	Low
37	SBH-30	Kalunagar, Hazaribagh	0.88	2.48	6.99	Moderate
38	SBH-31	Rab-10, Plot, Kamrangirchar	0.48	3.91	31.85	Very High

SL. No	ID	Location	Predominant Frequency, F_g (Hz)	H/V Ratio, A_g	Vulnerability Index, $K_g = \frac{A_g^2}{F_g}$	Remarks
39	SBH-32	Sosan Ghat, Kamrangirchar	1.22	4.78	18.72	High
40	SBH-33	Basundhara River view	1.05	3.51	11.73	High
41	SBH-34	Matuail, Demra	2.77	2.48	2.22	Low
42	SBH-35	Jilmil Project, Ecuria	1.00	3.26	10.63	Moderate to high
43	SBH-36	Rajendapur	1.17	2.59	5.73	Low
44	SBH-37	Bramangaon	1.08	3.55	11.67	High
45	SBH-38	Meradia, Uttar Banasree	1.26	2.84	6.40	Moderate

Figure 3.3 shows the classification of vulnerability site at 45 locations using Nakamura's Vulnerability Index (K_g). Figure 4.3 demonstrates four major and two in between vulnerability type. The number of low vulnerability type locations, which is 16, is the most common among 45 locations. The second most predominant number of vulnerability type is moderate type which varies between 6 and 10. The number of very high type vulnerable site is 4.

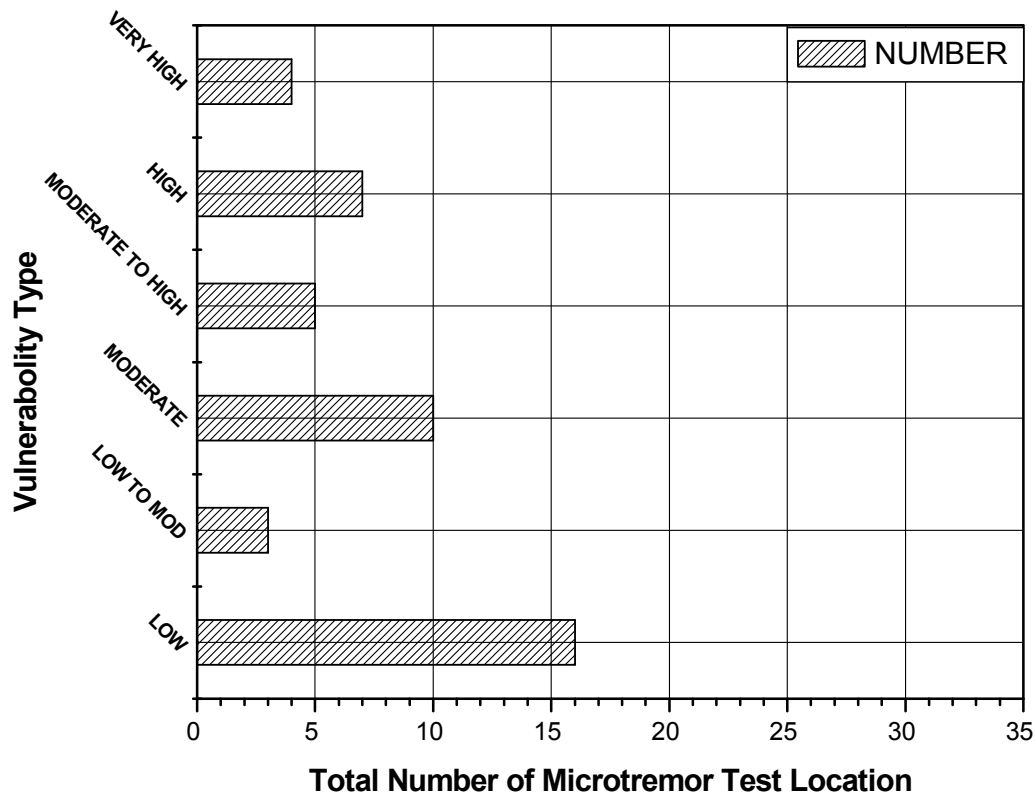


Figure 3.3: Damage assessment of 45 test locations using Nakamura’s Vulnerability Index (Kg).

To further ensure this, research on the acceleration of seismic waves in the basement need to be estimated. Vulnerability Index together with the acceleration of seismic waves in the basement has been suggested by Nakamura (2000) to calculate the value of shear strain (γ) of surface soil layers. Damaging earthquakes will occur when the limits are exceeded due to the shear strain deformation surface layer of soil. Soil is plastic at $\gamma = 1000 \times 10^{-6}$, whereas at $\gamma > 10.000 \times 10^{-6}$, the ground will deform. Only predominant frequency is not effective to classify a site due to Nakamura’s vulnerability index. Both predominant frequency and H/V ratio are required to estimate vulnerability type.

CONCLUSIONS AND RECOMMENDATIONS

4.1 GENERAL

The purpose of this research is to apply microtremor Horizontal to vertical spectral (H/V) ratio technique for site soil response analysis in and around the Dhaka city. For this purpose forty five selected locations in and around Dhaka city as well as one hundred and thirty two

points within BUET campus has been selected. The locations are selected on the basis of different geomorphic units.

After checking the stability of microtremor at different time instants microtremor observation has been carried out. The dynamic properties of soil, which are predominant frequency and amplification, have been estimated from microtremor analysis. The variation of microtremor H/V ratio due to various analysis windows have been carried out in this research.

The soil model using one dimensional response analysis using the programme SHAKE has been executed for the investigated sites. To carry out this research shear wave velocity data has been used as input for the programme SHAKE. Fourteen shear wave velocity data of the investigated site has been collected from the direct field test (PS logging and SSMM). The shear wave velocity of other investigated locations has been estimated using empirical correlation between SPT-N and shear-wave velocity. The comparison of amplitude ratio of microtremor and transfer function has been presented in this research. It should be mentioned that microtremor consists of different types of body and surface waves.

The resonance criteria between the site soil and buildings have been analyzed. Finally, vulnerability of site soil using Nakamura's (2000) technique has been carried out for this research.

4.2 CONCLUSIONS

From the overall result and analysis of the study following findings may be summarized.

(a) Stability of microtremor data on ground

In order to check the stability of microtremor data fourteen different locations of BUET campus have been selected to carry out microtremor observation from morning to midnight. The stability of microtremor H/V ratio for site amplification has been discussed in chapter 2. Fourier spectra depend on the source of vibration. This data does not show significant site amplification. That's why horizontal to vertical spectral ratio (H/V) of both East-West and North-South have been calculated. Microtremor H/V ratio do not show the source vibration effect. Whatever the source is, the amplification result is similar for different time instants. From this research, it can be concluded that Horizontal to Vertical spectral (H/V) ratio of microtremor is effective for site response analysis. This technique is reliable for site soil response compared to Fourier spectra.

(b) Resultant of EW and NS direction data

It is necessary to estimate the resultant H/V ratio because microtremor Horizontal to Vertical spectral (H/V) ratio data is found in East-West and North-South direction. Four resultant H/V ratio data are available to estimate the dynamic characteristics which are RM (Root multiplication), RMS (Root square mean), RS (Root square) and Mean. In this research the variations of four resultant H/V ratios have been carried out in three study locations (Bashundhara, Block-D; Board Bazar, Gazipur; Uttar Khan). From the observation it can be concluded that RM of H/V ratio data is close to other three resultants. Therefore, Root multiplication of East-West and North-South data have been used for the estimation of dynamic properties of soil.

(c) Various windows filtering technique

Five filtering windows are available for microtremor data analyses which are Rectangular, Welch, Hamming, Hanning and Blackman window. For this research, time history microtremor data at Bramangaon has been selected to be analyzed using five filtering windows. From analysis of data in filtering windows it can be concluded that the peak H/V ratio is almost same in five windows. Rectangular window has been selected for microtremor data analysis in this research.

(d) Smoothing effect on the microtremor data

Smoothing has significant effect on the of microtremor data. In this research six average smoothing points (2, 3, 5, 10, 15 and 20) have been applied on microtremor H/V ratio at four study locations (Bramangaon, Tongi Ershad Nagar, Ashiyan city and Agargaon Trade fair). From this research it can be concluded that suitable smoothing function helps to estimate peak H/V ratio and predominant frequency easily. The peak of H/V ratio decreases if higher average smoothing points is applied.

(e) H/V Ratio data in and around Dhaka city

Microtremor measurement has been carried out in 45 locations. Out of 45 locations, the overall predominant frequency is 1.25 Hz with standard deviation 0.014. On the other hand, the overall H/V ratio is 2.72 with standard deviation 0.177. The maximum predominant frequency is 3.65 Hz, where H/V ratio is 2.73 at Azampur School, Uttara. The Horizontal to Vertical spectral ratio (H/V) lies between 1.81 and 3.74. On the other hand, the minimum predominant frequency is 0.48 Hz, where H/V ratio is 3.91, Rab-10, Plot, Kamrangirchar.

The Horizontal to Vertical spectral ratio (H/V) lies between 2.23 and 5.65. The maximum Horizontal to Vertical spectral ratio (H/V) is 4.78 where as predominant frequency is 1.22 Hz, at Sosan Ghat, Kamrangirchar. The Horizontal to Vertical spectral ratio (H/V) lies between 4.07 and 5.71. The minimum Horizontal to Vertical spectral ratio (H/V) is 1.08 whereas predominant frequency is 2.57 Hz at Royer Bazar. From this classification of predominant frequency, it can be said that most of the locations predominant frequency varies from 1.0 Hz to 1.99 Hz. These are classified as **Type III**. From the classification of H/V ratio, the most common H/V ratio is **Type III** in 45 locations. The second most common H/V ratio is **Type IV**. The number of locations having H/V ratio ranging between 1.0 and 1.99 is eight. No location has been observed as **Type I**.

(f) Microtremor observation within BUET Campus

Microtremor observation at 132 selected points in soil has been carried out in BUET campus. Out of 132 locations, the overall predominant frequency is 1.39 Hz where as standard deviation is 0.289. On the other hand, the overall peak H/V ratio is 2.09 where as standard deviation is 0.523. The maximum predominant frequency is around 9.62 Hz where as H/V ratio is 2.43 at MT82. The Horizontal to Vertical spectral ratio (H/V) varies from 1.65 to 2.51. On the other hand, the minimum predominant frequency is around 0.25 Hz where as H/V ratio is 9.51 at MT72. This is the highest peak of H/V ratio in 132 selected locations within BUET campus. The Horizontal to Vertical spectral ratio (H/V) lies between 6.85 and 11.85. This lower predominant frequency and higher amplification ratio show that this location is highly susceptible due to any seismic hazard. The minimum Horizontal to Vertical spectral ratio (H/V) is 1.24 at MT 108. The Horizontal to Vertical spectral ratio (H/V) lies between 0.93 and 1.56.

From this classification of predominant frequency, it can be said that most of the locations predominant frequency ranging between 1.0 Hz and 1.99 Hz. These predominant frequencies are classified as **Type III**. The second most common type of predominant frequency is **Type II**. The number of locations predominant frequency classified as **Type V** is 21. There are sixteen **Type I** predominant frequency locations. From the classification of H/V ratio, most of the selected locations are classified as **Type III**. There are seventy five **Type III** locations. **Type II** is the second most predominant H/V ratio. There is no H/V ratio ranging between 0 and 0.99. The number of location H/V ratio greater than 3 is 15.

Microtremor observation on 45 buildings has been carried out within BUET campus. Fourier

Spectrum provides better result of predominant frequency for buildings. Out of 45 microtremor observation in buildings, the maximum predominant frequency is 5.56 Hz along both EW and NS directions at Controller of Examination Building. This is a four-storied frame structure building with 324sqm floor area. There are no lift and shear wall in this building. The foundation of the building is individual footing. There are no structural irregularities in building. But torsional irregularity, re-entrant corner and diaphragm discontinuity exist.

The minimum predominant frequency is 2.00 Hz along EW and NS directions at Eleven Story Tower Building. This is an eleven-storied frame structure with 673sqm floor area. There are three lift cores and a shear wall in the building. The foundation of the building is pile-raft system. No structural irregularity exists in this building. But torsional irregularity, re-entrant corner and diaphragm discontinuity exist. From this classification of predominant frequency along EW direction, most of the locations predominant frequency is more than 3.0 Hz. These are classified as **Type V**. The second most common type of predominant frequency is **Type IV**. The number of building predominant frequency ranging between 2.0 Hz and 2.99 Hz is 5. There is no predominant frequency of **Type I**, **Type II** and **Type III**. **Type V** is the most common predominant frequency in 45 buildings of BUET campus along NS direction. **Type IV** is the second most predominant frequency. There are no buildings of predominant frequency ranging between 0 and 1.99.

(g) Comparison between microtremor H/V ratio and Transfer Function using the program SHAKE

The comparison of amplitude ratio between transfer function and microtremor H/V ratio for forty two locations in and around the Dhaka city has been studied.

From the comparison between microtremor H/V ratio and transfer function using the programme SHAKE four types of characteristics curves have been observed. These curves are classified as similar, dissimilar, right side shifted and left side shifted compared to the microtremor H/V ratio curve. Among 42 models predominant frequency of thirty five transfer function have been shifted in the right side of microtremor and only one has been shifted in the left side. Similar pattern amplitude ratio curves have been found in six locations. The rest two locations have been found where no similarity between microtremor H/V ratio and transfer function.

The same amplitude ratio but higher frequencies of transfer function have been found in ten locations. The higher frequency but low amplified locations have been found in nineteen

different locations. On the other hand, both higher frequency and higher amplified locations of transfer function have been found in six locations. The similar predominant frequency but lower amplified transfer function has been found in three locations. But, the same predominant frequency but higher amplified location is Adabor. The dissimilar types of pattern curve have been found in three locations.

From these results, it can be said that although amplitude values of the ratios are close, the predominant frequency for the two cases differs slightly. The reason of this difference is that microtremor consists of different types of waves, but the theoretical transfer function is based on shear-wave only.

(h) Resonance between site soil and building

The resonance between the site soil and building has been analyzed using the H/V ratio of soil and Fourier spectra of building in both EW and NS direction. It has been found that resonance may occur at four BUET buildings. These buildings are Eleven Story Tower Building, URP Building, Titumir Hall and Building # 1. For most of the building predominant frequency is not close to the predominant frequency of soil. From the sub-soil characteristics within BUET campus, it can be concluded that stiff soil with higher SPT value exists in most of the investigated locations.

(i) Seismic Vulnerability Index (Kg) for soil

Seismic vulnerability index (Kg) is an index indicating the level of vulnerability of a layer of soil to deform. This index is useful for the detection of areas that are weak zone (unconsolidated sediment) at the time of occurrence of earthquakes. The details result of Vulnerability Index (Kg) of the investigated areas in 45 locations has been illustrated in section 4.3.2. The vulnerability index of forty five locations in and around the Dhaka city has been classified into four types which are low (0-5), moderate (6-10), high (11-20) and very high (>20). From the analysis the highest (Kg) value has been found at Rab-10, Plot, and Kamrangirchar. So, it can be concluded that this location is more weak zone than other locations. The seismic vulnerability index (Kg) for 45 sites varies between 0.45 and 31.85. Sixteen sites have been classified as low vulnerable of soil layers. Five sites have been identified as having moderate to high vulnerable of soil layers to deform.

REFERENCES

- Alam, M. K., Hasan, A.K.M. Shahidul, Khan, M. R. and Whitney, J. W. (1990). The Geological Map of Bangladesh, the Geological Survey of Bangladesh in Collaboration with United States Geological Survey.
- Ansary, M. A., Yamazaki, F. and Katayama, T. (1996). Application of microtremor measurements to the estimation of site amplification characteristics, Bulletin of Earthquake Resistant Structure Research Center, IIS, University of Tokyo, No. 29, PP. 95-113.
- Ansary, M. A., Rahman, S., Murad, E. M., Chowdhury, S. A. and Shuvra, D. P. (2010). Proposed Time History and Response Spectrum for Dhaka, Chittagong and Sylhet cities, Proceedings, 3rd International Earthquake Symposium, March 5-6, Dhaka, Bangladesh, PP. 349-356.
- ASTM (2000). Annual Book of ASTM Standards, vol. 04.08: Soil and Rock (I). Standard No. D 1586-99, Standard Test Method for Penetration Test and Split-Barrel Sampling of Soils, West Conshohocken, PA, PP. 139-143.
- Banglapedia (2006). National Encyclopedia of Bangladesh, Prepared by Asiatic Society of Bangladesh, CD edition.
- Bard, P. Y. (2004). Effects of surface geology on ground motion: Recent results and remaining issues, Proceedings of the 10th European Conference on Earthquake Engineering, Vienna, Austria, August 28 – September 2, 1994, PP. 305-325.
- Bilham, R., Gaur, V. K. and Molnar, P. (2001). Himalayan Seismic Hazard, SCIENCE, 293.
- CDMP (2009). Ongoing Research Work, CDMP-UNDP Fault Map Delineation for Bangladesh, 2009.
- Curry, J. R. and Moore, D. G. (1974). Sedimentary and Tectonic processes in Bengal Deep Sea Fan and Geosyncline, The geology of continental margins, Springer-Verlag, New York.
- Daryono (2009). Efek Tapek Lokal (Local site effect) di Graben Bantul Berdasarkan Pengukuran Mikrotremor. International Conference Earth Science and Technology. Yogyakarta.
- Dimitriu, P. P., Papaioannou, Ch. and Theodulidis, N. P. (1998). EURO-SEISTEST strong motion array near Thessaloniki, Northern Greece: a case study of site effects. Bulletin of seismological society of America, No. 3, PP. 862-873.

- Dravinski, M., Ding, G. and Wen, K. L. (1996). Analysis of spectral ratios for estimating ground motion in deep basins, *Bull. Seism. Soc. Am.*, 86, PP. 843-847.
- Field, E. H. and Jacob, K. H. (1993). The Theoretical Response of Sedimentary Layers to Ambient Seismic Noise, *Geophysical Research Letter*, 20, PP. 2925-2928.
- Field, E. H. and Jacob, K. H. (1995). A comparison and test of various site-response estimation techniques, including three that are not reference-site dependent, *Bulletin of the Seismological Society of America*, 85, PP. 1127-1143.
- Field, E. H., Clement, A. C., Jacob, K. H., Aharonian, V., Hough, S. E., Friberg, P. A., Bahaian, T. O., Karapetian, S. S., Hovanessian, S. M. and Abramian, H. A. (1995). Earthquake site response study in Giumri (Formerly Leninakan), Armenian using ambient noise observation. *Bull. Seism. Soc. Am.*, 85, PP. 349-353.
- Ghayamghamian, M. R. and Kawakami, H. (1997). Segmental cross-spectrum in microtremor spectral ratio analysis. 7th International Conference on Structural Safety and Reliability, Kyoto, November 1997, 24-28, PP. 1487-1494.
- Geological Survey of Bangladesh, GSB (2008). Geomorphological Map of Dhaka city, Prepared by GSB under the project of Comprehensive Disaster Management Programme (CDMP).
- Horike, M., Zhao, B. and Kawase, H. (2001). Comparison of site response characteristics inferred from microtremors and earthquake shear waves, *Bulletin of the Seismological Society of America*, 91, PP. 1526-1536.
- Hossain, M. T. (2009). Estimation of Earthquake Induced Liquefaction Potential of Selected areas of Dhaka City Based on Shear Wave Velocity, Thesis paper of Master of Science in Civil Engineering, November, 2009.
- Huang, H. C. and Tseng, Y. S. (2002). Characteristics of soil liquefaction using H/V of microtremors in Yuan-Lin area, Taiwan, *TAO*, Vol.13, No.3, 325-338, September, 2002.
- Kamal, A.S.M. Maksud and Midorikawa, S. (2003). GIS-based Landfill Mapping of Dhaka City area, Bangladesh, Using Remote sensing data, *Proceedings on the second International Symposium on New Technologies for Urban Safety of Mega cities in Asia*, University of Tokyo, Japan.
- Kanai, K., Tanaka, T. and Osada, K. (1954). Measurements of Micro-tremors 1. *Bulletin Earthquake Research Institute, Tokyo University*, 32, PP. 199-210.
- Khan, M. R. and Munimullah., compilers (1988). Stratigraphic lexicon of Banglades: Geology Survey of Bangladesh record, Vol. 5, pt. 1, PP. 61.
- Khan, F. H. (1991). *Geology of Bangladesh*, University Press Limited, PP. 1-207.

- Konno, K. and Ohmachi, T. (1998). Ground motion characteristics estimated from spectral ratio between horizontal and vertical components of microtremor», *Bull. Seism. Soc. Am.*, 88, N. 1, PP. 228-241.
- Lachet, C. and Bard, P. Y. (1994). Numerical and theoretical investigations on the possibilities and limitations of Nakamura's technique, *Journal of the Physics of the Earth*, 42, PP. 377-397.
- Lermo, L. and Chavez-García, F. J. (1993). Site effect evaluation using spectral ratios with only one station, *Bull. Seism. Soc. Am.*, 83, PP. 1574-1594.
- Lermo, J. and Chavez-Garcia, F. J. (1994). Are Microtremors Useful in Site Response Evaluation? *Bulletin of Seismological Society of America*, 84, PP. 1350-1364.
- Matin, M.A., Maroof Khan, M.A., Fariduddin, M., Boul. M.A., Taolad Hossain, M.M. and Kononov, A.I. (1983). *The Tectonic Map of Bangladesh-Past and Present*, Vol-2, PP. 29-36.
- Molnar, S., Cassidy, J. F. Monahan, P. A. and Dosso, S. E. (2007). Comparison of geophysical methods to determine shear-wave velocity, *Proceedings of the Canadian Conference on Earthquake Engineering*, June 24-27th 2007, Ottawa, ON, Paper 1173.
- Nakamura, Y. (1989). A Method for Dynamic Characteristics of Sub-surface Using Microtremors on the Ground Surface, *Quick Report of Railway Technical Research Institute*, 30, No. 1, PP. 25-33 (in Japanese).
- Nakamura, Y. (2000). Clear identification of fundamental idea of Nakamura's Technique and its applications, *Proc. Of the 12th World Conference on Earthquake Engineering*, Auckland, New Zealand, PP. 2656-2664.
- Ohmachi, T., Nakamura, Y. and Toshinawa, T. (1991). Ground motion characteristics in the San Francisco Bay area detected by microtremor measurements, *Proc. 2nd International Conference on Recent Advances in Geotech. Earth. Eng. & Soil Dyn.* Saint Louis, Missouri, PP. 11-15 March: PP. 1643-1648.
- Rodriguez, V. S. H. and Midorikawa, S. (2002). Applicability of the H/V Spectral Ratio of Microtremors in Assessing Site Effects on Seismic Motion, *Earthquake Engineering and Structural Dynamics*, 31, PP. 261-279.
- Russel, S. Z. R., Yasin, M., Ansary, M. A., Saha, R., Kamruzzaman, M. and Noor, M. A. (2006). Evaluation of the Seismic Vulnerability of Bangladeshi Building using Non-Destructive Testing, an unpublished BNUS annual Report, Bangladesh Network Office for Urban Safety, International Centre for Urban Safety Engineering, Institute of Industrial Science, The University of Tokyo.

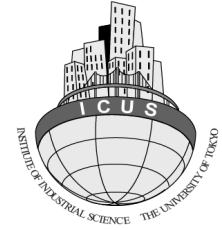
Sesoren, Atila (1984). Geological Interpretation of Landsat Imagery of Bangladesh Ganges Delta, ITC Journal, PP. 229-232.

Suzuki, T., Adachi, Y. and Tanaka, M. (1995). Application of Microtremor measurements to the estimation of earthquake ground motions in the Kushiro city during the Kushiro-Oki earthquake of 15 January 1993, Earthquake Eng. Struc. Dyn. 24, PP. 595-613.

TC4 (1993). Manual for Zonation on Seismic geotechnical hazards, published by ISSMFE.



**BANGLADESH NETWORK
OFFICE FOR URBAN SAFETY**



PART-III

ESTIMATION OF SHEAR WAVE VELOCITY USING 3D MICROTREMOR MEASUREMENT IN SYLHET CITY

**BANGLADESH NETWORK OFFICE FOR
URBAN SAFETY (BNUS), BUET, DHAKA**

Prepared By: Estiak Ahmed Murad

Mehedi Ahmed Ansary

Introduction:

Bangladesh is a small country situated at the south of The Himalayans. The Indian tectonic plate and the Asian tectonic plate had a collision in The Himalayans region. In 2001, Bilham et al. (2001) has shown the high possibility of large earthquake occurrence around the Himalayan region . Sylhet is one of the major cities of Bangladesh. There are several faults near Sylhet where past earthquake history is available. Shillong Fault and Douki Fault are prominent within them. So, seismic activity near Sylhet is higher than any other region of Bangladesh. According to Bangladesh National Building Code (BNBC) 1993 Sylhet is situated in the most vulnerable zone, “Zone-3” to Earthquake. Recently some studies have been taken to evaluate earthquake risk in some particular Educational Institutions. Several kinds of Structural and Geotechnical data have been collected for this study. For evaluation of site amplification and response of soil and structure, Shear wave velocity of soil is the key parameter. Shear wave velocity of soil has been determined using a Geophysical technique named microtremor array method. This method was developed and used in several projects like Network for Earthquake Engineering Simulation (NEES) funded by National Science Foundation (NSF), USA , Site Effects Assessment Using Ambient Excitation (SESAME) in Europe etc. In Bangladesh this method is a new one and this is the first time where it has been used.

Methodology:

There are several methods of determining shear wave velocity from surface wave. Spectral-Analysis-of-Surface-Waves (SASW) was proposed by Nazarian and Stokoe in 1984. Later a more easy and convenient method, Multi Channel spectral analysis was developed and proposed by Park et al. Tokimatsu, 1995; Zywicki, 1999 etc. but all these methods has one common disadvantages. There an energy source is required to create vibration. That energy source usually makes too much noise and vibration. So, in urban area those methods are unacceptable some time. To recover those problems in 2001, Louie proposed another method, Refraction Microtremor (ReMi) method. Ambient vibration is used in this method to get deep profile of shear wave velocity of soil.

The steps to get shear wave velocity starts with data acquisition. At first the different array type was proposed by different researchers. After Wathele (2005) an irregular array of microtremor was used in this research.

Five numbers of sensors are used in each sites except Zindabazar High School. Due to some limitations, three sensors were used for data collection. To reduce the effect of noise and to detect low frequency vibration one hour reading has been taken.

Using those data at first Spectral Auto Correlation (SPAC) was used to determine the correlation between waves detected from different location at the same time. According to Aki (1957) special auto correlation function between two sensors is defined by the following equation.

$$\phi(\xi) = \frac{1}{T} \int_0^T v_o(t)v_\xi(t)dt \dots\dots\dots(1)$$

Here,

ξ is the distance between two sensors, T is the data acquisition time, v_o & v_ξ are the signals recorded at the sensors of 0 and ξ distance respectively.

If a narrow frequency band filter is used of frequency ω_0 the auto correlation ratios are calculated for all pairs of receivers by the following equation.

$$\rho(\xi, \omega) = \frac{\phi(\xi, \omega)}{\phi(0, \omega)} \dots\dots\dots(2)$$

Akai (1957) has shown that, for a given inter sensor distance ξ the azimuthal average of $\rho(\xi, \omega)$ has the shape of Bessel function. That can be shown as,

$$\overline{\rho(\xi, \omega)} = J_0 \left(\frac{\omega_0 \xi}{c(\omega_0)} \right) \dots\dots\dots(3)$$

Here, J_0 is the Bessel function of the first order and $c(\omega_0)$ is the dispersion curve. Than using those correlation dispersion curve has been developed. There was Possibility of different dispersion curves, so a theoretical dispersion curve has been used to find the dispersion curve for the site. Theoretical dispersion curve was developed for Sylhet from soil data achieved by Comprehensive Disaster Management Program (CDMP). In the computation of theoretical dispersion curve in GPDC program is based on Eigenvalue problem by Thomson (1950) and Haskell (1953). For the computation the assumptions are, the soil layers are perfectly horizontal and isotropic, they are extended upto infinity horizontal distance. It can be shown by a figure given by Wathelet (2005),

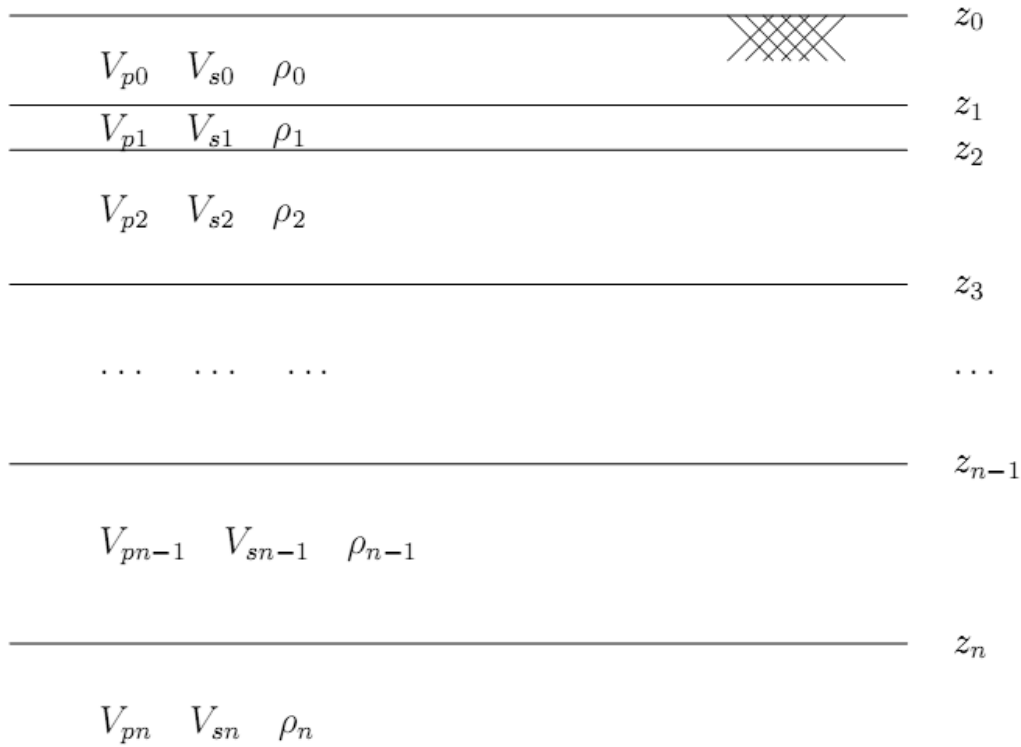


Fig 1: Schematic one dimensional soil model Wathelet (2005), .

For sylhet the soil property used are given below:

Thickness(m)	Vp (m/s)	Vs (m/s)	density (kg/m ³)
16	20	210	1600
24	800	400	1800
0	2000	1000	2200

The bottom most layer of thickness 0 m is actually the half space. Here 0 m thickness is given just because GPDC program considers the half space by reading 0 value in thickness.

The dispersion curve found is given below.

Than the inversion of those dispersion curve was done by using Neighbourhood Algorithm by Dinver (A software developed by Marc Wathele (2005). In the inversion process the assumptions were, Shear wave velocity increases with depth of the layer and poisson ratio is same for soil from any depth. There were less attention to the poison's ratio of soil layers because the poison ratio does not has a significant role in forward computation of dispersion curve from soil layer (Wathelet, 2005) . But it is necessary to relate shear wave velocity with p-wave velocity.

Collected Data:

Location of data collection are showed in the following figure.

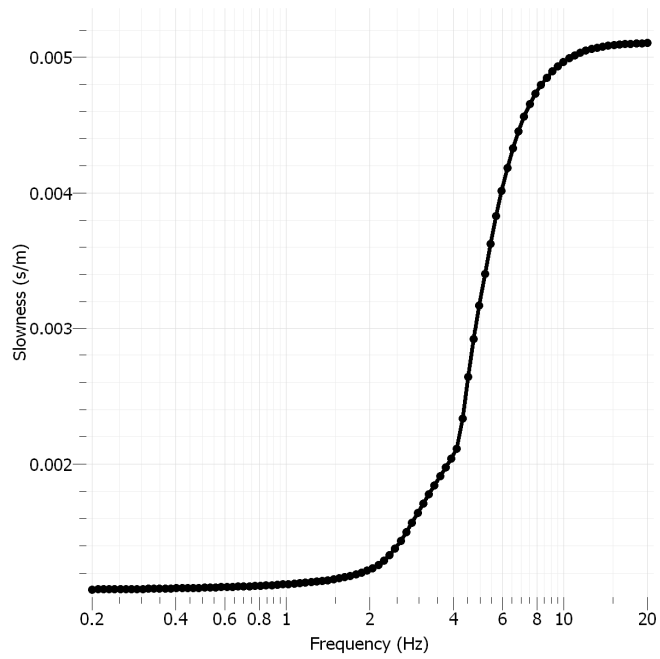


Fig 2: the dispersion curve for Sylhet.

Fig 3 : Location of Data Collection from Sylhet.

At Aided School, the playground was used for data collection. Two kind of array has been used in that case. Array formations are given below.

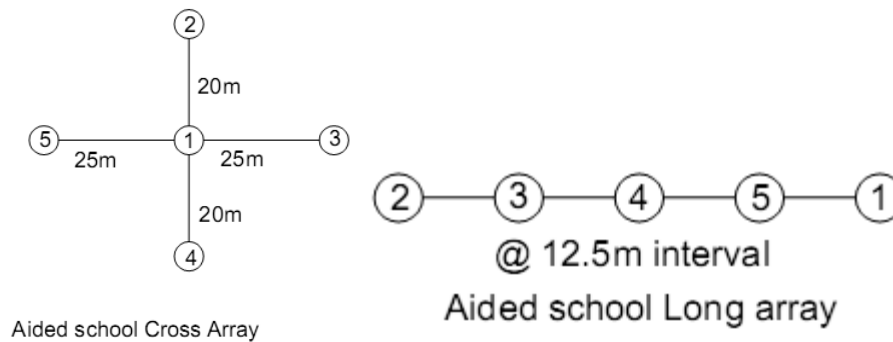


Fig 4 : Array formation at Aided school play ground.

At Gindabazar Govt. Primary School due to the limitation of enough free space, only one longitudinal array has been used.

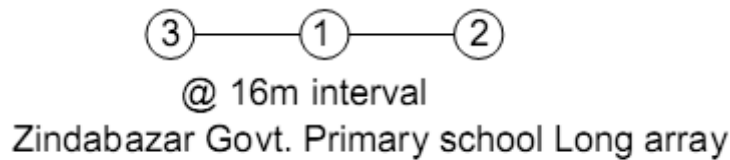


Fig 5: Array formation of Zindabazar Govt. Primary School.

At Raza G. C. High School, the play ground has been used. The array formation is given below.

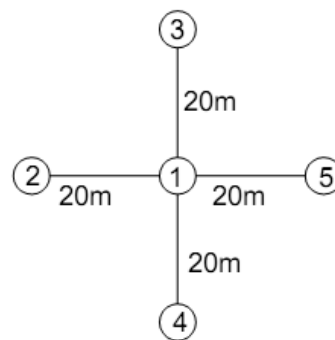


Fig 6: Array formation of Raza G.C. High School play ground .

At Taltola fire service office, the field adjacent office has been used. Two array has been used there. Array formations are given below.



Fig 7: Array formation of Taltola Fire service office.

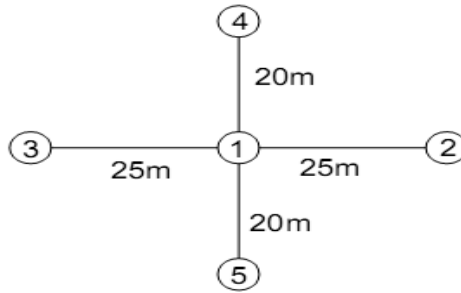


Fig 8: Upashar array formation.

Results:

After using all steps described in the methodology section, the shear wave velocity profiles found are presented below.

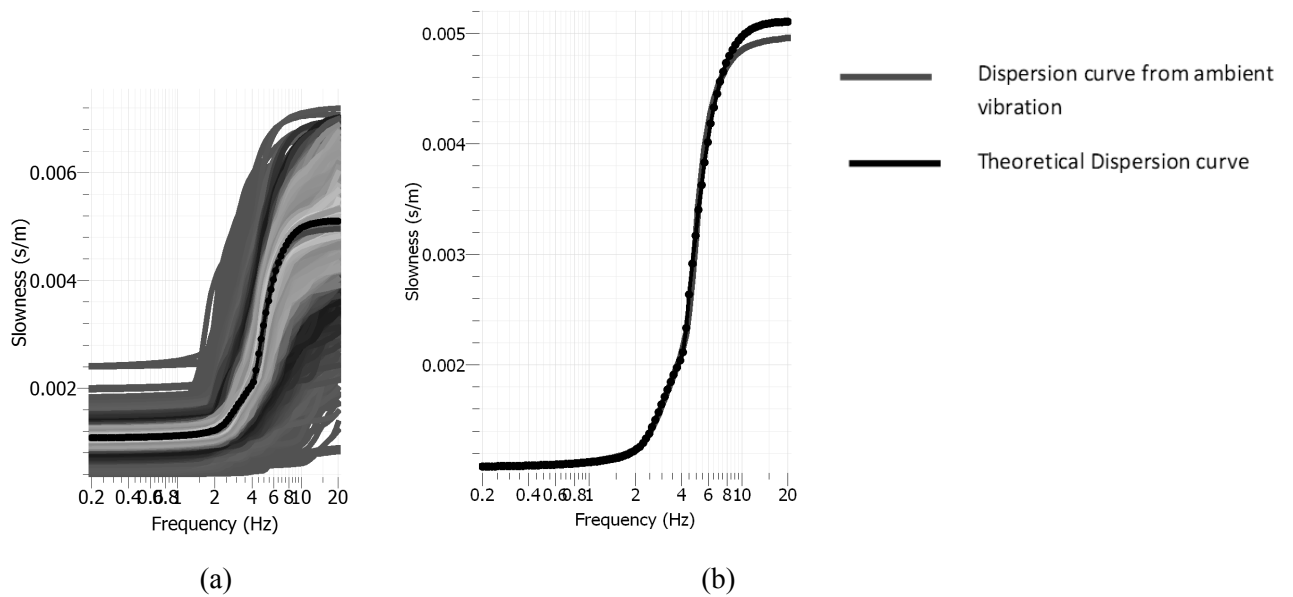
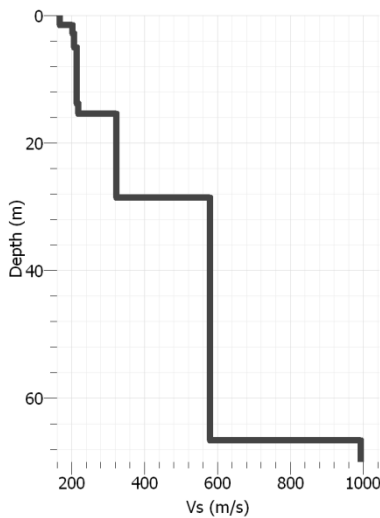


Fig 9: Dispersion Curve for Rayleigh wave of Aided School (From cross array). (a) All curves with misfit 0 to 1., (b) Curve with minimum misfit, (Misfit = 0.0176) .



Depth			Vs (m/s)	Vs (avg)
0	to	1.44	168.38	203
1.44	to	2.87	201.27	
2.87	to	4.83	205.97	
4.83	to	13.83	215.37	217
13.83	to	15.27	220	323
15.27	to	28.44	323.43	
28.44	to	66.43	579.51	579
66.43	to	70	991.45	991

Fig 10: Shear wave velocity profile of Aided School (From cross array).

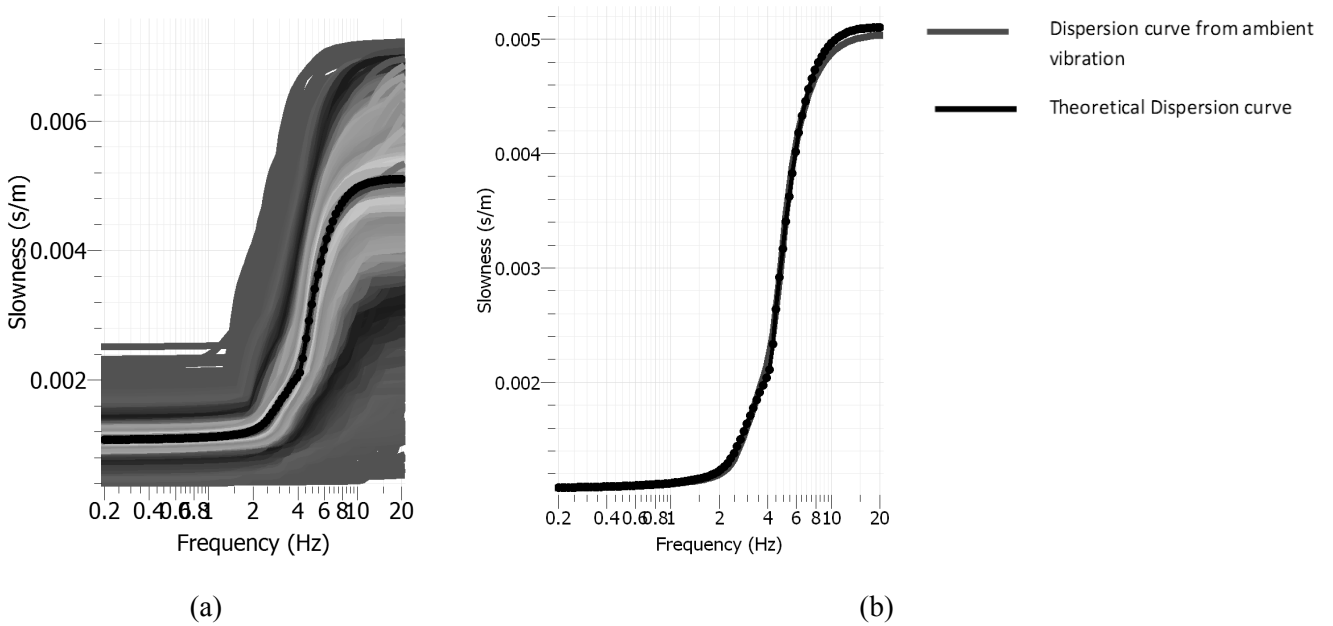
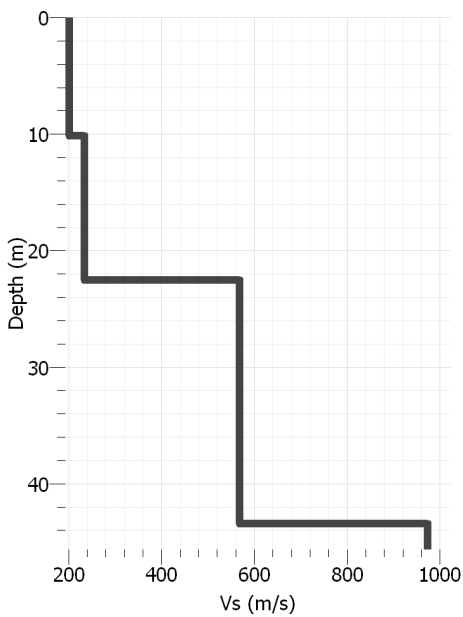


Fig 11: Dispersion Curve for Rayleigh wave of Aided School (From long array).

(a) All curves with misfit 0 to 1., (b) Curve with minimum misfit, (Misfit = 0.0176) .



Depth			Vs (m/s)	Vs (average)
0	to	10.04	200.09	200
10.04	to	22.48	234	234
22.48	to	43.39	469.43	469
43.39	to	45.52	974.03	974

Fig 12: Shear wave velocity profile of Aided School (From long array).

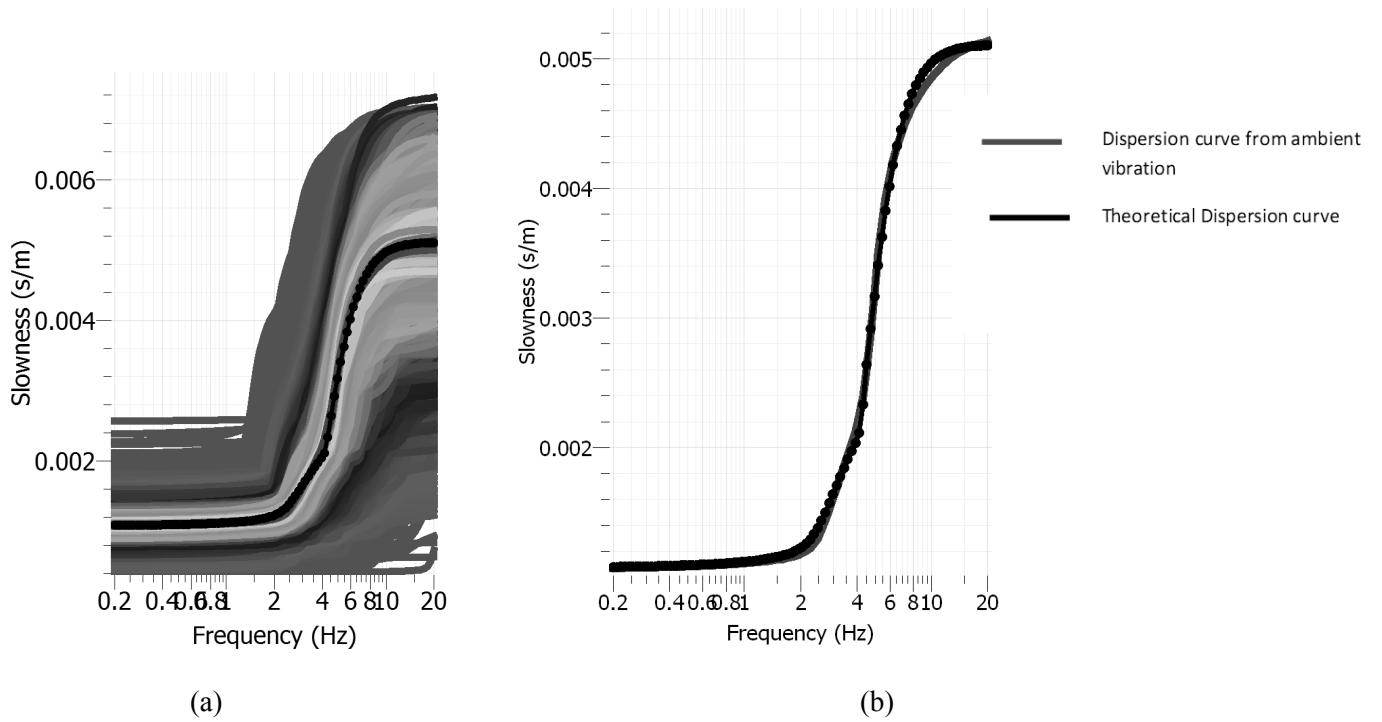
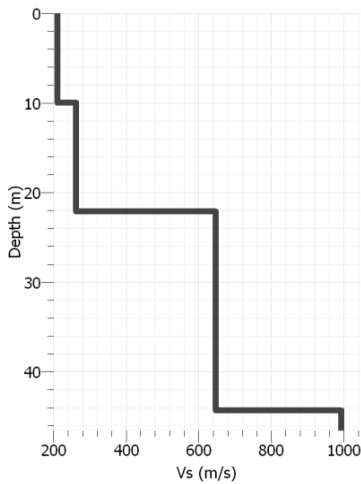


Fig 13: Dispersion Curve for Rayleigh wave of Raza GC School (From long array).
 (a) All curves with misfit 0 to 1., (b) Curve with minimum misfit,(Misfit = 0.022) .



Depth			Vs (m/s)	Vs avg
0	to	9.89	211.07	211
9.89	to	22.04	260.37	260
22.04	to	44.26	645.76	646
44.26	to	46.52	991.60	992

Fig 14: Shear wave velocity profile of Raza GC School (From long array).

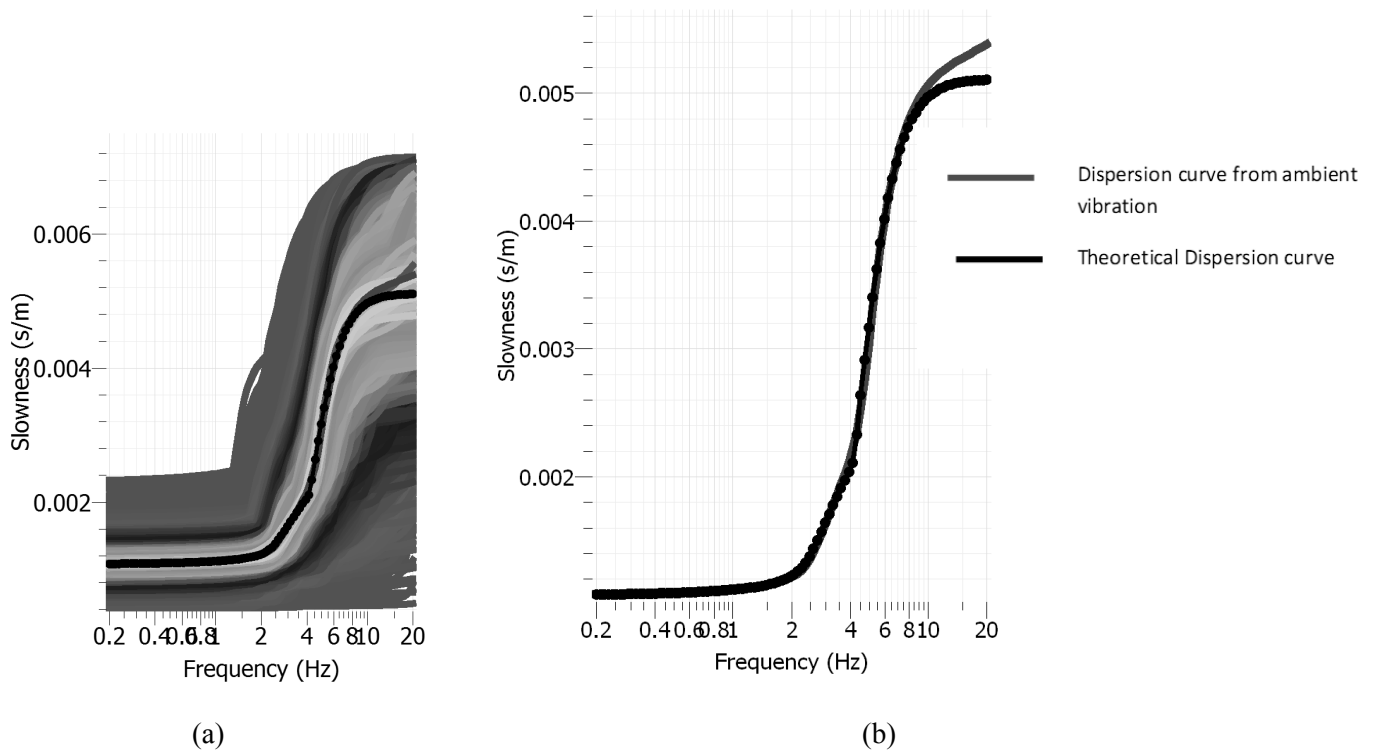
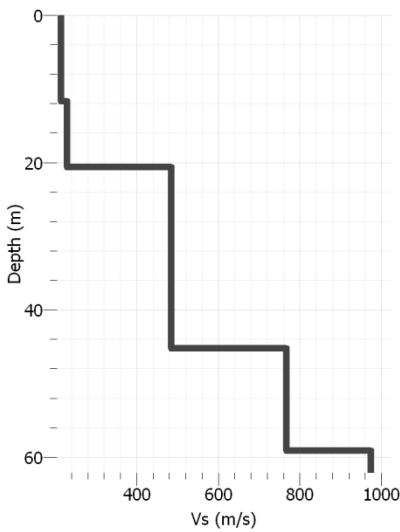


Fig 15: Dispersion Curve for Rayleigh wave of (From cross array).
 (a) All curves with misfit 0 to 1., (b) Curve with minimum misfit,(Misfit = 0.02)



Depth			Vs (m/s)	Vs avg
0	to	11.58	214.76	215
11.58	to	20.61	227.81	228
20.61	to	45.07	484.51	485
45.07	to	58.95	768.06	768
58.95	to	61.96	974.73	975

Fig 16: Shear wave velocity profile of Upashar (From cross array).

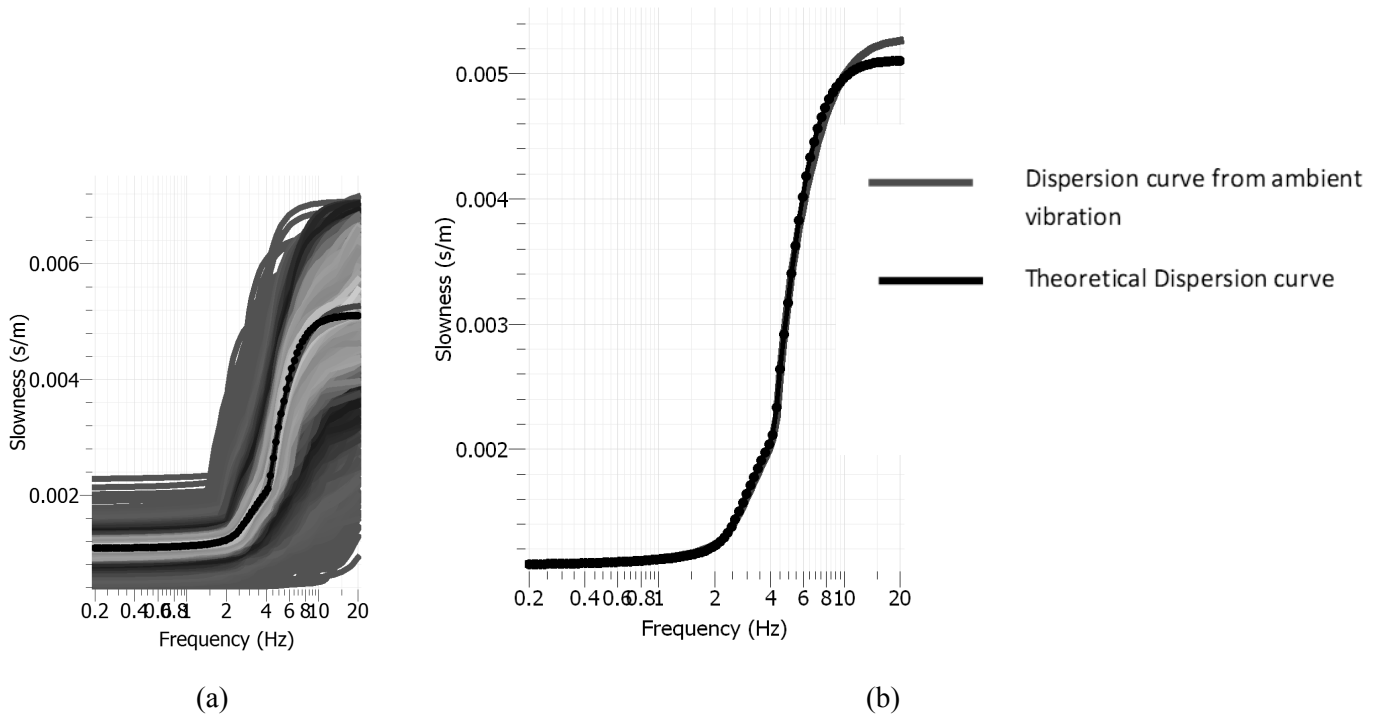


Fig 17: Dispersion Curve for Rayleigh wave of Taltola Fire service (From long array).
 (a) All curves with misfit 0 to 1., (b) Curve with minimum misfit,(Misfit = 0.015)

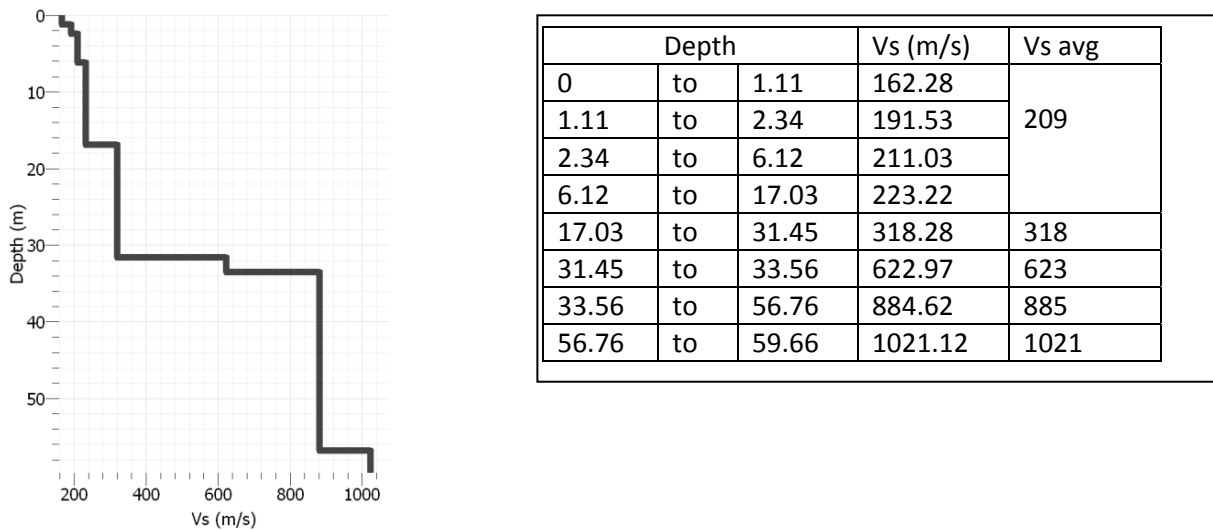


Fig 10: Shear wave velocity profile of Taltola Fire service (From long array).

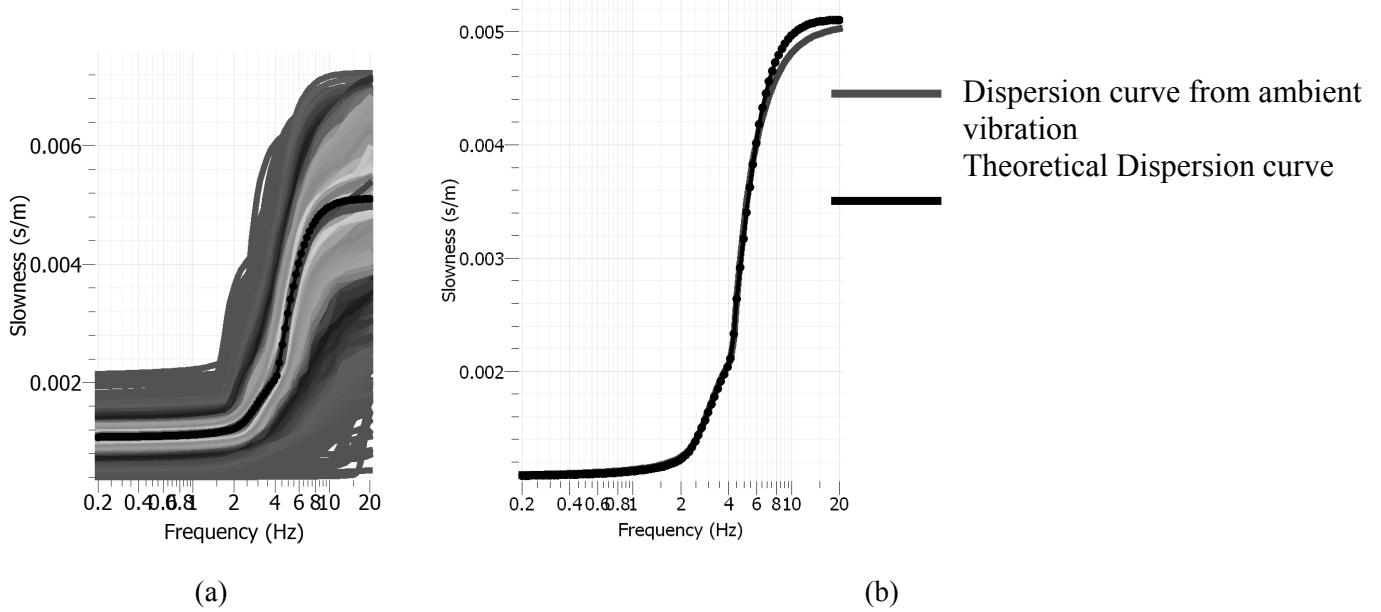
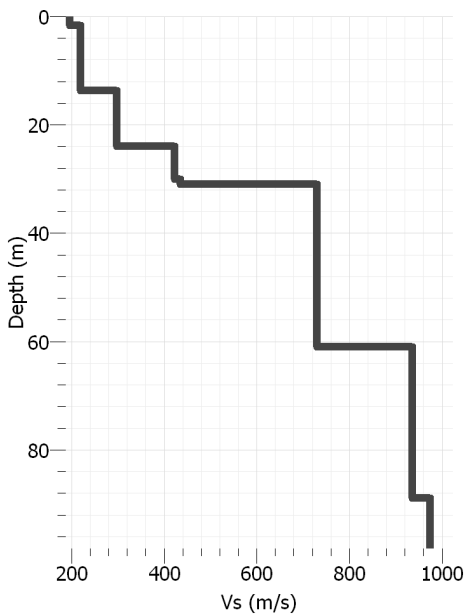


Fig 18: Dispersion Curve for Rayleigh wave of Zindabazar High School
 (a) All curves with misfit 0 to 1., (b) Curve with minimum misfit, (Misfit = 0.017).



Depth			Vs (m/s)	Vs avg
0	to	1.46	195.31	206
1.46	to	13.54	217.52	
13.54	to	23.97	293.07	293
23.97	to	30.01	419.71	427
30.01	to	30.84	435.26	
30.84	to	60.96	728.54	729
60.96	to	88.96	933.71	934
88.96	to	97.93	971.48	971

Fig 19: Shear wave velocity profile of Zindabazar High School (From long array).

Conclusion

Microtremor array method is an approximate method which is highly susceptible to some factors like array formation, noise in collected data, the theoretical dispersion curve and the parameterization. The noise was very high in most of the cases. Long time reading was taken to reduce the effect of noise. The shear wave velocity profiles found are average soil profile

of all the soil profiles below each sensor. So just because of the positioning of the sensors gave close but different soil profile in the same field. The theoretical dispersion curve was made by using judgment on some soil profiles found by seismic downhole method. In the parameterization phase, the poisson ratio and density of the soil strata kept same for all depth, but according to Wathele (2005) the effect of poisson ratio and density are insignificant. So it will not lead to a profile much different from real case. Another fact is, the profiles are found by using misfit less than 0.05. So there is probability of variation of real shear wave velocity from the shown profile.

Reference

- Aki, K. (1957). Space and time spectra of stationary stochastic waves, with special reference to microtremors, *Bull. Earthq. Res. Inst.* 35, 415-456.
- Bilham, R., V.K. Gaur and P. Molnar (2001). Himalayan Seismic Hazard, *SCIENCE*, 293.
- Haskell, N. A. (1953). The dispersion of surface waves on multilayered media, *Bull. Seism. Soc. Am.* 43, 17-34.
- Louie, J. N. (2001). "Faster, better: shear-wave velocity to 100 meters depth from refraction microtremor arrays." *Bulletin of the Seismological Society of American*, 91(2), 347-364.
- Nazarian, S., and Stokoe, K. H., II (1984). "In situ shear wave velocities from Spectral Analysis of Surface Waves." *Proceedings of the 8th World Conference on Earthquake Engineering*, Prentice-Hall, Inc., Englewood Cliffs, New Jersey, Vol. III, 31-38.
- Park, C.B., Miller, R.D., Xia, J. (1999). "Multichannel analysis of surface waves." *Geophysics*, 64, 800-808.
- Thomson, W. T. (1950). Transmission of elastic waves through a stratified solid medium, *Journal of Applied Physics* 21, 89-93
- Tokimatsu, K. (1995). "Geotechnical site characterization using surface waves." *Proceedings of 1st International Conference on Earthquake Geotechnical Engineering*, IS-Tokyo '95, Balkema, Rotterdam, 1333-1368.
- Wathelet, M. (2005). "Array recordings of ambient vibrations: surface-wave inversion." Ph.D. dissertation, Universite de Liege.
- Zywicki, D.J. (1999). "Advanced signal processing methods applied to engineering analysis of seismic surface waves." Ph.D. dissertation, Georgia Institute of Technology.



**BANGLADESH NETWORK
OFFICE FOR URBAN SAFETY**



PART-IV

STRONG MOTION RECORDINGS DURING SEPTEMBER 18, 2011 SIKKIM EARTHQUAKE

**BANGLADESH NETWORK OFFICE FOR
URBAN SAFETY (BNUS), BUET, DHAKA**

Prepared By: Mehedi Ahmed Ansary

Md. Shamsur Rahman

1. INTRODUCTION

The 4.8 km long Jamuna Multipurpose Bridge connects the eastern and western parts of Bangladesh. Being the only road and rail link between the two regions, the bridge bears immense economic and strategic importance for the whole country. But the bridge is located in a seismically active region that can be subjected to moderately strong earthquakes from a number of sources and special earthquake protection devices have been used in the bridge. The bridge has been designed for a peak ground acceleration of 0.2g due to a 7.0 magnitude earthquake in the Bogra fault zone, which is about 25 to 40 kms from the west end of the bridge, based on study by Bolt (1987).

Jamuna Multipurpose Bridge Authority (JMBA) took necessary steps for the installation of seismic instruments on and around the Jamuna Bridge. JMBA employed Bangladesh University of Engineering & Technology (BUET) as the technical consultant for this project. The Installation of the seismic instruments on the bridge structure and six other free-field (ground) stations was completed by Kinometrics, Inc. USA on July 10, 2003 (BUET, 2003). The Operating and Monitoring Phase of the project started on July 11, 2003.

In this report the September 18, 2011 Sikkim earthquake recorded by the earthquake monitoring system are presented.

2. EARTHQUAKE DATA ANALYSIS

The report gives the complete processed data of the three components of motion at the eight free-field stations which recorded the earthquake. The data processing, which includes necessary corrections and filtering, has been carried out using softwares SMA (Kinometrics, 2001) and Origin 6.0. The earthquake data has been formatted using USGS format. The acceleration, velocity and displacement time histories have been evaluated.

3. EARTHQUAKE PARAMETERS

The 6.9 Moment magnitude earthquake hit Sikkim on 18th September 2011 with its epicenter located at 27.72°N, 88.06°E, near India-Nepal border, about 68 km NW of Gangtok and at a focal depth of 19.7 km as reported by USGS. Three aftershocks of magnitude 5.7, 5.1 and 4.6 were also felt in Sikkim within 30 minutes of the earthquake.

The region is known for seismic activity between the Main Boundary Thrust (MBT) and the Main Central Thrust (MCT). Maximum observed shaking intensity during this earthquake was VIII on MSK scale. About 100 deaths are reported in India with the maximum of at least 60 in the state of Sikkim and total loss of property was about 15 Million US Dollar.

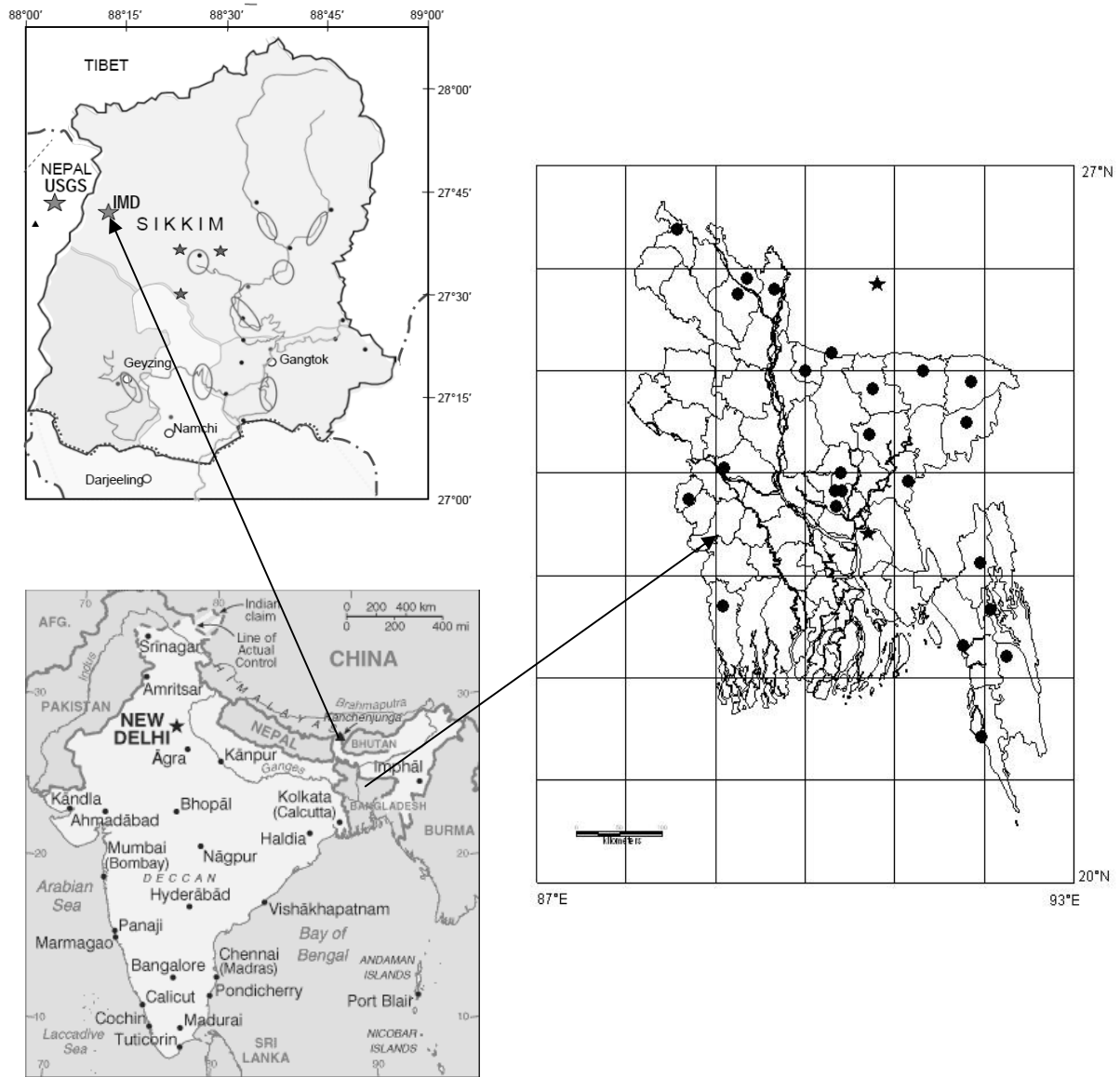


Figure 1 Earthquake and strong motion (accelerometer) locations

4. GROUND MOTION DUE TO EARTHQUAKE

Figure 2 to 24 show the time history (acceleration) data of Bogra, Comilla, Haji Camp, Khagrachari, Kurigram, Meherpur, Natore, Netrokona in EW, NS and UD directions. Table 1 gives a list of peak values of accelerations, velocities and displacements of all the free-field stations due to the 2011 Sikkim earthquake. The maximum recorded acceleration due to this earthquake is 33.55 cm/s^2 in Kurigram, the maximum velocity is 3.46 cm/s in Kurigram and the maximum displacement is 1.62 cm in Netrokona.

Table 1: Summary of Peak Ground Motion Acceleration in Free Field Stations

Station ID	Direction	Peak Ground Motion		
		Acceleration (cm/s^2)	Velocity (cm/s)	Displacement (mm)
Bogra	EW	21.49	2.00	0.54
	NS	-21.57	-1.41	0.32
	UD	10.67	0.68	-0.16
Comilla	EW	-5.56	0.28	0.022
	NS	-5.47	0.28	-0.017
	UD	2.27	0.08	0.007
Haji Camp	EW	7.95	1.198	-0.340
	NS	5.27	-0.842	-0.324
	UD	2.45	-0.348	-0.125
Khagrachari	EW	6.81	0.467	-0.093
	NS	-4.91	0.413	0.089
	UD	1.84	-0.215	0.038
Kurigram	EW	-33.55	-3.16	-0.904
	NS	29.87	3.46	0.565
	UD	31.81	1.39	-0.320

Meherpur	EW	-12.71	1.72	-0.585
	NS	-11.59	1.95	-0.614
	UD	5.73	-0.29	-0.125
Natore	EW	-17.34	1.58	0.589
	NS	17.68	1.46	0.413
	UD	-	-	-
Netrokona	EW	14.63	-2.89	1.623
	NS	12.19	2.18	0.793
	UD	-4.56	0.79	0.405

Note. EW represents East-West direction,
 NS represents North-South direction,
 UD represents Vertical direction

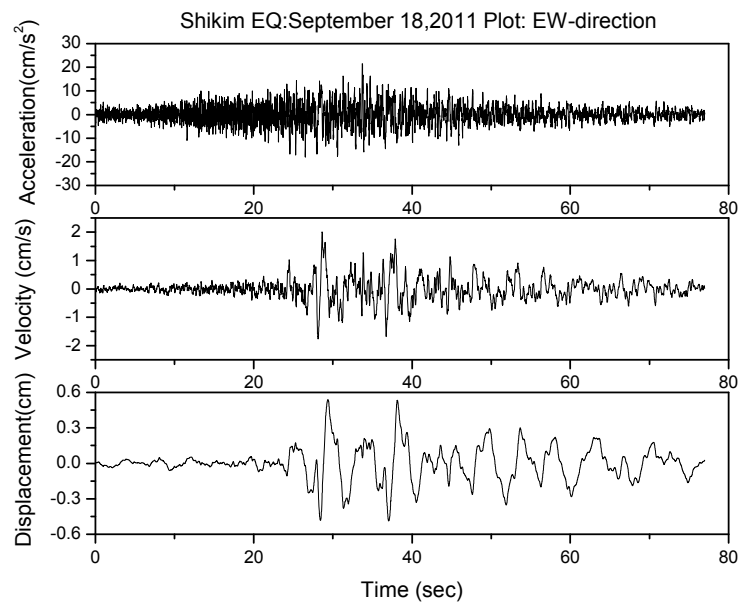


Figure 2 Recorded earthquake ground motion in Bogra, EW-direction

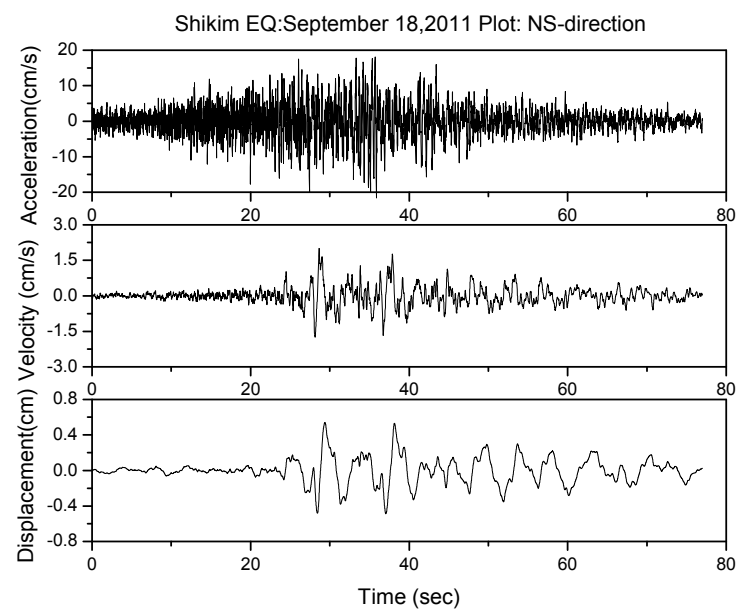


Figure 3 Recorded earthquake ground motion in Bogra, NS-direction

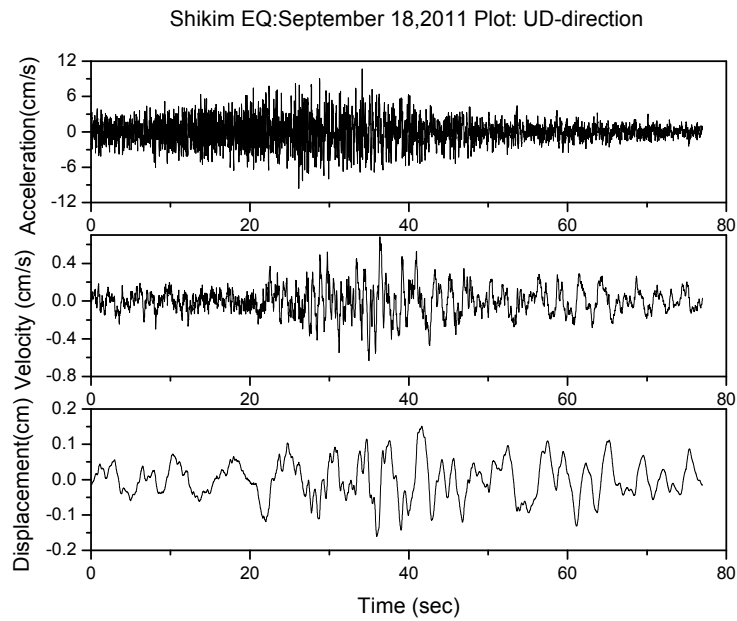


Figure 4 Recorded earthquake ground motion in Bogra, UD-direction

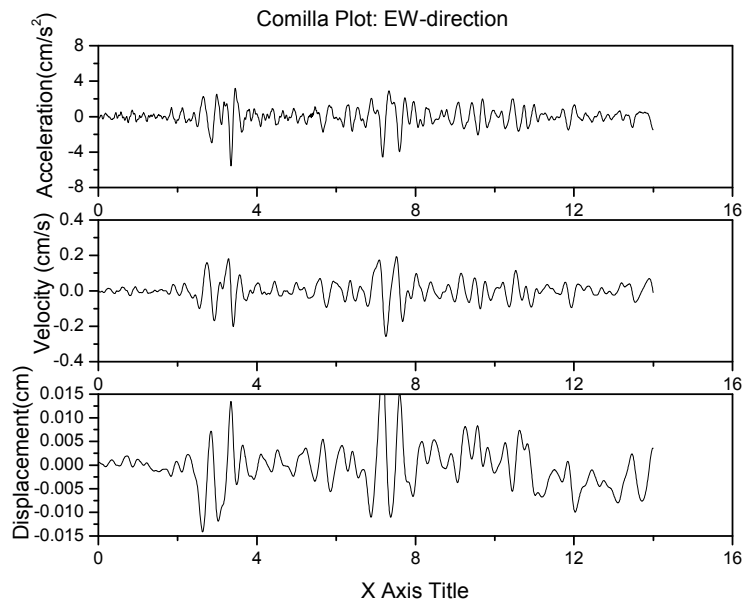


Figure 5 Recorded earthquake ground motion in Comilla, EW-direction

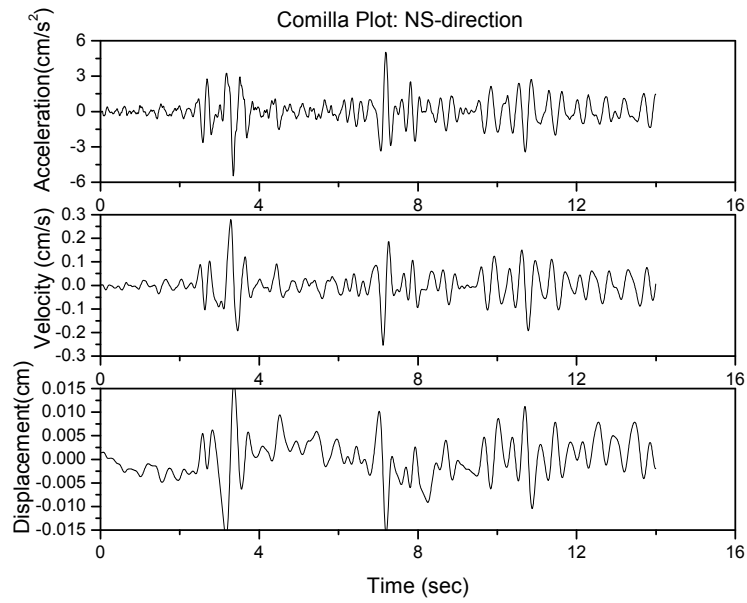


Figure 6 Recorded earthquake ground motion in Comilla, NS-direction

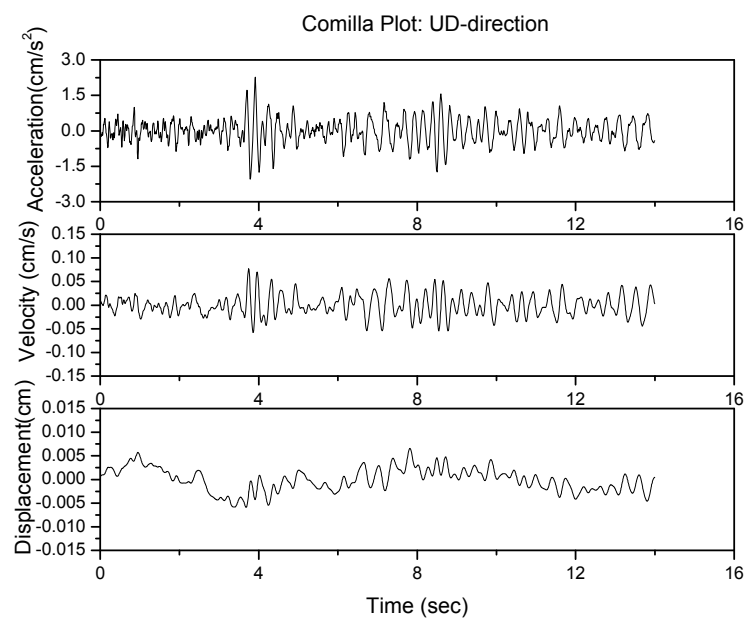


Figure 7 Recorded earthquake ground motion in Comilla, UD-direction

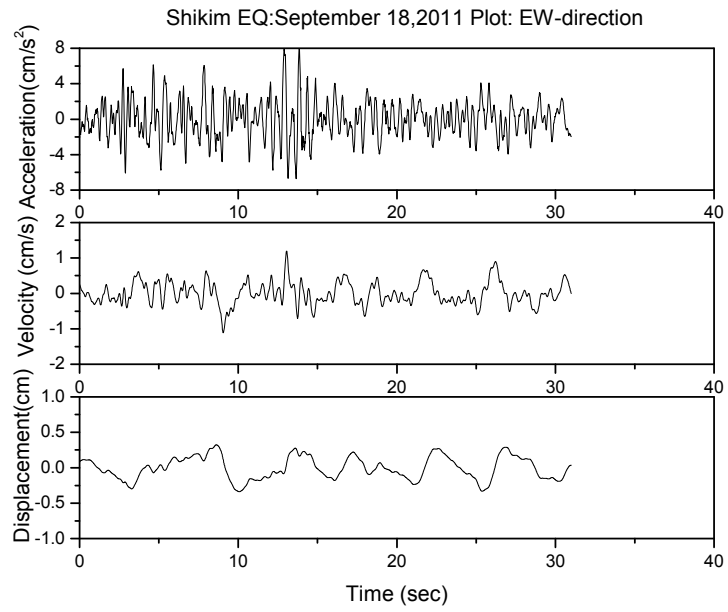


Figure 8 Recorded earthquake ground motion in Hazi Camp, EW-direction

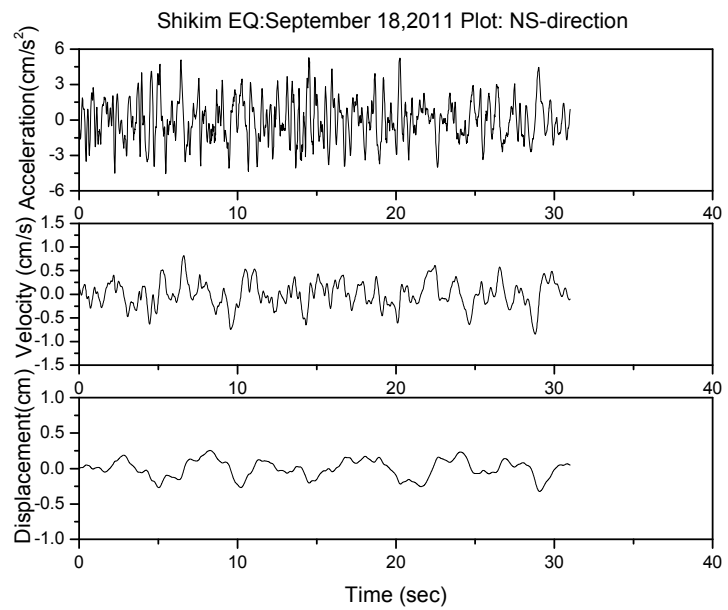


Figure 9 Recorded earthquake ground motion in Hazi Camp, NS-direction

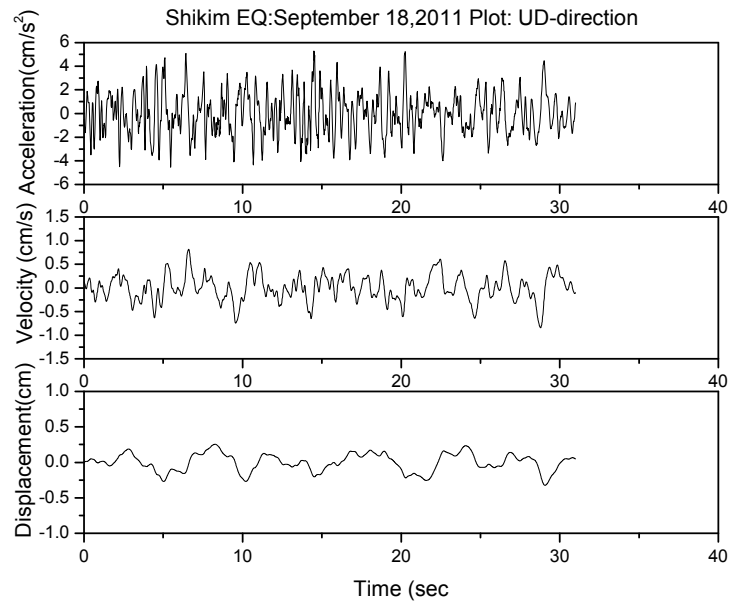


Figure 10 Recorded earthquake ground motion in Hazi Camp, UD-direction

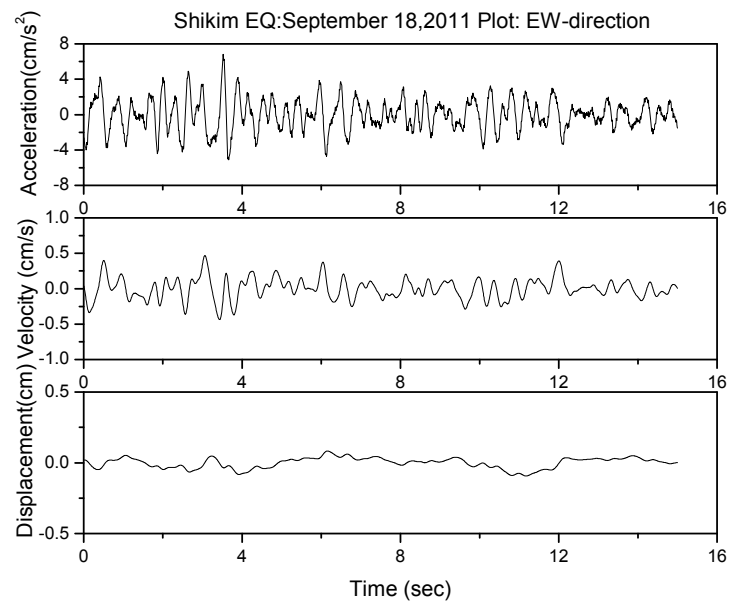


Figure 11 Recorded earthquake ground motion in Khagrachari, EW-direction

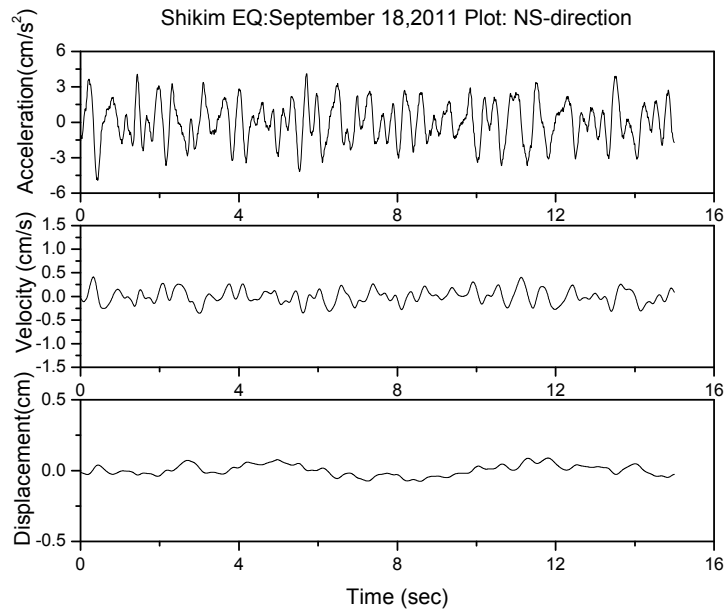


Figure 12 Recorded earthquake ground motion in Khagrachari, NS-direction

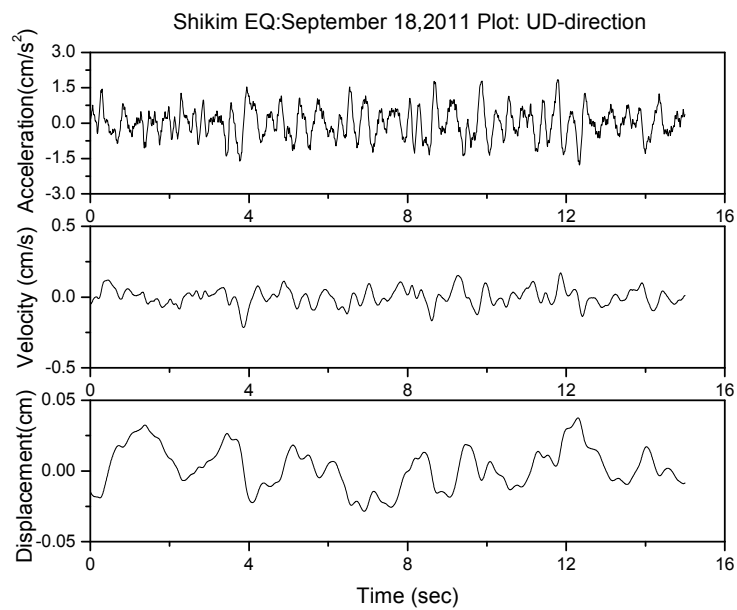


Figure 13 Recorded earthquake ground motion in Khagrachari, UD-direction

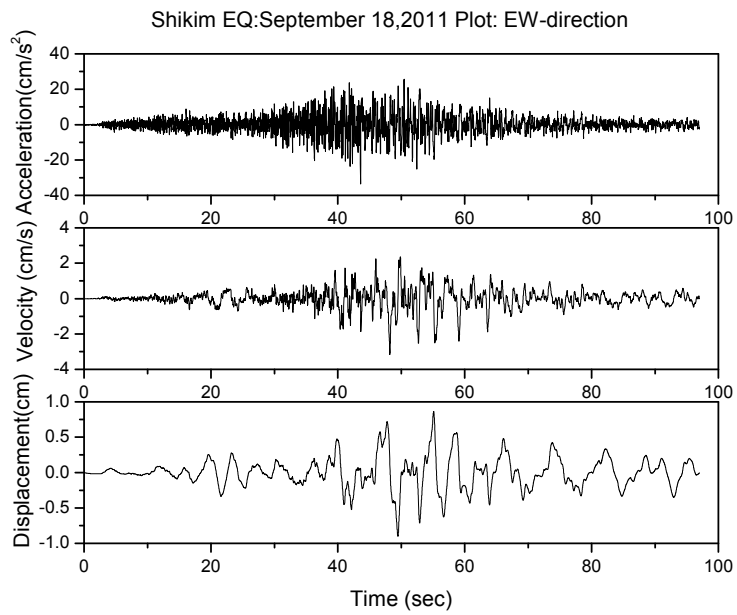


Figure 14 Recorded earthquake ground motion in Kurigram, EW-direction

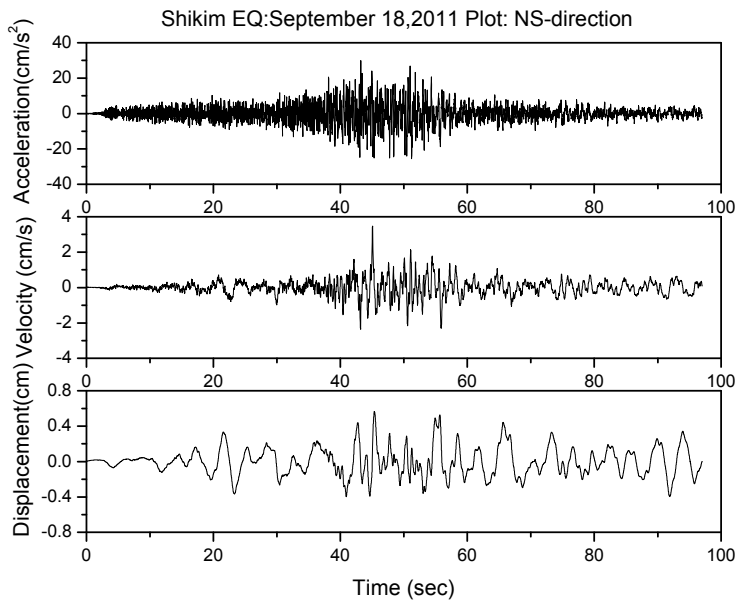


Figure 15 Recorded earthquake ground motion in Kurigram, NS-direction

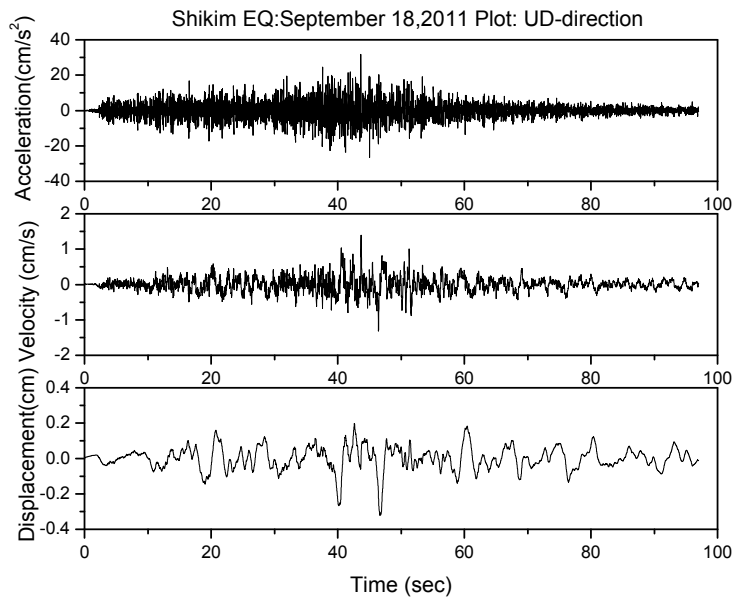


Figure 16 Recorded earthquake ground motion in Kurigram, UD-direction

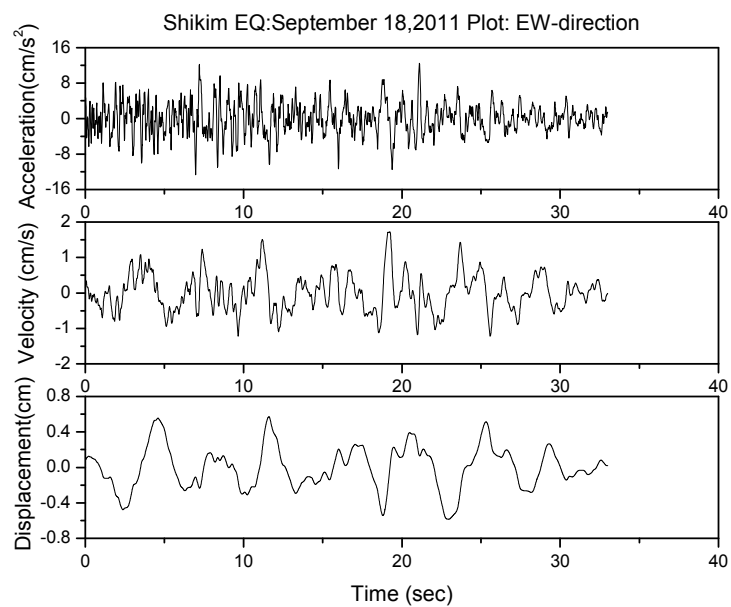


Figure 17 Recorded earthquake ground motion in Meherpur, EW-direction

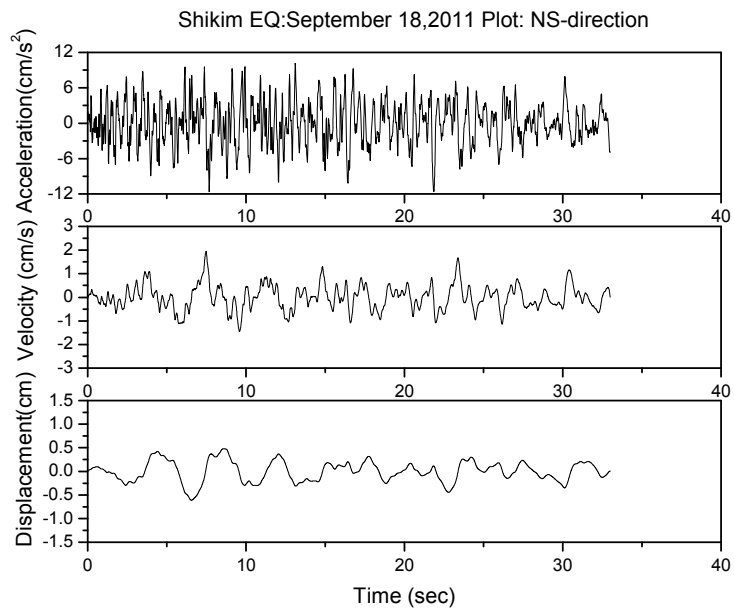


Figure 18 Recorded earthquake ground motion in Meherpur, NS-direction

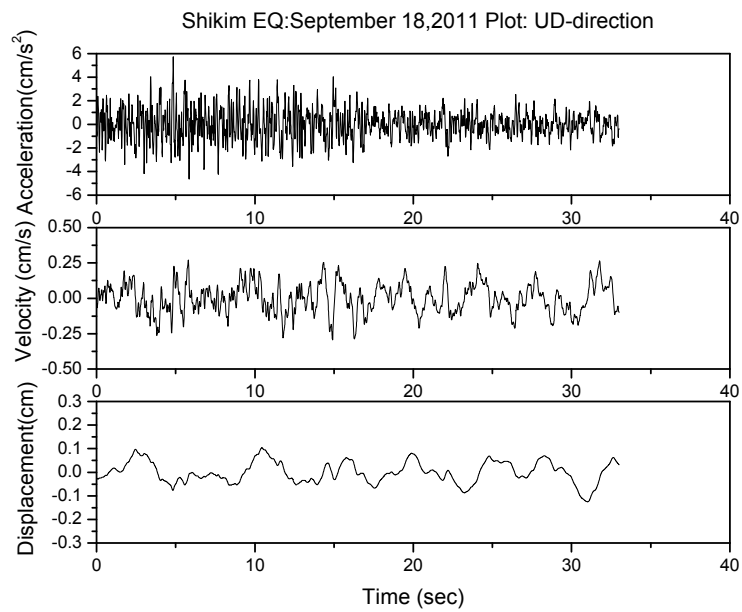


Figure 19 Recorded earthquake ground motion in Meherpur, UD-direction

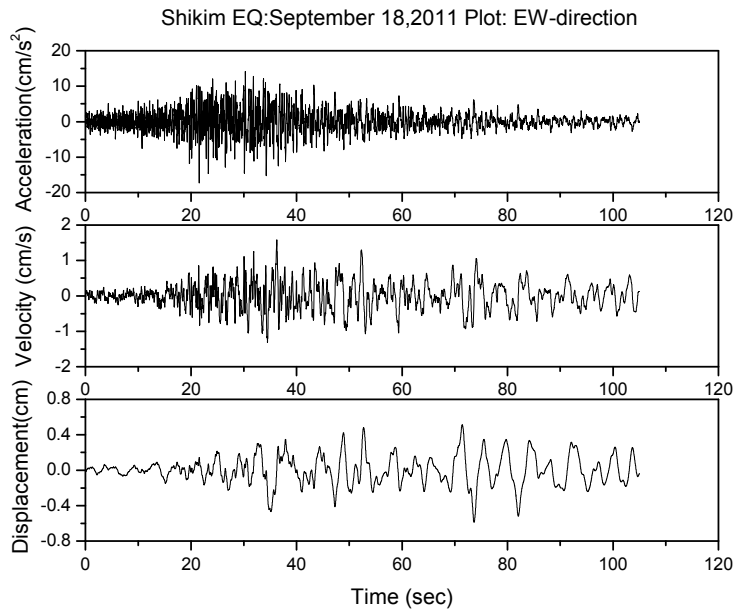


Figure 20 Recorded earthquake ground motion in Natore, EW-direction

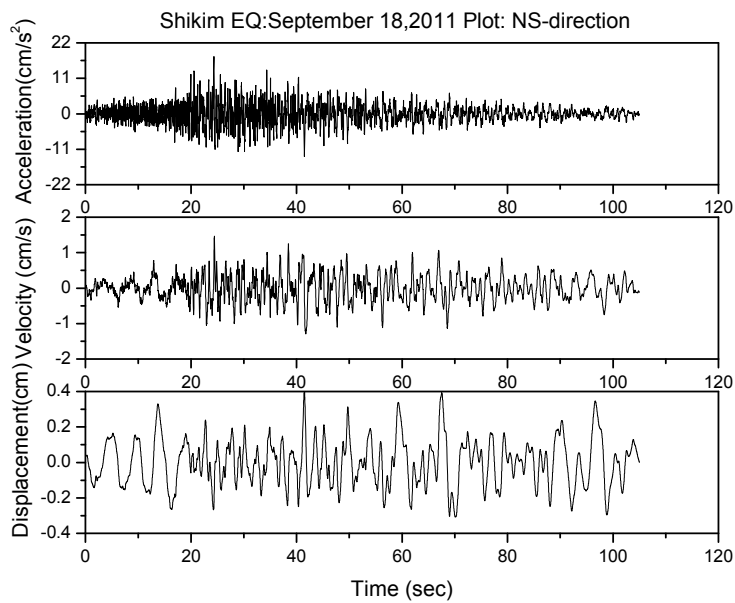


Figure 21 Recorded earthquake ground motion in Natore, NS-direction

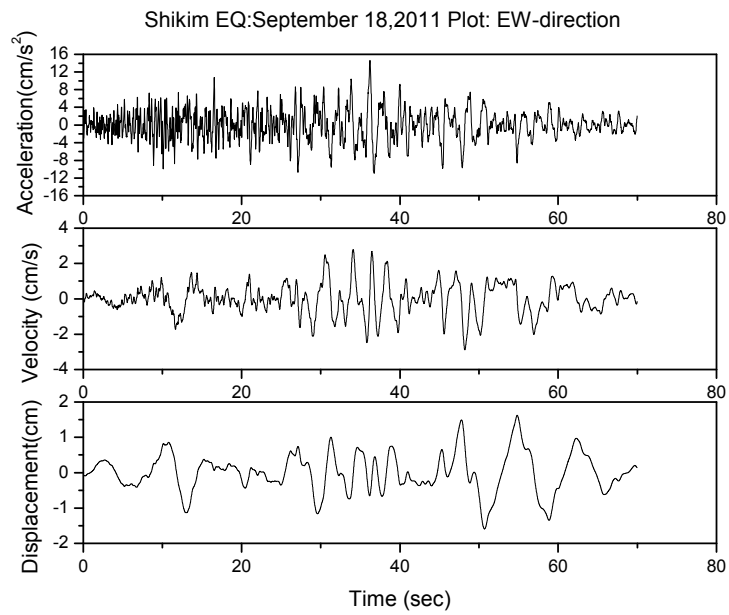


Figure 22 Recorded earthquake ground motion in Netrokona, EW-direction

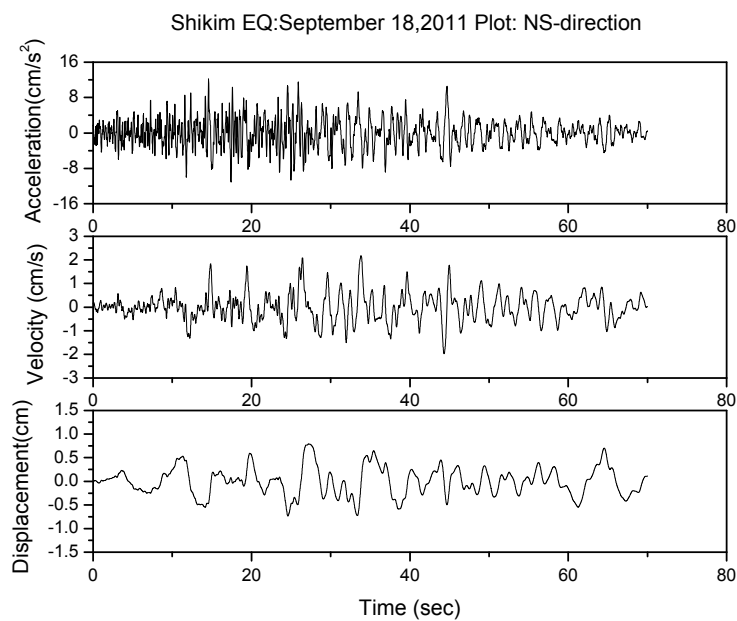


Figure 23 Recorded earthquake ground motion in Netrokona, NS-direction

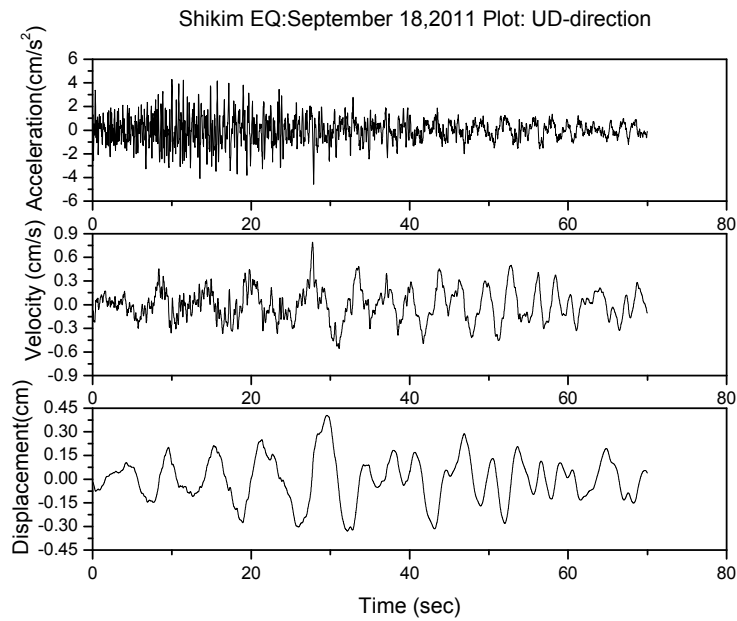


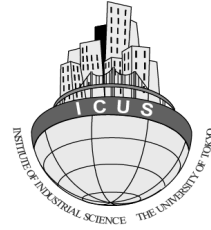
Figure 24 Recorded earthquake ground motion in Netrokona, UD-direction

REFERENCE

1. Bolt, B.A (1987) 'Site Specific Seismicity Study of seismic Intensity and Ground Motion Parameter for Proposed Jamuna Bridge, Bangladesh' Report prepared for seismic design of Jamuna Bridge.
2. BUET (2003) 'Final Report: Installation Phase, Jamuna Multipurpose Bridge Seismic Instrumentation Project', report submitted to JMBA.
3. KMI Strong Motion Analyst, Version 2.4, copyright 1998-2001, Kinematics, Inc. 222, Vista Avenue, Pasadena, California, USA 91107.



**BANGLADESH NETWORK
OFFICE FOR URBAN SAFETY**



PART-V

APPLICATION OF NON-DESTRUCTIVE TESTING TECHNIQUES FOR STRUCTURAL SAFETY EVALUATION IN BANGLADESH

**BANGLADESH NETWORK OFFICE FOR
URBAN SAFETY (BNUS), BUET, DHAKA**

Prepared By: Ram Krishna Mazumder

Mehedi Ahmed Ansary

1. INTRODUCTION

Assessment of an existing structure is a difficult task. The construction of a structure is never exactly as per a designer's specification and a number of defects and uncertainties crop up during the construction. Moreover, the quality of the materials deteriorated with time and the assessment of an existing structure becomes a time dependent problem.

The problem of assessment of an existing structure involves not only the current status of the structure but also its exploration in the life of the structure with or without repairs. There are three sources of deficiency in structures:

- a. Defect arising from the original design, such as under estimation of loads as per old standards or practices, inadequate section or reinforcement anchorage and detailing.
- b. Defects arising from original construction, such as under strength of concrete, poor compaction, poor construction joints, improper placing of reinforcement and honeycombing.
- c. Deterioration since the completion of the construction due to reinforcement corrosion, alkali-aggregate reaction, etc.

If the design documents are available, the first type of deficiency can be assessed with a satisfactory level of confidence. A number of techniques have been developed to detect the other two types of deficiency. Almost all of them depend on indirect measurement and have a low reliability (Singh, 2011). Further the variation of test result is large and interpretation of results requires experience and skills. However, modern NDT techniques have a much more reliability to condition assessment of buildings before taking up repair and upgrading work.

In Bangladesh, most of the houses are non-engineered constructions, which are mainly load bearing buildings. In urban areas, there are many RC frame buildings which have been constructed without any consideration to resist earthquake forces or without using current codal practice on Earthquake Resistance Design. For such type of seismically deficient buildings, a quick NDT assessment could be a good approach for safety measurement of buildings within considerable cost.

2. NON-DESTRUCTIVE TESTING EQUIPMENT

2.1 Ferrosan

Ferrosan is portable, non-destructive steel reinforcement detection system using electromagnetic pulse. It can reduce costly effort to drill, cut or physically break concrete surface to find out the bar. Ferrosan has been used for determining the position, depth and diameter of rebar in existing structure. This is a portable, quick and simple-to-operate system carrying out structural analyses quickly and exactly in a non-destructive manner. This also

determines coverage over the entire surface of a structure. The key elements of the system are the scanner and the monitor. After scanning a structure data has been transferred to the monitor. Collected data can be analyzed by monitor or in a PC using PS 200 software's. Maximum depth of scanning is 180 mm (at 36 mm rebar diameter) where rebar diameter range 6 - 36 mm. Accuracy of depth measurement for rebar is ± 1 mm, depending on depth range and scan mode used. Three types of scanning can be checked out by using Ferroskan device. Line scan is simple way to detect position and depth of rebar where Image scan provides detail information (diameter of bar, concrete cover, location etc.) with scanned image (2 ft x 2 ft grid) of any structure. Block scan is a combination of a set of image scan for a comparatively large area (Rahman et. al, 2010). Figure 1 shows monitor and scanning device.



Figure 1: Hilti PS 200 Monitor and Scanner device

2.2 Rebar Detector

Rebar Detector has been used to determine the exact location of rebar in existing structure. The Profoscope is a versatile, fully-integrated rebar detector and cover meter with a unique real-time rebar visualization allowing the user to actually see the location of the rebar beneath the concrete surface to a maximum depth of 180 mm. This is coupled with rebar-proximity indicators and optical and acoustical locating aids. Rebar diameter can also be estimated within the specified testing range. The Profoscope combines these unique features in a compact, light device that allows the user to operate this rebar detector with one hand making the task of locating rebars a simple and efficient process. In addition, Proceq's rebar detector convinces through its intuitive user interface making rebar detection easy. Figure 2(a) shows a Profoscope Rebar detector.

2.3 Rebound Hammer

A simple equipment known as Rebound Hammer or Schmidt Hammer is used to determine a surface hardness in order to establish the theoretical relationship between the strength of concrete and the rebound number of the hammer. The details of the equipment are shown in Figure 2b, 2c. Surface hardness measured during the test give an idea about the soundness and quality of cover concrete. Locations having very low rebound numbers indicate weak surface concrete and may be affected by corrosion.

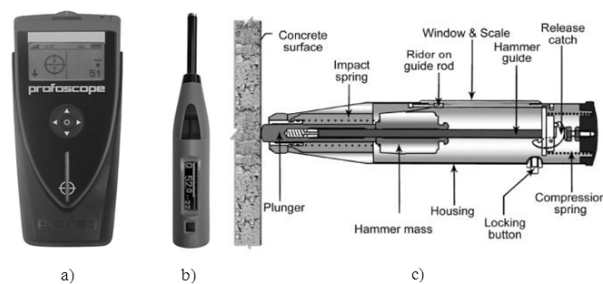
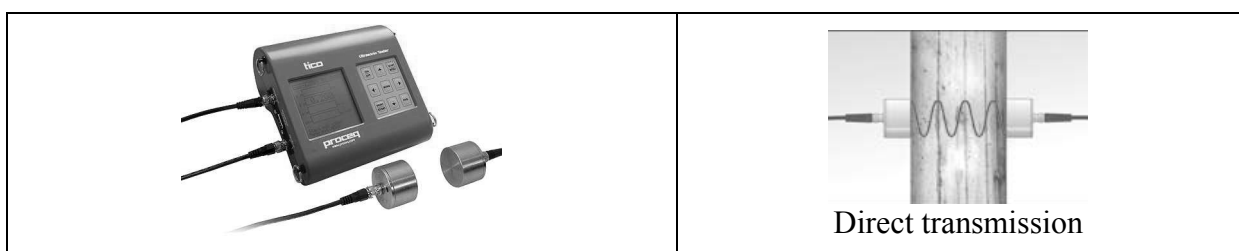


Figure 2: a) Profoscope Rebar Detector, b) Schmidt Hammer and c) Different parts of Schmidt Hammer

2.4 Ultrasonic Pulse Velocity (UPV) Instrument

The ultrasonic pulse velocity method is used to determine material strength and quality, based on the relationship to material density and elasticity. The test equipment has provisions for generating ultrasonic pulse, transmitting it to concrete, receiving and amplifying the pulse and measuring and displaying the pulse travel time. Good acoustic coupling between the transducers and concrete is to be established for correct measurement of the speed (IAEA, 2002). The instrument uses transducers as transmitters and receivers to calculate pulse velocity by measuring transmission time. This flexible unit can measure via direct transmission, semi-direct transmission, indirect or surface transmission to accommodate the demands of virtually any test site. Figure 3 shows UPV instrument and its observation.



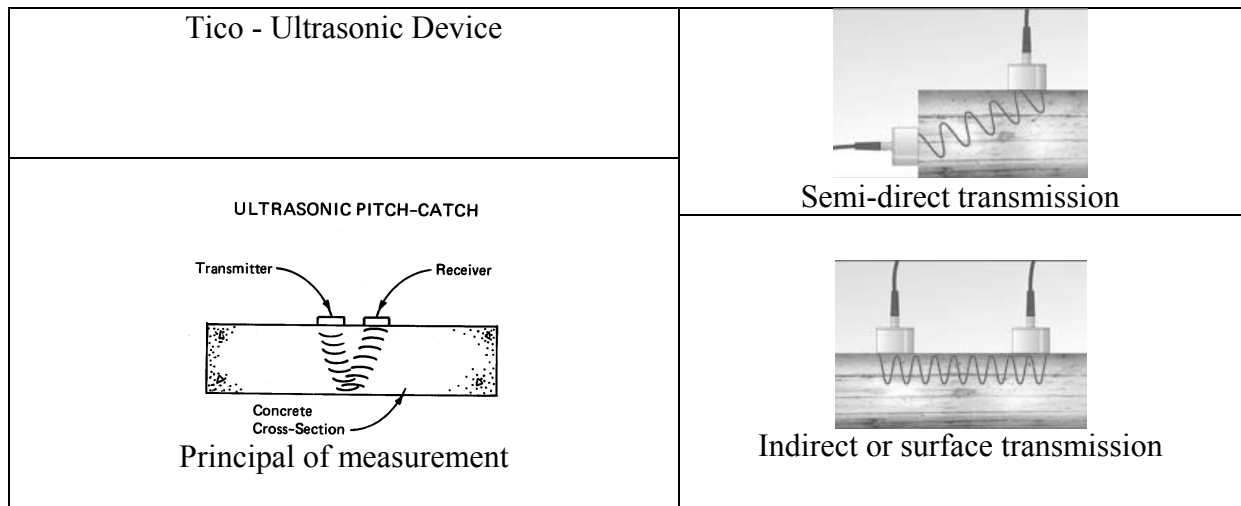


Figure 3: Ultrasonic concrete testing instruments and its observation

2.5 Microtremor Instrument

Microtremor measurement has been done with five component of sensor. At each site, microtremor ground motions were measured for 5 minutes. Each accelerometer recorded data in three direction two horizontal (N-S and E-W components) and one vertical direction (up-down). For free field near to building, First Fourier Transform (FFT) has been done in order to calculate H/V spectral ratio for microtremors. At the top and ground floors of the both buildings, horizontal X- and Y-component microtremor motions, which are in longitudinal and transverse directions of the buildings, were observed. Figure 4 shows Microtremor testing equipments.



Figure 4: Test equipments used in microtremor measurements.

2.6 Ground Penetrating Radar

Ground Penetrating Radar (GPR) is a technique of obtaining sub-surface images using electromagnetic radiation. The energy radiated by the antenna of the system penetrates the surface, and is either absorbed or reflected back at any discontinuities. GPR is valuable for in locating defects and voids in concrete structures, determining embedded reinforcement and other subsurface details. The StructureScan Standard system provides a nondestructive means to accurately inspect concrete structures. This StructureScan Standard used to safely locate

embedment within concrete structures prior to drilling, cutting or coring. Reach depths of 0-18 inches with confidence using a 1600 MHz antenna, survey cart and SIR-3000 control unit. This is generally used to locate metallic and non-metallic targets in walls, floors. Figure 5 shows GPR control units and a 1.6 GHz antenna for structure scan.

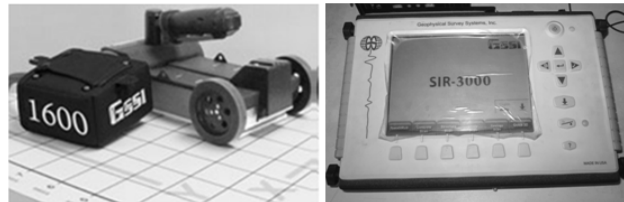


Figure 5: 1.6 GHz Antenna and Control Unit of GPR by Geophysical Survey System Inc. (GSSI)

3. STUDY AREA

In the last two years, these Non-Destructive Testing equipments have been used in different parts of Bangladesh. Important buildings of Chittagong hill tracts region (Khagrachari, Rangamati and Bandarban districts), new and old buildings in Dhaka and an electrical power plant building in Kushtia and two school buildings in Sylhet have been covered. Basically Unreinforced Masonry (URM) and Reinforced Concrete (RC) frame structure has been tested for structural safety. Figure 6 shows conducted NDT location in Bangladesh.

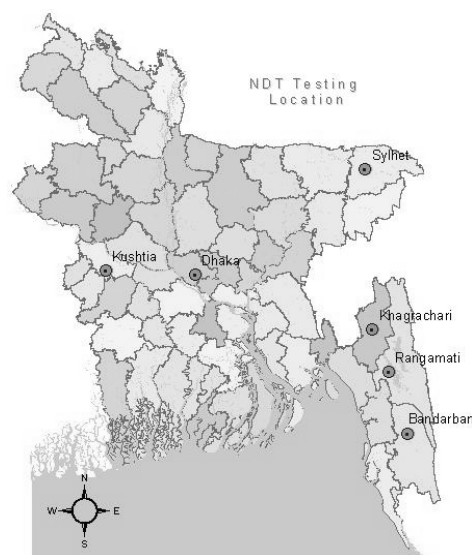


Figure 6: Locations of NDT conducted in Bangladesh

4. METHODOLOGY OF EVALUATION

Location and spacing requirements of column transverse reinforcement and beam stirrup have been checked by using Ferrosan and Rebar Detector. Existing beam and column have been scanned by those two equipments. Reinforcement configuration has been compared with seismic specification provided in ACI 318. Figure 7 and Figure 8 give reinforcement requirement for column where Figure 9 provides reinforcement requirement for beam (ACI, 2008). Slabs also scanned to check the existing reinforcement location as per design.

To measure the elastic properties or strength of concrete, Rebound hammer was used in all columns located at the ground floor of the surveyed building. Schmidt hammer was also used for some of the beams at ground floor. The quality of concrete may be interpreted as shown in the Table 1(GoI-UNDP, 2007).

Table 1: Average Rebound number and quality of concrete

Average Rebound number	Quality of Score
>40	Very good hard layer
30 to 40	Good layer
20 to 30	Fair
< 20	Poor concrete
0	Delaminated

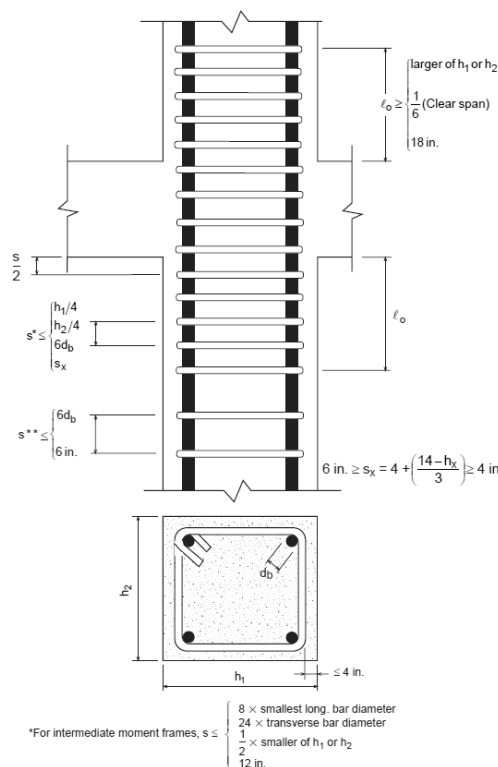


Figure 7: Column transverse reinforcement spacing requirements.

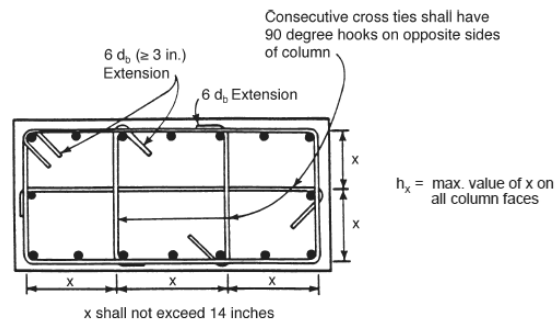


Figure 8: Transverse Reinforcement in Columns.

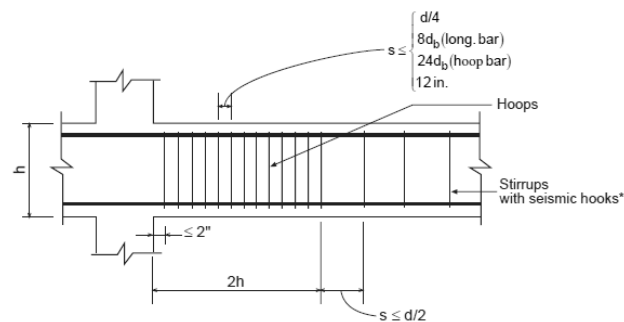


Figure 9: Transverse Reinforcement for Beams.

Using this ultrasonic method, the ultrasonic instrument determines, indirectly, the modulus of elasticity and concrete strength. The instrument is typically used on site to assess uniformly of concrete and to locate cracks, voids, cavities, and defects due to fire and frost. The quality of concrete may be interpreted from the Table 2(GoI-UNDP, 2007).

Table 2: UPV value and concrete quality

UPV value in m/sec (V)	Concrete quality
V > 4000.0	Very good
V = 3500 - 4000	Good, but may be porous
V = 3000 - 3500	Poor
V = 2500 - 3000	Very poor
V = 2000 - 2500	Very poor and low integrity
V < 2000 and reading fluctuating	No integrity, large voids suspected

Microtremor instruments measures predominant ambient frequency of the structures and soil. If predominant frequency of both structure and soil are close to each other, there will be more likelihood to damage during an earthquake.

GPR 1.6 GHz antenna can identify the rebar position in a structure by generating radar pulse. Semi-automatic mapping of deterioration zones within concrete structures can be identify using special RADAN software.

5. RESULTS

Among 65 buildings only 7 buildings are masonry, rest of all are reinforced concrete buildings. Considered masonry structures are situated at Dhaka and only microtremor test are performed for these masonry buildings in order to check the resonance criteria. Other NDT equipments have been used for all RC buildings.

Ferrosan and Rebar Detector have been used alternatively for RC buildings. Identified reinforcement spacings have been verified with ACI 318 guideline for seismic consideration. According to priority basis on structural configuration, at least three columns have been scanned for each building in different storey level. From 57 buildings, only 12 buildings comply with seismic provision for column middle part as per ACI 318 where 45 buildings didn't satisfy. For end portion of column, only 9 buildings are satisfied as per ACI 318. Beam reinforcement configuration also justified with ACI 318 provision. From 54 scanned cases, 19 cases have been satisfied for middle part of beam. Other hand, only 2 beams are satisfied for end portion check from 11 cases. Reinforcement identification of end portion hasn't been performed for most of the beams due to insufficient space. Scanned image of slabs have been generate using image scan mode by Ferrosan. Figure 10 and Figure 11 show typical image scan result and reinforcement position in structural elements respectively.

Schmidt hammer has been used for 55 buildings. Average of 10 impacts has been considered for each concrete surface. From the assessment it has been found that column rebound value is below 30 for 36 buildings. So, concrete conditions of those 36 buildings are fair to poor (see Table 1). Average rebound number more than 40 have been found for only 2 buildings, where 17 buildings have score greater than 30. Figure 12 shows impact data in Hammerlink software.

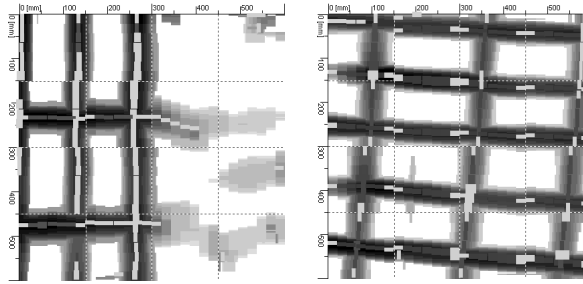


Figure 10: Typical image scan for column (left) and slab

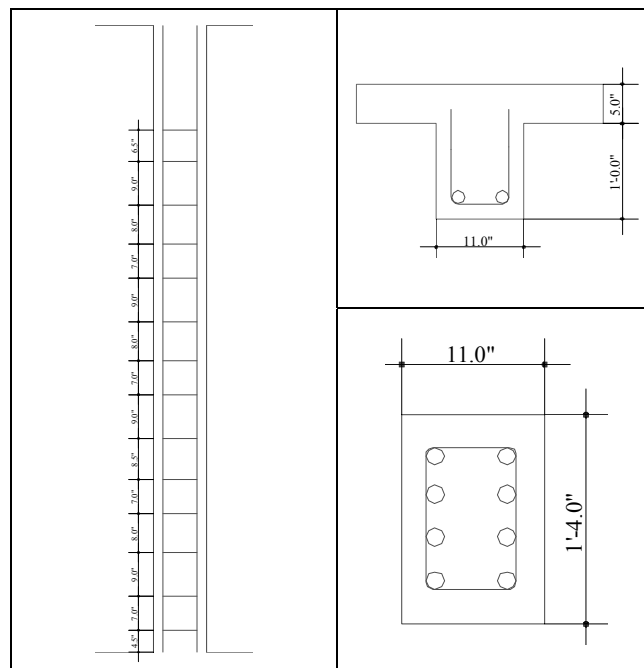


Figure 11: Identified reinforcement position in column and beam.

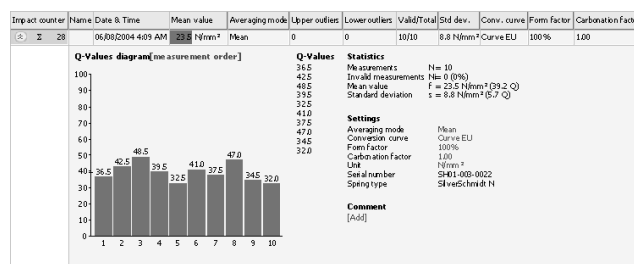


Figure 12: Impacts data analyzed in Hammerlink software.

Ultrasonic equipment has been used in three hill tract districts. Among 44 ultrasonic results, 2 buildings have very poor and low integrity, 4 buildings have very poor to poor condition, 21 buildings have good to very good condition (see Table 2).

Microtremor has been used for 21 buildings in Dhaka, Sylhet and Kushtia. First Fourier Transform (FFT) indicates that only 3 masonry buildings have likelihood to significant

damage during an earthquake. From other 14 RC buildings, 4 buildings have a high possibility to resonance during earthquake where 10 buildings have a moderate to low risk for resonance. Predominant frequency can be found from FFT (in Figure 13).

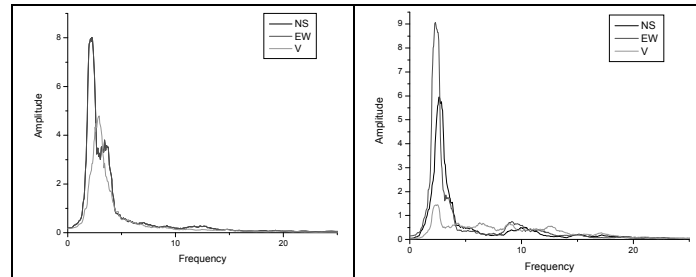


Figure 13: Typical FFT analysis for free field and roof of structure

A raft founded basement has been scanned by GPR. 3D data has been collected in order to investigate deterioration zones within concrete structures. After RADAN analysis, no deterioration has been found. Figure 14 shows 3D model of raft basement

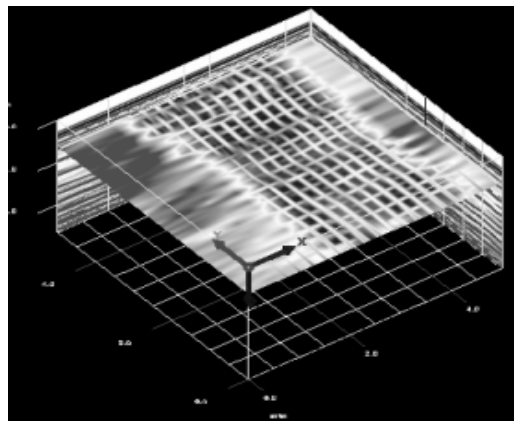


Figure 14: 3D data set showing rebar mat.

6. CONCLUSIONS

The importance and need for NDT assessment and evaluation of safety of existing buildings have been highlighted in this paper. Safety evaluation forms the basis for designing and carrying out strengthening of buildings to satisfy the safety and performance standards as per the extant building codes. An overview of the procedures and different investigations including tests involved in condition assessment and evaluation of safety is presented. It can be seen that detailed visual inspection and Non Destructive Testing (NDT) plays an

important role in condition assessment of existing buildings. It may be emphasized here that a great deal of expertise is required for interpretation of field observations and test results to make a proper assessment of the condition as well as for analyzing and evaluating safety.

References

American Concrete Institute (ACI) -318 (2008), “Building Code Requirements for Structural Concrete”.

GoI-UNDP Disaster Risk Management Programme, Government of India (2007), “Condition Assessment of Buildings for Repair and Upgrading Report”.

International Atomic Energy Agency (IAEA) (2002), “Guidebook on Non-Destructive Testing of Concrete Structures”, *Training Course Series No. 17*.

Rahman, M. S., Islam, B. and Ansary, M. A.. (2010), “Diagnosis of the Seismic Vulnerability of Buildings at Dhaka Using Non-Destructive Testing”, *9th Proceedings of New Technologies for Urban Safety of Mega Cities in Asia, Kobe, Japan*.

Singh, Y. (2011), “Seismic Vulnerability Assessment of Existing Buildings”, *Earthquake Risk Mitigation Training Manual, SAARC Disaster Management Center, L-18*.



PART-VI

VULNERABILITY EVALUATION FOR ZINDABAZAR GOVERNMENT PRIMARY SCHOOL, SYLHET, BANGLADESH

**BANGLADESH NETWORK OFFICE FOR
URBAN SAFETY (BNUS), BUET, DHAKA**

Prepared By: K .M. Khaleduzzaman Nayan

Istiaq Ahmed Murad

Mehedi Ahmed Ansary

1. General

The devastating social and economic impacts of recent earthquakes in urban areas have resulted in an increased awareness of the potential seismic hazard and the corresponding vulnerability of the built environment. Greater effort has been given to reasonably estimates, predictions and mitigation of the risks associated with these potential losses.

This report is based on engineering judgment arrived at from the site visit, review of available architectural drawings, and non-destructive test carried out at site. All possible efforts have been made to provide accurate and authoritative seismic vulnerability assessment of the building in the given circumstances of information provided by the client and limited number of field-tests. Therefore, neither BNUS nor any of its employees make any warranty, expressed or implied, nor assumes any responsibility for the accuracy, completeness, or usefulness of the statement made in this report in case the starting information does not stand correct.

2. Basic Information

Building Name	Zindabazar Government Primary School
Locality	Zindabazar, Sylhet
Estd.	1999
Shape in Elevation	Regular
Plan view	Rectangular
Comments	One side of 2 nd floor is not constructed
Populations	Day:220/250, Night: 2
Mass irregularity	Presence
Tall Unhooked Component	Light
Height of Ground Floor	10 ft
Hazard	Earthquake, Fire

3. Turkish Score

3.1. Level 1 Score

Turkish Level 1 Score										
Number of Story	Zone I	Zone II	Zone III	Soft Story	Heavy Overhang	Apparent Quality	Short Column	Pounding	Topography Effects	PS
3	90	120	140	-15	-10	-10	-5	-2	0	
VSM	1	0	0	0	0	1	0	0		80
$\Sigma \text{VSM} \times \text{VS}$	90	0	0	0	0	-10	0	0		
Remarks						Light				

Where,
 PS = Performance Score
 VSM=Vulnerability Score Modifiers

(Ref: Sucuglu et. al. 2003)

4. Building plan:

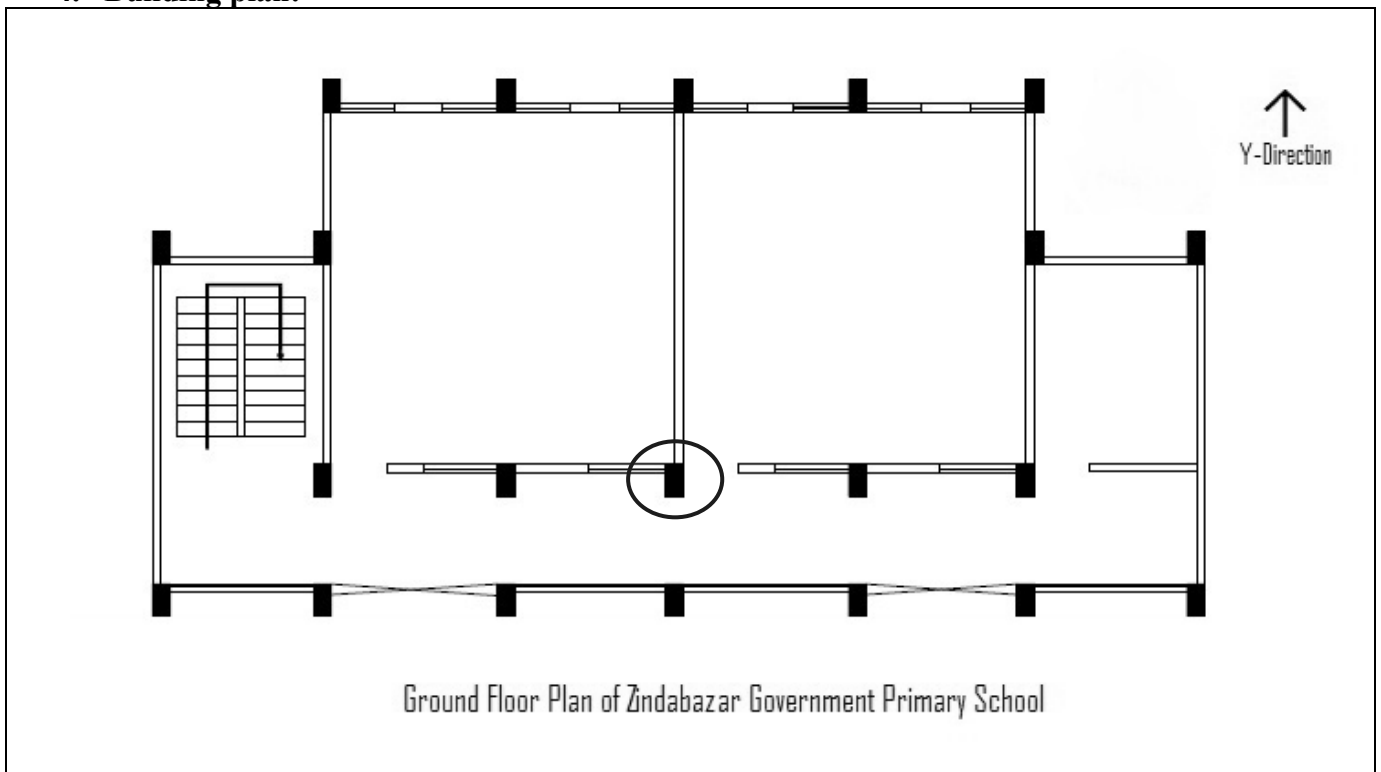


Figure 1 Building plan showing the location of tested column

5. Seismic Load Calculation

5.1. Lump Load Calculation Table

Load calculation for 1st Lump

S.N.	Item	Weight KN	Fraction Taken	Weight KN
1	GF Column	254.7	0.5	127.3
2	1F column	254.7	0.5	127.3
3	Beam	191.8	1.0	191.8
4	GF wall	422.9	0.5	211.5
5	1F wall	430.1	0.5	215.0
6	Parapet Wall	1.7	1.0	1.7
7	slab	192.6	1.0	192.6
8	Dead load	1748.5		

Load calculation for 2nd Lump

S.N.	Item	Weight KN	Fraction Taken	Weight KN
1	1F Column	254.7	0.5	127.3
2	2F column	127.3	0.5	63.7
3	Beam	191.8	1.0	191.8
4	1F wall	430.1	0.5	215.0
5	2F wall	258.9	0.5	129.5
6	Parapet Wall	1.7	1.0	1.7
7	slab	192.6	1.0	192.6
8	Dead load	1457.1		

Load calculation for 3rd Lump

S.N.	Item	Weight KN	Fraction Taken	Weight KN
1	2F Column	127.3	1.0	127.3
2	3F column	0.0	0.5	0.0
3	Beam	95.9	1.0	95.9
4	2F wall	258.9	0.5	129.5
5	3F wall	0.0	0.5	0.0
6	Parapet Wall	1.7	1.0	1.7
7	Slab	96.3	1.0	96.3
8	Dead load	580.2		

6. Base Shear Calculation

No. of Stories =	3	
Building Structural Type =	RC	
StoreyHt (Level)	Each st.Ht(m)	Ht. from GL(m)
0	3.05	3.05
1	3.05	6.10
2	3.05	9.15

Total StoreyHt (h_n) =	9.15	<i>m</i>
C_t =	0.073	
T =	0.38	<i>second</i>
S (Site Class) =	2.0	<i>S4</i>
Response reduction factor, R =	5.0	
C =	2.75	
Seismic Zone =	3	
Z =	0.25	
Importance factor, I =	1	
Seismic Weight, W =	3785.8	<i>KN</i>
Base Shear, V =	520.5	<i>KN</i>
F_t =	0.00	<i>KN</i>
V- F_t =	520.5	<i>KN</i>

Lump load (floor) level	weight w_i (<i>KN</i>)	Height h_i (<i>m</i>)	$w_i h_i$	Q_i	Storey Shear V_i (<i>KN</i>)	
3	580.2	9.15	5308.9	141.4994	141.499407	@2 Storey Shear
2	1457.1	6.10	8888.5	236.9105	378.40992	@1 Storey Shear
1	1748.5	3.05	5332.8	142.1372	520.547122	@0 Storey Shear
		Sum=	19530.2			

(Ref: Bangladesh National Building Code, 1993)

7. Ferro-Scan Test

7.1. 2D Image Scan

In Figure 1 circle indicates the scanned column. The results of the test are shown below.

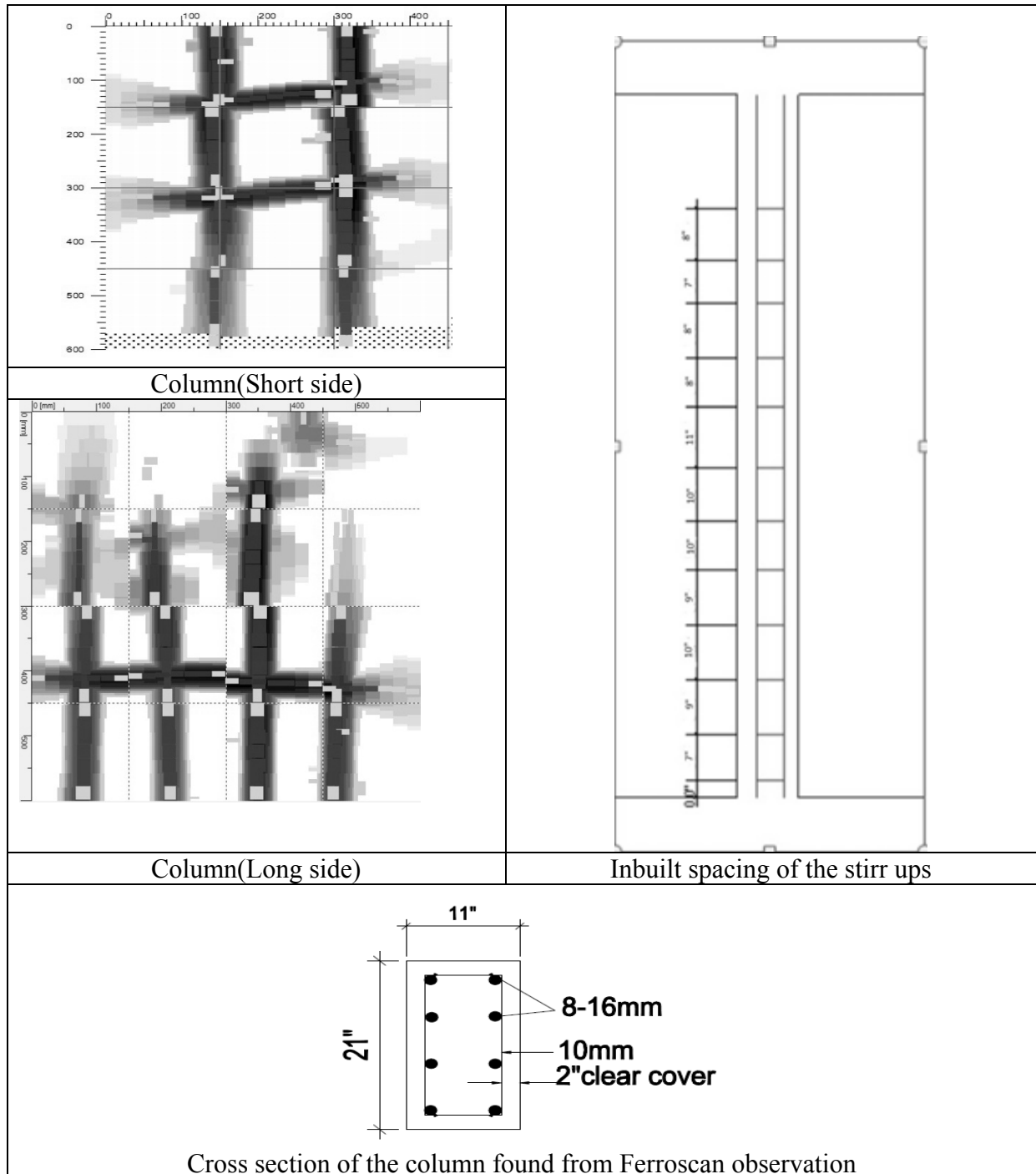


Figure 2: Image Scan results for different structural components

7.2. Line Scan

Table 6: Transverse Reinforcement Requirements - Rectangular hoop check reinforcement for Column (C1-1F)

Transverse Reinforcement Requirements - Rectangular hoop reinforcement for Column (C1-1F)				
Column Dimension	x	y	$L_0 \geq$	
	11	21	Larger of C1 or C2	21 in
Column Height (Clear Span)	9.5	ft	Clear Span/6	19 in
	114	in	18"	18 in
Longitudinal Bar Used	16	mm		
Diameter, D	0.63	in		
Max. Value between tie (in a plane), h_x	6	in		
End Strip Length	19	in		
Middle Strip length	76	in		
Spacing Recommended for End Strip :			$S \leq$	
S	2.75	in	0.25 X Smaller of C1 or C2	2.7 5 in
Existing Spacing	5.5	in	6 X Longitudinal Bar Diameter, D	3.7 5 in
Remark	Not Satisfied		$S_x = 4 + [(14 - h_x) / 3]$	66. 6 in
Spacing Recommended for Middle Strip				
S	3.75	in	$S \leq$	
Existing Spacing	10	in	6"	6 in
Remark	Not Satisfied		6 X Longitudinal Bar Diameter, D	3.7 5 in
Clear Cover				
Cover depth \geq	38.1	mm		
Existing min Depth	51	mm		
Remark	Satisfied			

(Ref: American Concrete Institute, 2002)

8. Microtremor Observations

Figure 3 shows individual time histories for X, Y and Z components for a building. Figure 4 shows FFT of those time histories. Table 5 presents the predominant frequency of the buildings in both directions.

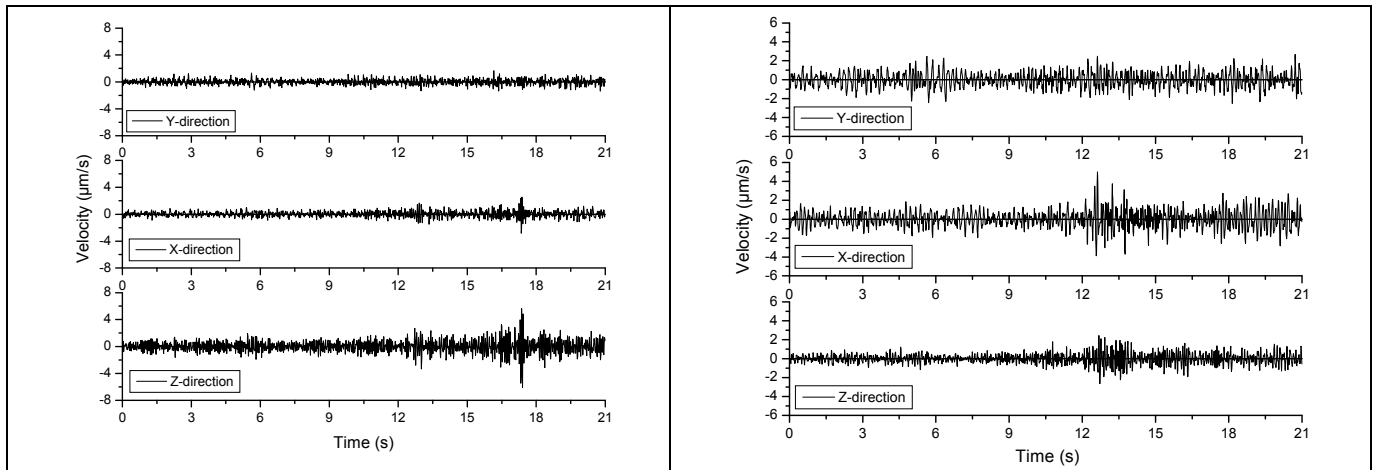


Figure 3: Time History of soil and building

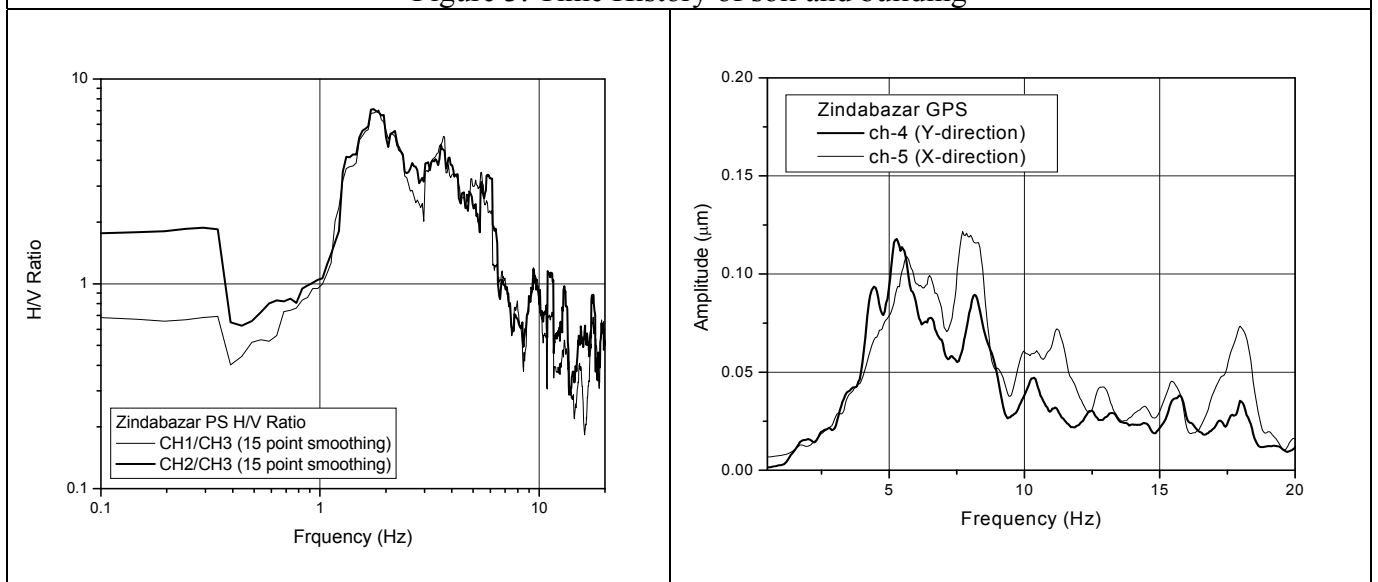


Figure 4: Fourier Spectrum of soil and building

At Zindabazar Govt. Primary School due to the limitation of free space, only one longitudinal array as shown in Figure 5 has been used to estimate shear-wave velocity.

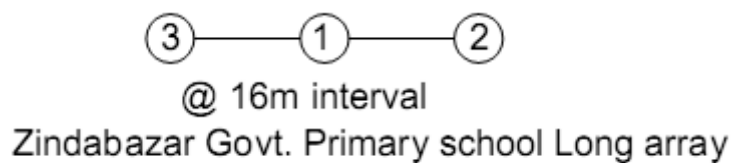


Fig 5: Array formation of Zindabazar Govt. Primary School.

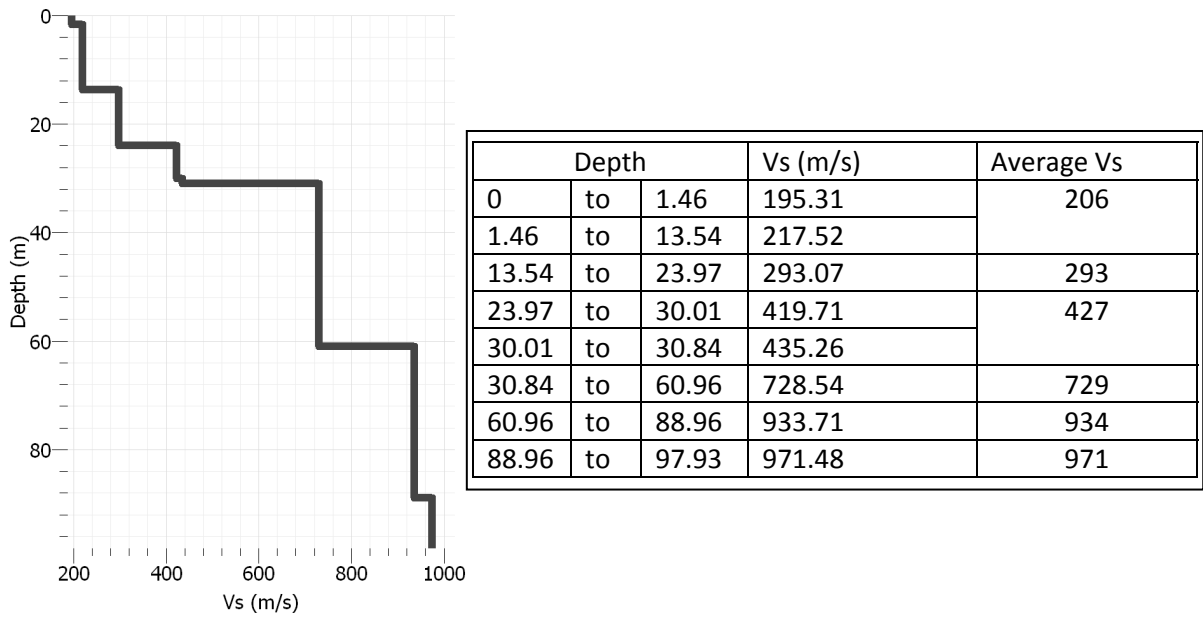


Figure 6: Shear wave velocity profile of Zindabazar High School (From long array).

9. ETABS MODEL

Computer model for the school buildings have been developed. In Figure 7, first mode of ETABS model and periods for different modes for Zindabazar Government Primary School have been shown. It can be seen that first mode from the computer model is 0.21 s which is longer than the actual period obtained from the microtremor observation (0.12 s). This is due to the presence of different walls located in the actual building whereas in the model no walls exist. Also we have run another model using cross bracing instead of wall which shows almost the same period (0.13 s) for the model.

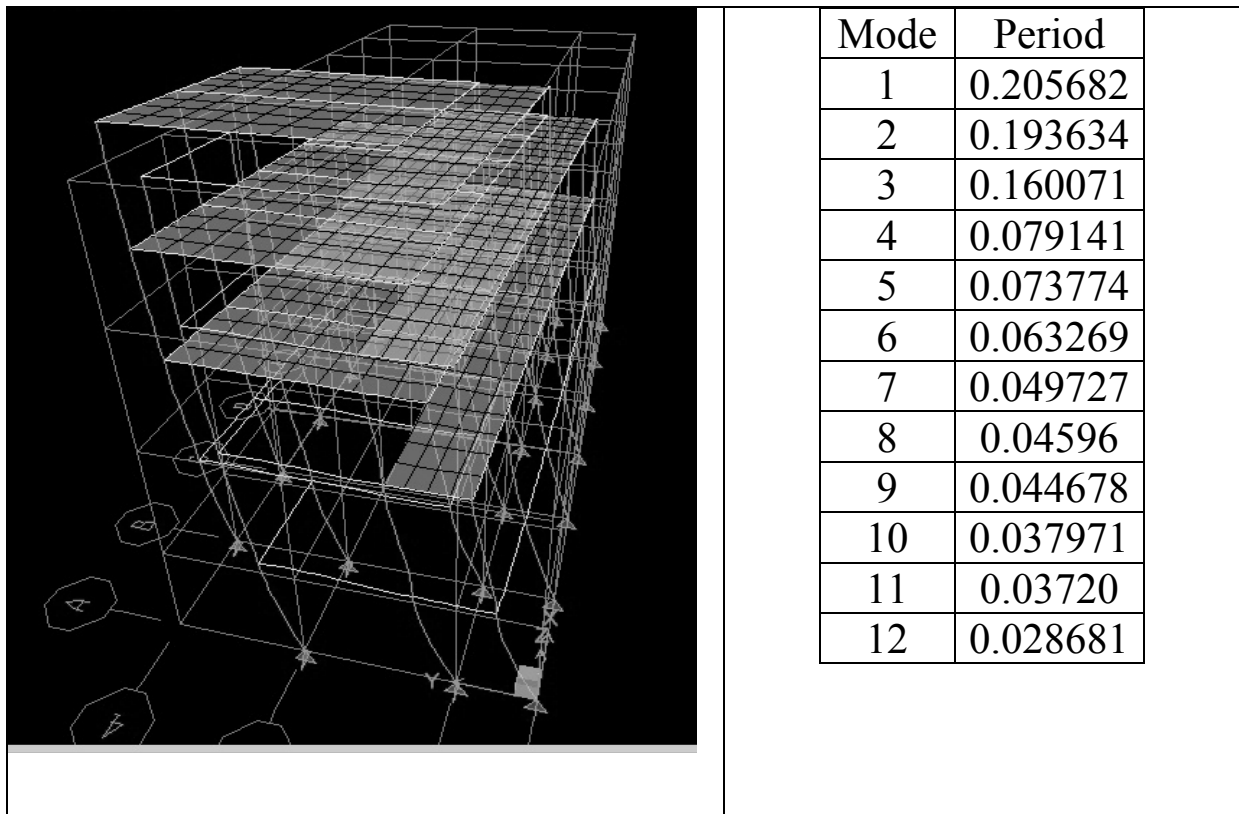
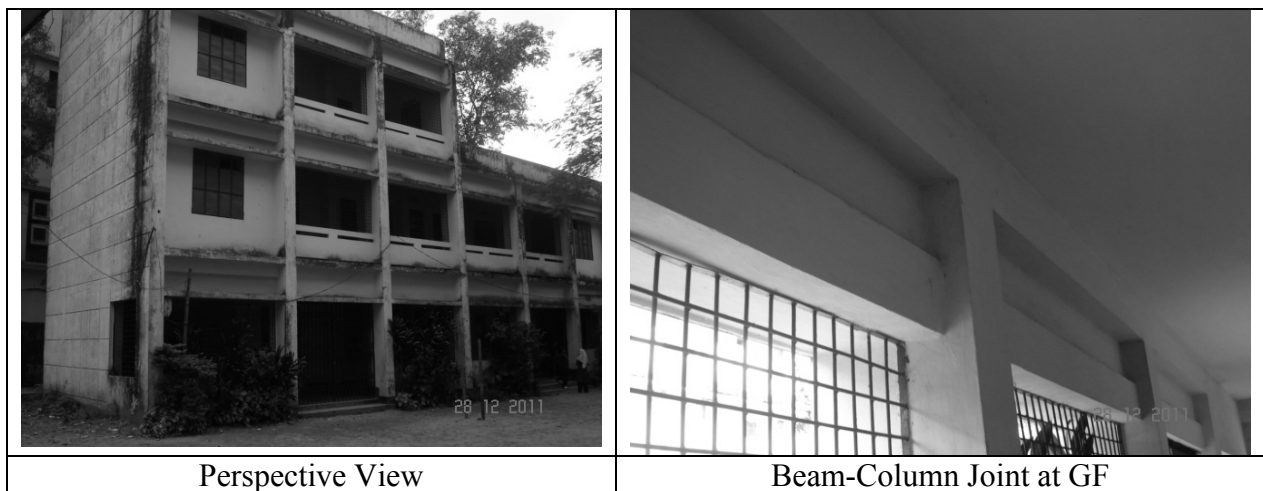


Figure 7: First mode of ETABS model and periods for different modes for Zindabazar School

10. Photographs



	
<p>Unhooked Component</p>	<p>Image Scan Survey</p>
	
<p>Side view of the structure</p>	<p>No Structure in circular portion</p>

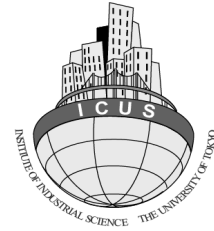
11. Conclusions and Recommendations

The columns of the buildings have inadequate reinforcement from the point of view of earthquake loadings. The columns may be retrofitted either by using ferrocement column jacketing or using FRP wrappings, which also need to be connected with the foundation of the building.

The predominant period of the building is 0.12 sec (8 Hz) and the predominant period of the soil is 0.50 sec (2 Hz), so there is no chance of resonance between the soil and building's vibration.



**BANGLADESH NETWORK
OFFICE FOR URBAN SAFETY**



PART-VII

GEOPHYSICAL INVESTIGATION AT MEGHNA DHONAGODA IRRIGATION PROJECT (MDIP) USING GROUND PENETRATING RADAR MET HOD

**BANGLADESH NETWORK OFFICE FOR
URBAN SAFETY (BNUS), BUET, DHAKA**

Prepared By: Ram Krishna Mazumder

Mehedi Ahmed Ansary

1. INTRODUCTION

The project is located at 19 km North of Chandpur Town and 40 km South East of Dhaka near the confluence of the Padma & the Meghna River. MDIP comprises the gross area of 17584 ha in Matlab Upazilla of Chandpur district is bounded on the North and the West by the mighty Meghna and on the East and the South by the Dhonagoda River.

The Project is encircled by a 60.7 km of flood embankment completed in 1987. After completion of the embankment, severe seepage and boiling were observed along the countryside of the embankment during floods. The embankment was breached during 1987 and 1988 floods causing severe damages. During the flood of 2004, a breach at Nandalalpur occurred but no damage could be caused as the Bangladesh Water Development Board (BWDB) authorities repaired the breach quickly with the help of local people. Furthermore, sliding of the slope of embankments occurred on the countryside at about 60 places, seepage problems developed at about 25 km length and boiling occurred at about 120 locations. Figure 1 shows the embankment location and the affected points. The damages were severe and it remained as a threat to future performance of the embankment during floods (Ansary et al., 2009).

To strengthening the embankment, currently BWDB authorities are injecting cement grouting up to 5 m to 12 m below the surface. This paper presents the geophysical study which was carried out to evaluate the performance of the embankment after the cement grouting was completed.

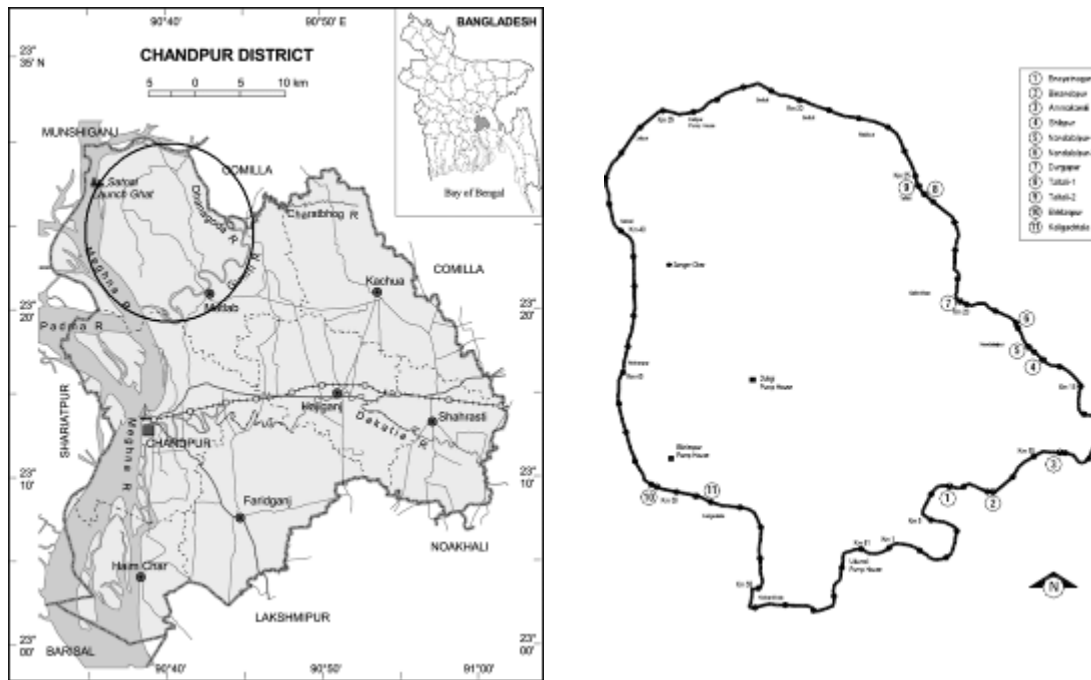


Figure 1: Location of Meghna Dhonagoda Irrigation Project (MDIP) and erosion points (right)

2. SUBSOIL INVESTIGATION

The field investigation at the embankment site consisted of drilling of boreholes, recording density or stiffness characteristics of soil layers by carrying out Standard Penetration Tests (SPT), collection of sufficient numbers of disturbed and undisturbed tube samples. Also portable seismograph was used to support the result obtained from SPT-N values. A total of fifty six boreholes at eleven sites were drilled vertically at this site using wash boring technique. The depth of boreholes below the ground surface varied from 10 m to 17 m. In general five boreholes were drilled at each site across an embankment section.

2.1 Soil Sampling

Disturbed and undisturbed samples were collected from the boreholes. A split-spoon sampler was used to obtain the disturbed samples in conjunction with the Standard Penetration Test. Undisturbed samples were also retrieved from cohesive layers of the boreholes by pushing conventional 76 mm external diameter thin-walled Shelby tubes following the procedure outlined in ASTM D1587. The locations of disturbed and undisturbed samples obtained from the boreholes are shown in the bore logs. The drilling of the fifty six boreholes at the project site, including collection of disturbed and undisturbed tube samples and performance of Standard Penetration Test (SPT) were carried out by the Groundwater Hydrology Division of BWDB.

2.2 Soil Profile and Parameters across Embankment Alignment

A typical soil profile across the embankment is shown in Figure 2.

Particle size distribution was obtained following procedures mentioned in ASTM D422, ASTM C136 and ASTM D1140 on samples from different boreholes and from different depths. Particle size characteristics (d_{10} , d_{15} , d_{30} , d_{50} , d_{60} , d_{85} , percentage of non plastic fines, C_u , C_c) are also presented tabular form. A summary of the amount of fine material (% finer than #200 sieves i.e. 0.074 mm) in soils at different depths and in different locations tested (Ansary et al., 2009).

As has been mentioned earlier the subsoil consisted mostly of cohesionless soil and undisturbed samples could not be retrieved from the boreholes. It therefore became apparent that shear strength parameters for this layer has to be interpreted from the field-N values based on appropriate corrections and available empirical relations. Since the soil mineralogy and grain characteristics could be different from those for which correlations is available, it was decided to perform laboratory shear strength tests on samples reconstituted from disturbed samples at different densities in order to achieve possible highest and lowest range of strength parameter (Ansary et al., 2009)..

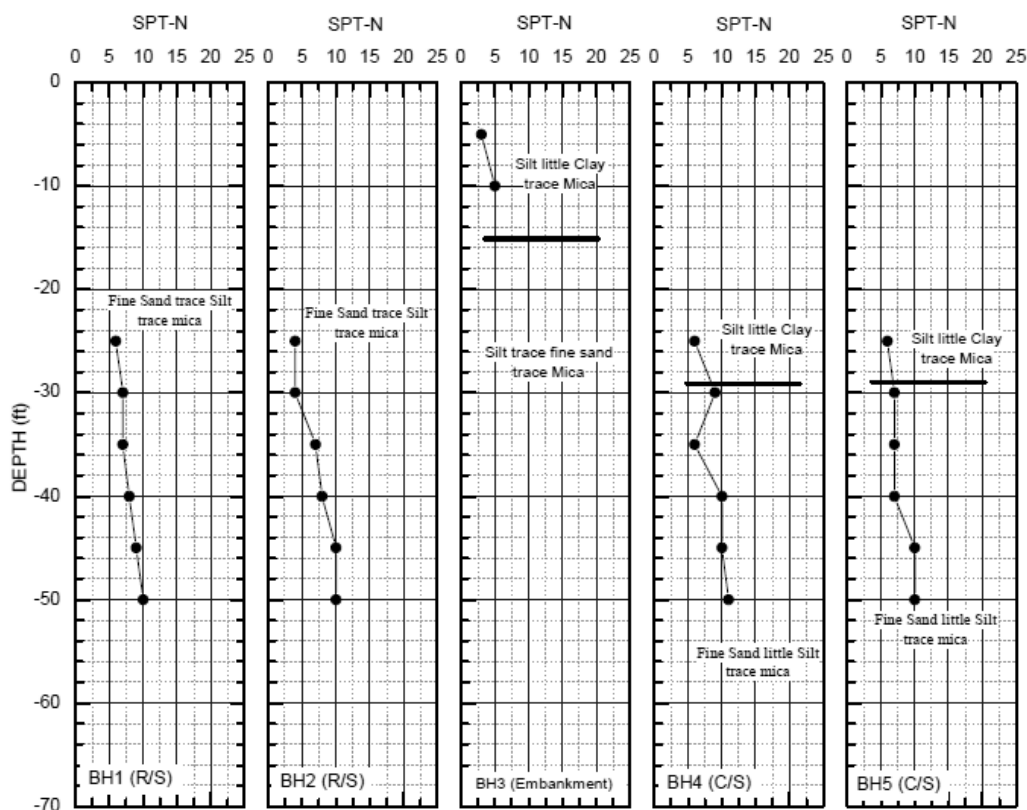


Figure 2: Typical Soil Profile across MDIP embankment (after Ansary et al., 2009)

Direct shear tests were performed on reconstituted (near to field density as depicted from SPT) disturbed soil samples from several location and depth to obtain the angle of internal friction, and cohesion intercept, c of the sub-soil. The tests were performed on air dry soil. Specimens were tested under three different normal stresses (45 kPa, 90 kPa, and 180 kPa) and the strength parameters were determined from the failure envelope with various physical properties of the soil encountered. For the soils tested apparent cohesion, c was found to be negligible and in the range of 0-16 kN/m. The angle of internal friction, the soils is in the range of 26.7 to 35.8. It can be seen that the range of void ratio (e) of the soil is 0.81 to 1.13 corresponding to porosities (n) of 0.45 to 0.53 respectively. The experimental results indicate that the soils of the site are predominantly fine sand existing in a loose to medium dense state.

Constant head permeability test was carried out on specimen prepared by mixing soils from different boreholes and depths. For better representation of field conditions the flow of water was allowed upward through the specimen by using a special constant head permeameter. The boiling phenomenon was simulated for the field conditions using this apparatus. The gradient was found to be lower than the theoretical value of 1.0. The permeability of the soil was also estimated using Allen Hazens well known empirical formula of $k=Cd_{10}^2$ using the range of C values of 100 to 150 (Lees and Chuaqui, 2004).

3. GPR PRINCIPLE

Geophysical exploration is a non-destructive, cost effective way to help locate and characterize features beneath the ground at many sites; GPR is one of the better techniques for this search in the shallow subsurface. GPR is a near-surface geophysical technique that can provide high resolution images of the dielectric properties about 20 meters of the earth. It is a very useful technique which employ the radio waves typically 16 to 2000 MHz frequency range, to study structure and features buried in the ground, groundwater, subsurface faulting, and underground cavities (natural or man).

A trigger pulse is generated in the control unit at a normal repetition rate of about 100 kHz. The trigger pulse is sent through the control cable to the transmitter electronics in the antenna. In the transducer, each trigger pulse is transformed into a bipolar pulse with higher amplitude than the trigger pulse. The pulse shape varies with the electronics and the antenna. The

transmit pulse then propagates along the antenna and is radiated into the subsurface. The size of the antenna and electrical properties of the subsurface determine the frequency of the propagating energy. In the subsurface, reflections occur at boundaries where there is a dielectric contrast. The reflected portion of the signal travels back to the antenna. The receiver in the antenna detects the returning signal and sends it back to the control unit. In the control unit the signal is processed and displayed. The output of the graphic recorder or the display on the video is a representation of the analog signal. Horizontal axis is distance along the surface and vertical axis is two-way travel time of the radar pulse in nanoseconds (ns). The signal amplitude determines the shade of grey on the paper or the color on the video display.

The penetration depth is controlled by the GPR centre frequency, the electrical conductivity and the attenuation of the subsurface deposits. In low-loss (i.e., resistive) deposits a low centre frequency achieves a large penetration depth whereas a high centre frequency results in a lower penetration depth. Figure 3 shows the fundamental principal of GPR.

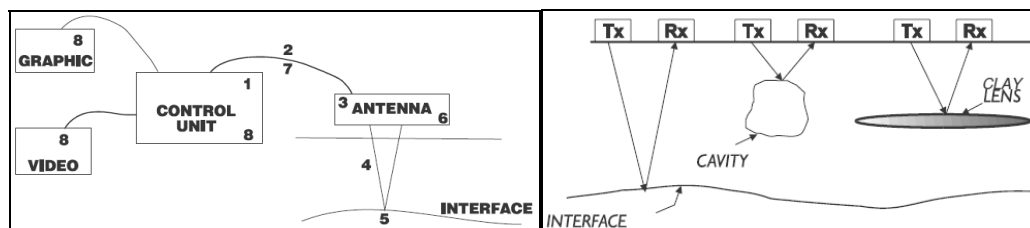


Figure 3: Fundamental principal of GPR

3.1 Modal propagation Theory

Modal propagation within a layer waveguide (of permittivity ϵ_2) refers to lossless propagation and is especially dispersive when the layer thickness is close to or less than an in-situ wavelength λ , (Arcone et al., 1998). In a two layer dielectric ground, lossless (nonleaky) modes occur when the confining layers (e.g. air above, for which $\epsilon_1=1$ and dry sand ϵ_3 below) have lower permittivities than the waveguide. In this case, a refraction will occur in the lower layer at the critical angle, and dispersive modes will develop in the upper layer (Figure 2). Depending on waveguide thickness d and ϵ_2 , higher order modes will develop which have phase fronts that propagate at speeds determined by discrete angles (measured from vertical)

greater than the critical angle. The lowest order mode is always the strongest and most important. The modes are determined by the modal equation (Budden, 1961) for either transverse electric (TE) or transverse magnetic (TM) waves, such that

$$R_{01}R_{12} \exp(i2k_2d \cos\theta) = 1$$

Where R_{01} and R_{12} are the TE or TM reflection coefficients for the upper and lower layer interfaces, respectively; $k_2=k_0\sqrt{\epsilon_2}$ is the propagation function for the refracting layer; and θ is the modal angle of a particular frequency with respect to vertical. The quantity $k_0=2\pi f/c$, where f is frequency in Hz and $c=30$ cm/ns. The phase velocity of any particular frequency is

$$v_{ph}=c/\sqrt{\epsilon_2}\sin \theta$$

For our case of parallel and facing antennas, we consider only TE waves. In this case all modes have a minimal cutoff frequency where phase and group velocities equal the velocity within an adjacent, refracting layer and a higher frequency at which minimum group velocity occurs and energy is theoretically maximized. This latter phenomenon is known as the Airy phase (Grant and West, 1965). For given values of d and the permittivities of each layer, several modes might exist, each of which can support all frequencies above their own particular cutoff frequency.

Modal propagation losses are caused by transmission through the waveguide interfaces, intrinsic attenuation within the medium itself, and geometric wavefront spreading. Interface transmission losses and intrinsic attenuation, such as caused by conduction currents or scattering, may be expressed through a complex, equivalent propagation angle $\theta + i\gamma$, for which the phase velocity then becomes

$$v_{ph}=c/\sqrt{\epsilon_2}\sin\theta \cosh\gamma$$

If $\epsilon_1 > \epsilon_2$, then transmission leakage into the lower layer can produce values of γ near unity and attenuation rates can approach several tens of decibels per meter. For the case of our refractive waveguide, however, real energy loss occurs strictly through medium attenuation mechanisms. Apparent energy loss at any particular frequency occurs from the dispersive process itself.

For geometric spreading losses we consider that the amplitudes of modes, refractions, and any kind of lateral surface wave decay in proportion to r^2 , where r is the range separation

between transmitter and receiver antennas. The range is both several wavelengths from the source and much greater than the surface layer depth. We assume this range dependency because very thin layers (in terms of γ) support nearly interfacial waves; interfacial waves along homogeneous ground follow this behavior (Annan, 1973), and so do seismic refractions (O'Brien, 1967). Furthermore, the low-frequency wave velocity that developed in our surface waveguide emulates refraction along the lower interface (Steven et. al., 2003)

4. FIELD TECHNICS

We used the Geophysical Survey Systems, Inc. (GSSI) model SIR-3000 control unit to set radar parameters and record data to hard disk. We used separate transmitter and receiver resistively loaded antennas with bandwidths nominally centered near dominant frequencies of 100 MHz (GSSI model 3207).

4.1 Reflection profiling

In reflection profiling mode the antennas are kept at constant separation, while they are moved along a profile (Figure 4). The electromagnetic pulses are transmitted at fixed time or distance interval. The signal is recorded and displayed immediately on a computer screen as GPR profiles, in which the vertical axis is two-way travel time in nanoseconds (ns) and the horizontal axis is distance along the measured profile. The GPR data are either collected along a single profile or in a grid of profiles to obtain 2D or pseudo 3D information on structures in the ground. The GPR data can also be acquired along lines so densely spaced that the line spacing equals the stepwise along the line. This leads to a 3D data cube, where data also can be displayed as time or depth slices. Study was conducted using bi-static high range profiling mode at distance interval according to Figure 4.

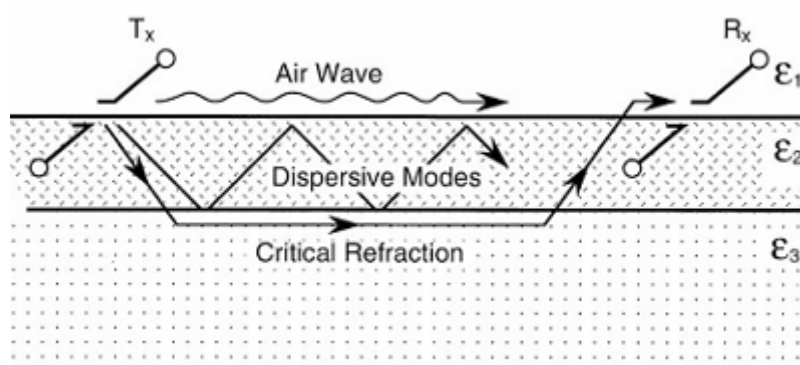




Figure 4: Diagram of the transmit (Tx) and receive (Rx) antennas, airwave, waveguide dispersive modes, and refraction (Top). 100-MHz antennas with fiber optic circuitry to trigger the receiver and antennas on the study line (bottom).

4.2 Common Depth Point

A common depth point dataset, CDP, is also called a velocity sounding, since the technique is commonly used for signal velocity establishment. In CDP mode the antennae separation is increased for each recording, while they are kept over a common midpoint (Figure 5a). A CDP plot contains the direct wave transmitted in the air above the ground, the direct wave transmitted in the ground and waves reflected from interfaces in the ground, where the dielectric properties change (Figure 5b). Refracted waves are seldom present in CDP soundings. This is related to the fact that the electromagnetic wave velocity decreases with depth together with increasing water content with depth.

5. RESULT ANALYSIS AND DISCUSSION

The test area of this study consisted of 75m along embankment foot and formed a 2-D section of underground stratum structure. Figure 6 displays the GPR section for distance on ground surface, at 0 m~40m. From the Figures, a clear surface of reflection can be observed along ground surface at underground depth of 6m, which shows different electrical properties of stratum above and below the reflection interface. This reflection interface is almost parallel to the ground level.

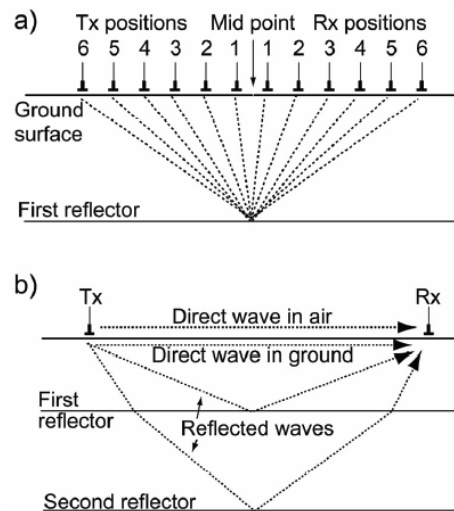


Figure 5: Principles of GPR in CDP mode. a) In CDP mode a set of a transmitting antenna (Tx) and a receiving antenna (Rx) are moved away from each other. The six first antenna positions are shown with the path of the reflected wave from the first reflector. b) Sketch of the path of the most common waves that is present in a CDP.

Groundwater table is present just below the 3m. Figure 6 implies that cement grouting has been successfully injected about 6m below the surface. The reflection signal is also very strong at 13m depth, which shows that the property of this layer differs a lot from the layers above and below it. Figure 7 shows the wiggle shape. This figure indicates that the strong signal of reflection below 6m depth is caused by rich content of underground water. Figure 8 shows the data collection in CDP mode. This data is used to estimate velocity of the soil with respect to depth profile.

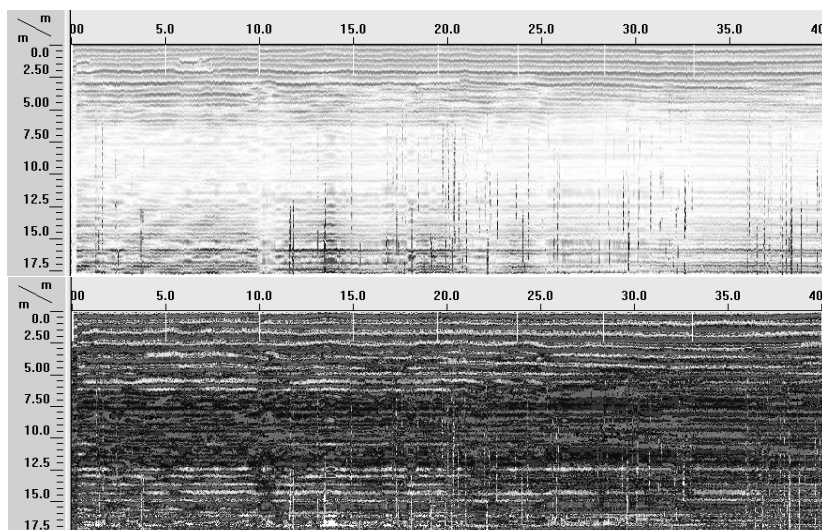


Figure 6: GPR Section at a distance of 0m~40m from ground surface (different color).

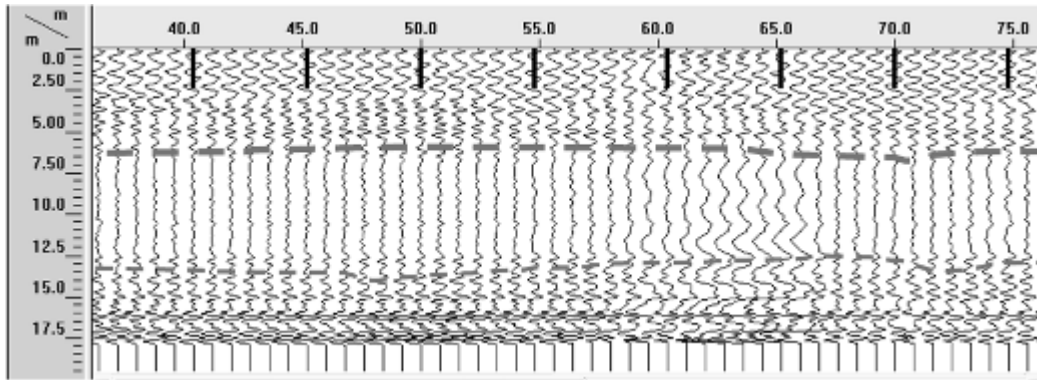


Figure 7: GPR Section in wiggle mode at a distance of 0m~75m from ground surface

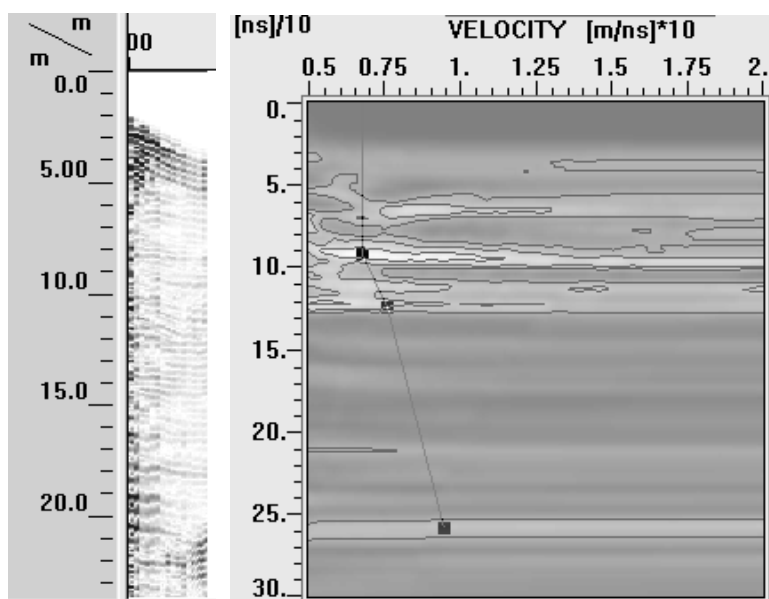


Figure 8: Multifold data are normally acquired or sorted in CDP gathers as represents in ray path form (left). An optimum stacking velocity versus travel time can be extracted which permits coherent summation of multifold survey data as well as a velocity depth function such as shown (right).

4. CONCLUSIONS

In this study, a 100 MHz frequency GPR antenna was used at Meghna Dhonagoda Irrigation Project (MDIP) site to evaluate the remedial measures undertaken using cement grouting technique at the river side in two affected embankment points. Common Depth Point (CDP) and bi-static high range reflection profiling was used for data collection. The collected data indicated that a water table did exist at a depth of 3m which was substantiated by the piezometer located at the investigated points. Also the collected GPR data indicated that the soil up to a depth of 6m might have improved by cement grouting technique.

REFERENCES

- Ansary, M. A., Yasin, S. J. M., Siddque, A., Abedin, M.Z. and Safiullah, A. M. M., (2009), Soil Investigation of Meghna Dhonagoda Irrigation Project (MDIP) Embankment, Proceedings of the Bangladesh Geotechnical Society's Conference in 2009 in Dhaka, Bangladesh.
- Annan, A. P., (1973), Radio interferometry depth sounding: Part I-Theoretical discussion, *Geophysics*, Vol. 38, pp. 557–580.
- Arcone, S. A., Lawson, D. E., Delaney, A. J., Strasser, J.C., and Strasser, J. D., (1998), Ground-penetrating radar reflection profiling of ground water and bedrock in an area of discontinuous permafrost. *Geophysics*, Vol 63, pp. 558-669.
- ASTM (2006), *American Society for Testing and Materials Standards*, Vol. 04.08.
- Budden, K. G., (1961), The wave-guide mode theory of wave propagation, *Prentice-Hall, Inc.*
- BWDB (2007), Cross Section of Flood Embankment at Boring Points of MDIP, Memo. No.PMO-JMREMP/ S-83/ 632, Project Director, JMREMP, *Bangladesh Water Development Board*, July 2007.
- Grant, F. S., and West, G. F., (1965), Interpretation theory in applied geophysics, *McGraw-Hill Book Co.*
- Lees, D. & Chuqui, M. (2004), Soil Grouting: Means, Methods and Design, *Grouting 2003*, pp. 1347-1359.
- O'Brien, P. N. S., (1967), The use of amplitudes in seismic refraction survey, in Musgrave, A. W., Ed., *Seismic refraction prospecting: Soc. Expl. Geophys*, pp. 85-118.
- Steven, A. A., Paige, R. P. and Lanbo, L., (2003), Propagation of a ground penetrating radar (GPR) pulse in a thin-surface waveguide, *Geophysics*, Vol. 68, No. 6 P. 1922–1933.



PART-VIII

TRAINING COURSES, SEMINARS AND WORKSHOPS

**BANGLADESH NETWORK OFFICE FOR
URBAN SAFETY (BNUS), BUET, DHAKA**

Prepared By: Mehedi Ahmed Ansary

BNUS Participates in Earthquake Risk Mitigation Training

Earthquake Risk Mitigation training program organized by Centre of Excellence in Disaster Mitigation & Management and Department of Earthquake Engineering, Indian Institute of Technology Roorkee (IITR). This two week training course conducted on Earthquake risk mitigation from 6th-17th June 2011 at IIT Roorkee Greater Noida Extension Center, New Delhi, India. This program is founded by SAARC Disaster Management Center (SDMC). A total of 27 participants representing SAARC member countries attended the training course. The main objective of the training course was to impart training to the participants to assess the earthquake hazard, vulnerability of buildings; mitigation measures to be undertaken for minimizing the earthquake effects; sharing knowledge on best practices in earthquake resistant design, construction and mitigation measures. Research Engineer *Ram Krishna Mazumder* from Bangladesh Network Office for Urban Safety (BNUS) has been participated in this training course which focused on Earthquake Risk and Mitigation.

The training program was inaugurated by Padmashree Dr. A. S. Arya, Former National Seismic Advisor, Government of India. Dr. S. C. Saxena, Director, IIT Roorkee welcomed the participants and Dr. O. P. Mishra Director/Officer-in-Charge SDMC elaborated history, genesis, vision and mission of SDMC, various training programs conducted by the center in collaboration with specialized agencies for the benefit of SAARC region.



Figure: Ram Krishna Mazumder from BNUS presenting country presentations on Bangladesh

The training programme was divided into 32 sessions covering Seismic Hazard and Vulnerability Assessment; Secondary Seismic Hazards; Earthquake – Resistant Design and Construction and

other related aspects of the Earthquake risk mitigation by several experts as resource persons affiliated with IIT Roorkee, National Institute of Disaster Management (NIDM) India, SDMC, Dhaka University Bangladesh, Taylor Devices India Pvt Ltd. The participants were also made field visits to New Delhi, Agra for on-spot observation of the mitigation measures executed for minimizing the effects of earthquake. The facilities available to the trainees included hands-on-exercises on aspects of earthquake risk mitigation. The session dedicated to country presentations enabled the trainees to be in tune with the recent developments in the related fields in the region. The trainees could also get a chance to evaluate themselves about the lessons learnt from the training through an evaluation test.

Dr. O. P. Mishra, Officer-in-charge, SDMC, distributed the certificates to the participants at the end of the training. In his valedictory speech he elaborated on the role played by SDMC in the rapidly evolving field of disaster mitigation and management. Dr. D. K. Paul, coordinator of the training presented the course completion report.

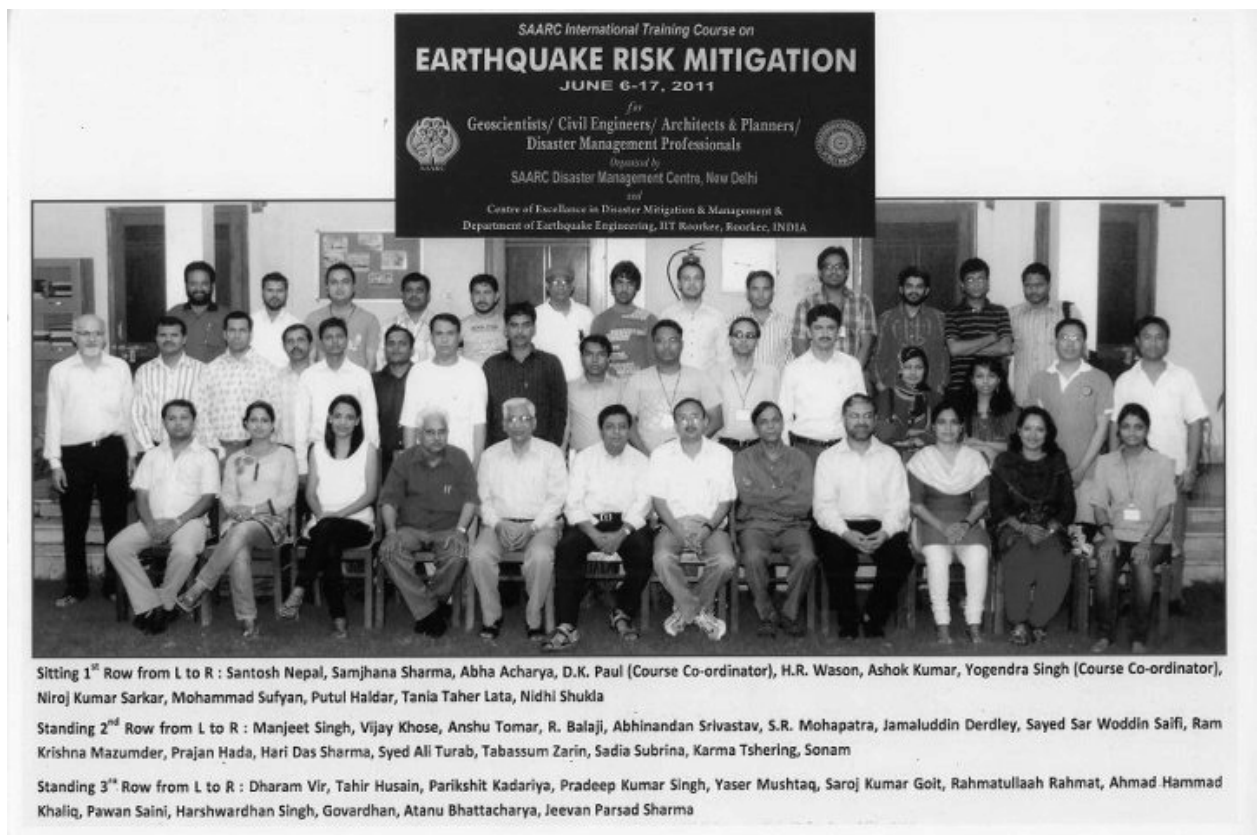


Figure: Participants and Program co-ordinators of Earthquake Risk Mitigation training at Roorkee, India.

Report on Training of Engineers on Earthquake Safe Construction



Jointly Organized by
Bangladesh Network Office for Urban Safety (BNUS), BUET
National alliance for Risk Reduction and Response Initiatives (NARRI)

Key Contents	Earthquake and Geotechnical Issues Structural Issues regarding earthquake
No of Participants	40
Level of Participants	B. Sc Engineer
Date	December 29-31, 2011
Venue	Hotel Supreme, Sylhet
Type of training	Non-residential
Facilitated by	Prof Dr. Mehedi Ahmed Ansary Prof. Dr. Raquib Ahsan Engr. Mehedi Hasan

SURVEY REPORT ON BURNT BUILDING AT OLD DHAKA

BNUS conducted a survey on two back to back fires in Ward 65 in Old Dhaka. The fires occurred in 15th and 16th January 2012 in Islambag and Lalbag areas. The first incident occurred in a plastic warehouse near the Eidgah ground in West Islambag at around 10:45 PM started with gas stove. Eventually the fire became so devastating that it burnt three houses around the warehouse. Fire service came after 30 minutes of fire occurrence and controlled the fire at 12:30 AM. Total economic loss of this hazard is Tk. 0.3 Million.

The next day again at the same time another fire occurred in Shahid Nagar area at Lalbag around 10:30 PM. In this case fire originated from a tin shed house. Around 100 shanties, five shops and a printing press were caught by fire. Ten units of Fire Service and Civil Defense (FSCD) from Lalbagh, Polashi, Sadarghat and the headquarters rushed to the spot and managed to extinguish the blazes around 12:40 AM. A man was injured during fire. Some photographs of the Islambag fire are as follow:



Burnt household objects



Burnt household objects



Burnt household objects



Source of fire: gas Stove



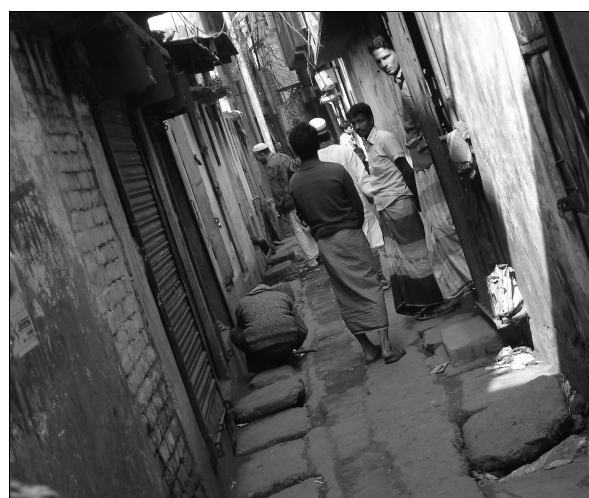
2 feet wide staircase within the burnt building



Nearby building affected by fire



Electric pole near the burnt building



4 feet wide road in front of the burnt building

INTERVIEW WITH OFFICIALS RELATED WITH STANDING ORDER ON DISASTER

BNUS and ICUS jointly conducted a number of interviews with some officials related with the Standing Order on Disaster (SoD) of Bangladesh from 4th January 2011 to 10th January 2011. They covered four government organizations including Disaster management Bureau (DMB), Comprehensive Disaster Management Programme (CDMP) Phase II, Fire Service and Civil Defense Directorate (FSCD) and Cycle Preparedness Programme (CPP). An international NGO Oxfam GB was also visited to know the gap between the planning and implementation of SoD.



Figure 1: BNUS and ICUS Officials in front of BNUS Office in BUET, Dhaka

DMB is directly related with the planning, implementing and monitoring of SoD. Two important personnels of DMB including the Director General Mr. Ahsan Zakir and the Communication Media Specialist Mr. Syed Ashraf are interviewed. The government of Bangladesh introduced its Standing Orders on Disaster (SoD) which specify the functions of each concerned Government Ministry, Division, Department and Agencies. The SoD is the compilation of all the disaster codes in Bangladesh. Cyclone codes of 1070, drought codes of 1979 and flood codes of 1985 are gathered together to form the first version of SoD in 1998 which was published in Bangla. In 1999, the SoD was translated into English and published. In 2000 and 2002 Bangladesh experienced two big floods and some big earthquakes occurred in the neighboring countries of this country. So there was a need to revise the SoD to incorporate earthquake. The revision process started in 2004. But it was running slowly until Cyclone Sidr hit Bangladesh in 2007. The DMB formed a committee to manage the revision process. The committee incorporated more functions for each organization related with disaster management. Then they called a validation workshop and invited all the DM organizations to participate in the workshop. After the validation made by the DM organizations about their responsibilities in DM, the DMB committee made a number of

corrections and finalized the revised SoD. The revised SoD was published in 2010 in English version. The DMB mainly involves in planning of the SoD rather than implementation. FSCD and Oxfam GB involve directly in the implementation process. FSCD is a service oriented emergency government organization under Ministry of Home Affairs of Bangladesh which responds first and remains alert for 24 hours a day for the management of any kind of fire and disaster. Its main mission is to provide service support to reduce mortality rate during fire or any disaster, ensure first aid to the victim, provide ambulance service to the patient, organize training, demonstration and consultancy to prevent fire incident and arrange civil defense measures. Director (Operation and Maintenance) Major Mohammad Mahub, Staff Officer Mr. Akram and Staff Officer Md. Abul Bashar of FSCD are interviewed to know the activities of BFSCD in the implementation process of SoD. FSCD involves in fire fighting, rescue operation and preparedness of disaster. Recently they are organizing several training program to instruct 62000 community volunteers throughout the country. They also conduct fire drill, simulation drill and evacuation drill frequently specially in high rise buildings and slum.



Figure 2: Community Volunteer Training Program



Figure 3: Demonstration Training Program



Figure 4: Fire Drill Program



Figure 5: Simulation Drill Program

Two officials of CPP including Assistant Director Mr. Hasanul Amin and Coordinator of Signal Mr. Abdul Hamid were interviewed to know how CPP responds in case of any cyclone after implementation of the SoD and the revised SoD. The CPP plays an important role in the dissemination of cyclone warning, evacuation, rescue, first aid and emergency relief work including mobilization of people toward cyclone shelters through its volunteers in the coastal districts. Currently, CPP has 203 paid employees, 49215 volunteers including 32810 male and 16405 female and 3281 Units covering 321 Unions, 37 Upazilas, 7 Zones and 13 District. Due to global warming, CPP has increased its preparedness and awareness building functions for the community people living in the coastal area of Bangladesh. CPP command area is expanded in more 5 Upazilas of Khulna, Bagerhat and Satkhira districts with the financial help of Comprehensive Disaster Management Program (CDMP) Phase I. Comprehensive Disaster Management Programme (CDMP) Phase II was also visited to know its involvement in the planning and implementation of SoD. Disaster Response Management Specialist Mr. Abdul Latif Khan, Communication Specialist Shaila Shahid and Project Coordinator (Inter Ministerial) Officer Md. Eusuf Ali were interviewed.

Apart from these government organizations, some international NGOs are currently working in DM sector. Six international NGOs viz. Action Aid, Concern Universal, Concern Worldwide, Islamic Relief Worldwide, Oxfam GB and Bangladesh government have established a consortium named National Alliance for Risk Reduction and Response Initiatives (NARRI). Among these NGOs, Oxfam GB was visited and the Programme Manager Manish Kumar Agrawal was the key interviewee.



International Center for Urban Safety Engineering
Institute of Industrial Science, The University of Tokyo

4-6-1 Komaba, Meguro-ku,

Tokyo 153-8505, Japan

Tel: +81-3-5452-6472

Fax: +81-3-5452-6476

<http://icus.iis.u-tokyo.ac.jp>

E-mail: icus@iis.u-tokyo.ac.jp

ISBN4-903661-54-7

